

# **Off the beaten track**

**How ecosystems fail to respond to environmental change**

The research presented in this dissertation was supported by a grant awarded to Max Rietkerk and Arjen Doelman by the Netherlands Organization for Scientific Research (NWO) and is part of the NWO Complexity programme.

**Printed by:** Gildeprint, The Netherlands

**Cover by:** Koen Siteur

**ISBN:** 978-94-623-3353-6

©2016, Koen Siteur. All rights reserved.



# **Off the beaten track**

**How ecosystems fail to respond to environmental change**

## **Buiten de gebaande paden**

**Hoe ecosystemen er niet in slagen te reageren op externe verandering**

(met een samenvatting in het Nederlands)

Proefschrift

ter verkrijging van de graad van doctor aan de Universiteit Utrecht op gezag van de rector magnificus, prof. dr. G.J. van der Zwaan, ingevolge het besluit van het college van promoties in het openbaar te verdedigen op vrijdag 23 september 2016 des avonds te 6.00 uur

door

Koen Siteur

geboren op 27 september 1987 te Utrecht

**Promotoren** Prof. dr. ir. M. Rietkerk

Prof. dr. A. Doelman

**Copromotor** Dr. M.B. Eppinga

# Contents

<b>1</b>	<b>Introduction</b>	<b>1</b>
1.1	Environmental science and dynamical systems theory . . . . .	1
1.2	Basic concepts and insights from dynamical systems theory . .	2
1.2.1	Feedbacks, equilibrium states and stability . . . . .	2
1.2.2	Environmental change and critical transitions . . . . .	3
1.2.2.1	Transitions to alternative equilibrium states . . . . .	4
1.2.2.2	Transitions to cyclic dynamics . . . . .	6
1.2.2.3	Transitions to spatially periodic patterns . . . . .	7
1.3	Problem definition and research questions . . . . .	9
1.3.1	Transitions from patterned to uniform states . . . . .	11
1.3.2	Frequency and magnitude of resource pulses . . . . .	13
1.3.3	Processes at multiple timescales . . . . .	13
1.3.4	Rapid environmental change . . . . .	14
1.4	Focus: water-limited ecosystems . . . . .	14
<b>2</b>	<b>Beyond Turing: the response of patterned ecosystems to environmental change.</b>	<b>17</b>
2.1	Introduction . . . . .	18
2.2	Model description and analyses . . . . .	20
2.2.1	Model description . . . . .	20
2.2.2	Analyses . . . . .	22
2.3	Stability of uniform and patterned states: from Turing instability to the Busse balloon . . . . .	23
2.3.1	Existence and stability of uniform system states . . . . .	23
2.3.2	Existence and stability of patterned system states . . . . .	25
2.3.3	Ecological implications . . . . .	27
2.4	System response to changing environmental conditions . . . . .	29
2.4.1	Bouncing through the Busse balloon . . . . .	30
2.4.2	Wavenumber selection: the role of rate of change and noise . . . . .	31
2.4.3	Competition between and rearrangement of patches . . . . .	33
2.5	Discussion and conclusions . . . . .	35

Appendix 2.A A non-dimensional extended Klausmeier model . . . . .	40
Appendix 2.B Wavenumber plotting by fast Fourier transform . . . . .	41
Appendix 2.C General equations for perturbations. . . . .	44
Appendix 2.D Analysis of the homogeneous steady states. . . . .	45
2.D.1 Existence of spatially homogeneous steady states . . . . .	45
2.D.2 Stability of the homogeneous steady states against homogeneous perturbations . . . . .	47
2.D.3 Turing analysis of the steady states . . . . .	50
Appendix 2.E Analysis of patterns . . . . .	51
2.E.1 Existence of patterns . . . . .	51
2.E.2 Stability of patterns . . . . .	53
<b>3 How will increases in rainfall intensity affect semiarid ecosystems? 55</b>	
3.1 Introduction . . . . .	56
3.2 Model description . . . . .	58
3.2.1 Soil moisture dynamics . . . . .	60
3.2.2 Plant growth . . . . .	60
3.2.3 Infiltration neglecting runon (for uniform case and interbands) . . . . .	61
3.2.4 Infiltration including runon (non-uniform case) . . . . .	63
3.2.5 Competition for surface water and spatial feedbacks .	65
3.2.6 Parametrization and analysis . . . . .	67
3.3 Results . . . . .	68
3.3.1 Competition for water along the hillslope . . . . .	68
3.3.2 Alternative stable system states . . . . .	70
3.3.3 The response of the model to changes in rainfall intensity	73
3.4 Discussion and conclusions . . . . .	78
Appendix 3.A Derivation of first and second order moments of infiltration rate . . . . .	81
Appendix 3.B Feedbacks between vegetation bands and interbands if infiltration is depth dependent. . . . .	83
Appendix 3.C Bifurcation diagram . . . . .	85
Appendix 3.D Region with alternative stable system states . . . . .	86
3.D.1 Upper rainfall limit . . . . .	86
3.D.2 Lower rainfall limit . . . . .	87
3.D.3 Robustness of the presented model results . . . . .	88

<b>4 Soil water repellency: a potential driver of vegetation dynamics in coastal dunes.</b>	<b>91</b>
4.1 Introduction . . . . .	92
4.2 Empirical observations of SWR . . . . .	94
4.2.1 Site description . . . . .	94
4.2.2 Linking SWR to infiltration . . . . .	94
4.2.3 Soil variables controlling infiltration . . . . .	95
4.3 Model description and analyses . . . . .	97
4.3.1 Model description . . . . .	97
4.3.2 Model analysis . . . . .	101
4.4 Model results . . . . .	102
4.4.1 SWR induced bistability in soil conditions . . . . .	102
4.4.2 The water-plants cycle: repetitive regime shifts . . . . .	103
4.4.3 Cyclic dynamics and the SWR lock . . . . .	105
4.4.4 The impact of SWR depends on plant species traits .	105
4.4.5 SWR can amplify drought stress . . . . .	107
4.5 Discussion and conclusions . . . . .	108
Appendix 4.A Composition of the hydrophobic compounds. . . . .	113
Appendix 4.B Gravimetric and volumetric soil moisture content .	114
Appendix 4.C Parameter values for the model . . . . .	114
Appendix 4.D Hydrophobic compound content in plant tissues .	115
Appendix 4.E Decomposition rates of hydrophobic compounds in soils. . . . .	117
Appendix 4.F Additional drought simulations . . . . .	119
<b>5 Ecosystems off track: Rate-induced critical transitions in ecological models.</b>	<b>121</b>
5.1 Introduction . . . . .	122
5.2 Critical transitions, Steady state analysis and Resilience . .	122
5.3 Rate-induced critical transitions . . . . .	125
5.4 Analysis of rate sensitive models . . . . .	130
5.4.1 Graphical analysis of Equation 5.1 . . . . .	131
5.4.2 Steady lag analysis of Equation 5.1 . . . . .	132
5.4.3 Understanding rate sensitivity of ecological models .	133
5.5 Identifying real rate sensitive ecosystems . . . . .	135
5.6 Discussion and conclusions . . . . .	138
Appendix 5.A Steady states and potential diagrams for Equation 5.1	141
Appendix 5.B Stability analysis for Equation 5.8 . . . . .	141

## *Contents*

Appendix 5.C Graphical analysis of the Rosenzweig-MacArthur model . . . . .	142
Appendix 5.D Steady lag analysis of the Rosenzweig-MacArthur model . . . . .	144
<b>6 Synthesis and perspectives</b>	<b>147</b>
6.1 Ecosystems "off the beaten track" and their response to environmental change . . . . .	147
6.2 Patterned ecosystems: multistability, gradual transitions and early-warning signals? . . . . .	149
6.3 Towards (speed) limits for environmental change . . . . .	151
6.3.1 Advanced model analysis and long-term experiments .	152
6.3.2 Acknowledging adaptations on population level . . . . .	155
6.4 Final remarks . . . . .	155
<b>Bibliography</b>	<b>156</b>
<b>Summary</b>	<b>183</b>
<b>Samenvatting</b>	<b>185</b>
<b>Dankwoord</b>	<b>189</b>
<b>Curriculum Vitae</b>	<b>192</b>
<b>Publications by Koen Siteur</b>	<b>195</b>

# 1 Introduction

## 1.1 Environmental science and dynamical systems theory

Species that change biotic or abiotic materials and thereby affect the availability of resources to other species are referred to as “ecosystem engineers” in ecology (Jones et al., 1994). Humans can be considered as the ultimate ecosystem engineer. Through changes in the biogeochemical cycles, land surface transformations and climate change humans are globally affecting species and, on a higher level, ecosystems. The affected ecosystems often provide essential services, such as the regulation of climate, floods and diseases, and the provision of food and fresh water (Reid et al., 2005). Understanding the exact effect of human-induced changes in the environment on ecosystems is of crucial importance and is currently one of the main challenges in the field of environmental science (Miller, 2005). To obtain insights in the effects of human-induced environmental changes, there is a strong need for environmental scientists to develop methods and tools that enable better understanding of ecosystem dynamics.

Dynamical systems theory provides ways to study human-environment interactions (Meadows, 2008) and the effect of (human-induced) environmental changes on ecosystems in particular. Dynamical systems theory, referred to as dynamical modelling or environmental modelling when applied in environmental sciences, is a field in mathematics that uses differential and difference equations to describe natural phenomena.

In this dissertation I will use dynamical systems theory to understand why some ecosystems fail to cope with environmental change. In the following sections I will first give an overview of the key insights gained by the application of dynamical systems theory in the field of environmental science and ecology in particular. I then identify current knowledge gaps and introduce the research questions that I aim to answer. Finally, I will explain how these questions apply to the particular type of ecosystem that will be the focus of this dissertation.

## 1.2 Basic concepts and insights from dynamical systems theory

### 1.2.1 Feedbacks, equilibrium states and stability

State variables are variables of a system that describe its state (e.g. nutrient concentration, population density, soil water content). State variables are influenced by fluxes (e.g. nutrient input, population growth, rainfall). The dynamics of ecosystems are controlled by feedbacks, which occur when a state variable affects its own fluxes, directly or through a loop of causal connections and possibly involving other state variables. Negative feedbacks are balancing and stabilizing, whereas positive feedbacks are reinforcing and destabilizing. The effect of feedbacks can be explained with Figure 1.1, which is a graphical representation of the logistic growth model (Verhulst, 1838). The population size in this model increases when population growth is positive and decreases when population growth is negative. In the model reproduction increases with population size, resulting in a positive feedback, whereas crowding hampers population growth at high population sizes, giving rise to a negative feedback. The sign of the dominating feedback can be read from the slope of the growth curve. If the slope is positive, then the positive feedback dominates, as an increase in the population further enhances population growth. If the slope of the growth curve is negative, then the negative feedback dominates, since now an increase in the population diminishes the growth rate, and thereby slows down further growth.

Systems are said to be in a (dynamic) equilibrium or steady state if, despite flows through the system (e.g. growth and mortality), the state of a system is unchanging. In Figure 1.1 these equilibrium states are located at the intersections of the growth curve with the  $x$ -axis. An important property of equilibrium states is their stability. Holling (1973, p. 17) defines it as follows: “Stability is the ability of a system to return to an equilibrium state after a temporary disturbance. The more rapidly it returns, and with the least fluctuation, the more stable it is”. This definition does not specify the magnitude of the temporary disturbance or perturbation. As we will see in the next section, however, the ability of a system to return to an equilibrium state can be affected by the magnitude of the perturbation. In this dissertation I will therefore use a narrower (mathematical) definition of stability: the ability of a system to return to an equilibrium state after a *small* perturbation. When defined as such, stability can be derived mathematically through linear stability analysis. Formally, this is done by perturbing an equilibrium state

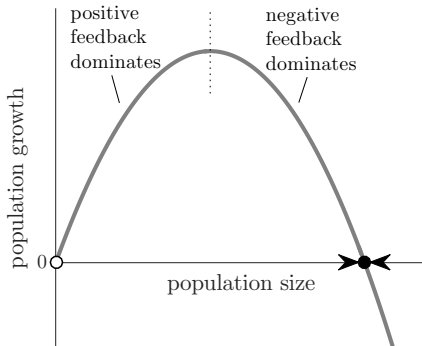


Figure 1.1: Example of a growth curve that can be used to get a qualitative understanding of differential equations with one state variable. Depicted is the growth curve for the logistic growth model (Verhulst, 1838). The closed dot is a stable equilibrium state and the open dot is an unstable equilibrium state.

and deriving (the sign of) the growth rate of the perturbation. A quick way to assess stability in the logistic growth model of Figure 1.1 is by reading the slope of the growth curve at the equilibrium points. If the slope at an equilibrium is negative, then negative feedbacks are dominant and the equilibrium is stable (filled dot). If the slope at an equilibrium is positive, then positive feedbacks are dominant and the equilibrium state is unstable (open dot). For systems with more than one state variable the stability of an equilibrium can be derived in a similar way using a so-called Jacobian matrix.

### 1.2.2 Environmental change and critical transitions

Environmental conditions (e.g. rainfall or temperature) control fluxes in ecosystems and thereby they affect the strength of the feedbacks that determine the stability of equilibrium states. When, as a result of gradual environmental change, positive feedbacks start to dictate the dynamics of an equilibrium state then a critical transition occurs. A critical transition is a shift of a system to a qualitatively different dynamical regime. Critical transitions are analogous to bifurcations, a term used in dynamical systems theory. However, in contrast to bifurcations, critical transitions include shifts to alternative regimes that are caused by perturbations of the system's state instead of gradual external change. Different types of critical transitions can

## 1 Introduction

be distinguished depending on their reversibility and the type of dynamics to which the system transitions. In the following I will discuss a selection of the different types of critical transitions, and reflect on their implications for ecosystem functioning.

### 1.2.2.1 Transitions to alternative equilibrium states

Critical transitions are either super- or subcritical. Supercritical transitions are reversible, whereas subcritical transitions are discontinuous and require disproportional efforts to reverse. Subcritical transitions between equilibrium states are often referred to as catastrophic shifts (Scheffer et al., 2001).

Catastrophic shifts can be understood by plotting the equilibrium states of a model as function of a parameter that represents the environmental conditions. Figure 1.2 shows such so-called bifurcation diagram for the over-harvesting model by Noy-Meir (1975), with plant biomass being the state variable and grazing pressure the parameter of interest. The figure shows that, when increasing the grazing pressure from I to II, the system obtains a second stable equilibrium state; it becomes bistable. When increasing the grazing pressure further, from II to III, positive feedbacks become dominant and a catastrophic shift occurs from a vegetated state to a degraded overgrazed bare state. Reversing this transition requires disproportional efforts because lowering the grazing pressure back to II will not result in recovery of the vegetation to its original state. Instead, grazing pressure needs to be reduced back to I in order allow the vegetation to recover.

Besides the over-harvesting model by Noy-Meir (1975), catastrophic shifts have been found in other ecological models as well as in (experiments on) real ecosystems (Scheffer et al., 2001; Schröder et al., 2005). Well-known examples are transitions of shallow lakes from clear to turbid states, triggered by increases in nutrient input (Scheffer et al., 1993; Carpenter, 2005), desertification resulting from plant-soil-water feedbacks (Rietkerk et al., 1996, 1997) and shifts in marine ecosystems driven by various factors, such as sea temperature rise and overfishing (Jackson et al., 2001; Petraitis, 2013).

The notion that slow continuous environmental change can result in rapid discontinuous ecosystem response has led to formulation of an ecosystem property called ecological resilience. A frequently used definition of ecological resilience is the one by Holling (1973, p. 17): “Resilience determines the persistence of relationships within a system and is a measure of the ability of these systems to absorb changes of state variables, driving variables, and parameters, and still persist”. Figure 1.3 shows how this definition relates

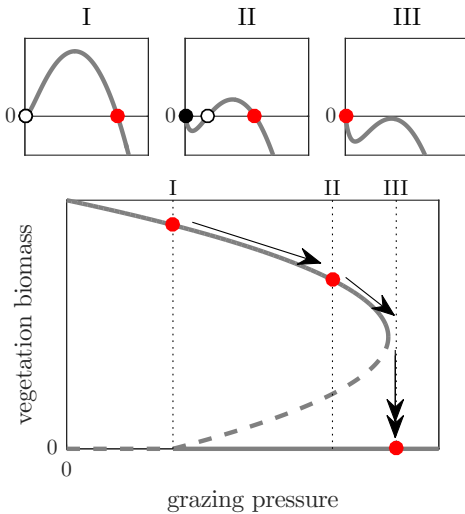


Figure 1.2: Example of a catastrophic shift triggered by gradually changing environmental conditions. The lower panel depicts a bifurcation diagram, with the dotted lines corresponding to the environmental conditions of the growth curves in the upper panels. The closed dots and solid lines are stable equilibrium states and the open dots/dashed lines are unstable equilibrium states. The red dots represent the actual state of the ecosystem.

to the bifurcation diagram of the model by Noy-Meir (1975). In this figure, the current state of the ecosystem is given by the red dot. The arrows depict two measures of the ability of ecosystems to absorb changes, i.e. measures of ecological resilience. The system is able to absorb environmental changes (i.e. changes in driving variables/parameters) of a magnitude up to  $a$  and perturbations of the system state (i.e. changes in state variables) of a magnitude up to  $b$  without shifting to an alternative stable equilibrium state.

Catastrophic shifts and ecological resilience are now well embedded concepts in ecology and the environmental sciences. Recent efforts in these fields focus on establishing the architectural features in ecosystems that are responsible for catastrophic shifts (Scheffer et al., 2012) and on assessing the proximity of ecosystems to critical thresholds (i.e.  $a$  in Figure 1.3) through so-called early-warning signals (Scheffer et al., 2009). The concept of catastrophic shifts also inspired the formulation of “planetary boundaries” that border the safe operating space for humanity regarding environmental issues such as climate change, ocean acidification and land-use change (Rockström et al., 2009; Scheffer, 2015; Steffen et al., 2015).

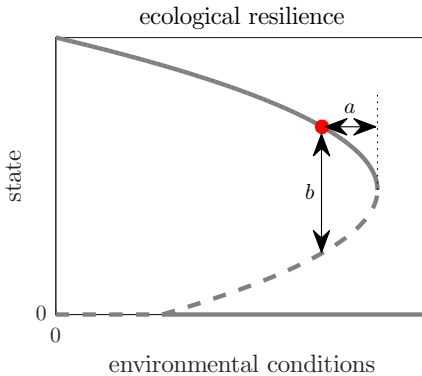


Figure 1.3: Bifurcation diagram of the model by Noy-Meir (1975). Arrows  $a$  and  $b$  represent measures of ecological resilience following the definition by Holling (1973).

### 1.2.2.2 Transitions to cyclic dynamics

When positive feedbacks become dominant ecosystems need not shift to an alternative equilibrium state, but can also transition to cyclic dynamics. In differential equations, such cyclic dynamics are the result of (at least) two interacting state variables, with contrasting effects on each other (for more conditions see Kolmogorov, 1936; Edelstein-Keshet, 1988, p. 351). The most well-studied examples of cyclic dynamics are found in predator-prey models. In these models predators negatively affect the prey population. The preys, in turn, positively affect the predator population. The first model to describe cyclic predator-prey dynamics is the model by Volterra (1928). In this model, cycles of neutral stability (i.e. neither stable nor unstable) emerge if the system is brought out of equilibrium. Later extensions of this model (Edelstein-Keshet, 1988, p. 223) showed that changes in parameters can trigger a critical transition from steady to cyclic dynamics. Such stable limit cycles emerge as a result of what is called an Andronov-Hopf bifurcation in dynamical systems theory. A famous example of a stable limit cycle that emerges from an equilibrium state is described by Rosenzweig and MacArthur (1963) and Rosenzweig (1971) (Figure 1.4a). In their models an increase in prey productivity results in destabilization of the equilibrium state, a phenomenon known as the paradox of enrichment (Rosenzweig, 1971).

Predator-prey models successfully explain the temporal dynamics observed in real ecosystems. A well-known dataset of Canadian lynx and hare abundances shows cyclic dynamics in both populations (Figure 1.4b). The dynamics in lynx and hares were first studied separately, leading various hypotheses on

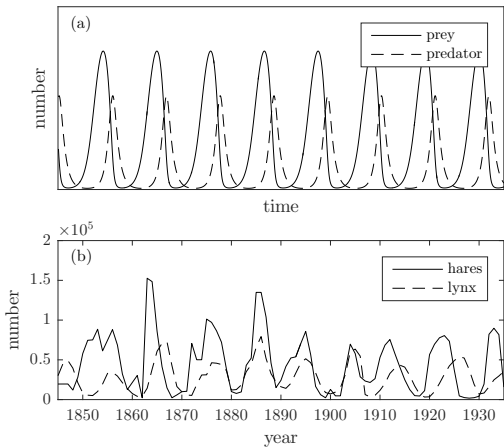


Figure 1.4: (a) Cyclic dynamics between predators and preys in the model by Rosenzweig and MacArthur (1963). (b) Cyclic dynamics in the abundance of lynx and snowshoe hare, indicated by the number of pelts received by the Hudson's Bay Company, Canada (Elton and Nicholson, 1942; Odum, 1953).

the cause of the cycles, ranging from climate forcing (Elton and Nicholson, 1942) to the sunspot cycle (Elton, 1924; Moran, 1949). However, when the datasets were combined there appeared to be good match between them (Odum, 1953), suggesting that, as in the models, the cycles were intrinsically driven.

In predator-prey models, or more generally in consumer-resource models, distinct repetitive catastrophic shifts can emerge when there is a large difference in timescales at which the state variables operate (e.g. Ludwig et al., 1978). In such fast-slow systems, temporal dynamics of the fast variable are characterized by periods of little change, separated by rapid shifts (Figure 1.5).

### 1.2.2.3 Transitions to spatially periodic patterns

Besides alternative steady and cyclic dynamics, ecosystems can transition to a different spatial structure in response to environmental change. A well-studied phenomenon is the formation of spatially periodic patterns out of uniform ecosystem states. This process is known as spatial self-organization (Rietkerk and Van de Koppel, 2008) and is the result of positive feedbacks that dominate locally (short range activation) in combination with distal negative feedbacks (long range inhibition; Gierer and Meinhardt, 1972). This combination of

## 1 Introduction

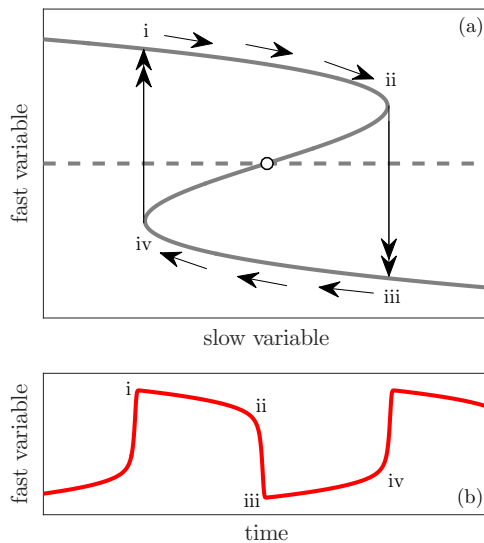


Figure 1.5: Repetitive catastrophic shifts in a fast-slow system. (a) Repetitive shifts occur when the isocline of the slow variable (dashed line; here the change in the slow variable equals zero) separates the two stable branches of the bifurcation diagram of the fast variable (solid line). (b) Temporal dynamics of the fast variable are characterized by periods of little change, separated by rapid shifts (Rinaldi and Scheffer, 2000).

positive and negative feedbacks is referred to as scale-dependent feedbacks (Figure 1.6; Rietkerk and Van de Koppel, 2008).

Pattern formation is a ubiquitous property of reaction-(advection-)diffusion models that combine local processes (reactions) and spatial processes (advection/diffusion). Two types of pattern forming reaction-(advection-)diffusion systems can be distinguished: the activator-inhibitor system and the activator-depleted substrate system (Edelstein-Keshet, 1988). In the activator-inhibitor system an activator produces more of itself and of an inhibitor that inhibits the production of the activator (Figure 1.7a). In the activator-depleted substrate system an activator produces more of itself and depletes a substrate that is required for activator production (Figure 1.7b). If the activator spreads with a lower rate than the inhibitor or the substrate, these mechanisms can lead to pattern formation through what is called a Turing instability (Turing, 1953) (for a detailed derivation of the required conditions see Segel and Jackson, 1972; Edelstein-Keshet, 1988, pp. 516-520).

Observed patterns in ecosystems have been successfully reproduced by models of both activator-inhibitor and activator-depleted substrate type. Van de Koppel and Crain (2006) for instance, were able to model spatial patterns in freshwater marshes, in which *Carex stricta* acts as an activator and its litter as an inhibitor. Models by Klausmeier (1999) and Rietkerk et al. (2002) suggest that patterns observed in arid ecosystems can be explained by considering arid vegetation as activator and surface water, for which plants compete by enhancing soil infiltrability, as (depleted) substrate (Figure 1.8).

Model studies suggest that the short range positive feedbacks involved in pattern formation (Figure 1.6) enable patterned ecosystem states to persist into harsher environmental conditions when compared to uniform states and that as conditions change further, a catastrophic shift to a degraded uniform system state can occur (Rietkerk et al., 2004). This means that observing particular patterns could indicate that a system has alternative stable states (Kéfi et al., 2010) and that patterns may serve as an early-warning signal for catastrophic shifts (Rietkerk et al., 2004).

## 1.3 Problem definition and research questions

In the previous section I gave a brief overview of relevant insights in environmental sciences and ecology that have been obtained through the application of dynamical systems theory. However, the presented theory strongly relies on stability analysis of uniform equilibrium states. This means that, in order to

## 1 Introduction

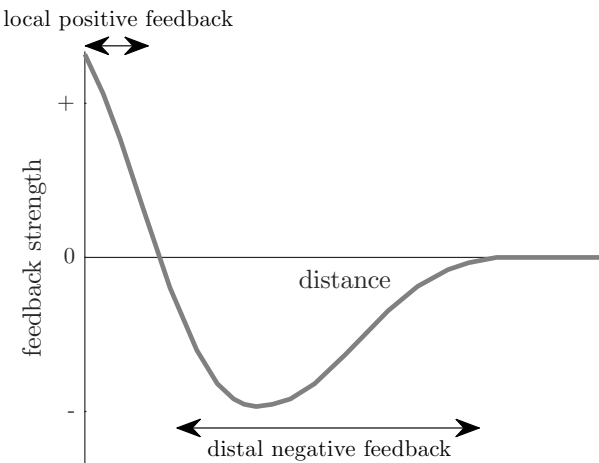


Figure 1.6: Pattern formation results from scale-dependent feedbacks (Rietkerk and Van de Koppel, 2008).

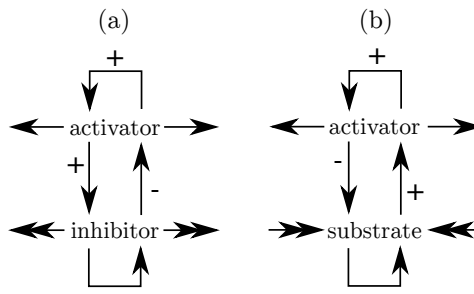


Figure 1.7: (a) Activator-inhibitor system and (b) activator-depleted substrate system. The horizontal arrows indicate direction of diffusion patch of activator. For pattern formation, the diffusion rate of the inhibitor/substrate needs to be faster than that of the activator, as indicated by the double horizontal arrows.

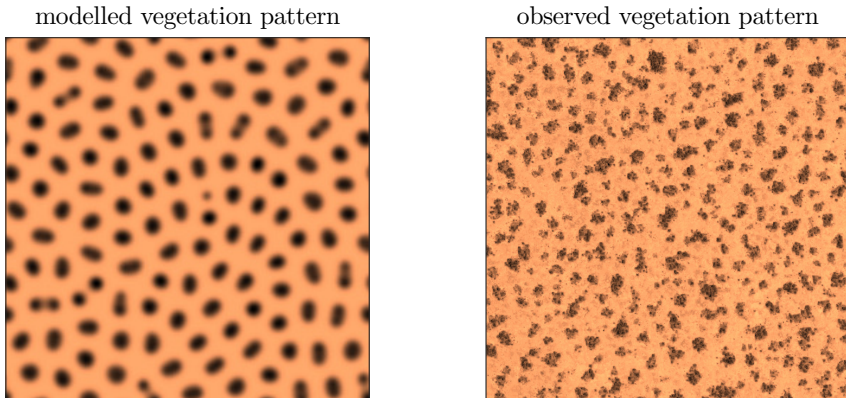


Figure 1.8: Patterns in arid vegetation (dark: vegetation, bright: bare soil). Left: vegetation patterns produced by the model of Rietkerk et al. (2002). Right: vegetation patterns in a satellite image (Sudan, 11°32' N, 27°57' E; ©2004 Google Earth. ©2004 DigitalGlobe). The dimensions of the depicted area are  $1 \times 1$  km.

Table 1.1: Critical transitions in ecological models that are well understood because they can be studied analytically (indicated by the check marks).

to from \	uniform equilibrium states	cyclic dynamics	patterned states
uniform equilibrium states	✓	✓	✓
cyclic dynamics			
patterned states			

understand how ecosystems respond to environmental change, one is required to assume that the system under consideration is spatially uniform and that it is in equilibrium. This limits research on critical transitions to transitions between uniform states or from uniform states to cyclic dynamics or patterned states (see Table 1.1). Furthermore, the equilibrium assumption may not be appropriate because of slow ecosystem dynamics, rapid environmental change or stochastic events. As a result, a number of key questions remain to be answered, as I will point out in this section.

### 1.3.1 Transitions from patterned to uniform states

When ecosystems are subject to environmental change, pattern formation can occur due to an interplay of local positive feedbacks and distal negative

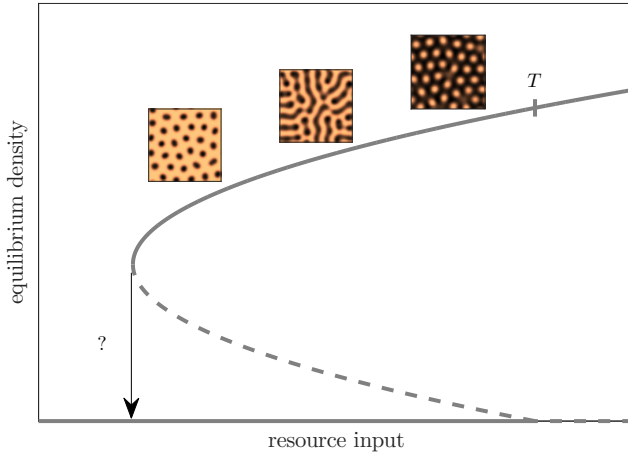


Figure 1.9: Turing instability (indicated with  $T$ ) is responsible for pattern formation, but what mechanisms are responsible for the transition to the uniform degraded state? (Rietkerk et al., 2004).

feedbacks, as discussed in the previous section. To study under which conditions such scale dependent feedbacks are strong enough to trigger pattern formation, ecologists have relied on Turing analysis (e.g. Klausmeier, 1999; HilleRisLambers et al., 2001; Kefi et al., 2008; Eppinga et al., 2009). Turing analysis consists of assessing the stability of uniform equilibrium states by applying spatially heterogeneous perturbations. If a uniform system state is unstable against such heterogeneous perturbations, then patterns can be expected to form.

Although Turing analysis gives an indication on when patterns form, it does not provide any information about the stability of the patterns that form. Hence, it cannot be used to study when and how patterned ecosystems transition to (degraded) uniform states. An open question therefore remains: *How do patterned ecosystems transition to uniform degraded states?*

In order to study how patterned ecosystems respond to change one would have to study the stability of patterned states of ecological models. Advanced analyses that enable studying the stability of patterned states have recently been applied to ecological models (Van der Stelt et al., 2013; Sherratt, 2013a). In Chapter 2 of this dissertation I will use these techniques to understand the response of patterned ecosystems to environmental change.

### 1.3.2 Frequency and magnitude of resource pulses

In some cases ecosystem dynamics are controlled by discrete events, such as rain storms, floods, fires and predation. In order to apply equilibrium analysis, such events are sometimes aggregated to capture their resulting effect in a single parameter or function. Rainfall, for example, is often treated as a constant parameter (Rietkerk et al., 1997; Klausmeier, 1999; Rietkerk et al., 2002), predation as a function of prey density (Holling, 1959) and disturbances are modelled as a constant loss term (Hastings, 1980; Nee and May, 1992; Tilman, 1994). While this approach benefits analysis, information is also lost regarding the frequency and magnitude of the events. This information may be particularly important when studying ecosystems that depend on resource pulses and that have a limited capacity to take up resources. In these ecosystems, infrequent, high magnitude pulses may lead to greater resource losses than frequent low magnitude pulses. However, in patterned ecosystems, and in activator-depleted substrate systems in particular, the loss of resource at one location may be beneficial elsewhere. Therefore, patterned ecosystems may function well if resource pulses are of high magnitude.

In Chapter 3 of this dissertation I will derive a function that aggregates resource pulses without losing information about their frequency and magnitude. This allows answering the following question using equilibrium analysis: *How do changes in the frequency and magnitude of resource pulses affect (patterned) ecosystems with limited resource uptake capacity?*

### 1.3.3 Processes at multiple timescales

The rates of processes within ecosystems often differ widely. These differences in timescales can be advantageous for model analysis as they allow studying fast and slow processes separately, providing more detailed insights into cyclic ecosystem dynamics for instance (e.g. as in Figure 1.5; Rinaldi and Scheffer, 2000). However, how processes should be divided into fast and slow processes is not always *a priori* clear. Within the same ecosystem, processes may operate on the time scale of seconds (e.g. infiltration of water, overland flow), months (e.g. growth of herbs), decades (e.g. tree growth) and centuries (e.g. soil formation), without being trivially dividable into two groups. One solution is to limit the number of state variables in ecological models by leaving out the extremes, thereby focussing on specific timescales only. However, very fast or very slow processes may be key in explaining ecosystem dynamics. Furthermore, very slow processes, that operate on

## 1 Introduction

ecosystem development timescales, may have effects that are too slow to observe in empirical studies, meaning that modelling studies are required to understand their role in ecosystem dynamics. This raises the following question: *How do interactions between processes at multiple timescales affect ecosystem dynamics?*

In Chapter 4 of this dissertation I will demonstrate that dividing processes into three groups, rather than two, still allows detailed analysis of ecological models, providing ways to understand both the emergence and stagnation of cyclic dynamics and explaining both rapid short-term shifts and long-term ecosystem development.

### 1.3.4 Rapid environmental change

Equilibrium analysis can only be applied to models without explicit time dependency (i.e. to autonomous models). As a result, environmental changes are generally assumed to be very slow when studying ecological models. However, the current anthropogenic environmental changes can often not be regarded as slow. Recent model studies outside ecology have suggested that rapid change in parameters can trigger critical transitions (Wieczorek et al., 2010; Luke and Cox, 2011; Ashwin et al., 2012; Perryman, 2015), even when slow changes of the same magnitude would not. These findings lead to the following questions that will be treated in Chapter 5: *Can rapid environmental change trigger critical transitions in ecological models? If so, what mechanisms are responsible and how can “rate sensitive” ecosystems be identified?*

## 1.4 Focus: water-limited ecosystems

Although the posed research questions apply to various ecosystems, they all apply to water-limited ecosystems.

Periodically patterned vegetation has been observed in (semi-)arid drylands (Macfadyen, 1950; Deblauwe et al., 2008, Figure 1.10a) and has been successfully reproduced by models (e.g. Klausmeier, 1999; Von Hardenberg et al., 2001; Rietkerk et al., 2002; Gilad et al., 2004). Advanced analysis of these models would help understanding how patterned arid ecosystems transition to uniform bare states (i.e. desertification; Problem 1.3.1).

Water-limited ecosystems rely on pulsed resource input in the form of rain events. In addition, these events are projected to become more intense and to become more intermittent due to climate change (Tebaldi et al., 2006;

Solomon et al., 2007). Affected regions include (semi-)arid regions such as the Sahel and the Horn of Africa (Figure 1.10b). Explicitly incorporating rain events in an ecological model may provide insights into how the projected changes in rainfall patterns affect the ecosystems in these regions (Problem 1.3.2).

Coastal dune ecosystems in temperate climates can also be water-limited for at least part of the year, because of high wind velocities and sandy soil textures. Dry sandy dune soils are also known to be water repellent (Dekker and Jungerius, 1990; Ritsema et al., 1993), a soil property caused by the very slow accumulation hydrophobic compounds originating from plant material (Mao et al., 2015). Soil water repellency potentially hampers infiltration into the rootzone, meaning that fast soil water dynamics, slower plant dynamics and very slow soil dynamics are linked in coastal dunes (Figure 1.10c). This provides ways to understand their dynamics in detail through separation of timescales (Problem 1.3.3).

Finally, arid regions are home to about one third of the human population and with a growth rate of over 18 % population density in arid regions increases more rapidly than in any other ecological zone (Safriel et al., 2005; UNEP, 2007, Figure 1.10d). This not only means that many people depend on the services provided by arid ecosystems, but also that rapid anthropogenic environmental changes are currently imposed on these ecosystems (Problem 1.3.4).

For the above reasons, the focus of the remaining chapters of this dissertation will be on water-limited ecosystems.

## 1 Introduction

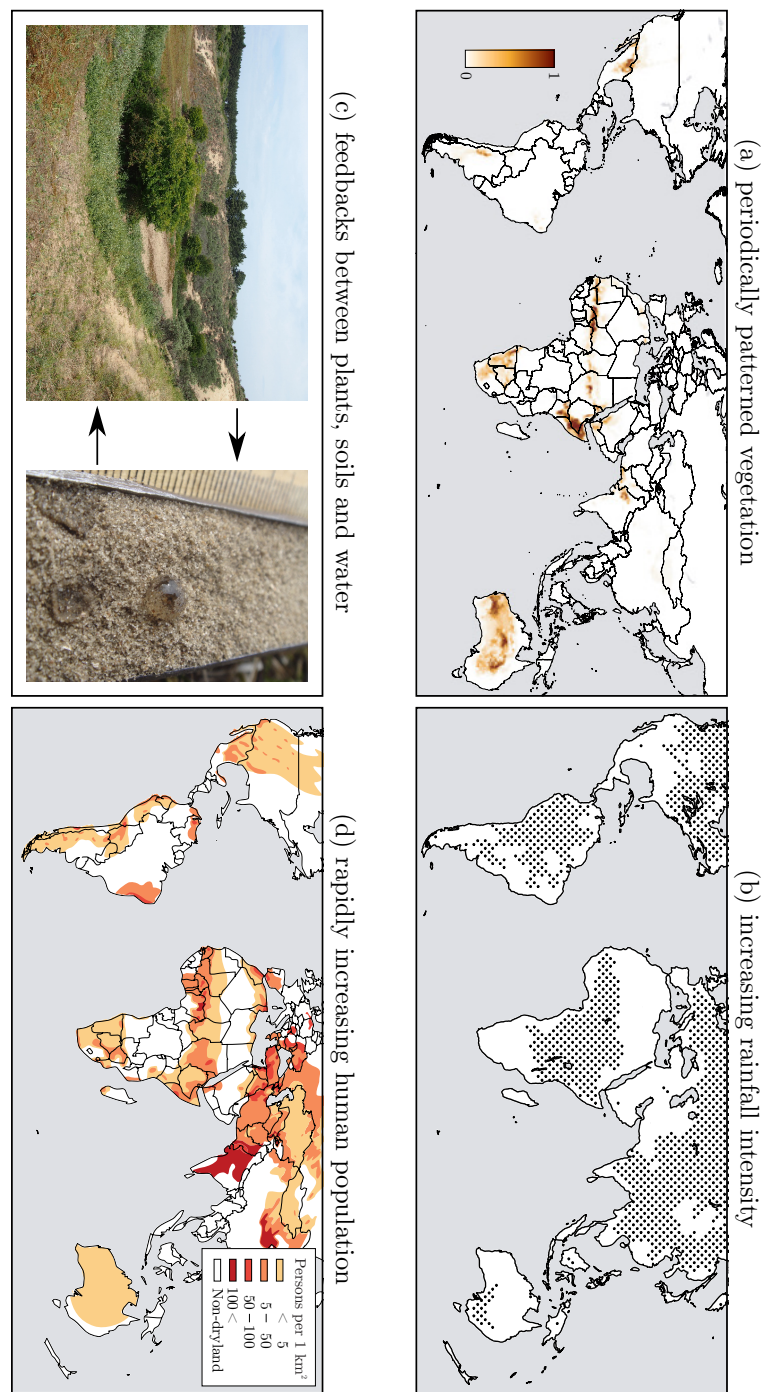


Figure 1.10: (a) Distribution of periodically patterned arid vegetation obtained with an empirical predictive model (Deblauwe et al., 2008). (b) Regions where a majority of the global climate models shows a statistically significant increase in precipitation intensity (period 2080-2099 relative to 1980-1999 for the A1B scenario Solomon et al., 2007). (c) Coastal dune vegetation (left) causes water repellency of sandy soils (right) which may feed back to dune vegetation by decreased infiltration (Photos by Jiefei Mao, 2012, 2014). (d) Population density in drylands is high and growing rapidly with over 18% per decade (UNEP, 2007).

## **2 Beyond Turing: the response of patterned ecosystems to environmental change.**

Siteur, K., Siero, E., Eppinga, M. B., Rademacher, J. D. M., Doelman, A. and Rietkerk, M. (2014), Beyond Turing: The response of patterned ecosystems to environmental change. *Ecological Complexity* 20:81-96.

### **Abstract**

Spatially periodic patterns can be observed in a variety of ecosystems. Model studies revealed that patterned ecosystems may respond in a nonlinear way to environmental change, meaning that gradual changes result in rapid degradation. We analyse this response through stability analysis of patterned states of an arid ecosystem model. This analysis goes one step further than the frequently applied Turing analysis, which only considers stability of uniform states. We found that patterned arid ecosystems systematically respond in two ways to changes in rainfall: 1) by changing vegetation patch biomass or 2) by adapting pattern wavelength. Minor adaptations of pattern wavelength are constrained to conditions of slow change within a high rainfall regime, and high levels of stochastic variation in biomass (noise). Major changes in pattern wavelength occur under conditions of either low rainfall, rapid change or low levels of noise. Such conditions facilitate strong interactions between vegetation patches, which can trigger a sudden loss of half the patches or a transition to a degraded bare state. These results highlight that ecosystem responses may critically depend on rates, rather than magnitudes, of environmental change. Our study shows how models can increase our understanding of these dynamics, provided that analyses go beyond the conventional Turing analysis.

## 2.1 Introduction

Spatially periodic patterning of sessile biota can be observed in a variety of ecosystems including arid ecosystems (Macfadyen, 1950), mussel beds (Van de Koppel et al., 2005), boreal peatlands (Malmström, 1923) and tropical peatlands (Baldwin and Hawker, 1915). Such spatially periodic patterns can typically not be explained by underlying heterogeneity in the environment, which suggests that they are self-organized. Self-organization into periodic patterns is the result of positive feedbacks that act locally (short range activation) in combination with distal negative feedbacks (long range inhibition; Gierer and Meinhardt, 1972). This combination of feedbacks is also referred to as scale-dependent feedbacks (Rietkerk and Van de Koppel, 2008). In arid ecosystems, the combination of locally reduced evaporation through shading and water uptake by laterally extended roots is known to induce such scale-dependent feedbacks (Gilad et al., 2004; Meron, 2012). Scale-dependent feedbacks can also result from the fact that in arid ecosystems plants tend to improve soil structure which allows more water to infiltrate during rain events (Rietkerk et al., 2000; Thompson et al., 2010a). This results in increased water availability and increased plant growth, meaning that locally a positive feedback loop is active. However, water availability farther away is negatively affected by this facilitative effect: surface water accumulates on bare soils during intense rain events and moves towards vegetated areas due to a gentle slope or due to infiltration differences on flat terrain (Klausmeier, 1999; Rietkerk et al., 2002). In arid ecosystems, local positive feedbacks are therefore linked to a flux of resource that results in long range inhibition and consequently in pattern formation. This type of scale-dependent feedback is referred to as the resource-concentration mechanism (Rietkerk et al., 2004). The positive feedbacks that are often involved in pattern formation (Rietkerk and Van de Koppel, 2008) are associated with nonlinear ecosystem response to environmental change (DeAngelis et al., 1980; Rietkerk et al., 2004). This means that gradual changes in environmental conditions may result in sudden significant losses in productivity and in degradation of patterned ecosystems.

Reaction-(advection-)diffusion models have been developed to understand the mechanisms responsible for pattern formation, to study the conditions under which scale-dependent feedbacks are strong enough for patterning to occur and to get more insight in the possible nonlinear behaviour of patterned ecosystems (e.g. Klausmeier, 1999; Von Hardenberg et al., 2001; Rietkerk et al., 2002; Gilad et al., 2004). In these models, patterns typically arise from a uniform system state that becomes unstable to heterogeneous

perturbations. This type of instability is referred to as Turing instability (after A.M. Turing, 1912-1954; Turing, 1953) and is thought to be involved in for example the formation of patterns on animal coats (Meinhardt, 1982), on sea shells (Meinhardt, 1995) and in chemical systems (Gray and Scott, 1984; Pearson, 1993). Using linear stability analysis, it is possible to find the parameter ranges for which a uniform system state is Turing unstable.

At present, Turing analysis is used as a relatively simple way to study the environmental conditions under which one would expect periodic patterns to be observed (e.g. Klausmeier, 1999; HilleRisLambers et al., 2001; Meron et al., 2004; Gilad et al., 2004; Kefi et al., 2008; Eppinga et al., 2009). However, since Turing analysis only considers the stability of uniform system states, it provides very little information about the behaviour of ecosystems that are in a patterned state. Therefore, previous studies have been exploring this behaviour using numerical approaches. These studies revealed a number of interesting properties of patterned ecosystems. Various model studies suggest that patterns can be expected under conditions where uniform system states are still stable and under conditions too harsh for uniform cover to be sustained (e.g. Von Hardenberg et al., 2001; Rietkerk et al., 2002). These findings imply that stable uniform and stable patterned states can coexist for a range of environmental conditions (Rietkerk et al., 2004). The coexistence of alternative stable ecosystem states can result in so-called critical transitions (Scheffer, 2009) if environmental conditions change, which are associated with sudden losses of productivity and ecosystem degradation (Scheffer et al., 2001). Numerical studies that looked in more detail to the dynamics of patterned ecosystem states suggest that multiple stable patterned states, with different wavelength or spatial configurations, can coexist and that this can result in hysteresis and more gradual ecosystem adaptation if environmental conditions change (Sherratt and Lord, 2007; Bel et al., 2012).

Although studies with numerical approaches uncovered some interesting characteristics of patterned ecosystems, recent studies have been exploring whether the use of analytically based methods provides more detailed insights (Van der Stelt et al., 2013; Sherratt, 2013a). These approaches go one step further than Turing analysis as they consider the stability of patterned rather than uniform ecosystem states. By combining stability analysis on patterned states with model runs Sherratt (2013a) demonstrated that hysteresis can be explained by the coexistence of multiple stable states. His study also suggests that the rate at which environmental conditions change may affect system response. This is of particular importance as current human activities induce anomalous rates of environmental change (e.g. Joos and Spahni,

2008). Although these results suggest that information about the stability of patterned states is essential in understanding ecosystem response to changing environmental conditions, the application of stability analysis on patterned states in the field of ecology has been limited so far and various ecologically relevant questions remain to be answered (Van der Stelt, 2012, p.95-100).

One of the processes that are not well understood is the process of pattern wavelength adaptation. Patterned ecosystems can respond to environmental change by adapting pattern wavelength and the study by Sherratt (2013a) showed that this process is affected by the rate of environmental change. It is, however, unknown why and how patterned ecosystems adapt and why this depends on the rate of change. In this study we therefore aim to provide a mechanistic understanding of how patterned ecosystems respond to environmental change, considering both the magnitude of change as well as the rate of change. By applying stability analysis on patterned system states, we first show that the use of Turing analysis can yield false negatives and false positives with regard to predicting the existence of observable (i.e. stable) patterns. Based on the mechanisms that are involved in pattern destabilization, we then discuss possible types of pattern adaptation. Using model runs, we demonstrate that knowledge about the stability of patterned states is crucial in understanding the response of ecosystems subject to environmental change and show how the rate of change in environmental conditions and the level of imposed spatio-temporal noise affect system response. Finally, we propose that competition for resources between patches of vegetation provides a possible ecological explanation for the obtained results. In this study we use an extended version of an arid ecosystem model by Klausmeier (1999) as introduced by Van der Stelt et al. (2013), which we will discuss in the next section.

## 2.2 Model description and analyses

### 2.2.1 Model description

The extended version of the Klausmeier model is a reaction-advection-diffusion model in which the formation of spatial vegetation patterns is the result of competition for surface water. The model has two state variables that are functions of both time  $t$  and space  $x$  ( $x \in \mathbb{R}$ ): plant biomass  $n$  and surface water  $w$ . Notice that we will consider only one spatial dimension ( $x$ ), following Van der Stelt et al. (2013) and Sherratt (2013a). The model is given by Equation 2.1 and 2.2. We use a non-dimensional version the model

in order to reduce the number of parameters. For a dimensional version of the model and the physical meaning of the parameters, see Appendix 2.A.

$$\frac{\partial w}{\partial t} = a - w - wn^2 + v \frac{\partial w}{\partial x} + e \frac{\partial^2 w^\gamma}{\partial x^2} \quad (2.1)$$

$$\frac{\partial n}{\partial t} = wn^2 - mn + \frac{\partial^2 n}{\partial x^2} \quad (2.2)$$

The change in surface water  $w$  (Equation 2.1) is controlled by rainfall  $a$ , surface water losses (second term) and uptake by plants through infiltration and transpiration (third term). As in the original model by Klausmeier (1999), the movement of surface water due to gradients in the terrain is captured with an advection term (fourth term). We extended the model by adding diffusion of surface water (fifth term). We did this for three reasons. First, the diffusion term has a physical basis as it can be derived from the shallow water equations (Gilad et al., 2004). Second, it allows us to capture the movement of surface water induced by spatial differences in infiltration rate (Rietkerk et al., 2002). Third, it enables us to demonstrate that the type stability analysis we use to study the system's response to change can be applied to both reaction-advection-diffusion and reaction-diffusion model ( $v \neq 0$  and  $v = 0$  respectively).

The dynamics in plant biomass  $n$  (Equation 2.2) are determined by plant growth which is linearly related to water uptake (first term) and by plant mortality (second term). As in the original model, plant dispersion is modelled with a diffusion term (third term).

The non-dimensional version of the model has five parameters. We chose parameter values that are valid for grass as reported by Klausmeier (1999). Plant mortality was set to  $m = 0.45$  and for flat and sloped terrain  $v = 0$  and  $v = 182.5$  respectively. As we are interested in the response of the system to changes in rainfall, we use rainfall  $a$  as bifurcation parameter and let it vary between  $a = 0$  to  $a = 3.5$ . For simplicity we chose  $\gamma = 1$ . Van der Stelt et al. (2013) showed that the value of  $\gamma$  does not qualitatively affect the structure of stability regions. Therefore the results presented in the following sections are not expected to differ qualitatively for other values of  $\gamma$ . Finally,  $e$  was calibrated to obtain patterns in a realistic rainfall range according to studies listed by Deblauwe et al. (2008), which appeared to be for  $e = 500$ . For conversion of these dimensionless parameters to dimensional parameters, see Appendix 2.A.

The extended Klausmeier model falls in the broader class of reaction(-

advection)-diffusion models referred to as activator-depleted substrate systems (Edelstein-Keshet, 1988) with vegetation being the activator and surface water being the substrate. In addition, it shows strong similarities with other well studied models, depending on parameter choice. Naturally, if  $e = 0$  we return to the original (one dimensional) Klausmeier model (Klausmeier, 1999). With  $v = 0$  and  $\gamma = 1$  the model is equal to the model studied by Kealy and Wollkind (2012) and the well studied chemical model by Gray and Scott (1984). Finally, the model has been studied by Van der Stelt et al. (2013) for constant rainfall  $a$ .

It should be mentioned that apart from the model by Klausmeier (1999) and derivations thereof (Van der Stelt et al., 2013; Kealy and Wollkind, 2012) a large body of model studies have been published that dedicate pattern formation in arid ecosystems to a variety of mechanisms, including competition for surface water (Dunkerley, 1997; HilleRisLambers et al., 2001; Rietkerk et al., 2002), competition through soil water uptake by roots (Von Hardenberg et al., 2001; Meron et al., 2004), a combination of these mechanisms (Gilad et al., 2004) or plant-plant interactions only (Lefever and Lejeune, 1997; Lejeune and Tlidi, 1999; Lejeune et al., 1999, 2002). These models may be suitable depending on system characteristics such as climate, soil and plant properties and can be used to answer specific research questions. However, here we limit our study to the analysis of the more generic extended Klausmeier model as it captures pattern formation in a relatively parsimonious way.

### 2.2.2 Analyses

In order to study the response of the system to changes in rainfall  $a$ , knowledge is required about the rainfall ranges for which stable spatially uniform and patterned states of Equations 2.1 and 2.2 exist. We derived the existence of system states and assessed their stability by performing linear stability analysis. This type of analysis, together with the obtained stability regions in parameter space, will be discussed in detail in the next section. The boundaries of the stability regions were obtained by tracking the marginally stable patterned system states (Doelman et al., 2012; Sherratt, 2013b) using AUTO continuation software (AUTO-07p; Doedel, 1981).

As the rainfall  $a$  changes stable states may lose their stability. The stability regions, as obtained using stability analysis, provide insight in when a system state destabilizes. However, the behaviour of the system after destabilization (e.g. re-stabilization) is a priori unknown. To study this, we performed runs of

the model with linearly increasing and decreasing rainfall  $a$ . The model runs were performed in MATLAB (version 2012a - 7.14.0.739; The MathWorks, Inc.) using a vector of 1024 elements that represent a domain with a size of 1000 (500 meters). Periodic boundary conditions were used to diminish boundary effects and to mimic an infinite domain. We studied the response of the system under different rates of change in  $a$  ( $\frac{da}{dt} = -10^{-7}$ ,  $-10^{-4}$  and  $-10^{-2}$ ). We added spatially and temporally uncorrelated multiplicative uniformly distributed noise to both components of the model every  $\frac{1}{4}$  year (noise amplitude = 0,  $5 \cdot 10^{-5}\%$  and  $0.05\%$ ). The noise was added to diminish numerical artefacts, such as the system residing in unstable system states, and represents potential sources of noise that are not captured by the deterministic equations.

The state of the system can be expressed in terms of pattern wavenumber  $\kappa$  ( $= \frac{2\pi}{\text{wavelength}}$ ). To enable comparison between the model runs and the stability regions, we assessed the wavenumber of the patterns as generated by the model by applying discrete Fourier transformations. This is explained in detail in Appendix 2.B.

## 2.3 Stability of uniform and patterned states: from Turing instability to the Busse balloon

In this section we discuss the stability of uniform and patterned states of the extended Klausmeier model. In Section 2.3.1 we briefly review well-known linear stability analysis (Turing analysis) as applied to uniform system states. We then continue by discussing the mathematically more challenging stability analysis of patterned states in Section 2.3.2. Finally we compare the stability regions obtained in both subsections and discuss the ecologically relevant results in Section 2.3.3.

### 2.3.1 Existence and stability of uniform system states

Determining the stability of uniform steady states to uniform perturbations is a fairly easy task: first one derives the steady states of the system, and then one perturbs the steady states. The stability of the system state is then defined by the sign of the exponential growth rate of the perturbation: the maximum real part of eigenvalues  $\lambda$ . Solely negative real parts of eigenvalues imply a (asymptotically) stable state, whereas a positive real part means that the system state is unstable. A bifurcation occurs when due to a parameter

change the growth rate of a perturbation  $\max(\Re(\lambda))$  becomes positive (here  $\max()$  refers to the maximum of a set values and  $\Re()$  takes the real part of a complex number). The system is marginally stable at such an onset of instability. Marginal stability marks the boundaries of stability regions in parameter space.

Uniform system states can be derived by setting Equations 2.1 and 2.2 to zero while neglecting advection and diffusion fluxes. The extended Klausmeier model presented in the previous section has three uniform steady states for  $a > 2m$  (see Appendix 2.D.1 for a derivation). Two of the steady states are vegetated (so  $\bar{n} > 0$ ), of which one is stable to uniform perturbations for ecologically relevant parameter values ( $m < 2$ ) and one is unstable (see Appendix 2.D.2 for stability analysis). A stable bare desert state ( $\bar{n} = 0$ ) exists for all values of  $a$ . At  $a = a_{SN} := 2m$  a saddle-node bifurcation occurs. Here the vegetated states cease to exist, meaning that for  $a < a_{SN}$  only a stable bare state exists.

Perturbations in natural systems are generally heterogeneous. To account for this in the stability analysis, spatially heterogeneous perturbations can be added to the uniform states (Turing, 1953; Edelstein-Keshet, 1988). Heterogeneous perturbations can be represented as sinusoids with wavenumber  $\kappa$  ( $= \frac{2\pi}{\text{wavelength}}$ ) of which the amplitude grows (or decays) with a rate of  $\max(\Re(\lambda(\kappa)))$ .

When perturbing the stable uniformly vegetated state of the extended Klausmeier model with such sinusoids (Appendix 2.D.3), a range of values for  $a$  can be found for which the state is Turing unstable. Here the amplitude of a perturbing sinusoid grows over time ( $\max(\Re(\lambda(\kappa, a))) > 0$ ). Whether this occurs does not only depend on intrinsic model parameters, such as  $a$ , but also on the wavenumber of the sinusoid  $\kappa$ . The solid red line in Figure 2.1a,b borders the region in  $(a, \kappa)$ -space for which the uniformly vegetated state is Turing unstable. Assuming that the amplitude of the imposed perturbations grow while their wavenumber is preserved, one would expect patterns to exist in this region. Therefore this can be seen as a *Turing prediction region*. If rainfall decreases over time, patterns will form directly after the Turing bifurcation  $T$  (or Turing-Hopf bifurcation  $TH$  if  $v \neq 0$ ; Van der Stelt et al., 2013) as here the uniform state becomes unstable. These patterns will have a wavenumber close to  $\kappa_T$  (or  $\kappa_{TH}$ ): the wavenumber of the perturbation that initializes the Turing bifurcation. Model runs show that when randomly perturbing uniform states that are Turing unstable, the system tends to evolve to a state with a pattern wavenumber close to the wavenumber of the perturbation with the largest growth rate, also referred to as most unstable

mode (dashed red line in Figure 2.1a,b; Sherratt and Lord, 2007). As we will show in Section 2.4 however, pattern wavenumber can strongly deviate from the this wavenumber if environmental conditions change.

### 2.3.2 Existence and stability of patterned system states

So far we have discussed the stability of uniform system states. The patterned states that arise from a Turing unstable uniform state are, however, not necessarily stable themselves. Unlike uniform steady states, it is generally not possible to find explicit expressions for patterned states by hand. For this and subsequent determination of stability we rely on numerics.

Patterns may exist in the form of so-called *wavetrains*: vegetation bands that slowly migrate in uphill direction. In fact for  $v = 182.5$  this is the case for all patterns. To deal with this a comoving frame  $\xi = x - st$  is introduced. Here  $s$  is equal to the migration speed: a pattern dependent property that is assumed to be constant in space and time. This results in additional advection terms in both equations. A pattern  $(w_p, n_p)$  with wavenumber  $\kappa$  exists for rainfall  $a$  if and only if it is a solution to the system

$$0 = a - w_p - w_p n_p^2 + (v + s) \frac{dw_p}{d\xi} + e \frac{d^2 w_p^\gamma}{d\xi^2} \quad (2.3)$$

$$0 = w_p n_p^2 - m n_p + s \frac{dn_p}{d\xi} + \frac{d^2 n_p}{d\xi^2} \quad (2.4)$$

on the domain  $[0, \frac{2\pi}{\kappa}]$  with periodic boundary conditions. See Appendix 2.E.1 for a derivation of these equations. Notice that, besides the parameters of the extended Klausmeier model (Equations 2.1 and 2.2), migration speed  $s$  and wavenumber  $\kappa$  now appear as additional parameters. Parameters  $s$  and  $\kappa$  can be used to express the state of the system.

Since the existence of unstable patterned states is not of immediate interest we also require stability. To determine this we need to linearise about  $(w_p, n_p)$  leading to ordinary differential equations with a dependency on  $w_p$  and  $n_p$  (Appendix 2.E.2). The perturbations are no longer represented by sinusoidals. Instead they are given by products of two functions: a sinusoidal  $e^{i\nu}$  (with wavenumber  $\nu$ ) and an a priori unknown periodic function with the same wavenumber  $\kappa$  as the pattern. The eigenvalues of the corresponding perturbations are complex and depend on  $\nu$ .

Stable patterns exist in what is referred to as the *Busse balloon* (after F.H. Busse; Busse, 1978): the region in (parameter,  $\kappa$ )-space for which at least one

stable periodic solution exists (Van der Stelt et al., 2013). If a patterned state is stable, it is said to be in the Busse balloon. Busse balloons for the extended Klausmeier model are depicted in Figure 2.1a,b (bordered by the black solid line). Apart from the patterned states, a stable uniform bare state ( $\kappa = 0$ ) exists for all rainfall values.

Stability regions are bordered by marginally stable solutions. Therefore a Busse balloon can be constructed by finding marginally stable solutions. If one marginally stable solution is known it is possible to track marginal stability while changing a parameter (with the use of continuation software AUTO; Doedel, 1981). A precise description of this procedure can be found in the article by Rademacher et al. (2007). The Busse balloon is obtained by plotting the wavenumbers  $\kappa$  of the marginally stable solutions against the changing parameter. In order to track marginal stability we also need to know exactly how the eigenvalues obtain a positive real part: what is the destabilization mechanism?

In Van der Stelt et al. (2013) it is rigorously proven through the derivation of amplitude equations (Ginzburg-Landau analysis) that stable patterns exist close to the Turing(-Hopf) bifurcation: it is derived that the bifurcation is supercritical (for the scalings considered). Close to the Turing(-Hopf) bifurcation the region in  $(a, \kappa)$ -space where stable patterns exist is bounded by a parabola of marginally stable patterns (Van der Stelt et al., 2013). Also, the destabilization mechanism is identified as being a *sideband instability* or *Eckhaus instability*.

The sideband instability is characterized by a change in sign of the curvature of the eigenvalues attached to the origin ( $\nu = 0$ ), as depicted in Figure 2.1c. For marginally stable patterns, which separate stable from unstable patterns, there is no curvature at  $\nu = 0$ . This corresponds to a second derivative at  $\nu = 0$  that equals zero. If, due to changing rainfall, patterns lose their stability, perturbations with  $\nu$  close (but unequal) to zero become able to destabilize patterned states.

With the current parameter combination the sideband is the dominant destabilization mechanism for the extended Klausmeier model (Van der Stelt et al., 2013). Only for very small wavenumbers  $\kappa$  it is superseded by intertwining Hopf instabilities (Doelman et al., 2012). In this case, onset of instability occurs away from  $\nu = 0$ , but continuation with AUTO is still possible (Rademacher et al., 2007; Doelman et al., 2012).

The perturbations, which consist of products of  $e^{i\nu}$  and functions with the same wavenumber as the pattern  $\kappa$ , need not be periodic, but can be for particular values of  $\nu$ . For example, perturbations with  $\nu = 0$  are

periodic with pattern wavenumber  $\kappa$ , since  $e^0 = 1$ . As shown in Figure 2.1c, perturbations with wavenumber  $\kappa$  ( $\nu = 0$ ) are not able to destabilize a patterned state: due to translation symmetry the growth rates of these perturbations remain zero. Perturbations with  $\nu = \pi$  are periodic with wavenumber  $\kappa/2$  since  $e^{\pi i} = -1$ . If perturbations with wavenumber  $\kappa/2$  ( $\nu = \pi$ ) become able to destabilize a patterned state, a so-called spatial *period doubling bifurcation* occurs. Growth of these perturbations results in a halving of the pattern wavenumber. Recall that the wavelength is inversely proportional to the wavenumber, so the wavelength (spatial period) doubles. According to Figure 2.1c, perturbations of this kind are the last to destabilize a patterned state as rainfall  $a$  decreases, however they do attain the largest growth rate soon after. The black dashed line in Figure 2.1a,b depicts the period doubling instability.

In summary, we discussed that the stability of patterned states can be assessed by tracking marginal stability. To do this, knowledge about the destabilization mechanisms is required. For the extended Klausmeier model the sideband instability is the dominant destabilization mechanism, meaning the curvature (second derivative) of the curve of eigenvalues (Figure 2.1c) can be used to trace the boundary of the stable pattern region.

### 2.3.3 Ecological implications

We determined the stability of patterned ecosystem states and discussed some important destabilization mechanisms, but what ecologically relevant information can we extract from Figure 2.1?

First, we observe that the Turing prediction region and the Busse balloon only partly overlap. A large part of the patterns in the Turing prediction region turn out to be unstable, and are therefore unlikely to be observed. Furthermore, stable patterns exist outside the Turing prediction region for  $a < a_{SN}$  and if  $v \neq 0$ , also for  $a > a_{SN}$ . These patterns cannot form directly from a Turing unstable uniform state. Although stable patterns do not appear at rainfall values above the Turing(-Hopf) bifurcation for the extended Klausmeier model, this may be different for other models (e.g. Rietkerk et al., 2002). The differences between the Turing prediction region and the Busse balloon suggest that a relatively simple Turing analysis gives very limited information about the parameter regimes for which one can expect patterns to be observed.

Second, Figure 2.1 shows that for a given rainfall value a range of stable patterned states exists. Since the system has many stable states, it can

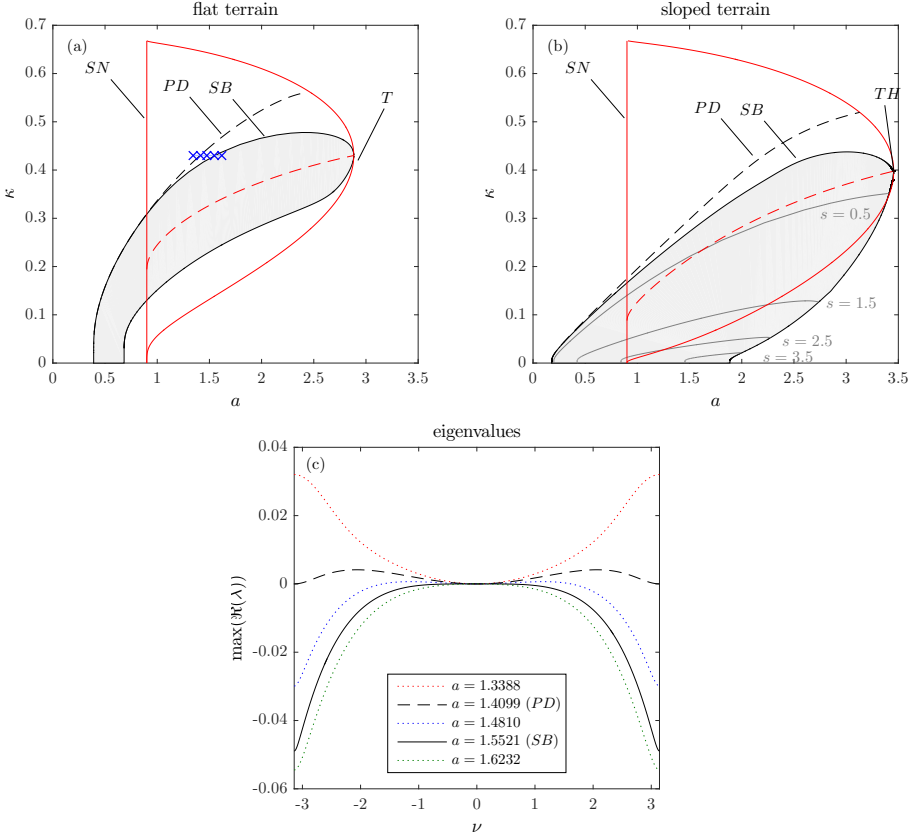


Figure 2.1: Stability regions of the non-dimensional extended Klausmeier model (Equations 2.1 and 2.2) in  $(a, \kappa)$ -space for flat ( $a; v = 0$ ) and sloped terrain ( $b; v = 182.5$ ). In (a) and (b)  $a$  represents rainfall and  $\kappa$  is the wavenumber of the patterned state. The black solid curve indicates the location of the sideband instability and borders the stable pattern region or Busse balloon (shaded area). A period doubling bifurcation occurs on the black dashed line. The grey curves in (b) show the contours of constant uphill pattern migration speed  $s$ . The red solid line borders the Turing prediction region where perturbations of the uniformly vegetated state grow in amplitude. On the right hand border of the Turing prediction region uniform states are marginally stable to spatial perturbations. On the left hand border of this region the Turing unstable uniform state ceases to exist (saddle-node bifurcation  $SN$ ;  $a = a_{SN} := 2m$ ). The wavenumber of the perturbation with the largest growth rate is indicated by the red dashed line. The highest rainfall value at which the uniformly vegetated state is Turing unstable is marked as the Turing bifurcation point  $T$  (or Turing-Hopf bifurcation point  $TH$  if  $v \neq 0$ ). (c) The maximum real part of eigenvalues for perturbations of patterned states plotted against Floquet wavenumber  $\nu$ . The perturbed patterned states have a wavenumber of  $\kappa = 0.43009 (\approx \kappa_T)$ . Notice that the perturbed states are marked with crosses in (a). At  $a \approx 1.5521$  a sideband bifurcation ( $SB$ ) occurs. Here the curvature at  $\nu = 0$  changes sign. At  $a \approx 1.4099$  a period doubling bifurcation ( $PD$ ) occurs. Here  $\max(\Re(\lambda(\nu)))$  at  $\nu = \pi \approx 3.14$  becomes positive.

be considered *multistable*. The current state, in terms of wavenumber  $\kappa$ , consequently depends on history, meaning that hysteresis can be expected.

Third, a pattern with a given wavenumber  $\kappa$  is stable for a range of  $a$ . This means that the same pattern wavenumber can in theory be observed for a range of external conditions. Furthermore, if external conditions change, one would expect the wavenumber of a pattern to remain constant as long as it is stable, i.e. as long as the external conditions remain within the range for which the pattern is stable.

Fourth, the shape of the Busse balloon allows high wavenumbers to be stable only at high values of  $a$ . The opposite is true for low wavenumbers. The presence of a slope affects the shape of the Busse balloon. Pattern formation occurs at higher rainfall rates and patterned states can sustain under more arid conditions on sloped terrains. The absence of a slope allows high wavenumber patterns to be stable, while the rainfall range for which stable low wavenumber patterns exist is narrow. On sloped terrains in contrast low wavenumber patterns can be expected to be observed for a wide rainfall range.

Finally, we observe that the period doubling instability approaches the boundary of the Busse balloon as rainfall  $a$  decreases. Meaning that at low rainfall values, period doubling takes place almost simultaneously with the destabilization of a pattern. In addition, the boundary of the Busse balloon is steeper at low rainfall values. This means that at low rainfall values an incremental decline in rainfall could result in desertification if the system is close to the boundary of the Busse balloon.

## 2.4 System response to changing environmental conditions

The obtained information about the stability and destabilization of patterned states is not enough to fully understand the behaviour of patterned ecosystems when subject to changing environmental conditions. This is because the linearisation we implicitly apply only enables us to describe the behaviour of the system close to the steady state. Consequently, if the system is pushed away from a steady state (during pattern destabilization) it is a priori unknown to which state it will evolve (restabilisation). In this section we study the behaviour of the system while gradually changing the rainfall parameter and relate this behaviour to the findings presented in the previous section. First we describe history dependence within the system resulting

from multistability in Section 2.4.1. In Section 2.4.2 we then study in more detail the restabilisation of the system and its dependence on the rate with which rainfall changes and on the level of noise imposed on the system. Finally, in Section 2.4.3 we propose an ecological mechanism that controls system restabilisation.

### 2.4.1 Bouncing through the Busse balloon

The non-dimensional extended Klausmeier model (Equations 2.1 and 2.2) was run with the rainfall  $a$  changing over time with a rate of  $\frac{da}{dt} = \pm 10^{-4}$ . This rate of change corresponds to a change in annual rainfall of about  $0.1 \text{ mm year}^{-1}$ .

Figure 2.2 shows how the system responds to changing rainfall on flat terrain ( $v = 0$ ). When rainfall decreases, patterns in plant biomass emerge shortly after the uniformly vegetated state becomes Turing unstable (Figure 2.2a). The mean plant biomass of the patterned state does not differ much from that of the Turing unstable uniform system state (Figure 2.2d). The wavenumber of the pattern does not change as long as the pattern is stable. The pattern amplitude in contrast increases during pattern formation after which it slowly decreases with declining  $a$ . At some point, the decreasing rainfall forces the system outside the Busse balloon and the pattern destabilizes (Figure 2.2c). This results in a pattern with a lower wavenumber and a larger amplitude. These transitions are not distinguishable in mean biomass (Figure 2.2d). The adaptation of the wavenumber is accompanied by the extinction of what can be considered as vegetation patches. When  $a$  reaches a value for which no stable patterned state exists, desertification occurs and all remaining patches go extinct simultaneously.

If rainfall increases over time similar behaviour can be observed (Figure 2.2b), however now patterns destabilize at the lower border of the Busse balloon and the wavenumber increases until eventually a uniformly vegetated state is reached (Figure 2.2c). During wavenumber adaptation vegetation patches split up. Since the trajectories for decreasing and increasing rainfall differ, hysteresis occurs (Sherratt, 2013a).

On sloped terrain (Figure 2.3), patterns emerge in the form of vegetation bands that migrate in uphill direction (travelling waves). As the Busse balloon is wider in terms of wavenumber  $\kappa$  the hysteresis effect is more pronounced when compared to flat terrain. As shown by Figure 2.3, the migration speed of the vegetation bands gets lower as rainfall decreases. However, during wavenumber adaptation vegetation bands accelerate leading

to slightly elevated migration speeds directly after transition.

Although wavenumber adaptation occurs some time after patterned states destabilize, as discussed earlier by Sherratt (2013a), Figures 2.2 and 2.3 indicate that the Busse balloon helps in understanding how patterned ecosystems respond to changes: 1) as long as the system is in the Busse balloon it responds by changing the amplitude (and migration speed) of the patterns, 2) if, due to changing rainfall  $a$ , the system is forced outside the Busse balloon it responds by changing its pattern wavenumber.

At first sight, the Busse balloon does not seem to provide insight in what determines the selection of a new wavenumber after pattern destabilization. In the next section we show how wavenumber selection is affected by the rate at which the rainfall changes and by the amount of spatio-temporal noise to which the system is exposed.

#### 2.4.2 Wavenumber selection: the role of rate of change and noise

The model was run for  $v = 0$  with different rates of change in rainfall  $|\frac{da}{dt}|$  (with  $\frac{da}{dt} < 0$ ) and different noise levels. As shown in Figure 2.4, wavenumber adaptation occurs with increasing step size (in terms of wavenumber  $\kappa$ ) for increasing rates of change. At high rates of change, desertification can take place at rainfall levels for which stable patterned states still exist. For the level of noise imposed on the system, the opposite is true: higher noise levels result in smaller step size. At sufficiently high noise levels, patches go extinct one-by-one and the system tends to closely follow the boundary of the Busse balloon.

We observe that during some wavenumber adaptations period doubling occurs, meaning that half of the vegetation patches go extinct simultaneously (Yizhaq et al., 2005). The occurrence of period doubling is related to the position of the system in  $(a, \kappa)$ -space at which the wavenumber adaptation is initiated, which is in turn determined by rate of change and noise level. If wavenumber adaptation takes place close to the boundary of the Busse balloon, which is the case for low rates of change or high noise levels, period doubling does not occur. If wavenumber adaptation is initiated farther away from the boundary of the Busse balloon, period doubling occurs, provided that the system surpassed the period doubling instability  $PD$  and that period doubling results in a stable patterned solution.

At low rainfall values we find that period doubling occurs more frequently (even at high noise levels). Here the period doubling instability  $PD$  approaches the sideband instability  $SB$  (boundary of the Busse balloon). As a

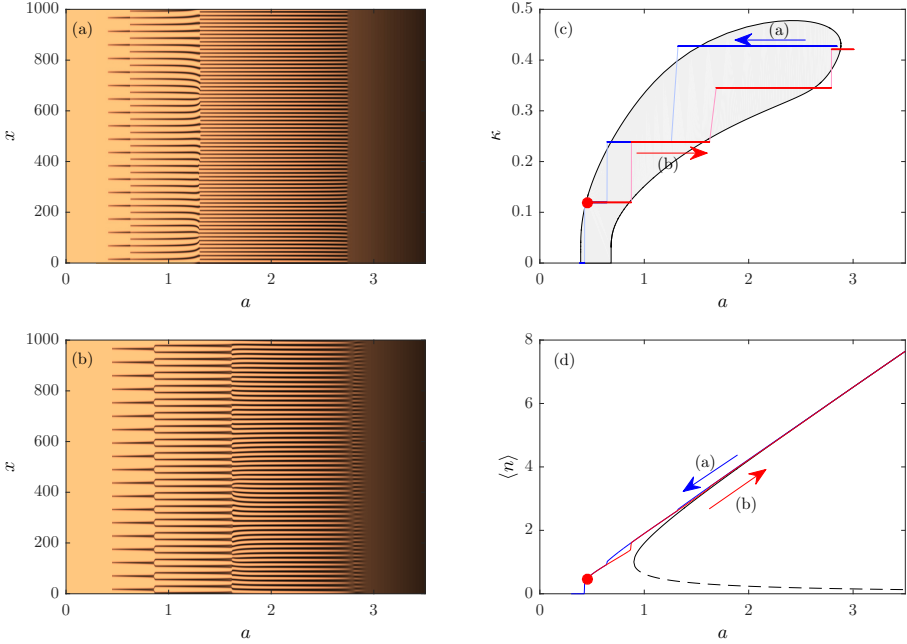


Figure 2.2: Plant density  $n$  in space for runs of the non-dimensional extended Klausmeier model with  $v = 0$  (flat terrain), for  $\frac{da}{dt} = -10^{-4}$  (a) and  $\frac{da}{dt} = 10^{-4}$  (b). The former run starts from the homogeneously vegetated steady state. The latter is initiated with the patterned solution of the first at  $a = 0.45$ . Spatially and temporally uncorrelated multiplicative uniformly distributed noise with an amplitude of  $5 \cdot 10^{-5}\%$  is added to the plant density every  $\frac{1}{4}$  year. The trajectories through the Busse balloon in (c) were obtained by applying a discrete Fourier transformation with respect to  $x$  (see Appendix 2.B). In (d), the mean biomass is plotted for both runs. The solid and dashed black lines are the uniform steady states.

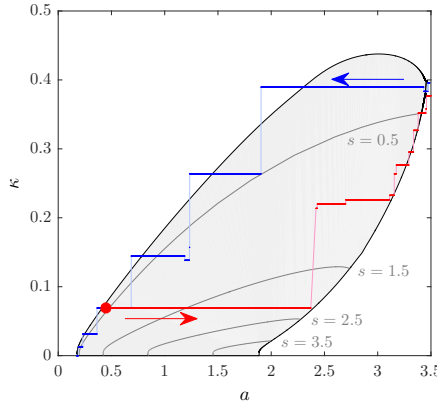


Figure 2.3: See the caption of Figure 2.2, but now  $v = 182.5$  (sloped terrain). The grey curves show the contours of constant uphill pattern migration speed.

result the period doubling instability  $PD$  is surpassed even at low rates of change.

### 2.4.3 Competition between and rearrangement of patches

In the previous subsections we showed that wavenumber adaptation driven by changing environmental conditions can be a discontinuous process: many patches can go extinct simultaneously if a pattern destabilizes. In addition, we found that rainfall, the rate of change in rainfall and the level of noise on the system affect the number of patches that go extinct. Here we provide an interpretation of the observed system responses by taking a closer look to what happens during wavenumber adaptation.

Figure 2.5 shows plant biomass and surface water for part of the modeled domain during one of the wavenumber adaptations in a model run with declining rainfall. The figure shows that the extinction of one vegetation patch results in growth of its neighbouring patches, which in turn negatively affects their neighbours. This triggers a cascade, eventually resulting in extinction of half of the patches.

The interaction between neighbouring patches in the extended Klausmeier model can be explained by the competition for water. Vegetation patches harvest water from an area bordered by water divides where  $\frac{dw}{dx} = 0$ . The uptake of water by patches that share a water divide, which is controlled by patch biomass, determines the position of the water divide. An increase

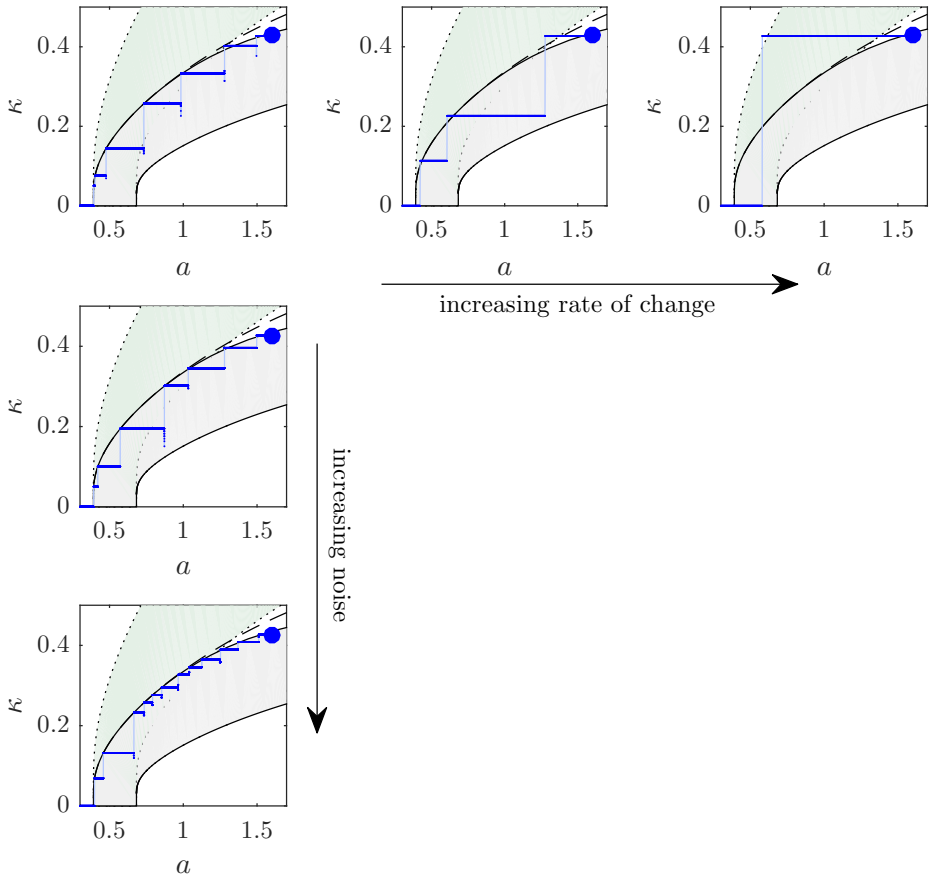


Figure 2.4: Trajectories through the Busse balloon for runs with decreasing rainfall and with different rates of change in  $a$  and different noise levels. The trajectories were obtained by applying a discrete Fourier transformation with respect to  $x$  (see Appendix 2.B). The runs were initiated with a stable pattern solution at  $\kappa \approx \kappa_T$  and  $a = 1.6$  and end in the desert state  $\kappa = 0$ . The solid line depicts the sideband instability  $SB$ , the dashed line is the period doubling instability  $PD$ . The green area bordered by the dotted curves was extrapolated from the Busse balloon and depicts the area in which period doubling would result in a stable patterned solution. No noise was added to the three runs in the upper panels. In these panels the rate of change in rainfall  $|da/dt|$  increases from left to right from  $10^{-7}$  to  $10^{-4}$  to  $10^{-2}$ . The runs depicted in panels on the left have the same rate of change in  $a$ , but an increasing noise amplitude ( $0, 5 \cdot 10^{-5}\%$  and  $0.05\%$ ).

in patch biomass with respect to neighbouring patches will widen the water harvesting area of a patch. The opposite occurs if a patch is weaker than its neighbours. Since the water harvesting area affects water availability, it feeds back to patch biomass eventually resulting in growth or extinction of a patch.

We observe (Figure 2.6) that wavenumber adaptations during which less than half of the vegetation patches goes extinct are accompanied by rapid spatial rearrangement of patches, while no movement of patches can be observed if half (period doubling) or all patches go extinct (desertification). The movement of neighbouring patches during rearrangement seems to weaken the feedbacks described above: if one patch goes extinct its neighbouring patches fill up the created space, thereby diminishing the stress on remaining patches.

Patch rearrangement generally occurs if wavenumber adaptation is initiated between the sideband instability and the period doubling instability. At low rainfall values, the period doubling instability approaches the sideband instability. At these rainfall values rearrangement of patches becomes less likely, as pattern destabilization almost coincides with the period doubling instability  $PD$ . High rates of change in rainfall also do not allow for patch rearrangement. High noise levels in contrast can trigger wavenumber adaptation before the system crosses the period doubling instability  $PD$ , resulting in patch rearrangement and one-by-one extinction of vegetation patches.

## 2.5 Discussion and conclusions

In this study we showed that patterned ecosystems systematically respond in two ways to changing environmental conditions: 1) by adjusting patch biomass (pattern amplitude) or 2) by changing pattern wavelength (wavenumber). In the latter case patches go extinct or split up and may rearrange. In arid ecosystems, gradual wavelength adaptation is constrained to conditions of high rainfall, slow changes in rainfall and high levels of stochastic spatial variation in biomass (noise). The adaptation process is less gradual under conditions of either low rainfall, rapid change or low levels of noise. Such conditions do not allow vegetation patches to rearrange, and facilitate the simultaneous extinction of half the patches or even a transition to a degraded state without any patches.

We found that an overview of stable patterned states, the Busse balloon, is a powerful tool in understanding the response of patterned ecosystems to

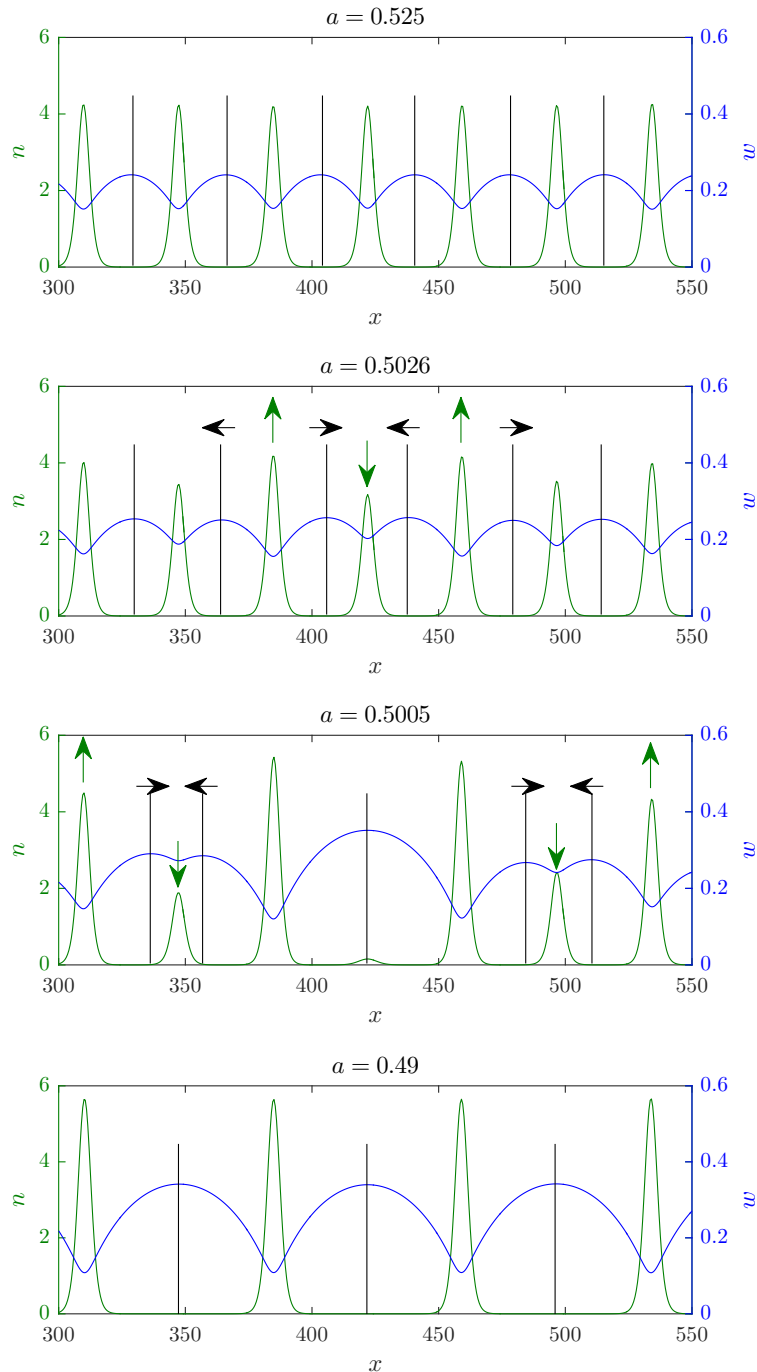


Figure 2.5: Plant biomass  $n$  and water  $w$  against space  $x$ , for  $v = 0$  and  $\frac{da}{dt} = -10^{-4}$ . The black lines mark the position of water divides. The black arrows indicate the direction of the movement of the water divides. The green arrows indicate the growth or decay in  $n$ .

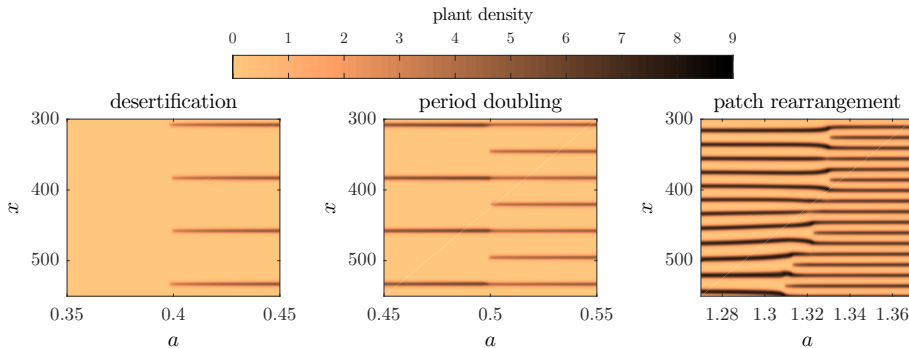


Figure 2.6: Plant density  $n$  in space  $x$  against rainfall  $a$  during different wavenumber adaptations in a model run with declining rainfall. Rearrangement of patches during a transition only occurs at high rainfall values. At low rainfall patches do not rearrange promptly and period doubling or desertification occurs.

changing environmental conditions. If a system is in a stable patterned state (i.e. in the Busse balloon), a pattern tends to solely adapt its amplitude, while if the system leaves the Busse balloon, a pattern adapts its wavenumber. The ability of patches to rearrange is determined by the period doubling instability. Once the system surpasses this instability, patches do not rearrange, leading to extinction of half or all the patches.

Our findings suggest that the response of patterned ecosystems to environmental change does not only depend on the magnitude of change, but also on the rate with which conditions change: patterned ecosystems may not be able to respond in a gradual way to rapid environmental change. Similar behaviour can be observed in a number of non-spatial models (e.g. Scheffer et al., 2008; Luke and Cox, 2011). Nonlinear response to rapid environmental change may as well occur in more comprehensive models that are used for policy making. This may imply that merely setting targets for tolerable change may not be sufficient to prevent ecosystem degradation and that to ensure gradual ecosystem adaptation, identification of critical rates of change is required as well.

Besides the rate of change in environmental conditions, the level of noise to which the system is exposed seems to play an essential role in ecosystem response. Our study shows that relatively small amplitude noise brings heterogeneity in the population of patches which leads to more gradual ecosystem adaptation to environmental change. Larger amplitude noise, on the other hand, is known to be a cause of critical transitions (Horsthemke and Lefever, 2006).

Our findings are in agreement with a recent study by Deblauwe et al. (2011) based on areal images of patterned vegetation in Sudan. Like Deblauwe et al. (2011) we found that pattern wavenumber declines with increasing aridity and that, when compared to flat terrain, a wider range of pattern wavenumbers can be found on sloped terrain. Although our stability analysis suggest that low wavenumber patterns are stable (and thus can be observed in theory), Deblauwe et al. (2011) did not find such patterns. This might be explained by the fact that, at least for flat terrain, low wavenumber patterns are stable only for a relatively small rainfall range (Figure 2.1a). A second explanation can be found in the steepness of the boundary of the Busse balloon. Wavenumber adaptation forced by environmental changes generally results in increased ecosystem resilience as it increases the distance to critical thresholds (the boundary of the Busse balloon). However, if the boundary of the Busse balloon is steep, as is the case for low wavenumber patterns at low rainfall values (Figure 2.1a), the system remains close to the boundary of the Busse balloon meaning that the increase in ecosystem resilience is relatively small. As a result patterned arid ecosystems are relatively fragile in this parameter region. Variations in seasonal and annual precipitation, to which all arid ecosystems are exposed, can easily trigger desertification. Consequently, low wavenumber patterns are less likely to be observed.

By assessing the existence and stability of patterned system states we went one step further than Turing analysis, frequently applied in previous studies (e.g. Klausmeier, 1999; HilleRisLambers et al., 2001; Meron et al., 2004; Gilad et al., 2004; Kefi et al., 2008; Eppinga et al., 2009). In a wide range of ecosystems, scale-dependent feedbacks are thought to involve local positive feedbacks (Rietkerk and Van de Koppel, 2008). Such local positive feedbacks allow stable patterned states to exist under conditions where uniform cover can no longer be sustained. Analysis of patterns in these parameter regions is of importance because of proximity to critical thresholds. Using conventional Turing analysis, however, it is fundamentally impossible to do so. The novel approach we presented in this paper is a promising way forward in understanding the behaviour of spatially explicit ecosystem models under these conditions.

The findings presented in this paper are in accordance with previous model studies. Analysis of the original Klausmeier model by Sherratt and Lord (2007) and Sherratt (2013a) already suggested the existence of patterned states in parameter regions where Turing unstable states are absent (see also Rietkerk et al., 2002) and that hysteresis can occur in pattern wavenumber and migration speed. In contrast to the study by Sherratt (2013a) we

used wavenumber as state variable instead of migration speed. In practice, wavenumber is a property that is easier to assess than migration speed (Couteron and Lejeune, 2001; Deblauwe et al., 2012). In addition, migration speed cannot be used as state variable if all patterns are stationary. This is the case on flat terrain in the extended Klausmeier model, but on sloped terrain patterns can be fixed as well (Thompson et al., 2008; Dunkerley, 2013). The existence of a multitude of stable patterned states has been demonstrated in other models as well (Sherratt, 2013a; Bel et al., 2012; Zelnik et al., 2013; Meron, 2012). In this paper we showed that transitions between stable patterned states can be forced by changing environmental conditions. Previous studies show that such transitions can also be triggered by disturbances in the form of the uniform biomass removal (Meron, 2012) or patch removal (Zelnik et al., 2013). Although our findings seem to be in line with observations (Deblauwe et al., 2011), most findings remain to be tested using areal images and field data. Empirical proof for a Busse balloon requires a constant pattern wavelength to be observed for a range of environmental conditions or, alternatively, a range of pattern wavelengths to be observed for a fixed set of environmental conditions. It would also be interesting to see if competition between neighbouring patches indeed occurs and how the competition strength depends on environmental stress. If time series of areal images are available, it may also be possible to observe hysteresis in pattern wavelength.

To get more insight in the behaviour of real ecosystems we propose that future studies apply stability analysis on patterned system states of other (more realistic) models. Constructing Busse balloons for other models will allow to relate findings to measurable parameters. Stability analysis of models in which multiple pattern forming mechanisms are captured, such as the model by Gilad et al. (2004), would allow studying how the relative strength of these mechanisms affects the global behaviour of patterned ecosystems (Kinast et al., 2014). In addition, future studies could consider two spatial dimensions as this may qualitatively affect the model behaviour described in this paper. Accounting for more than one spatial dimension in stability analysis is mathematically challenging, since more complex spatial patterns can evolve (gaps, labyrinths and spots; Pearson, 1993; Rietkerk et al., 2002) and more destabilization mechanisms may potentially destabilize a patterned system state (Hoyle, 2006). Finally, as soon as bare ground forms between patches, the movement and stability of patches can be described by pulse interaction (see Doelman and Kaper, 2003; Sun et al., 2005, and references therein). This may provide insight in the ecologically relevant process of

wavenumber adaptation forced by environmental change.

The changes in climate projected for the coming decades (Solomon et al., 2007) are likely to affect the functioning of patterned ecosystems worldwide. We showed that in order to understand the behaviour of patterned ecosystems that are subject to change, mathematical techniques are required that go beyond conventional Turing analysis. By assessing the stability of patterned ecosystem states and by studying the relevant destabilization mechanisms we were able to explain when and how arid ecosystems may adapt their pattern wavelength. Identification of the Busse balloon, together with the period doubling instability, provides a theoretical framework for future theoretical and empirical studies. These studies may provide enhanced insights in the response of other ecological models to change, the response of real ecosystems to change, and the ecological mechanisms responsible for this response.

## Acknowledgments

This study is supported by a grant within the Complexity programme of the Netherlands Organization for Scientific Research (NWO). The research of MR is also supported by funding from the European Union's Seventh Framework Programme (FP7/2007-2013) under grant agreement no. 283068 (CASCADE).

## Appendix 2.A A non-dimensional extended Klausmeier model.

The extended Klausmeier model is given by Equations 2.5 and 2.6. In Table 2.1, the values of the parameters are listed for both grass and trees, as estimated by Klausmeier (1999). The diffusion term was calibrated to obtain patterns in a realistic parameter range. A non-dimensional version of the model (Equations 2.7 and 2.8) is used throughout the paper. Table 2.2 shows how the dimensionless parameters can be obtained.

$$\frac{\partial W}{\partial T} = A - LW - RWN^2 + V \frac{\partial W}{\partial X} + E \frac{\partial^2 W^\Gamma}{\partial X^2} \quad (2.5)$$

$$\frac{\partial N}{\partial T} = RJWN^2 - MN + D \frac{\partial^2 N}{\partial X^2} \quad (2.6)$$

## 2.B Wavenumber plotting by fast Fourier transform

$$\frac{\partial w}{\partial t} = a - w - wn^2 + v \frac{\partial w}{\partial x} + e \frac{\partial^2 w^\gamma}{\partial x^2} \quad (2.7)$$

$$\frac{\partial n}{\partial t} = wn^2 - mn + \frac{\partial^2 n}{\partial x^2} \quad (2.8)$$

Table 2.1: Values and units for the variables and parameters of the extended Klausmeier model (Equations 2.5 and 2.6). Values adopted from Klausmeier (1999).  $E$  was calibrated to obtain patterns in a realistic parameter range, according to Deblauwe et al. (2008).

Parameter/Variable	Value (grass)	Value (tree)	Unit
$W$			$\text{kg m}^{-2}$ (=mm)
$N$			$\text{kg m}^{-2}$
$X$			m
$T$			year
$A$	0 - 950	0 - 950	$\text{kg m}^{-2} \text{ year}^{-1}$ (= mm year $^{-1}$ )
$L$	4	4	year $^{-1}$
$R$	100	1.5	$\text{kg m}^{-2} \text{ year}^{-1} \text{ kg}^{-2}$ (=mm year $^{-1}$ kg $^{-2}$ )
$V$	0 or 365	0 or 365	$\text{m year}^{-1}$
$E$	500	500	$\text{m}^2 \text{ year}^{-1} \text{ mm}^{1-\Gamma}$
$\Gamma$	1	1	-
$J$	0.003	0.002	$\text{kg kg}^{-1}$ (=kg L $^{-1}$ )
$M$	1.8	0.18	year $^{-1}$
$D$	1	1	$\text{m}^2 \text{ year}^{-1}$

## Appendix 2.B Wavenumber plotting by fast Fourier transform

In this appendix we explain how we compute the trajectories through (parameter, $\kappa$ )-space, as depicted in the main text, by using the discrete or *fast Fourier transform*.

In the model runs the plant biomass  $n(x)$  is represented by a vector  $n(j)$ ,  $j = 1, 2, \dots, N$ , of  $N = 1024$  elements and the spatial domain size is  $L = 1000$ . The vector can be expressed as a linear combination of vectors  $v_l(j) = e^{\frac{2\pi i l}{N} j}$ ,

Table 2.2: Physical meaning and values for the variables and parameters of the non-dimensional extended Klausmeier model (Equations 2.7 and 2.8)

Parameter/Variable	Physical meaning	Value (grass)	Value (tree)
$w$	$WR^{1/2}L^{-1/2}J$	$0.015W$	$0.0012W$
$n$	$NR^{1/2}L^{-1/2}$	$5N$	$0.61N$
$x$	$XL^{1/2}D^{-1/2}$	$2X$	$2X$
$t$	$TL$	$4T$	$4T$
$a$	$AR^{1/2}L^{-3/2}J$	$0.00375A$	$0.0003062A$
$m$	$ML^{-1}$	$0.25M$	$0.25M$
$v$	$VL^{-1/2}D^{-1/2}$	$0.5V$	$0.5V$
$e$	$ED^{-1}$	$E$	$E$
$\gamma$	$\Gamma$	$\Gamma$	$\Gamma$

where  $l = 0, 1, 2, \dots, N - 1$ . The  $v_l$  represent sinusoidals with wavenumber  $\kappa = \frac{2\pi l}{L}$ . The weight of  $v_l$  in  $n$  can be computed by the discrete Fourier transform

$$Y(\kappa) = \sum_{j=1}^N n(j)v_l(-j). \quad (2.9)$$

The absolute value of  $Y(\kappa)$  is a measure of how much  $n$  resembles a sinusoidal with wavenumber  $\kappa$ . If a single  $Y(\kappa)$  has a large absolute value compared to all other  $Y$  ( $\kappa \neq 0$ ), then the state is (nearly) periodic with wavenumber  $\kappa$ .

The trajectories through (parameter,  $\kappa$ )-space, as depicted in the main text, were obtained by picking the wavenumber where  $|Y|$  attained its maximum,  $\kappa = 0$  excluded. The wavenumber is only plotted when the maximum is relatively large, which suppresses plotting during transient dynamics.

Figure 2.7 shows that during wavenumber adaptation the spread in  $\kappa$  increases. After wavenumber adaptation the spread decreases slowly. As the pattern settles, the maximum wavenumber can still change. As  $l$  is an integer,  $\kappa$  can only attain certain values. Therefore the settling of the pattern can result in small jumps in pattern wavenumber.

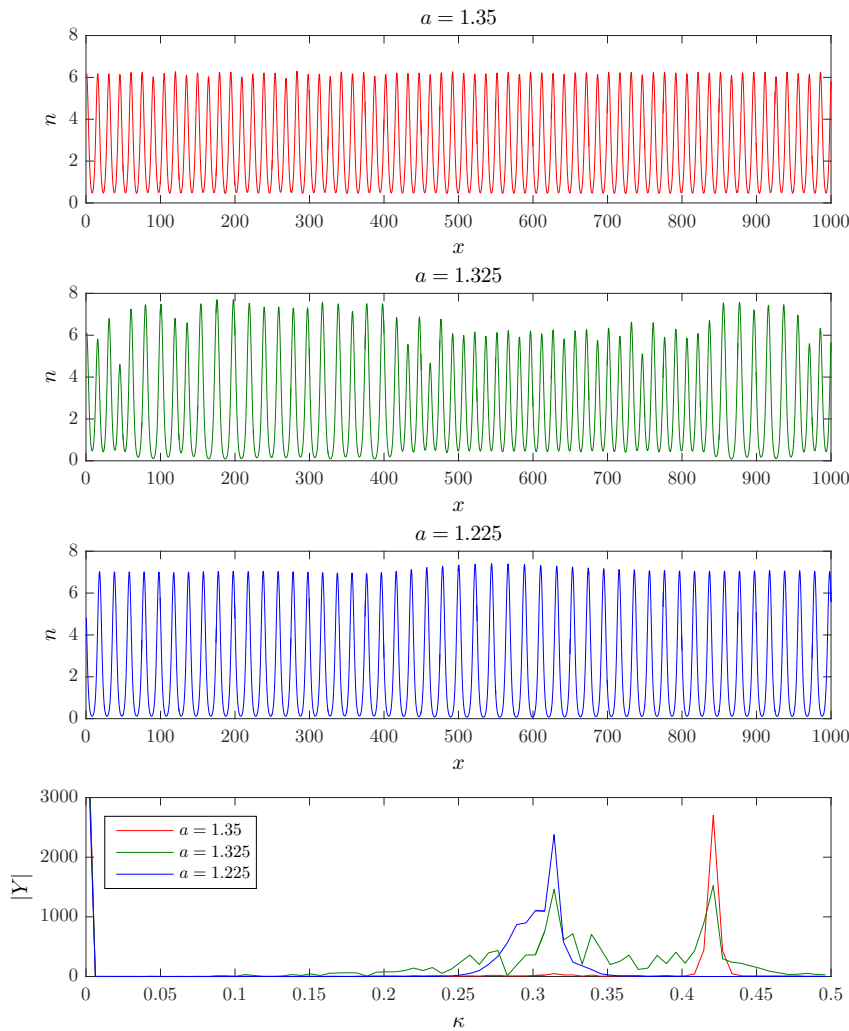


Figure 2.7: Plant biomass  $n$  against space  $x$  before, during and after wavenumber adaptation in the model run with declining rainfall of Figure 2.2 and the Fourier transform of the corresponding vectors.

## Appendix 2.C General equations for perturbations.

We derive equations for perturbations of a general system state in the extended Klausmeier model. These equations will be of use in Appendix 2.D.2, 2.D.3 and 2.E.2. For ease of the computations we restrict to the linear diffusion case  $\gamma = 1$ . Let  $(w, n)$  be a system state that is perturbed by  $(w', n')$ . We obtain an expression for the governing equations of the perturbation by the following calculations:

$$\begin{aligned} \frac{\partial w'}{\partial t} &= \frac{\partial(w + w')}{\partial t} - \frac{\partial w}{\partial t} \\ &= e \frac{\partial^2(w + w')}{\partial x^2} + v \frac{\partial(w + w')}{\partial x} + a - (w + w') - (w + w')(n + n')^2 \\ &\quad - \left( e \frac{\partial^2 w}{\partial x^2} + v \frac{\partial w}{\partial x} + a - w - wn^2 \right) \\ &= e \frac{\partial^2 w'}{\partial x^2} + v \frac{\partial w'}{\partial x} - w'(1 + n^2) - 2n'wn - 2w'n'n - n'^2w - w'n'^2 \\ &\approx e \frac{\partial^2 w'}{\partial x^2} + v \frac{\partial w'}{\partial x} - w'(1 + n^2) - 2n'wn \end{aligned} \tag{2.10}$$

$$\begin{aligned} \frac{\partial n'}{\partial t} &= \frac{\partial(n + n')}{\partial t} - \frac{\partial n}{\partial t} \\ &= \frac{\partial^2(n + n')}{\partial x^2} + (w + w')(n + n')^2 - m(n + n') \\ &\quad - \left( \frac{\partial^2 n}{\partial x^2} + wn^2 - mn \right) \\ &= \frac{\partial^2 n'}{\partial x^2} + w'n^2 + n'(2wn - m) + 2w'n'n + n'^2w + w'n'^2 \\ &\approx \frac{\partial^2 n'}{\partial x^2} + w'n^2 + n'(2wn - m) \end{aligned} \tag{2.11}$$

The final approximate equalities are equalities in a linear approximation: for small perturbations  $(w', n')$  the products  $w'n'$  and  $n'^2$  are negligible.

In an abstract formulation equations 2.10 and 2.11 can be rewritten as:

$$\frac{\partial}{\partial t} \begin{pmatrix} w' \\ n' \end{pmatrix} = A \begin{pmatrix} w' \\ n' \end{pmatrix} \tag{2.12}$$

where the so-called spectrum, a generalization of the concept of eigenvalues,

of the differential operator  $A = \begin{pmatrix} e\frac{\partial^2}{\partial x^2} + v\frac{\partial}{\partial x} - 1 - n^2 & -2wn \\ n^2 & \frac{\partial^2}{\partial x^2} + 2wn - m \end{pmatrix}$  determines the stability of  $(w, n)$ .

## Appendix 2.D Analysis of the homogeneous steady states.

For completeness we will give a thorough analysis of the homogeneous steady states of the extended Klausmeier model. This also serves the purpose of showing how easily results can be obtained by hand in this case, compared to the restricted possibilities for the analysis of patterns in Appendix 2.E. The results of Section 2.D.1 and 2.D.2 also hold for  $\gamma = 2$ .

### 2.D.1 Existence of spatially homogeneous steady states

If  $w$  and  $n$  are spatially homogeneous, gradients in  $w$  and  $n$  are absent, and the advection-diffusion terms of Equations 2.1 and 2.2 vanish. Since only a single type of derivative remains, the partial differential equations become ordinary differential equations. The steady uniform states can then be found by solving Equations 2.13 and 2.14.

$$\frac{dw}{dt} = a - w - wn^2 = 0 \quad (2.13)$$

$$\frac{dn}{dt} = wn^2 - mn = (wn - m)n = 0 \quad (2.14)$$

Clearly  $\bar{n}_B = 0$  solves Equation 2.14 and consequently  $\bar{w}_B = a$ . This is a bare desert state, as plant biomass equals zero. Alternatively Equation 2.14 is solved if  $n = \frac{m}{w}$ . Substituting this in Equation 2.13 and multiplying with  $-w$  we obtain the quadratic equation  $w^2 - aw + m^2 = 0$ . This quadratic equation can be solved to obtain two solutions for  $w$  and from  $n = \frac{m}{w}$  the

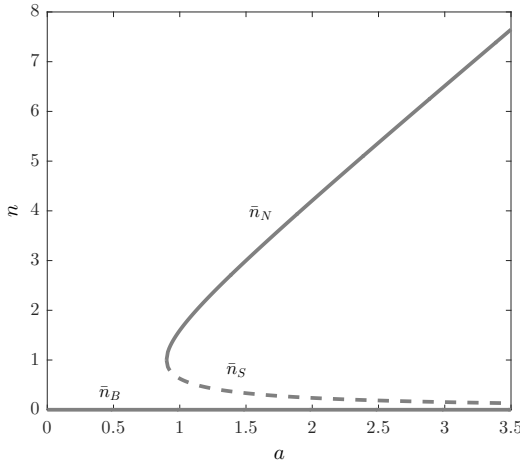


Figure 2.8: Homogeneous steady states of the (extended) Klausmeier model expressed in plant biomass  $n$  as function of rainfall  $a$  for  $m = 0.45$ .

corresponding solution for  $n$  can be computed. The outcome is given by:

$$\bar{w}_S = \frac{2m^2}{a - \sqrt{a^2 - 4m^2}} \quad (2.15)$$

$$\bar{n}_S = \frac{a - \sqrt{a^2 - 4m^2}}{2m} \quad (2.16)$$

$$\bar{w}_N = \frac{2m^2}{a + \sqrt{a^2 - 4m^2}} \quad (2.17)$$

$$\bar{n}_N = \frac{a + \sqrt{a^2 - 4m^2}}{2m} \quad (2.18)$$

Here the argument of the square root needs to be positive, so these states only exist for  $a \geq 2m$ . Note that the two states coincide at  $a = 2m$ , in fact here a so-called saddle-node bifurcation takes place. In the following section we will show that  $(\bar{w}_S, \bar{n}_S)$  has a stable and an unstable direction (saddle, unstable) and  $(\bar{w}_N, \bar{n}_N)$  either has two stable or unstable directions (node). Note that we have covered all possible cases of Equations 2.13 and 2.14 and thus no other homogeneous steady states can exist. Moreover, all the steady states are non-negative. We will continue by studying their stability.

## 2.D.2 Stability of the homogeneous steady states against homogeneous perturbations

By perturbing the steady states obtained in Appendix 2.D, their stability can be determined. If a perturbation grows over time, the steady state is unstable. The steady state is stable, if all perturbations decay. In this Appendix, we show how linear stability analysis can be used to assess the stability of uniform system states to homogeneous perturbations. We will do this by using the equations derived for perturbations in Appendix 2.C.

Since the perturbations are assumed to be homogeneous Equations 2.10 and 2.11 simplify to:

$$\frac{\partial w'}{\partial t} = -w'(1 + \bar{n}^2) - 2\bar{n}'w\bar{n} \quad (2.19)$$

$$\frac{\partial n'}{\partial t} = w'\bar{n}^2 + n'(2\bar{w}\bar{n} - m) \quad (2.20)$$

This can be compactly written as:

$$\begin{pmatrix} \frac{dw'}{dt} \\ \frac{dn'}{dt} \end{pmatrix} = \begin{pmatrix} -1 - \bar{n}^2 & -2\bar{w}\bar{n} \\ \bar{n}^2 & 2\bar{w}\bar{n} - m \end{pmatrix} \begin{pmatrix} w' \\ n' \end{pmatrix} \quad (2.21)$$

where the matrix is readily identified as the Jacobian matrix  $J$  of the reaction terms. As is well-known, the stability can be determined by looking at the real parts of the eigenvalues of the Jacobian.

For the bare state plugging in  $\bar{n}_B = 0$  in the Jacobian matrix yields  $J = \begin{pmatrix} -1 & 0 \\ 0 & -m \end{pmatrix}$ . The eigenvalues can now be read off from the diagonal ( $\lambda_1 = -1$ ,  $\lambda_2 = -m$ ) so the bare state is always stable (for  $m > 0$ ).

In case of the saddle-node states we recall that  $n w = m$  (Appendix 2.D.1). So the Jacobian matrix becomes  $J = \begin{pmatrix} -1 - \bar{n}_{S,N}^2 & -2m \\ \bar{n}_{S,N}^2 & m \end{pmatrix}$ . The eigenvalues can be computed directly by solving the characteristic equation involving the determinant  $\det$ :

$$\begin{aligned} \det(J - \lambda I) &= \det \begin{pmatrix} -1 - \bar{n}^2 - \lambda & -2m \\ \bar{n}^2 & m - \lambda \end{pmatrix} \\ &= \lambda^2 + \lambda(1 + \bar{n}^2 - m) - m + m\bar{n}^2 = 0 \end{aligned} \quad (2.22)$$

Solving this we obtain:

$$\lambda_{\pm} = -\frac{1}{2} (1 + \bar{n}^2 - m) \pm \sqrt{m(1 - \bar{n}^2) + \frac{1}{4}(1 + \bar{n}^2 - m)^2} \quad (2.23)$$

Which has the form:

$$\lambda_{\pm} = \alpha \pm \sqrt{\beta + \alpha^2} \quad (2.24)$$

For this general form it holds:

	$\beta > 0$	$\beta < 0$
$\alpha > 0$	$\Re(\lambda_+) > 0$	$\Re(\lambda_+) > 0$
	$\Re(\lambda_-) < 0$	$\Re(\lambda_-) > 0$
$\alpha < 0$	$\Re(\lambda_+) > 0$	$\Re(\lambda_+) < 0$
	$\Re(\lambda_-) < 0$	$\Re(\lambda_-) < 0$

We first show that  $(\bar{w}_S, \bar{n}_S)$  has both a stable and an unstable direction (saddle, unstable), as was claimed in Appendix 2.D.1. For this it suffices to show that  $\beta = m(1 - \bar{n}_S^2) > 0$ . Since  $a > 2m$  (Appendix 2.D.1)

$$\bar{w}_S = \frac{2m^2}{a - \sqrt{a^2 - 4m^2}} = \frac{2m^2 \left( a + \sqrt{a^2 - 4m^2} \right)}{a^2 - a^2 + 4m^2} = \frac{a}{2} + \frac{1}{2}\sqrt{a^2 - 4m^2} > m \quad (2.25)$$

Now  $\bar{n}_S = \frac{m}{\bar{w}_S} < 1$  so  $\beta > 0$ .

Second we show that  $(\bar{w}_N, \bar{n}_N)$  is a node (i.e. is either stable or unstable in both directions), as was claimed in Appendix 2.D.1, but we will not directly determine the stability. This is equivalent to  $\beta = m(1 - \bar{n}_N^2) < 0$ . Since  $a > 2m$  we have

$$\bar{n}_N = \frac{a + \sqrt{a^2 - 4m^2}}{2m} = \frac{a}{2m} + \frac{1}{2m}\sqrt{a^2 - 4m^2} > 1 \quad (2.26)$$

So indeed  $\beta < 0$ .

Finally the eigenvalues belonging to the node can have positive (unstable) or negative (stable) real parts. Both eigenvalues are negative if and only if  $\alpha = -\frac{1}{2}(1 + \bar{n}_N^2 - m) < 0$ , this is automatically satisfied if  $m < 1$ , so in particular if  $m = 0.45$ . For general  $m$  it can be calculated that the stability

## 2.D Analysis of the homogeneous steady states.

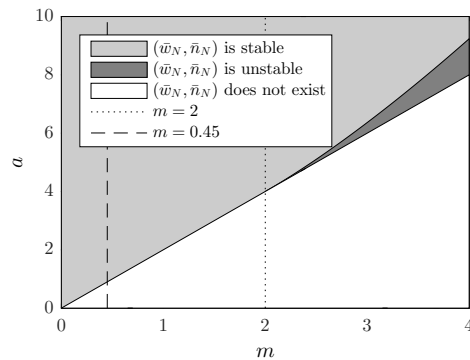


Figure 2.9: Region in parameter space where  $(\bar{w}_N, \bar{n}_N)$  is stable, unstable or does not exist.

boundary is given by pairs  $(m, a)$  that satisfy:

$$a = \frac{m^2}{\sqrt{m-1}} \text{ and } m \geq 2 \quad (2.27)$$

This boundary is plotted in Figure 2.9.

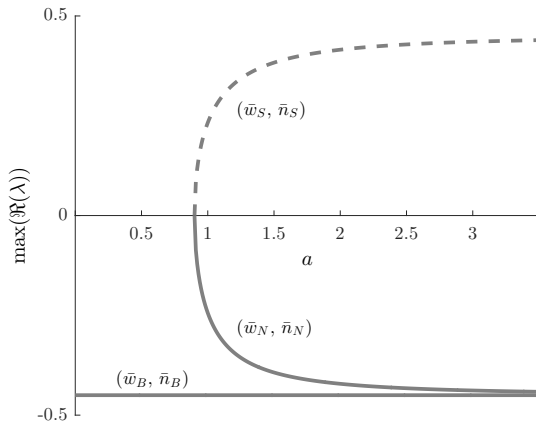


Figure 2.10: The maximum real part of  $\lambda$  for the spatially uniform steady states plotted against  $a$ . Perturbations are assumed to be spatially homogeneous and  $m = 0.45$ .

### 2.D.3 Turing analysis of the steady states

In the full model the steady states are also subject to heterogeneous perturbations. States that were thought of as being stable against homogeneous perturbation may be unstable against a wider class of perturbations. For simplicity we restrict to  $\gamma = 1$ .

The usual approach is to assume that the spatial dependence of the perturbation has the form of a sinusoid: we represent it by a complex exponential  $e^{i\kappa x}$ .<sup>1</sup> This is convenient because  $\frac{d}{dx}e^{i\kappa x} = i\kappa e^{i\kappa x}$  and  $\frac{d^2}{dx^2}e^{i\kappa x} = -\kappa^2 e^{i\kappa x}$ . Substituting  $\begin{pmatrix} w'(t,x) \\ n'(t,x) \end{pmatrix} = e^{i\kappa x} \begin{pmatrix} \tilde{w}(t) \\ \tilde{n}(t) \end{pmatrix}$  in Equation 2.10 and 2.11 and dividing by  $e^{i\kappa x}$  yields:

$$\frac{\partial \tilde{w}}{\partial t} = -\kappa^2 e \tilde{w} + i\kappa v \tilde{w} - \tilde{w}(1 + n^2) - 2\tilde{n}wn \quad (2.28)$$

$$\frac{\partial \tilde{n}}{\partial t} = -\kappa^2 \tilde{n} + \tilde{w}n^2 + \tilde{n}(2wn - m) \quad (2.29)$$

---

<sup>1</sup>If there are only second order spatial derivatives present, assuming the form  $\cos(\kappa x)$  or  $\sin(\kappa x)$  is equivalent.

This can be written in a single matrix equation:

$$\begin{pmatrix} \frac{d\tilde{w}}{dt} \\ \frac{d\tilde{n}}{dt} \end{pmatrix} = \begin{pmatrix} -\kappa^2 e + i\kappa v - 1 - \bar{n}^2 & -2\bar{w}\bar{n} \\ \bar{n}^2 & -\kappa^2 + 2\bar{w}\bar{n} - m \end{pmatrix} \begin{pmatrix} \tilde{w} \\ \tilde{n} \end{pmatrix} \quad (2.30)$$

The justification of the assumption that the perturbation is sinusoidal is given by the Fourier transform, which links the spectrum of the operator  $A$  in the abstract formulation Equation 2.12 to the eigenvalues of the above matrix.

For the bare state  $\bar{n}_B = 0$ , so the matrix simplifies to  $\begin{pmatrix} -\kappa^2 e + i\kappa v - 1 & 0 \\ 0 & -\kappa^2 - m \end{pmatrix}$  so  $\lambda_1 = -\kappa^2 e + i\kappa v - 1$  and  $\lambda_2 = -\kappa^2 - m$ . Since the real parts  $\Re(\lambda_1) = -\kappa^2 e - 1$  and  $\Re(\lambda_2) = -\kappa^2 - m$  both remain negative for any  $\kappa$ , the bare state is also stable against heterogeneous perturbations. Because the saddle is already unstable against homogeneous perturbations we focus our attention on the node. Since  $\bar{w}_N \bar{n}_N = m$  the matrix becomes  $\begin{pmatrix} -\kappa^2 e + i\kappa v - 1 - \bar{n}_N^2 & -2m \\ \bar{n}_N^2 & -\kappa^2 + m \end{pmatrix}$ , from which we can obtain the eigenvalues by solving the dispersion relation:

$$\det \begin{pmatrix} -\kappa^2 e + i\kappa v - 1 - \bar{n}_N^2 - \lambda & -2m \\ \bar{n}_N^2 & -\kappa^2 + m - \lambda \end{pmatrix} = 0 \quad (2.31)$$

This again yields a quadratic equation in  $\lambda$ , which can be solved for  $\lambda$ . The eigenvalues  $\lambda$  are now not only a function of model parameters, but also a function of wavenumber  $\kappa$ . Figure 2.11 shows solutions of Equation 2.31 (which depends on  $a$  through  $\bar{n}_N$ ) for several values of  $a$  for  $m = 0.45$ . The curves pass through the real axis between  $a = 4$  and  $a = 2.5$  in both the case  $v = 0$  and  $v = 182.5$ , the node becomes Turing unstable somewhere in between (precise values are given in the caption of Figure 2.1).

## Appendix 2.E Analysis of patterns

In the previous appendix all of the analysis could be done by hand. This is very much in contrast to the analysis of patterns. Here we give some results that can be obtained analytically for the extended Klausmeier model.

### 2.E.1 Existence of patterns

Here we derive that patterns are solutions of the Equations 2.3 and 2.4. These equations are solved numerically.

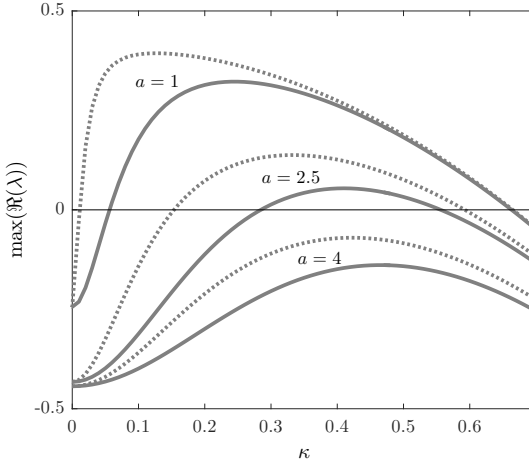


Figure 2.11: The maximum real part of  $\lambda$  for heterogeneous perturbations of  $(\bar{w}_N, \bar{s}_N)$ , plotted as function of  $\kappa$ , for different values of  $a$  and for  $v = 0$  (solid lines) and  $v = 182.5$  (dotted lines),  $m = 0.45$ . The boundary of the Turing prediction region depicted in Figure 2.1 is located at the intersection points of the curves with the  $x$ -axis. The maxima of the curves correspond to the most unstable wavenumber.

In general, patterned states may migrate uphill (if  $v \neq 0$ ). We will denote the migration speed (in the direction of increasing  $x$ ) of these so-called wavetrains by  $s$ . Allowing for  $s = 0$ , any pattern can be written in the form  $(w(t, x), n(t, x)) = (w_p(x - st), n_p(x - st)) = (w_p(\xi), n_p(\xi))$ , where  $w_p$  and  $n_p$  are periodic functions describing the wave profile and  $\xi = x - st$  is a comoving frame coordinate. By using the chain rule, e.g.

$$\frac{\partial w(x, t)}{\partial t} = \frac{dw_p(\xi)}{d\xi} \frac{\partial \xi}{\partial t} = -s \frac{dw_p}{d\xi} \quad (2.32)$$

after substituting the forms in Equations 2.1 and 2.2 we obtain

$$0 = a - w_p - w_p n_p^2 + (v + s) \frac{dw_p}{d\xi} + e \frac{d^2 w_p}{d\xi^2} \quad (2.33)$$

$$0 = w_p n_p^2 - m n_p + s \frac{dn_p}{d\xi} + \frac{d^2 n_p}{d\xi^2} \quad (2.34)$$

which are the equations we set out to find.

## 2.E.2 Stability of patterns

We will study the stability of a pattern  $(w(t, x), n(t, x))$  in the case  $\gamma = 1$ , so the equations for the perturbation 2.10 and 2.11 hold. We show these equations again, now with explicit dependence on the coordinates:

$$\begin{aligned} \frac{\partial w'(t, x)}{\partial t} &= e \frac{\partial^2 w'(t, x)}{\partial x^2} + v \frac{\partial w'(t, x)}{\partial x} \\ &\quad - w'(t, x) (1 + n(t, x)^2) - 2n'(t, x)w(t, x)n(t, x) \end{aligned} \quad (2.35)$$

$$\frac{\partial n'(t, x)}{\partial t} = \frac{\partial^2 n'(t, x)}{\partial x^2} + w'(t, x)n(t, x)^2 + n'(t, x)(2w(t, x)n(t, x) - m) \quad (2.36)$$

Here  $w$  and  $n$  are not constant, which prevents us from applying a sinusoidal substitution as in Turing analysis (Appendix 2.D.3). As in Appendix 2.E.1 we write  $(w(t, x), n(t, x)) = (w_p(\xi), n_p(\xi))$  with  $\xi = x - st$ . To make optimal use of this form we apply a change of coordinates  $(t, x) \mapsto (t, \xi)$ . Simultaneously we substitute  $(w', n') = e^{\lambda t} (\tilde{w}(\xi), \tilde{n}(\xi))$  and after division by  $e^{\lambda t}$  we obtain:

$$\lambda \tilde{w} = e \frac{d^2 \tilde{w}}{d\xi^2} + (v + s) \frac{d\tilde{w}}{d\xi} - \tilde{w}(1 + n_p^2) - 2\tilde{n}w_p n_p \quad (2.37)$$

$$\lambda \tilde{n} = \frac{d^2 \tilde{n}}{d\xi^2} + s \frac{d\tilde{n}}{d\xi} + \tilde{w}n_p^2 + \tilde{n}(2w_p n_p - m) \quad (2.38)$$

This is a system of two second order ordinary differential equations. After defining  $\tilde{q} = \frac{d\tilde{w}}{d\xi}$  and  $\tilde{r} = \frac{d\tilde{n}}{d\xi}$  it can be rewritten as a first order system of four ordinary differential equations:

$$\frac{d}{d\xi} \begin{pmatrix} \tilde{w} \\ \tilde{q} \\ \tilde{n} \\ \tilde{r} \end{pmatrix} = \begin{pmatrix} 0 & 1 & 0 & 0 \\ \frac{\lambda+1+n_p^2}{e} & \frac{-v-s}{e} & \frac{2w_p n_p}{e} & 0 \\ 0 & 0 & 0 & 1 \\ -n_p^2 & 0 & m - w_p n_p & -s \end{pmatrix} \begin{pmatrix} \tilde{w} \\ \tilde{q} \\ \tilde{n} \\ \tilde{r} \end{pmatrix} \quad (2.39)$$

Since the matrix of coefficients is periodic, we are ready to use Floquet theory. Through Floquet theory it is possible to express the spectrum as the union of curves of eigenvalues of a related problem. The spatial part of the

perturbations that act as eigenfunctions satisfy:

$$\tilde{w} \left( \xi + \frac{2\pi}{\kappa}; \nu \right) = e^{i\nu} \tilde{w}(\xi; \nu) \quad (2.40)$$

$$\tilde{n} \left( \xi + \frac{2\pi}{\kappa}; \nu \right) = e^{i\nu} \tilde{n}(\xi; \nu) \quad (2.41)$$

where  $\kappa$  is now the pattern wavenumber and  $\nu \in (-\pi, \pi]$ . Note that  $\frac{2\pi}{\kappa}$  is the wavelength of the pattern. A corresponding curve of eigenvalues was exhibited as a function of  $\nu$  in Figure 2.1c, for different values of  $a$ . Regarding the stability we will not go into more details but note that the procedure for assessing stability is explained further in Rademacher et al. (2007).

A special case is when  $\nu = \pi$ . Then  $e^{i\nu} = -1$ . It follows that  $\tilde{w}(\xi + \frac{4\pi}{\kappa}; \pi) = -\tilde{w}(\xi + \frac{2\pi}{\kappa}; \pi) = \tilde{w}(\xi; \pi)$ , and similarly for  $\tilde{n}$ , so the perturbation has twice the wavelength of the pattern. When the real part of the corresponding eigenvalue becomes positive, the pattern can be destabilized by such a perturbation and the period will be doubled (period doubling instability).

### **3 How will increases in rainfall intensity affect semiarid ecosystems?**

Siteur, K., Eppinga, M. B., Karssenberg, D., Baudena, M., Bierkens, M. F. P. and Rietkerk, M. (2014). How will increases in rainfall intensity affect semiarid ecosystems? *Water Resources Research* 50 (7):5980-6001.

#### **Abstract**

Model studies suggest that semiarid ecosystems with patterned vegetation can respond in a non-linear way to climate change. This means that gradual changes can result in a rapid transition to a desertified state. Previous model studies focused on the response of patterned semiarid ecosystems to changes in mean annual rainfall. The intensity of rain events, however, is projected to change as well in the coming decades. In this paper we study the effect of changes in rainfall intensity on the functioning of patterned semiarid ecosystems with a spatially explicit model that captures rainwater partitioning and runoff processes with simple event based process descriptions. Analytical and numerical analyses of the model revealed that rainfall intensity is a key parameter in explaining patterning of vegetation in semiarid ecosystems as low mean rainfall intensities do not allow for vegetation patterning to occur. Surprisingly, we found that, for a constant annual rainfall rate, both an increase and a decrease in mean rainfall intensity can trigger desertification. An increase negatively affects productivity as a greater fraction of the rainwater is lost as runoff. This can result in a shift to a bare desert state only if the mean rainfall intensity exceeds the infiltration capacity of bare soil. On the other hand, a decrease in mean rainfall intensity leads to an increased fraction of rainwater infiltrating in bare soils, remaining unavailable to plants. Our findings suggest that considering rainfall intensity as a variable may help in assessing the proximity to regime shifts in patterned semiarid ecosystems and that monitoring losses of resource through runoff and bare soil infiltration could be used to determine ecosystem resilience.

## 3.1 Introduction

In semiarid environments plants can locally modulate their environment in a way that enables better access to resources, such as nutrients and water, thereby acting as so called ecosystem engineers (Jones et al., 1994). If the positive effect of plants on enhanced access to resources outweighs the negative effect of increased resource uptake, this may result in a positive feedback loop: an increase in plant biomass results in higher resource availability and consequently enhanced plant growth. This mechanism allows high plant densities to be maintained under harsher conditions, but it can also result in bistability (or multistability) of the ecosystem (Rietkerk et al., 1997), meaning that alternative stable system states exist under a given range of external conditions (Lewontin, 1969). Changes in external conditions can alter the stability and the number of system states. In the case of semiarid ecosystems, increasing grazing pressure or decreasing resource input may push the system over a critical threshold, resulting in a sudden critical transition from a vegetated state to a bare state (Noy-Meir, 1975; Rietkerk et al., 1997). As such regime shifts are accompanied by significant and irreversible losses in biological productivity, they are often related to the process of desertification (e.g. Kéfi et al. (2007); Von Hardenberg et al. (2001); although formal definitions of desertification are more complex and include changes in soil resources, soil geochemistry and vegetation composition as pointed out by Schlesinger et al. (1990) and D'Odorico et al. (2013)).

Although it is generally hard to determine whether ecosystems will indeed respond in such a non-linear way to changing environmental conditions, model studies show that particular periodic spatial patterns may be used as indicator for alternative stability (Rietkerk et al., 2004; Kéfi et al., 2010). This is the case if local facilitative interactions, responsible for non-linear system behaviour (DeAngelis et al., 1980), are linked to distal competitive interactions that are responsible for pattern formation (Gierer and Meinhardt, 1972; Rietkerk and Van de Koppel, 2008). In semiarid ecosystems such a link between local facilitative and distal competitive interactions exists and yields so called scale-dependent feedbacks (Rietkerk and Van de Koppel, 2008). More specifically, in these ecosystems plants can locally enhance the infiltration capacity of a soil by preventing crust formation and changing the soil structure. On sloped terrain, surface water accumulates on the barren or sparsely vegetated impenetrable soils during intense rain events, and flows downhill to the more densely vegetated soils where it can infiltrate, resulting in increased productivity. The depletion of surface water

by vegetation uphill on the other hand has a negative effect on infiltration and plant growth downhill. This particular scale dependent feedback, referred to as the resource concentration mechanism (Rietkerk et al., 2004), can result in the formation of regularly spaced vegetation bands perpendicular to the slope separated by interbands of bare soil (Klausmeier, 1999; Rietkerk et al., 2002, Figure 3.1).

A large body of spatially explicit mechanistic models have been published that describe pattern formation in semiarid ecosystems (see for example Lefever and Lejeune (1997); Klausmeier (1999); Von Hardenberg et al. (2001); Rietkerk et al. (2002); Gilad et al. (2004) and Borgogno et al. (2009) for a review). These models were successful in identifying possible mechanisms driving pattern formation in semiarid ecosystems such as the resource concentration mechanism, and provided insights in the non-linear response of these systems when subject to gradual changes in mean annual rainfall.

Changes in annual and seasonal rainfall volumes in arid and semiarid regions, as projected by global climate models, are however subject to much uncertainty. Projections of changes in rainfall intensity in contrast, show strong trends (Tebaldi et al., 2006; Solomon et al., 2007). For the Sahel region and the Horn of Africa for example, a majority of the global climate models predicts significant elevations in rainfall intensity at the end of this century with respect to the 1980s and 1990s (Tebaldi et al., 2006; Solomon et al., 2007).

Model studies show that spatio-temporal patterns in infiltration and soil moisture are to a large extent determined by rainfall intensity and storm size. Rodriguez-Iturbe et al. (1999) show that average soil moisture increases with rainfall depth, and that there is bell shaped relation between rainfall depth and variance. A study by Thompson et al. (2011) shows that the spatial infiltration patterns in patchy arid ecosystems are strongly controlled by rainfall intensity. During intense events, enhanced infiltration occurs for a large portion of vegetated sites, whereas during low intensity events increased recharge occurs only at the edges of vegetation patches. Although hydrological models show that rainfall intensity plays a key role in rain water partitioning and lateral surface water redistribution, it is unknown if and exactly how the projected changes in rainfall intensity are going to affect the productivity and functioning of patterned semiarid ecosystems.

Modelling the effect of changes in rainfall intensity on these ecosystems requires the coupling of processes that act on the timescale of a single rain event with processes, such as plant growth, that act on much longer timescales. The current spatially explicit models mostly capture rainfall in a continuous

### *3 Rainfall intensity and semiarid ecosystems*

manner, and thereby they do not explicitly deal with this issue (Konings et al., 2011). These models, as well the few that do consider rainfall to consist of separate events (Kletter et al., 2009; Ursino and Contarini, 2006), also assume infiltration to depend on surface water depth (e.g. HilleRisLambers et al., 2001; Rietkerk et al., 2002; Gilad et al., 2004; Meron et al., 2007), which is in contrast with conventional depth independent infiltration models (e.g. Horton, 1939; Philip, 1957). The study by Thompson et al. (2011), shows that this assumption leads insensitivity of surface water redistribution to changes in rainfall intensity. The use of depth dependent infiltration models may therefore underestimate the potential effects such changes may have on ecosystem functioning.

In this paper we study the response of semiarid ecosystems to changes in rainfall intensity using a spatially explicit version of the water limitation model by Rietkerk et al. (1997) that is coupled with a hydrological hillslope model that explicitly describes depth independent infiltration and infiltration excess (Hortonian) runoff generation on an event basis with simple conditional rules. The full model acknowledges both the processes that operate on short temporal scales, such as rainwater partitioning and redistribution, as well as processes that operate on longer temporal scales, such as plant growth. Temporal upscaling of short term processes and a minimalistic modelling approach enabled analytical analysis of the model.

## **3.2 Model description**

To study the role of rainfall intensity in semiarid ecosystems we need to account for relatively slow processes that operate on long temporal scales, such as plant growth, as well as fast processes that operate on short temporal scales, such as the partitioning and redistribution of rainwater during a rain event.

The slow long-term processes are modelled using a spatially extended version of the water-limitation model by Rietkerk et al. (1997), which describes the essential dynamics of plant density and available soil moisture in a minimalistic way (Rietkerk, 1998, p.4-5), thereby enabling detailed analytical analysis. Rainwater partitioning and the runoff-runon processes are fast short-term processes that are modelled with event based descriptions in the form of simple conditional rules. Temporal upscaling of the obtained infiltration rates yields a continuous formulation for infiltration, which is then used in the spatially extended version of the water-limitation model by

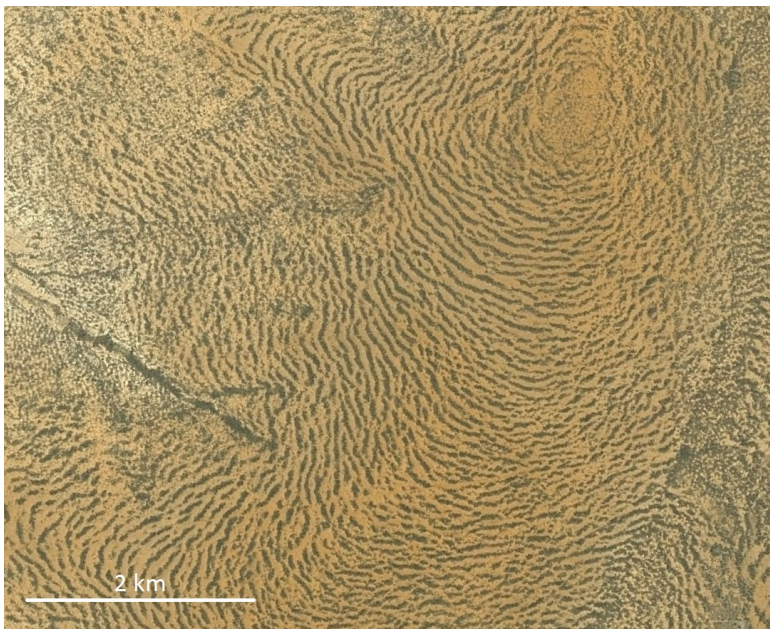


Figure 3.1: Periodically banded vegetation in Sudan ( $11^{\circ}17'$  N,  $28^{\circ}13'$  E, mean annual precipitation:  $450 \text{ mm year}^{-1}$ ) (Deblauwe et al., 2008). ©2013 Google Earth. ©2013 Cnes/Spot Image.

### 3 Rainfall intensity and semiarid ecosystems

Rietkerk et al. (1997).

In subsections 3.2.1 and 3.2.2, we will describe the water-limitation model. In Section 3.2.3 infiltration for uniform system states will be discussed and in Section 3.2.4 we account for spatial heterogeneity by including runoff-runon processes. The mechanism governing spatial patterning in this model is the resource concentration mechanism mentioned earlier, however, spatial feedbacks in our model differ from previous models because of the alternative modelling approach, as we will briefly discuss in Section 3.2.5.

#### 3.2.1 Soil moisture dynamics

Soil moisture dynamics comprise infiltration, plant uptake, soil evaporation and percolation losses, and lateral soil water movement. The change in available soil water  $W$  [mm] over time  $t$  [year] at location  $x$  [m] on the one-dimensional hillslope is modelled with Equation 3.1.

$$\frac{\partial W}{\partial t} = i_{ag} - u \frac{W}{W + k} P - rW + d_W \frac{\partial^2 W}{\partial x^2} \quad (3.1)$$

Here  $i_{ag}$  is the mean aggregated infiltration rate of water into the soil [mm year $^{-1}$ ], further discussed in Section 3.2.3 and 3.2.4. The second term represents the uptake of water by plants, which is assumed to depend on local plant density. Here  $u$  is the maximum specific soil water uptake [mm m $^2$  g $^{-1}$  year $^{-1}$ ],  $P$  is the plant density [g m $^{-2}$ ] and  $k$  is the half saturation constant of soil water uptake [mm]. Losses in available soil water are modelled with the third term, in which  $r$  is the specific soil water loss due to soil evaporation and percolation [year $^{-1}$ ]. The last term represents soil water movement, with  $d_W$  being the diffusion rate of soil water [m $^2$  year $^{-1}$ ] and  $x$  space [m]. Note that soil water is assumed to diffuse in a linear way and that also percolation and evaporation losses depend linearly on soil water availability (following Rietkerk et al., 2002).

#### 3.2.2 Plant growth

In the model, plant dynamics is captured by growth, mortality and grazing, and plant dispersion. The change in plant density  $P$  is given by Equation 3.2.

$$\frac{\partial P}{\partial t} = cu \frac{W}{W + k} P - mP + d_P \frac{\partial^2 P}{\partial x^2} \quad (3.2)$$

The first term represents plant growth, which is linearly related to water uptake. Here  $c$  is the conversion of water uptake by plants to plant growth [ $\text{g mm}^{-1} \text{ m}^{-2}$ ]. The second term covers both mortality and grazing losses, with  $m$  being the specific plant loss due to mortality and herbivory [ $\text{year}^{-1}$ ]. Plant dispersal is modelled with the last term. Here  $d_P$  is the dispersion rate of plants [ $\text{m}^2 \text{ year}^{-1}$ ].

### 3.2.3 Infiltration neglecting runon (for uniform case and interbands)

In this subsection we will solely consider the partitioning of rainwater into infiltration and runoff, and neglect runon, which we define as the infiltration of runoff generated uphill. This assumption is valid for uniform system states and interbands, as we will explain later.

The partitioning of rainwater into infiltration and runoff differs per rain event. In this model the infiltration rate during a given event  $i_{ev}$  [ $\text{mm hour}^{-1}$ ] is limited by either the infiltration capacity of the soil  $i_{cap}$  [ $\text{mm hour}^{-1}$ ] or the intensity of the rain event  $p_{ev}$  [ $\text{mm hour}^{-1}$ ], which is considered to be a random variable. In the former case not all rainwater infiltrates, but part is lost in the form of runoff. The infiltration rate  $i_{ev}$  for a rain event with intensity  $p_{ev}$  in a soil with infiltration capacity  $i_{cap}$  is given by:

$$i_{ev}(x, p_{ev}) = \begin{cases} p_{ev} & \text{if } p_{ev} < i_{cap}(x) \\ i_{cap}(x) & \text{if } p_{ev} \geq i_{cap}(x) \end{cases} \quad (3.3)$$

By using this relationship, we assume steady state infiltration conditions (Karssenberg, 2006). In other words: during the rain event  $i_{ev}$ ,  $p_{ev}$  and  $i_{cap}$  are constant over time. For soils with high sorptivity, this time independency results in underestimation of infiltration during short events and overestimation during long events. On average however, the error will be negligible provided that rainfall intensity and event duration are mutually independent. Notice that, although we consider infiltration to be independent of surface water depth (Horton, 1939; Philip, 1957), there may be situations, including soil cracking and crusting, in which surface water depth is important (Dunne et al., 1991; Fox et al., 1998; Novak et al., 2000).

The interarrival time between rain events is assumed to be sufficiently large, so that infiltration conditions, which are affected by antecedent soil moisture content, are similar for all events. With this assumption we neglect possible interactions between storm events, which allows analytical analysis of the model. Infiltration capacity  $i_{cap}$  increases with plant density  $P$  (Van

### 3 Rainfall intensity and semiarid ecosystems

Wijngaarden, 1985; Rietkerk et al., 2000; Thompson et al., 2010a) and is modelled with Equation 3.4.

$$i_{cap}(x) = i_0 + aP(x) \quad (3.4)$$

Here  $i_0$  is the infiltration capacity of bare soil [mm hour $^{-1}$ ], and  $a$  is the increase of infiltration capacity with plant density [mm m $^2$  hour $^{-1}$  g $^{-1}$ ].

We assume rainfall intensity  $p_{ev}$  to be an exponentially distributed random variable with mean  $\mu_{p_{ev}}$  [mm hour $^{-1}$ ] (Hoogmoed, 1981) that is uniform in space. Its probability density function is given by Equation 3.5.

$$f(p_{ev}) = \frac{1}{\mu_{p_{ev}}} e^{-\frac{p_{ev}}{\mu_{p_{ev}}}} \quad (3.5)$$

The fact that  $p_{ev}$  is a random variable, makes  $i_{ev}$  a random variable (if  $i_{cap} > 0$ ). In other words: the amount of water that infiltrates is different for each rain event. Although we consider infiltration to be a random process, the equilibrium analysis and model runs will be done using the expected value (or long term average) of  $i_{ev}$ . Thereby we assume the response of vegetation to individual rain events is slow. Working with the expected infiltration rate makes the model deterministic and allows studying the system's equilibria and the effects of changes in mean rainfall intensity on the system. Note, however, that the obtained solutions for  $P$  and  $W$  presented in Section 3.3 only approximate the expected values of  $P$  and  $W$  at first order. This means that we neglect the effects of variance and higher order moments of infiltration rate on available soil water and plant productivity.

The expected infiltration rate  $E(i_{ev})$  is obtained by summing the infiltration rates (Equation 3.3) over all possible event intensities ( $p_{ev} > 0$ ) while multiplying with the probability of occurrence of the events (Equation 3.5). As shown in Appendix 3.A this yields:

$$E(i_{ev}(x, p_{ev})) = \mu_{p_{ev}} \left( 1 - e^{-\frac{i_{cap}(x)}{\mu_{p_{ev}}}} \right) \quad (3.6)$$

If we assume the arrival of rain events to be a Poisson process (Bierkens and Puente, 1990) and the events to have a mutually independent duration and intensity (Hoogmoed, 1981), then the mean rainfall rate aggregated over a period of time  $p_{ag}$  [mm year $^{-1}$ ] is given by the product of the mean frequency of the events  $\lambda$  [year $^{-1}$ ], the mean duration of an event  $\tau$  [hour] and the mean rainfall intensity  $\mu_{p_{ev}}$  [mm hour $^{-1}$ ]. The aggregated infiltration rate  $i_{ag}(x)$  [mm year $^{-1}$ ], used in Equation 3.1, can now be written as function of

aggregated rainfall  $p_{ag}$ :

$$i_{ag}(x) = \lambda\tau E(i_{ev}(x, p_{ev})) = p_{ag} \frac{E(i_{ev}(x, p_{ev}))}{\mu_{p_{ev}}} = p_{ag} \left( 1 - e^{-\frac{i_{cap}(x)}{\mu_{p_{ev}}}} \right) \quad (3.7)$$

Similar to infiltration in the model by Rietkerk et al. (1997), the aggregated infiltration rate  $i_{ag}(x)$  increases asymptotically to  $p_{ag}$  for  $P \rightarrow \infty$ .

In this subsection, we neglected the infiltration of runoff produced uphill (runon). As mentioned, this assumption is valid under particular conditions. For example, if plant density and infiltration capacity are spatially homogeneous, runoff is produced if  $i_{cap}(x)$  is exceeded ( $p_{ev} > i_{cap}(x)$ ). However, if  $p_{ev} > i_{cap}(x)$  and if  $i_{cap}(x)$  is equal for all  $x$ , runoff will not infiltrate downhill as the maximum infiltration rate  $i_{cap}(x)$  is already reached for all  $x$ . In the case that  $p_{ev} < i_{cap}(x)$ , no runoff is generated at any  $x$ , and therefore runon can be neglected as well. If plant density is not uniform and infiltration capacity is spatially heterogeneous, still areas exist where runon does not occur and infiltration is approximated by Equation 3.7, as will be discussed in Section 3.2.5.

### 3.2.4 Infiltration including runon (non-uniform case)

In this subsection we will continue with the approach of Section 3.2.3, but now we include the infiltration of runoff produced uphill (runon). Runoff generation and its infiltration downhill are modeled similarly to Karssenberg (2006), with the difference that we use a spatially continuous formulation, which allows to calculate the expected infiltration rate as in the previous subsection. Runoff is generated where rainfall intensity  $p_{ev}$  exceeds infiltration capacity  $i_{cap}(x)$  and is transported downhill. Again two cases can be distinguished: (1) Infiltration rate  $i_{ev}(x)$  equals infiltration capacity  $i_{cap}(x)$  in areas where runoff is generated (i.e.  $p_{ev} > i_{cap}(x)$ ) and directly downhill of these areas due to runon. (2) In areas that do not receive surface water (e.g. due to depletion uphill) infiltration rate equals the rainfall intensity. A critical rainfall intensity  $\tilde{p}_{ev}(x)$  separates the two cases (see Figure 3.2):

$$i_{ev}(x, p_{ev}) = \begin{cases} p_{ev} & \text{if } p_{ev} < \tilde{p}_{ev}(x) \\ i_{cap}(x) & p_{ev} \geq \tilde{p}_{ev}(x) \end{cases} \quad (3.8)$$

The critical rainfall intensity  $\tilde{p}_{ev}(x)$  in mm hour<sup>-1</sup> is the minimum rainfall intensity required for surface water to reach position  $x$  on the hillslope and

### 3 Rainfall intensity and semiarid ecosystems

can be derived as follows.

In order for surface water to reach site  $x$ , the cumulative rainfall intensity uphill of  $x$  needs to exceed the cumulative infiltration capacity uphill of  $x$ . The cumulative infiltration capacity  $\hat{i}_{cap}$  [m mm hour $^{-1}$ ] upslope of  $x$  increases with distance  $l$  [m] from  $x$ .

$$\hat{i}_{cap}(l, x) = \int_{x-l}^x (i_{cap}(x')) dx' \quad (3.9)$$

Since rainfall is assumed to be spatially uniform, the cumulative rainfall intensity between  $x - l$  and  $x$ , ( $\hat{p}_{ev}$  in m mm hour $^{-1}$ ) is independent of  $x$  and is given by:

$$\hat{p}_{ev}(l, p_{ev}) = lp_{ev} \quad (3.10)$$

If  $\hat{p}_{ev}(l, p_{ev})$  exceeds  $\hat{i}_{cap}(l, x)$  for any positive value of  $l$ , surface water reaches  $x$ . The critical rainfall intensity equals the minimum rainfall intensity for which  $\hat{p}_{ev}(l, p_{ev}) = \hat{i}_{cap}(l, x)$  for some value of  $l$  (with  $l > 0$ ). From Equations 3.9 and 3.10 follows that the critical rainfall intensity is given by:

$$\tilde{p}_{ev}(x) = \min_{l>0} \left( \frac{\hat{i}_{cap}(l, x)}{l} \right) \quad (3.11)$$

Here  $\min()$  takes the minimum value of a given function. Note that by allowing  $l$  to have any positive value, we assume the hillslope to have an infinite length. If  $l$  tends to zero, then  $\frac{\hat{i}_{cap}(l, x)}{l}$  tends to  $i_{cap}(x)$ . Therefore, if the minimum in Equation 3.11 is located at  $l$  close to zero, then  $\tilde{p}_{ev}(x) = i_{cap}(x)$ . This is the case for some areas on the hillslope depicted in Figure 3.2.

The expected infiltration rate  $E(i_{ev})$  can again be obtained by summing the infiltration rates (Equation 3.8) over all possible event intensities ( $p_{ev} > 0$ ) while multiplying with the probability of occurrence of the events (Equation 3.5). As shown in Appendix 3.A, this yields:

$$E(i_{ev}(x, p_{ev})) = \mu_{p_{ev}} + (i_{cap}(x) - \tilde{p}_{ev}(x) - \mu_{p_{ev}}) e^{-\frac{\tilde{p}_{ev}(x)}{\mu_{p_{ev}}}} \quad (3.12)$$

The aggregated infiltration rate  $i_{ag}(x)$  [mm year $^{-1}$ ] used in Equation 3.1 now becomes:

$$i_{ag}(x) = p_{ag} + p_{ag} \left( \frac{i_{cap}(x) - \tilde{p}_{ev}(x)}{\mu_{p_{ev}}} - 1 \right) e^{-\frac{\tilde{p}_{ev}(x)}{\mu_{p_{ev}}}} \quad (3.13)$$

The full model is described by Equations 3.1, 3.2 and 3.13. In case of uniform infiltration conditions  $\tilde{p}_{ev} = i_{cap}$ , meaning that Equation 3.13 reduces to Equation 3.7.

Infiltration and runoff/runon process are modelled in a simple parsimonious way. Notice for example that hillslope gradient is not a parameter in Equation 3.13. This is because we assume instantaneous surface water redistribution: all runoff generated uphill infiltrates downhill as long as infiltration capacity is not met. Models that, besides spatial infiltration contrasts, also incorporate contrasts in surface roughness and resistance to flow, suggest that such sophisticated approaches are only required on terrains with a slope up to around 0.1% (Thompson et al., 2011). This supports our simplified approach, as the banded patterns we aim to model can only be found on hillslopes with a gradient greater than 0.2% to 0.25% (Valentin et al., 1999; Deblauwe et al., 2011). Finally, the spatial infiltration patterns depicted in Figure 3.2 are comparable, though less smooth, to those found by more advanced models (Thompson et al., 2011).

### 3.2.5 Competition for surface water and spatial feedbacks

The competition for surface water in this model is fundamentally different from other conceptual models that describe pattern formation in semiarid ecosystems (e.g. HilleRisLambers et al., 2001; Rietkerk et al., 2002; Gilad et al., 2004; Meron et al., 2007). These models do not consider soils to have a finite capacity to take up water. Instead, infiltration rate is considered to be a function of surface water depth which is modelled as a separate state variable. Since surface water accumulates on the bare interbands and is depleted as it is transported through the vegetation bands, bare areas positively affect infiltration in downhill vegetated areas while vegetated areas have a negative effect on the infiltration rate in the bare interbands in these models (see Appendix 3.B). The positive effect enables patterned states to exist under harsher conditions than would be the case if vegetation was uniformly distributed (Rietkerk et al., 2002; Sherratt and Lord, 2007), while the negative effect is responsible for the formation of patterns (Gierer and Meinhardt, 1972; Van de Koppel and Crain, 2006; Rietkerk and Van de Koppel, 2008) and explains why bare areas emerge when uniform cover is still possible (i.e. Turing instability).

In our model the positive effect is still active: runoff is generated on the bare interbands if rainfall intensity exceeds the infiltration capacity of bare soil (i.e.  $p_{ev} > i_0$ ) and feeds the vegetation bands where the infiltration

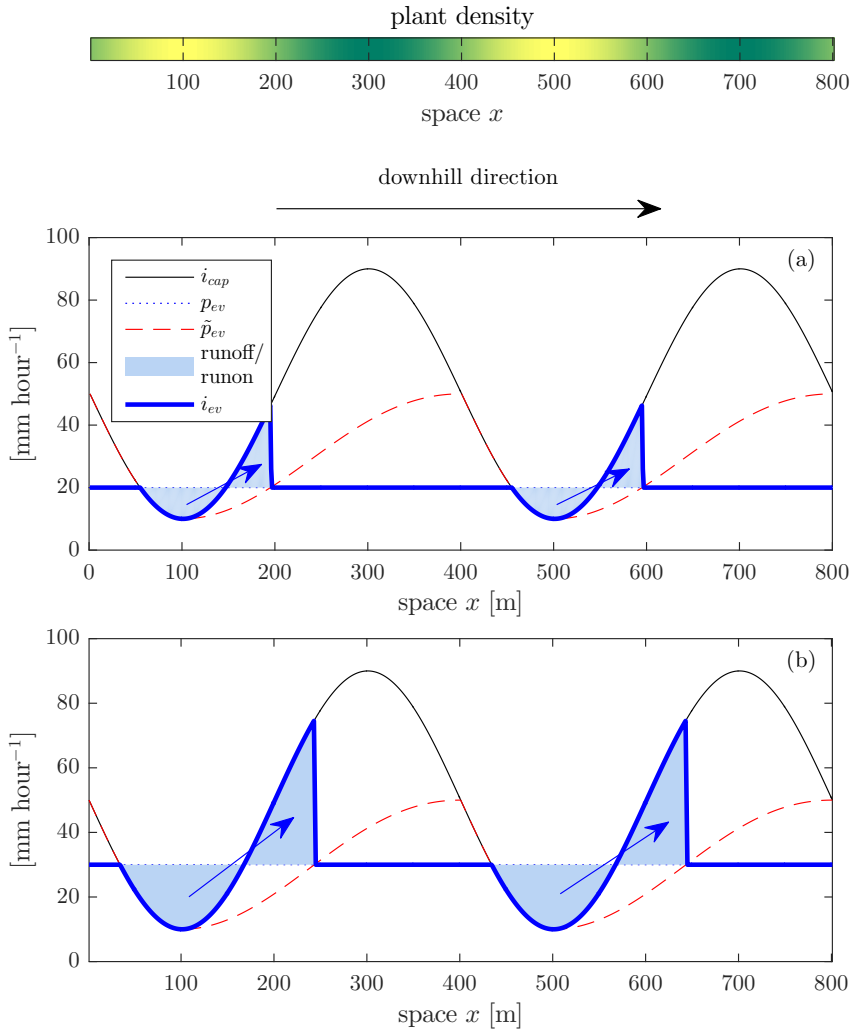


Figure 3.2: Infiltration capacity  $i_{cap}$ , critical rainfall intensity  $\tilde{p}_{ev}$  and infiltration rates  $i_{ev}$  for rain events with intensities  $p_{ev}$  of (a) 20 mm hour<sup>-1</sup> and (b) 30 mm hour<sup>-1</sup> on a hillslope with an imposed periodic pattern in plant density ( $P$  ranges from 0 to 40 g m<sup>-2</sup>). The critical rainfall intensity  $\tilde{p}_{ev}$  is the minimum rainfall intensity required for a particular location on the hillslope to receive surface water. The arrows indicate how the generated runoff is relocated. For some areas on the hillslope  $\tilde{p}_{ev}(x) = i_{cap}(x)$ . Notice that the amount of runon is equal to the amount of runoff that is generated and that surface water is transported further downhill during more intense rain events.

capacity is higher. However, the negative effect of the vegetation bands on the interbands is absent: the infiltration in the interbands is not affected by uphill vegetation. This is because runoff is only generated if  $p_{ev} > i_0$ , meaning that bare areas receive surface water only if, due to local rainfall, infiltration already occurs with a maximum rate of infiltration capacity. Consequently, additional infiltration due to runon does not occur on bare soil, regardless of rainfall intensity or the depth of the surface water layer. This means that for these areas Equation 3.13 reduces to Equation 3.7, meaning that infiltration in the interbands is independent of infiltration capacity uphill.

Because of the absence of a negative effect of areas with high plant densities on areas with lower plant densities, the behaviour of our model can be expected to differ from that of the mentioned conceptual models. This will be discussed in Section 3.3.

### 3.2.6 Parametrization and analysis

We implemented the model in MATLAB (Mathworks, 2012). The partial differential equations are solved numerically using a time-explicit scheme with a constant time step  $\Delta t$ . A vector of  $n$  elements, with each element having a length of  $\Delta x$ , represents the one dimensional hillslope.

The model can be analysed along only one spatial dimension, as we assume all water to flow downhill and neglect the exchange of surface water perpendicular to the hillslope. In models that do consider the exchange of water in this direction found that vegetation bands may break up to form dashed patterns (Von Hardenberg et al., 2001), which can also be found on imagery (Valentin et al., 1999). These patterns are not considered in our analysis.

In the model runs, Equation 3.11 was evaluated for  $0 < l \leq n\Delta x$  only. Following Klausmeier (1999); Rietkerk et al. (2002); Lejeune et al. (2004); Gilad et al. (2004); Sherratt and Lord (2007), we run the model using periodic boundary conditions. Thereby we minimize the boundary effects, such as deviating pattern orientation in proximity to ridges (McGrath et al., 2012) and increasing pattern wavelength close to streams (Penny et al., 2013), which makes our results independent of site-specific properties, such as topography. The use of periodic boundary conditions implies that we only consider the hillslope far from ridges and streams. Notice, however, that it does not imply that surface water cannot escape from the modelled hillslope: it is either depleted along the hillslope (as in Figure 3.2) or discarded once infiltration capacity is met along the entire hillslope.

### 3 Rainfall intensity and semiarid ecosystems

We performed runs of the model to study the patterned steady states. The model runs were initiated with random peaks in plant density in a fraction of the elements. To study the existence of stable patterned steady states with a particular wavelength, the peaks in plant density were distributed in a periodic fashion.

If environmental conditions, such as mean rainfall intensity, change, patterned states may cease to exist. The parameter range for which patterns with a particular wavelength exist was obtained using the bisection method (or binary search method) (Burden and Faires, 1985).

We analytically derived the uniform steady states of the system (expressed in plant density and water availability), as well as a rainfall range for which (patterned) vegetation and a stable bare desert state co-exist (as discussed in Appendices 3.C and 3.D). This information, combined with runs of the model, allowed to examine the response of the system to changes in aggregated rainfall rate  $p_{ag}$  and mean rainfall intensity  $\mu_{pev}$ . Table 3.1 gives an overview of the parameters used in the model.

## 3.3 Results

In this section we first describe the competition for water and feedbacks in the model on a local scale (Section 3.3.1) in order to understand the global behaviour of the model (Section 3.3.2). In Section 3.3.3, we will then discuss how the model responds to changes in rainfall intensity.

### 3.3.1 Competition for water along the hillslope

With the parameter values of Table 3.1, the model generates spatially periodic patterns in plant density along the hillslope (Figure 3.3a). These periodic vegetation bands migrate in uphill direction: colonization occurs directly uphill from the vegetation bands, while plant density slowly decays in the downhill part of the bands. This is in line with observations (Worrall, 1959; Deblauwe et al., 2012) and modelling studies (Klausmeier, 1999), although fixed patterns have also been reported (Thompson and Katul, 2009; Dunkerley, 2013). Available soil water is generally higher in the vegetation bands compared to the bare interbands, however a small depression in soil water availability can be found in the downhill part of the vegetation bands (Figure 3.3b).

Figure 3.3c shows the infiltration capacity  $i_{cap}(x)$  and critical rainfall intensity  $\tilde{p}_{ev}(x)$  in space. Expected infiltration rates (Equation 3.12) are high

Table 3.1: Parameter values, units and meaning. These parameter values are used throughout this work, unless indicated differently.

Parameter	Description	Value	Unit	Reference
$k$	Half saturation constant of soil water uptake	5	mm	Rietkerk et al. (2002)
$u$	Maximum specific water uptake	18	$\text{mm m}^2 \text{g}^{-1} \text{year}^{-1}$	Rietkerk et al. (1997)
$r$	Specific soil water loss due to evaporation and percolation	36	$\text{year}^{-1}$	Rietkerk et al. (1997)
$m$	Specific loss of plant density due to mortality and grazing	126	$\text{year}^{-1}$	Rietkerk et al. (1997)
$c$	The conversion of water uptake by plants to plant growth	10	$\text{g mm}^{-1} \text{m}^{-2}$	Rietkerk et al. (1997)
$d_P$	Dispersion rate of plants	36	$\text{m}^2 \text{year}^{-1}$	Rietkerk et al. (2002)
$d_W$	Diffusion rate of water	36	$\text{m}^2 \text{year}^{-1}$	Rietkerk et al. (2002)
$p_{ag}$	Aggregated rainfall rate	600	$\text{mm year}^{-1}$	Rietkerk et al. (2002)
$\mu_{pev}$	Mean intensity of the rain events	20	$\text{mm hour}^{-1}$	Deblauwe et al. (2008)*
$i_0$	Infiltration capacity of bare soil	10	$\text{mm hour}^{-1}$	Deblauwe et al. (2008)*
$a$	Increase of the infiltration capacity with plant density	2	$\text{mm m}^2 \text{hour}^{-1} \text{g}^{-1}$	Deblauwe et al. (2008)*
$\Delta t$	Time step size	$5 \cdot 10^{-4}$	year	
$\Delta x$	Cell length	0.2	m	
$n$	Number of elements	4000	-	

\*Parameters were calibrated to obtain patterns in a realistic rainfall range according to the mentioned study.

### 3 Rainfall intensity and semiarid ecosystems

if the critical rainfall intensity is low and infiltration capacity is high. The infiltration capacity increases linearly with plant density, following Equation 3.4, and is therefore higher for more densely vegetated soils. In the vegetation bands, critical rainfall intensity increases in downhill direction. This means that a higher rainfall intensity is required for runoff to occur in the downhill part as compared to the upslope part. In the interbands the critical rainfall intensity is equal to the infiltration capacity. Here runoff does not occur and the infiltration equation for the uniform case is valid (Equation 3.6).

When considering the effect of single rain events on the system, three types of rain events can be distinguished. *Low intensity events* have an intensity lower than the lowest infiltration capacity on the hillslope. These events do not trigger runoff generation, meaning that all rainwater infiltrates locally. Since the infiltration rate during such low intensity events is equal for every location along the hillslope, these events have a homogenizing effect on the spatial distribution of soil water and consequently vegetation. During *intermediate intensity events* runoff is generated on the bare interbands and is transported to the vegetation bands where it is fully depleted. Since runoff occurs in the uphill part of the vegetation bands and not in the downhill part spatial competition occurs: uphill vegetation negatively affects infiltration downhill. Such negative spatial interactions are a requirement for regular pattern formation (Gierer and Meinhardt, 1972; Van de Koppel and Crain, 2006; Rietkerk and Van de Koppel, 2008). During *high intensity events* the rainfall intensity exceeds the maximum critical rainfall intensity on the hillslope. Now surface water reaches all locations on the hillslope and infiltration rate equals infiltration capacity for the entire hillslope. Plants may still benefit from runoff produced uphill, however since surface water is not fully depleted on its way through the vegetation bands spatial competition does not occur. In addition, not all generated runoff is able to infiltrate downhill, meaning that some water flows through the vegetation bands and is eventually lost from the system.

The categorization of rain events as described above helps in understanding the response of the system when subject to changes in mean rainfall intensity, as discussed in Section 3.3.3.

#### 3.3.2 Alternative stable system states

Apart from the patterned state discussed so far, uniformly vegetated states and/or a bare desert state exist depending on parameter setting. Figure 3.4a shows a bifurcation diagram with aggregated rainfall  $p_{ag}$  as bifurcation

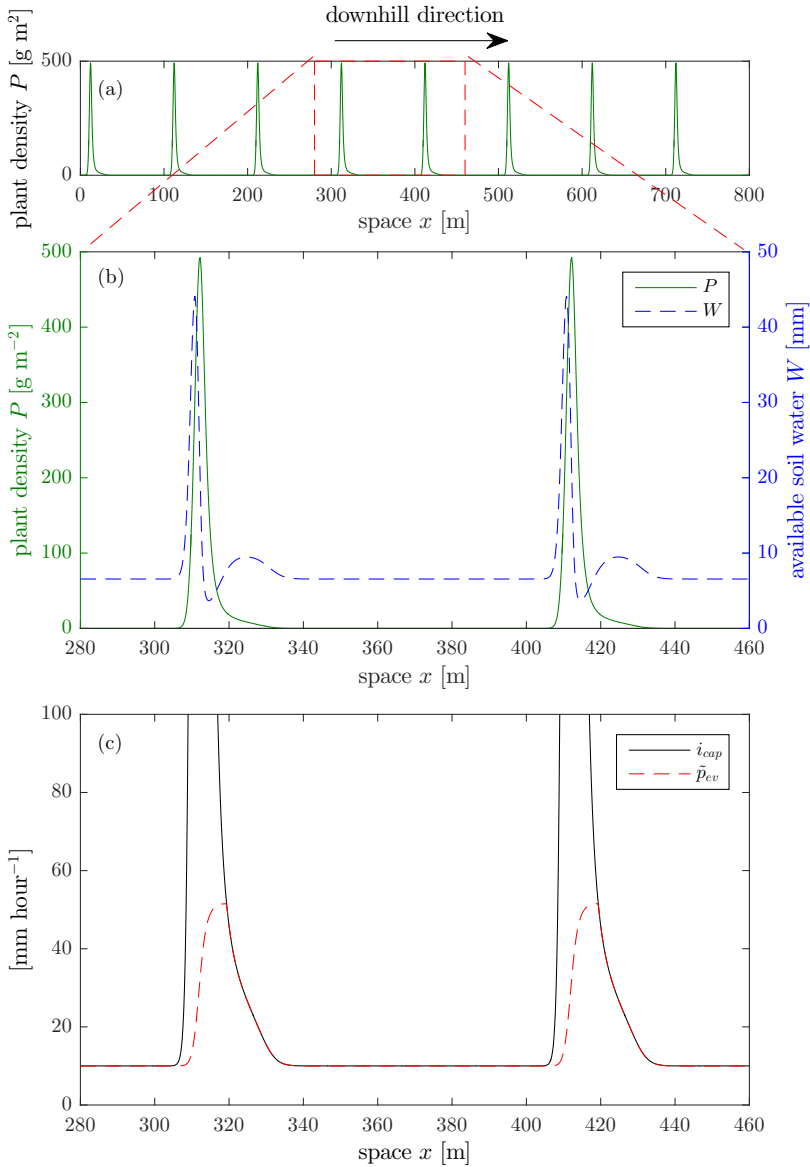


Figure 3.3: (a) Plant density  $P$  [g m<sup>-2</sup>], (b) plant density  $P$  [g m<sup>-2</sup>] and available soil water  $W$  [mm] and (c) infiltration capacity  $i_{cap}$  [mm hour<sup>-1</sup>] and critical rainfall intensity  $\tilde{p}_{ev}$  [mm hour<sup>-1</sup>] along the hillslope. Notice that the minimum infiltration capacity on the hillslope - separating low intensity events from intermediate intensity events - is equal to the infiltration capacity of bare soil  $i_0$ . The maximum critical rainfall intensity - separating intermediate intensity events from high intensity events - equals the mean infiltration capacity of the hillslope. In (c) infiltration capacities above 100 mm hour<sup>-1</sup> were cut off due to limited space. The peak infiltration capacity in the vegetation bands is about 1000 mm hour<sup>-1</sup>

### 3 Rainfall intensity and semiarid ecosystems

parameter and with a constant mean rainfall intensity  $\mu_{pev}$ . For high rainfall values only a uniformly vegetated state is stable and for very low rainfall values only a stable bare desert state exists. For intermediate aggregated rainfall values the system has alternative stable states: stable patterned states or a stable uniformly vegetated state coexist with a stable bare state.

Notice that multiple stable patterned states with different pattern wavelengths can exist for a given parameter configuration. For high wavelength patterns the plant density in the vegetation bands is higher compared to low wavelength patterns (see Figure 3.5). This is because high wavelengths come with a greater interband area, which enables plants to harvest more surface water (Yizhaq et al., 2005). We found that the plant density in the vegetation bands needs to be higher than a certain threshold value in order for plants to grow and ultimately sustain themselves. This minimum plant density depends on aggregated rainfall rate  $p_{ag}$  as shown in Figure 3.4b (see Appendix 3.C for a derivation). Since plant density in the vegetation bands increases with wavelength and because the minimum required plant density increases with aridity (Figure 3.4b), high wavelength patterns can persist under more arid conditions. As rainfall decreases, an adaptation of pattern wavelength occurs once a patterned state with a certain wavelength can no longer be sustained (Sherratt, 2013a). At low rainfall values ( $p_{ag} < 210 \text{ mm year}^{-1}$  for the current parameter setting) the minimum required plant density tends to infinity. Here stable patterned system states can not exist. For our model we were able to derive this lower rainfall limit at which patterned system states cease to exist (see Appendix 3.D).

$$p_{ag} = \frac{m\mu_{pev} e^{\frac{i_0}{\mu_{pev}}}}{ca} \quad (3.14)$$

This is the rainfall value at which desertification occurs: the transition from a vegetated (patterned) state to a bare desert state.

The upper rainfall limit for which patterns exist is equal to the rainfall value at which uniformly vegetated states cease to exist ( $p_{ag} \approx 700 \text{ mm year}^{-1}$  for the current parameter setting), meaning that stable patterned states and stable uniformly vegetated states do not coexist in this model. This can be explained by the absence of a negative effect of areas with high plant biomass on areas with lower plant biomass, as discussed in Section 3.2.5. Since no runoff occurs in the interbands, Equation 3.13 reduces to Equation 3.7, meaning these areas behave as if they are uniform system states. If no stable uniformly vegetated state exists ( $p_{ag} < 700 \text{ mm year}^{-1}$ ), plant density

decays to zero in the interbands directly downhill of the vegetation bands, as in the case of the model run of Figure 3.3. If however a stable uniform vegetated state does exist, plant density no longer decays in the interbands while the uphill parts of the vegetation bands keep propagating in uphill direction. This eventually results in a uniformly vegetated state.

A stable bare desert state exists for the entire parameter range in which patterns can be found. The desert state remains stable up to a rainfall level of  $p_{ag} \approx 1070 \text{ mm year}^{-1}$ . This value, above which revegetation occurs regardless of the amount of biomass introduced, can be obtained analytically (see Appendix 3.D):

$$p_{ag} = \frac{rW^*}{1 - e^{-\frac{i_0}{\mu_{pev}}}} \quad (3.15)$$

in which  $W^*$  is the resource level at which plant growth equals plant losses (Tilman, 1982):  $W^* = \frac{mk}{cu-m}$ .

Equations 3.14 and 3.15 give the aggregated rainfall rates between which the system can have alternative stable states and where respectively desertification and revegetation can be expected to occur. However, we found that desertification may as well occur at a much higher rainfall level than given by Equation 3.14. If the system is in a uniformly vegetated state and rainfall declines over time, a transition to a desert state occurs where uniformly vegetated states cease to exist. Such a transition is not preceded by the formation of vegetation patterns. This system behaviour can be attributed to the fact that in our model the patterned states are isolated from the uniform steady states. In most models, patterns arise from a uniformly vegetated state that becomes unstable to heterogeneous perturbations (Turing instability; Turing, 1953; Edelstein-Keshet, 1988). As a result, these models predict a sequence of uniform vegetation, patterned vegetation and desert with increasing aridity. In our model, in contrast, the uniformly vegetated state remains stable and patterns only form if the desert state is perturbed by sufficiently large perturbations. Notice that, although the bare desert state is stable up to  $p_{ag} \approx 1070 \text{ mm year}^{-1}$ , relatively small perturbations are required for revegetation to occur as  $p_{ag}$  increases (Figure 3.4), meaning that bare desert states are unlikely to be observed at such high rainfall values.

### 3.3.3 The response of the model to changes in rainfall intensity

So far we have seen that the ability of plants to harvest water depends on rainfall intensity and that during intense rain events an amount of rain water

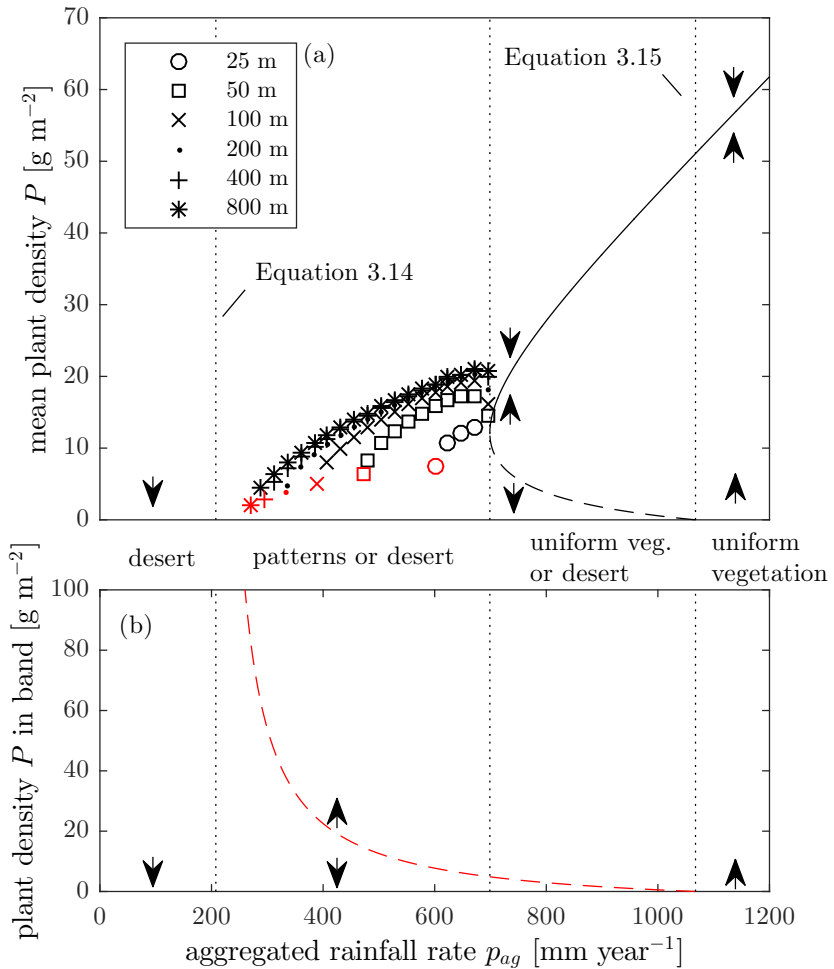


Figure 3.4: (a) The steady states of the system expressed in mean plant density  $P$  [g m $^{-2}$ ] plotted against aggregated rainfall rate  $p_{ag}$  [mm year $^{-1}$ ]. The solid and dashed lines depict the uniformly vegetated equilibria and can be written in terms of  $p_{ag}$  as shown in Appendix 3.C. For this parameter setting a stable uniform bare state exists for  $p_{ag} < 1070$  mm year $^{-1}$  (Equation 3.15). The markers show the mean plant density for patterned states with different wavelengths obtained with runs of the model. The red markers are obtained using the bisection method and depict the mean plant density at which the stable patterned states cease to exist. (b) The red dashed line shows the minimum plant density in a vegetation band required for plants to grow and ultimately sustain themselves (see Appendix 3.C for a derivation). For  $p_{ag} < 210$  mm year $^{-1}$  (Equation 3.14) infinite plant density is required to accomplish this. The arrows in (a) and (b) indicate whether plant density increases or decreases if the system is out of equilibrium.

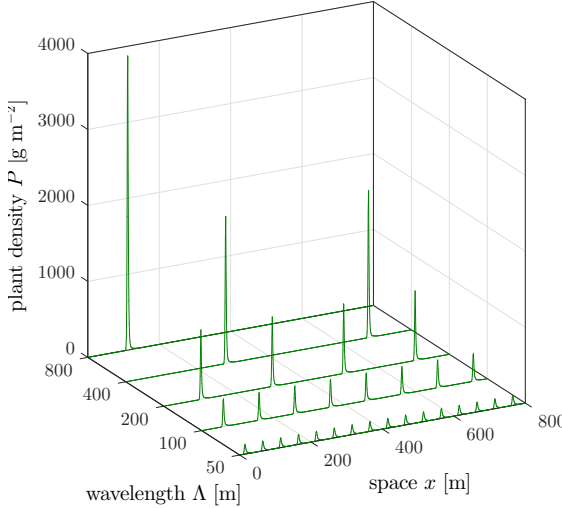


Figure 3.5: Patterns in plant density  $P$  with different wavelengths  $\Lambda$  but with a fixed parameter setting (Table 3.1). Notice that the plant density in the vegetation bands increases with wavelength, enabling high wavelength patterns to persist in drier climates (Figure 3.4b).

is lost from the system in the form of runoff (Section 3.3.1). In addition, we found that alternative stable states can co-exist, and that the rainfall range for which this occurs depends on mean rainfall intensity (Section 3.3.2). Using Equations 3.14 and 3.15 we can now study the response of the system to changes in mean rainfall intensity  $\mu_{pev}$ . Figure 3.6 shows that an increase in mean rainfall intensity will widen the rainfall range for which the system has alternative stable system states (this is the case only if  $\frac{m}{c} + \frac{rka}{i_0} > u$  as derived in Appendix 3.D). At low mean rainfall intensities, the system does not have alternative stable states and also patterns cannot exist. Short wavelength patterns are most likely to be observed in regions with high mean rainfall intensity. Plants can persist in very dry climates if the mean rainfall intensity is close to the infiltration capacity of bare soil  $i_0$  ( $\mu_{pev} = i_0$  is a minimum of Equation 3.14, see Appendix 3.D) and patterning is most likely to be observed where mean rainfall intensity is higher than the infiltration capacity of bare soil  $\mu_{pev} > i_0$ , which is consistent with observations that link vegetation patterns to low infiltrability of soils (Valentin et al., 1999).

The response of the system to changes in mean rainfall intensity is affected by model parameters that control infiltration into bare soil  $i_0$  and the impact

### 3 Rainfall intensity and semiarid ecosystems

of plants on soil structure  $a$  (Figure 3.7). The parameters  $i_0$  and  $a$  are related to soil type and vegetation composition. The infiltration capacity of sandy soils is generally higher than that of clayey soils, whereas vegetation composed of perennial grasses has a greater impact on soil structure when compared to annual grasses (Kelly and Walker, 1976; Rietkerk et al., 2000). Increasing mean rainfall intensity causes a more pronounced increase of the rainfall range with alternative stable states if the infiltration capacity of bare soil  $i_0$  is low and if the impact of plants on soil structure  $a$  is high. Also notice that plants can persist into higher aridity if bare soil infiltration capacity is low and if the impact of plants on soil structure is high.

As indicated by the arrows in Figure 3.6, changes in mean rainfall intensity can also induce a critical transition to a desert state or cause recovery from a desert state, even if aggregated rainfall rates remain unchanged. If the system is in a patterned state, an increase in mean rainfall intensity can result in desertification (arrow 1 in Figure 3.6). Such a transition is the result of an increased fraction of events that lead to runoff losses from the hillslope (high intensity events, as defined in Section 3.3.1) and is only possible if the mean rainfall intensity exceeds the infiltration capacity of bare soil  $i_0$ . The likelihood that desertification due to increasing mean rainfall intensity occurs is related to the slope of the lower rainfall limit, as given by Equation 3.14, and decreases with impact of plants on soil structure  $a$  (see Figure 3.7). As discussed in the previous subsection, a transition to a bare desert state can also occur if the system is in a uniformly vegetated state (arrow 2 in Figure 3.6).

Less intuitive is the fact that a transition to a desert state can result from a decrease in mean rainfall intensity (arrow 3 in Figure 3.6). This is caused by the fact that a decrease in mean rainfall intensity does not only lead to decreased runoff losses, but also to a lower fraction of events that are intense enough to trigger redistribution of water (intermediate and high intensity events as defined in Section 3.3.1). Consequently, more rainwater infiltrates locally and a greater fraction of the rainwater infiltrates in the bare interbands. As plants are absent in the interbands, this water is eventually lost due to soil evaporation and percolation. Desertification as a result of decreasing rainfall intensity can only occur if the system is in a patterned state (and if  $\frac{m}{c} + \frac{rka}{i_0(e-1)} > u$ ; see Appendix 3.D). If the system is in the desert state, decreasing rainfall intensity can also result in revegetation (if  $p_{ag} > rW^*$ ; arrow 4 in Figure 3.6).

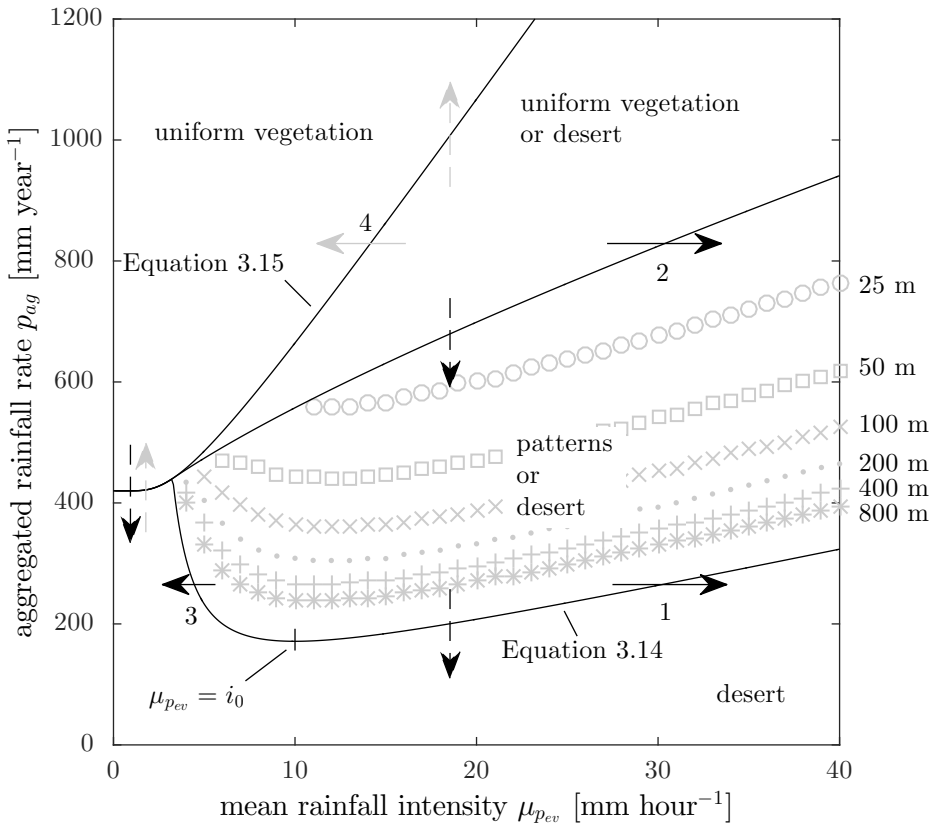


Figure 3.6: (a) Regions in  $(\mu_{p_{ev}}, p_{ag})$ -space for which uniform vegetation, patterns and/or desert states exist. The markers show the lower rainfall limits of patterned states with the indicated wavelengths and were obtained using the bisection method. The arrows indicate how changes in aggregated rainfall rate (dashed) and mean rainfall intensity (solid) can result in a transition to the desert state (black) or in recovery from a desert state (gray). The parameter regions were obtained by plotting Equations 3.14 and 3.15, as derived in Appendix 3.D. The border between uniform vegetation and patterned vegetation was obtained by finding the minimum of Equation 3.24. Note that, since rainfall intensity  $\mu_{p_{ev}}$  can change while aggregated rainfall  $p_{ag}$  remains constant 3.13, the interarrival time and/or event duration change along the  $x$ -axis, implying that the on the left end of this figure the rainfall is characterized by continuous drizzle, whereas on the right hand side rainfall consists of sporadic intense events.

### 3 Rainfall intensity and semiarid ecosystems

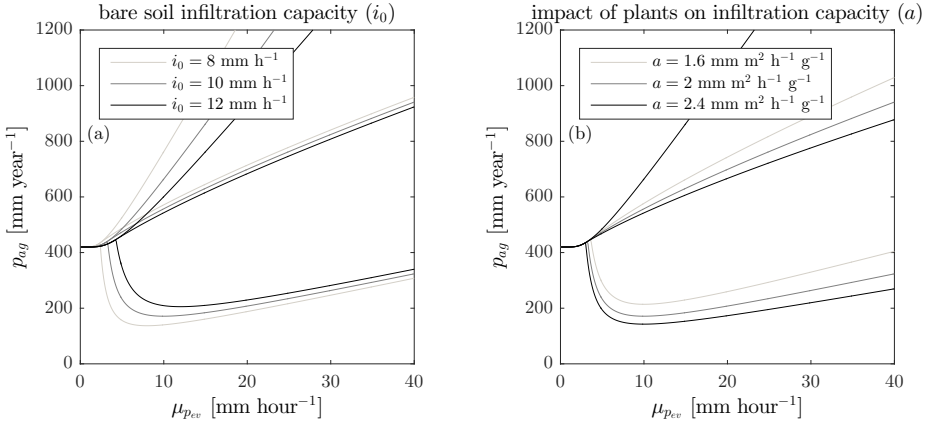


Figure 3.7: The parameter space as depicted in Figure 3.6, but now with different values for (a) bare soil infiltration capacity  $i_0$  [mm hour $^{-1}$ ] and (b) the increase of infiltration capacity with plant density  $a$  [mm m $^2$  hour $^{-1}$  g $^{-1}$ ].

## 3.4 Discussion and conclusions

In the coming decades global climate change may affect the functioning of ecosystems in a gradual or sometimes drastic manner. Model studies addressed that semiarid ecosystems can respond in a non-linear way to changes in variables like grazing and mean annual rainfall (Noy-Meir, 1975; Rietkerk et al., 1997). This means that gradual changes can lead to a rapid and significant loss of biological productivity, which is also referred to as desertification. While projections of global climate models are subject to much uncertainty regarding changes in mean annual and seasonal rainfall in arid and semiarid regions, strong trends in rainfall intensity have been reported (Tebaldi et al., 2006; Solomon et al., 2007). By combining an ecological model with a simple event based hydrological hillslope model, we were able to study the response of patterned semiarid ecosystems to changes in rainfall intensity.

From analysis of the model we conclude that projected increases in rainfall intensity can induce and enhance alternative stability of semiarid ecosystems. We found that periodically banded vegetation, resulting from surface water redistribution, cannot exist in regions with low mean rainfall intensity and that these ecosystems are less likely to be alternatively stable. Finally, we found that under certain conditions both an increase and a decrease in mean rainfall intensity can push the system over a critical threshold, resulting in a regime shift to a bare desert state. This finding was attributed to the fact

that water can be lost from the system in two ways. During high intensity rain events a fraction of the water flows through the vegetation bands and is lost as runoff, while during low intensity events a large portion of the water infiltrates in the bare interbands, where it is not available to plants and eventually lost due to soil evaporation and percolation.

The categorization of rain events into low, intermediate and high intensity events - as done in this paper to explain the response of the system to changes in mean rainfall intensity - is analogous to field observations by McDonald et al. (2009). In their study on the ecohydrology of banded vegetation patterns in the Chihuahuan Desert (USA), a threshold in storm size was identified above which a part of the runoff from interbands flows through the vegetated bands. In Section 3.3.1, we classified events with an intensity above this threshold as high intensity events. After small rain events wetting depths do not significantly differ between the vegetation bands and the interbands (low intensity events in our classification) (McDonald et al., 2009), while during larger storms infiltration in the vegetated bands was significantly higher (intermediate and high intensity events in our classification) (McDonald et al., 2009).

Our model differs from other conceptual models in that a (Turing unstable) uniformly vegetated system state and patterned system states do not co-exist in our model. This means that patterns cannot form out of uniform vegetation and that if the system is subject to change, a regime shift from a vegetated state to a desert state can occur without a warning in the form of vegetation patterns. We attribute this difference in model behaviour to model assumptions that lead to the absence of a negative effect of uphill vegetation on infiltration in the interbands. While we considered infiltration to be limited by the infiltration capacity of a soil, other conceptual models (HilleRisLambers et al., 2001; Rietkerk et al., 2002; Gilad et al., 2004; Meron et al., 2007) assume infiltration rates to be controlled by the depth of the surface water layer. Both infiltration models can be justified depending on the type system that is being considered, however, our study indicates that during model development infiltration models should be selected with care, as this choice can fundamentally affect the global behaviour of pattern formation models.

The minimalistic modelling approach used in this study enabled us to derive expressions for which the system exhibits alternative stable states and allowed us to derive the conditions required for the occurrence of critical transitions induced by changes in rainfall intensity. However, the choice for an analytically tractable and simplified model may have affected the

### 3 Rainfall intensity and semiarid ecosystems

presented findings in a number of ways.

Firstly, although the model captures the processes of infiltration and surface water redistribution in a hydrologically sensible way, it does not consider the possible interactions between rain events induced by antecedent soil moisture. If the interarrival time between rain events is short, i.e. in climates with frequent rain events (on left side of Figure 3.6), soils may be moist at the onset of a rain event leading to decreased infiltration capacities and possibly to the generation of runoff. A study by Baudena et al. (2007), shows similar mechanisms can lead to decreased productivity of drylands for interarrival times smaller than 3 days. In climates with infrequent high intensity events on the other hand, rainfall induced seal formation may significantly affect soil drying and consequently infiltration (Assouline and Mualem, 1997, 2002, 2003).

A second shortcoming of the model is that it does not fully account for the intermittent nature of rainfall, as it does not consider dry down periods and associated vegetation dynamics between rain events. In climates with sporadic high intensity rain events (on the right side of Figure 3.6) the length of these dry periods may have a great impact on plant mortality, while the effect of infiltration rates on plant growth is of less importance. Model studies show that models that do not consider the intermittent properties of rainfall systematically underestimate the productivity of semiarid ecosystems (Baudena et al., 2007; Baudena and Provenzale, 2008; Kletter et al., 2009). This underestimation is less pronounced if spatial feedbacks, such as resource redistribution due to infiltration contrasts, govern the system as in our model (Kletter et al., 2009; Baudena and Provenzale, 2008). Nonetheless, these effects may still be important if soil water uptake is non-linear (Kletter et al., 2009).

A third issue not accounted for in this study, is the fact that the magnitude of variability imposed on the system changes with rainfall intensity. Variability in infiltration rates (see Equation 3.18 in Appendix 3.A) and soil moisture (see Rodriguez-Iturbe et al. (1999)) are especially high at intermediate intensities. Variability in environmental conditions can affect model outcome in various ways. It can cause convergence of the system to a stochastically stable state between the two deterministically stable states (D'Odorico et al., 2005), it can result in a shrinkage of the region of bistability (Guttal and Jayaprakash, 2007), or it may induce the formation of patterns where one would expect uniform vegetation cover (D'Odorico et al., 2006).

Finally, microtopography can play an important role in infiltration and runoff generation. The hydrological part of our model is valid for sheet flow

### **3.A Derivation of first and second order moments of infiltration rate**

conditions, i.e. the surface water layer is deep compared to the depth of microtopographic depressions. This assumption is justified for sufficiently intense events, but for less intense events surface storage in depressions delays runoff initiation and increases infiltration locally (Thompson et al., 2010b). High intensity events on the other hand, may trigger changes in geomorphology. This may cause changes in flow patterns and infiltration, and may eventually affect vegetation patterning (Saco et al., 2007). We believe that studying such processes could be done by extending the framework presented here.

Future studies could attempt to verify our findings using areal images. For example, our model suggests that regular patterning only occurs in climatic regions with high mean rainfall intensities. If mean rainfall intensity is indeed a key parameter in explaining regular patterning, it can be used to further improve empirical predictive models such as the one by Deblauwe et al. (2008). Our study also suggests that changes in rainfall intensity may lead to increased resource losses, due to bare soil infiltration and runoff, and that these losses can potentially trigger desertification. Field data could be used to assess the rainfall intensities that separate the different event types as identified in our model study. These values, combined with the frequency distribution of rainfall intensity, can be used to estimate the fractional loss of water from the system in current and future climates, and may thereby help in assessing the proximity of semiarid ecosystems to critical thresholds.

## **Acknowledgments**

We thank Eric Siero, Arjen Doelman and Jens Rademacher for the fruitful discussions we had on the topic of patterning in semiarid ecosystems. This study is supported by a grant within the Complexity programme of the Netherlands Organization for Scientific Research (NWO). The research of MB and MR is also supported by funding from the European Union's Seventh Framework Programme (FP7/2007-2013) under grant agreement no. 283068 (CASCADE).

## **Appendix 3.A Derivation of first and second order moments of infiltration rate**

Equation 3.6 is the expected infiltration rate when neglecting runoff and is based on Equation 3.5 and Equation 3.3. The expected infiltration rate can

### 3 Rainfall intensity and semiarid ecosystems

be derived as follows.

$$\begin{aligned}
E(i_{ev}) &= \int_0^\infty i_{ev} f(p_{ev}) dp_{ev} \\
&= \int_0^{i_{cap}} p_{ev} f(p_{ev}) dp_{ev} + \int_{i_{cap}}^\infty i_{cap} f(p_{ev}) dp_{ev} \\
&= \int_0^{i_{cap}} \frac{p_{ev}}{\mu_{p_{ev}}} e^{-\frac{p_{ev}}{\mu_{p_{ev}}}} dp_{ev} + \int_{i_{cap}}^\infty \frac{i_{cap}}{\mu_{p_{ev}}} e^{-\frac{p_{ev}}{\mu_{p_{ev}}}} dp_{ev} \\
&= \left[ -(\mu_{p_{ev}} + p_{ev}) e^{-\frac{p_{ev}}{\mu_{p_{ev}}}} \right]_0^{i_{cap}} + \left[ -i_{cap} e^{-\frac{p_{ev}}{\mu_{p_{ev}}}} \right]_{i_{cap}}^\infty \\
&= \mu_{p_{ev}} - (\mu_{p_{ev}} + i_{cap}) e^{-\frac{i_{cap}}{\mu_{p_{ev}}}} + i_{cap} e^{-\frac{i_{cap}}{\mu_{p_{ev}}}} \\
&= \mu_{p_{ev}} \left( 1 - e^{-\frac{i_{cap}}{\mu_{p_{ev}}}} \right)
\end{aligned} \tag{3.16}$$

The expected infiltration rate including runon (Equation 3.12) is based on Equation 3.5 and 3.8:

$$\begin{aligned}
E(i_{ev}) &= \int_0^\infty i_{ev} f(p_{ev}) dp_{ev} \\
&= \int_0^{\tilde{p}_{ev}} p_{ev} f(p_{ev}) dp_{ev} + \int_{\tilde{p}_{ev}}^\infty i_{cap} f(p_{ev}) dp_{ev} \\
&= \int_0^{\tilde{p}_{ev}} \frac{p_{ev}}{\mu_{p_{ev}}} e^{-\frac{p_{ev}}{\mu_{p_{ev}}}} dp_{ev} + \int_{\tilde{p}_{ev}}^\infty \frac{i_{cap}}{\mu_{p_{ev}}} e^{-\frac{p_{ev}}{\mu_{p_{ev}}}} dp_{ev} \\
&= \left[ -(\mu_{p_{ev}} + p_{ev}) e^{-\frac{p_{ev}}{\mu_{p_{ev}}}} \right]_0^{\tilde{p}_{ev}} + \left[ -i_{cap} e^{-\frac{p_{ev}}{\mu_{p_{ev}}}} \right]_{\tilde{p}_{ev}}^\infty \\
&= \mu_{p_{ev}} - (\mu_{p_{ev}} + \tilde{p}_{ev}) e^{-\frac{\tilde{p}_{ev}}{\mu_{p_{ev}}}} + i_{cap} e^{-\frac{\tilde{p}_{ev}}{\mu_{p_{ev}}}} \\
&= \mu_{p_{ev}} + (i_{cap} - \tilde{p}_{ev} - \mu_{p_{ev}}) e^{-\frac{\tilde{p}_{ev}}{\mu_{p_{ev}}}}
\end{aligned} \tag{3.17}$$

### 3.B Feedbacks between vegetation bands and interbands if infiltration is depth dependent.

The variance in infiltration rate is related to the mean rainfall intensity  $\mu_{pev}$  as shown in Equation 3.18.

$$\begin{aligned}
 \text{VAR}(i_{ev}) &= \int_0^{\infty} (i_{ev} - \text{E}(i_{ev}))^2 f(p_{ev}) dp_{ev} \\
 &= \int_0^{i_{cap}} (p_{ev} - \text{E}(i_{ev}))^2 f(p_{ev}) dp_{ev} + \int_{i_{cap}}^{\infty} (i_{cap} - \text{E}(i_{ev}))^2 f(p_{ev}) dp_{ev} \\
 &= \int_0^{i_{cap}} \frac{(p_{ev} - \text{E}(i_{ev}))^2}{\mu_{pev}} e^{-\frac{p_{ev}}{\mu_{pev}}} dp_{ev} + \int_{i_{cap}}^{\infty} \frac{(i_{cap} - \text{E}(i_{ev}))^2}{\mu_{pev}} e^{-\frac{p_{ev}}{\mu_{pev}}} dp_{ev} \\
 &= \left[ -(\mu_{pev}^2 + (\text{E}(i_{ev}) - \mu_{pev} - p_{ev})^2) e^{-\frac{p_{ev}}{\mu_{pev}}} \right]_0^{i_{cap}} \\
 &\quad + \left[ -(i_{cap} - \text{E}(i_{ev}))^2 e^{-\frac{p_{ev}}{\mu_{pev}}} \right]_{i_{cap}}^{\infty} \\
 &= \mu_{pev}^2 + (\text{E}(i_{ev}) - \mu_{pev})^2 + 2\mu_{pev}(\text{E}(i_{ev}) - \mu_{pev} - i_{cap}) e^{-\frac{i_{cap}}{\mu_{pev}}} \\
 &= \mu_{pev} \left( \mu_{pev} - 2i_{cap} e^{-\frac{i_{cap}}{\mu_{pev}}} - \mu_{pev} e^{-2\frac{i_{cap}}{\mu_{pev}}} \right)
 \end{aligned} \tag{3.18}$$

For  $0 < \mu_{pev} \ll i_{cap}$  the variance increases quadratically with  $\mu_{pev}$ . The variance in infiltration rate reaches a maximum at  $\mu_{pev} \approx 0.89i_{cap}$ , after which it slowly declines with increasing rainfall intensity. A similar response can be found in soil moisture variance (Rodriguez-Iturbe et al., 1999) which is not only determined by the mean rainfall depth (the product of rainfall intensity and duration) but also by the interarrival time or frequency of the rain events and soil water losses.

## Appendix 3.B Feedbacks between vegetation bands and interbands if infiltration is depth dependent.

In the model presented in this paper infiltration rate is independent of surface water depth. In most models that generate patterns and that account for a surface water related pattern forming mechanism, infiltration rate is (linearly) related to surface water depth. An equation commonly used in conceptual

### 3 Rainfall intensity and semiarid ecosystems

models is given by Equation 3.19 (HilleRisLambers et al., 2001; Rietkerk et al., 2002; Gilad et al., 2004; Meron et al., 2007).

$$I(O, P) = \alpha O \frac{P + kW_0}{P + k} \quad (3.19)$$

Here  $I$  is the infiltration rate,  $\alpha$  is the maximum infiltration rate,  $O$  is the surface water depth,  $P$  is the plant density,  $k$  is a half saturation constant and  $W_0$  is the fraction of water that infiltrates in absence of plants.

Modeling infiltration with surface water depth dependence, as in Equation 3.19, results in a negative effect of the vegetation bands on the bare interbands because surface water is depleted in the vegetation bands and consequently surface water depth is lower downhill of vegetation bands (see Figure 3.8a,b). As a result infiltration rate in the interbands is lower than in absence of vegetation bands as shown in Figure 3.8c,d.

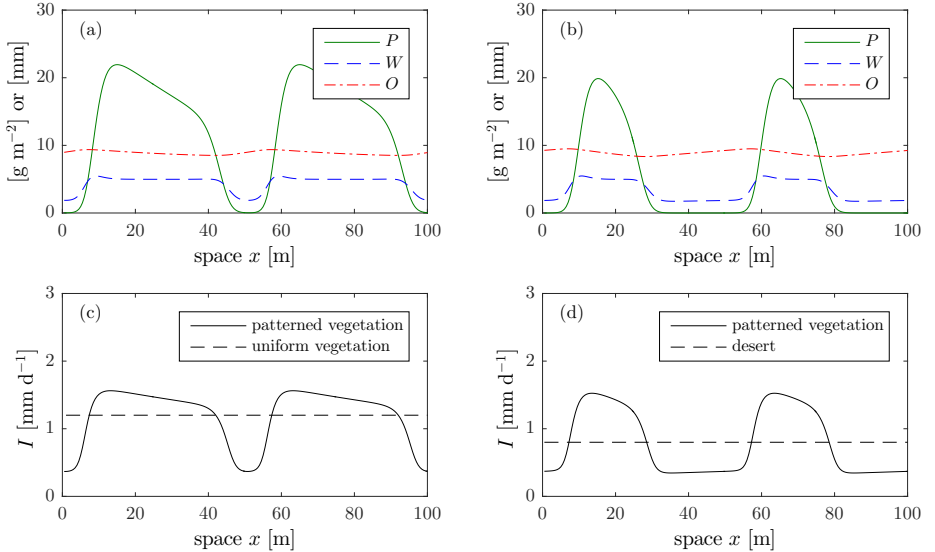


Figure 3.8: (a,b) Surface water  $O$  [mm], soil water  $W$  [mm] and plant density  $P$  [ $\text{g m}^{-2}$ ] along a hillslope generated using a one dimensional version of the model by Rietkerk et al. (2002) with mortality rate  $d = 0.25 \text{ day}^{-1}$ , downhill flow rate  $v = 10 \text{ m day}^{-1}$  and surface water diffusion  $D_O = 0 \text{ m}^2 \text{ day}^{-1}$ . In (a) rainfall rate  $R = 1.2 \text{ mm day}^{-1}$  and in (b)  $R = 0.8 \text{ mm day}^{-1}$ . Surface water flows from left to right. (c,d) Infiltration rate  $I$  [ $\text{mm day}^{-1}$ ] for the patterned states of (a,b) (solid line) and for uniform states (dashed line).

## Appendix 3.C Bifurcation diagram

The equilibria shown in Figure 3.4 can be derived by setting Equation 3.1 and 3.2 to zero and neglecting diffusion terms  $d_W \frac{\partial^2 W}{\partial x^2} = d_P \frac{\partial^2 P}{\partial x^2} = 0$ .

$$\frac{\partial W}{\partial t} = i_{ag} - u \frac{W}{W+k} P - rW = 0 \quad (3.20)$$

$$\frac{\partial P}{\partial t} = cu \frac{W}{W+k} P - mP = 0 \quad (3.21)$$

Solving gives:

$$\begin{aligned} \frac{\partial W}{\partial t} &= 0 \text{ at:} \\ W &= \frac{i_{ag} - uP - rk \pm \sqrt{(uP + rk - i_{ag})^2 + 4rki_{ag}}}{2r} \end{aligned} \quad (3.22)$$

$$\begin{aligned} \frac{\partial P}{\partial t} &= 0 \text{ at:} \\ P &= 0 \text{ and } W^* = \frac{mk}{cu - m} \end{aligned} \quad (3.23)$$

By plotting solutions 3.22 and 3.23 with  $\tilde{p}_{ev} = i_{cap}$  we obtain the phase planes for the homogeneous system shown in Figure 3.9. The stability and the number of system states changes with aggregated rainfall rate  $p_{ag}$ . The behavior of the system is very similar to the original model by Rietkerk et al. (1997). The isocline of soil water availability losses its humped shape if rainfall intensity is low, meaning that the transition from and to a bare desert state becomes supercritical (see Figure 3.6).

The uniform steady states depicted in Figure 3.4a were obtained by writing aggregated rainfall as a function of plant density:

$$p_{ag} = \frac{\frac{m}{c}P + rW^*}{1 - e^{-\frac{i_0 + aP}{\mu_{pev}}}} \quad (3.24)$$

The minimum plant density needed for plants to grow or sustain in Figure 3.4b is basically an unstable equilibrium above which the plant density in a vegetation band on an infinitely long bare hillslope increases. The soil uphill of the vegetation band is bare, therefore runoff will occur if  $p_{ev} > i_0$ , meaning that the critical rainfall intensity  $\tilde{p}_{ev}$  can be assumed to equal the infiltration capacity of bare soil  $i_0$ . Since the hillslope is assumed to be

### 3 Rainfall intensity and semiarid ecosystems

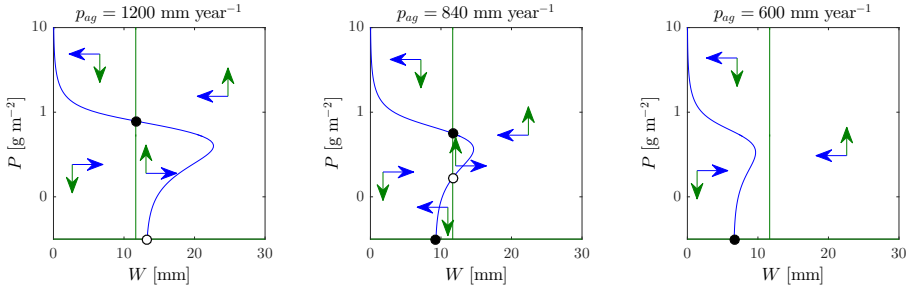


Figure 3.9: Phase planes for uniform conditions ( $dW \frac{\partial^2 W}{\partial x^2} = dP \frac{\partial^2 P}{\partial x^2} = 0$  and  $\tilde{p}_{ev} = i_{cap}$ ) with decreasing aggregated rainfall rates. In blue the isocline of available soil water ( $\frac{dW}{dt} = 0$ , Equation 3.22). In green the isoclines of plant density ( $\frac{dP}{dt} = 0$ , Equation 3.23). The system is in equilibrium if  $\frac{dW}{dt} = \frac{dP}{dt} = 0$ , i.e. where the isoclines intersect. Open circles indicate unstable equilibria and closed circles indicate stable equilibria. The vectors show the direction of change if the system is out of equilibrium.

infinitely long, runoff occurs along the full width of the vegetation band. We again need to neglect losses of soil water and plant density due to diffusion  $dW \frac{\partial^2 W}{\partial x^2} = dP \frac{\partial^2 P}{\partial x^2} = 0$ , meaning that the vegetation band needs to be sufficiently wide so that in its center diffusion losses approach zero. The phase planes depicted in Figure 3.10 can again be obtained by plotting solutions 3.22 and 3.23, but now with  $\tilde{p}_{ev} = i_0$ .

The curve of minimum plant density required for recovery as depicted in Figure 3.4 was obtained by writing aggregated rainfall as a function of plant density:

$$p_{ag} = \frac{\frac{m}{c}P + rW^*}{1 + \left(\frac{aP}{\mu_{pev}} - 1\right)e^{-\frac{i_0}{\mu_{pev}}}} \quad (3.25)$$

## Appendix 3.D Region with alternative stable system states

### 3.D.1 Upper rainfall limit

Equation 3.26 (Equation 3.15 in main text) gives the highest value of  $p_{ag}$  for which the system has multiple stable system states (solid line in Figure 3.6b). Here the bare desert state changes stability: the isoclines for available soil water and plant density intersect at  $P = 0$ . Equation 3.26 can be obtained by filling in  $P = 0$  in Equation 3.24.

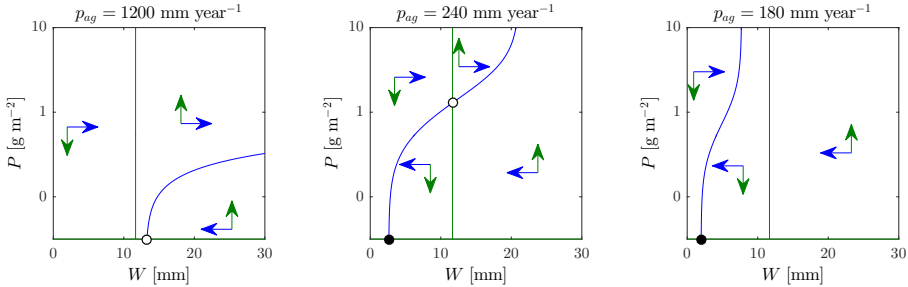


Figure 3.10: See caption of Figure 3.9 but now  $\tilde{p}_{pev} = i_0$  and  $P$  reflects the plant density in a vegetation band. Notice that plant density either decreases to zero or increases to infinity. The latter is due to the fact that we neglect the diffusion losses ( $dW \frac{\partial^2 W}{\partial x^2} = dP \frac{\partial^2 P}{\partial x^2} = 0$ ) that, in the full model, would slow down plant growth as plant density increases.

$$p_{ag} = \frac{rW^*}{1 - e^{-\frac{i_0}{\mu_{pev}}}} \quad (3.26)$$

The derivative of Equation 3.26 with respect to mean rainfall intensity  $\mu_{pev}$  is given by:

$$\frac{dp_{ag}}{d\mu_{pev}} = \frac{i_0 r W^* e^{\frac{i_0}{\mu_{pev}}}}{\mu_{pev}^2 (e^{\frac{i_0}{\mu_{pev}}} - 1)^2} \quad (3.27)$$

Given that  $cu > m$  ( $W^* > 0$ ) and that all parameter values are positive,  $\frac{dp_{ag}}{d\mu_{pev}} > 0$ . This means that the aggregated rainfall required for recovery from the desert state increases with rainfall intensity.

As the mean rainfall intensity  $\mu_{pev}$  increases, Equation 3.26 approaches a asymptote with a constant slope:

$$\left. \frac{dp_{ag}}{d\mu_{pev}} \right|_{\mu_{pev} \rightarrow \infty} = \frac{rW^*}{i_0} \quad (3.28)$$

### 3.D.2 Lower rainfall limit

Assuming that alternative stable (patterned) states exists as long as the plant density is required to recover from the bare state is finite, the lower limit of the region with alternative stable system states is given by Equation 3.29 (Equation 3.14 in main text). This is the aggregated rainfall rate  $p_{ag}$  that is

### 3 Rainfall intensity and semiarid ecosystems

approached as  $P \rightarrow \infty$  in Equation 3.25.

$$p_{ag} = \frac{m\mu_{pev} e^{\frac{i_0}{\mu_{pev}}}}{ca} \quad (3.29)$$

The derivative of Equation 3.29 with respect to mean rainfall intensity  $\mu_{pev}$  is given by:

$$\frac{dp_{ag}}{d\mu_{pev}} = \frac{m(\mu_{pev} - i_0)e^{\frac{i_0}{\mu_{pev}}}}{ca\mu_{pev}} \quad (3.30)$$

Equation 3.30 is positive if  $\mu_{pev} > i_0$  and negative if  $\mu_{pev} < i_0$ . A minimum of Equation 3.29 can be found at  $\mu_{pev} = i_0$ . As the rainfall intensity  $\mu_{pev}$  increases, Equation 3.29 approaches an asymptote with slope:

$$\left. \frac{dp_{ag}}{d\mu_{pev}} \right|_{\mu_{pev} \rightarrow \infty} = \frac{m}{ca} \quad (3.31)$$

#### 3.D.3 Robustness of the presented model results

In the main text (subsection 3.3.3) we state that if the aggregated rainfall rate remains unchanged, then both an increase and a decrease in mean rainfall intensity can result in desertification. In addition, we claim that the bistable region, in terms of aggregated rainfall, increases with mean rainfall intensity. These findings hold for the parameter combination listed in Table 3.1 as shown in Figure 3.6. Here we study the robustness of these findings: what are parameter combinations required for these findings to be valid?

Assuming that the transition from a patterned state to a desert state occurs at an aggregated rainfall rate given by Equation 3.29, both an increase and a decrease in mean rainfall intensity can result in desertification, only if the second derivative of Equation 3.29 with respect to  $\mu_{pev}$  in  $\mu_{pev} = i_0$  is positive:

$$\left. \frac{d^2 p_{ag}}{d\mu_{pev}^2} \right|_{\mu_{pev} = i_0} = \frac{me}{i_0 ac} > 0 \quad (3.32)$$

This is always true since all parameter values are positive. Desertification induced by declining mean rainfall intensity can only occur if the desert state is stable at this minimum. Filling in  $\mu_{pev} = i_0$  in Equation 3.26 and 3.29 results in the following condition:

### 3.D Region with alternative stable system states

$$\frac{rW^*}{1 - e^{-1}} > \frac{mi_0e}{ca} \quad (3.33)$$

Rewriting gives:

$$\frac{m}{c} + \frac{rka}{i_0(e - 1)} > u \quad (3.34)$$

The region of bistability, in terms of aggregated rainfall, increases with mean rainfall intensity. This is always true for  $\mu_{p_{ev}} \leq i_0$ , since here the slope of the lower rainfall limit (Equation 3.30) is negative while the slope of the upper rainfall limit is positive (Equation 3.27). From Equation 3.28 and 3.31 follows that for high values of mean rainfall intensity, the bistable region increases with mean rainfall intensity if:

$$\frac{rW^*}{i_0} > \frac{m}{ca} \quad (3.35)$$

Rewriting gives:

$$\frac{m}{c} + \frac{rka}{i_0} > u \quad (3.36)$$



# **4 Soil water repellency: a potential driver of vegetation dynamics in coastal dunes.**

Siteur, K., Mao, J., Nierop, K. G. J., Rietkerk, M., Dekker, S. C. and Eppinga, M. B. (2016). Soil water repellency: a potential driver of vegetation dynamics in coastal dunes. Accepted for publication in *Ecosystems*.

## **Abstract**

Coastal dunes are valuable and complex ecosystems, meaning that predicting their response to anthropogenic pressure is challenging. A potential driver of complexity that links soil, water and vegetation dynamics is soil water repellency (SWR). SWR is mainly caused by plant-derived hydrophobic compounds that are released during litter decomposition, and leads to dry sandy soils resisting infiltration of precipitation. Until now, studies have focused on soil physical and chemical properties associated with SWR, but the potential of SWR generating soil-water-vegetation feedbacks that drive ecosystem dynamics is yet to be assessed. This study assessed the role of SWR on coastal dune ecosystem dynamics by combining field observations and laboratory experiments with theoretical ecological modelling that incorporated the empirically established relationships. We observed large differences in soil infiltration capacity in the field, and the laboratory experiments showed that soil hydrophobic compound concentrations and antecedent soil moisture conditions can explain these differences. Theoretical model analyses suggested that SWR can trigger cyclic vegetation dynamics, including long periods in which vegetation is absent. Water competitive plants with low hydrophobic compound content (e.g. woody species) exhibit stable temporal dynamics, whereas species with opposite traits (e.g. grasses) are more likely to induce cyclic dynamics. For the latter species, SWR can amplify drought stress. In northwest Europe this effect could become more important in coming decades due to the projected increases in drought severity. Our study explains how SWR may contribute to coastal dune ecosystem complexity, providing insights that may aid effective dune conservation and restoration.

## 4.1 Introduction

Coastal dune ecosystems provide a broad range of natural and socio-economic functions (Everard et al., 2010), motivating conservation and restoration efforts in northwest Europe (Jensen, 1994; Grootjans et al., 2001; Van Der Meulen et al., 2004). Managing coastal dunes is complicated, as the stability and dynamics of these systems are controlled by an interplay between wind erosion, sand supply and vegetation dynamics (Aagaard et al., 2007; Klijn, 1990; Arens et al., 2007). In turn, these factors are affected by on-going changes in climate and human activities. Due to the inherent complexity of coastal dunes it is difficult to assess the impact of such changes on dune dynamics (Provoost et al., 2009). Vegetation significantly contributes to the complexity of coastal dunes. Vegetation displays long term dynamics with the abundance of dominant plant species varying over centuries (Zagwijn, 1970) but also short term dynamics driven by seasonality (Xu et al., 2013). Seasonal changes in temperature and precipitation, for example, control the productivity of plants. In addition, vegetation in coastal dunes shows strong spatial heterogeneity and generally has a very diverse composition. Finally, complex developments of vegetation, such as retrogression, have been reported (Van Dorp et al., 1985; Van der Maarel et al., 1985).

To understand the factors that control the complexity of the coastal dune ecosystem, interactions between vegetation and the abiotic environment need to be considered (Le Bagousse-Pinguet et al., 2013; Adema and Grootjans, 2003). In this context, the relationship between vegetation and available soil water deserves particular interest (Voortman et al., 2015), as climate change is projected to include increasing severity of summer droughts in northwest Europe (KNMI, 2014). This change may have undesired consequences for vegetation composition and cover, as well as groundwater recharge and wind erosion (Witte et al., 2008). When considering potential responses to changing precipitation patterns, soil hydrophobicity, a widely observed property of dry sandy dune soils, may be important to consider (Dekker and Jungerius, 1990; Ritsema et al., 1993). This property is commonly referred to as soil water repellency (SWR). SWR is caused by hydrophobic compounds in the soil that mainly originate from plants (Bisdom et al., 1993; DeBano, 2000; Horne and McIntosh, 2000; De Blas et al., 2013) and to a lesser extent from microorganisms (Home, 2015; McGhie and Posner, 1980). These soil hydrophobic compounds differ in concentration and composition depending on their origin and they also vary in their impact on SWR (Mao et al., 2014, 2015). SWR is a potentially important driver of dune vegetation

dynamics as it may hamper infiltration of water into the rootzone, thereby negatively affecting plant productivity. However, previous studies on SWR have mostly focused on soil characteristics (Dekker and Ritsema, 1996; Doerr et al., 2000; Doerr and Thomas, 2000) or on the identification of compounds at the molecular level (Franco et al., 1995, 2000; De Blas et al., 2013; Mao et al., 2014, 2015). Hence, how SWR mediates the relationship between vegetation and soil water availability, and what the consequences of this altered relationship are for ecosystem functioning remains to be investigated.

To assess the role of SWR in coastal dune ecosystem functioning, the relative importance of feedbacks associated with SWR needs to be understood. Three feedbacks may potentially be important regarding the role of SWR on ecosystem level. The first feedback is a negative feedback between plants and available water, which results from the positive effect of available water on plant growth and the negative effect of plant biomass on water through water uptake. A second negative feedback is caused by accumulation of hydrophobic compounds in the soil through the decomposition of plant litter, which hampers infiltration and subsequent plant growth, resulting in less plant biomass and decreased litter production. Finally, a positive feedback could be caused by the fact that SWR only occurs on dry soils (Dekker and Ritsema, 1994, 1996; Doerr and Thomas, 2000). For a given amount of precipitation, SWR may cause dry soils to remain dry, while the same amount of precipitation may lead to additional wetting of (already) wet soils. The relative contribution of these feedbacks on ecosystem dynamics may depend strongly on plant species traits, such as water competitiveness, which controls the feedback between plants and available water, and hydrophobic compound content of plant tissue, which affects the accumulation of hydrophobic compounds in the soil and consequently its repellency. However, a systematic analysis of these three feedbacks within a modelling framework is required to understand how they interactively affect the coastal dune ecosystem dynamics.

This study aims to incorporate the described feedbacks into an ecological model in order to understand the role of SWR on coastal dune ecosystem functioning and to assess possible implications of projected climatic change for the complex vegetation dynamics of the coastal dune ecosystems. We did this by performing measurements and experiments using soil samples collected at a field site in the national park Zuid-Kennermerland (the Netherlands) to get insights regarding the effect of soil physical and soil chemical properties on SWR. The obtained relationships were then incorporated into an ecological model with which we aim to answer the following research questions: i)

what is the potential role of SWR on vegetation dynamics in the coastal dune ecosystem? ii) how do plant species traits affect the role of SWR on vegetation dynamics? iii) how does SWR affect vegetation response to droughts with increasing severity?

## 4.2 Empirical observations of SWR

### 4.2.1 Site description

The relationships used as input for the ecological model were obtained through experiments at a field site in a national park in northwest Europe (Zuid-Kennemerland, the Netherlands,  $52^{\circ}25'17''\text{N}$ ,  $4^{\circ}35'13''\text{E}$ ) and laboratory measurements and experiments using soil samples collected at the same site. Zuid-Kennemerland is a coastal sand dune system typical for the west of the Netherlands. A part of the study area is bare soil, however most of it is covered by algae and various groups of plant species, including mosses, grasses, sedges, herbs, shrubs and trees. In the area, annual rainfall amounts to  $835 \text{ mm year}^{-1}$ . The annual potential evapotranspiration is lower with  $635 \text{ mm year}^{-1}$  but shows strong seasonal variability (KNMI, 2015). As a result, monthly averaged potential evapotranspiration frequently exceeds precipitation during the months March to September, resulting in a precipitation deficit (see Figure 4.1). During this period, as water becomes scarce, plants start competing for water and can experience drought stress.

### 4.2.2 Linking SWR to infiltration

In order to assess the role of SWR on ecosystem dynamics, we first examined how SWR is linked to infiltration. SWR is commonly measured using the Water Drop Penetration Time (*WDPT*) test (Van 't Woudt, 1959; Wessel, 1988; Dekker and Ritsema, 1994), which measures the time it takes for one water droplet to penetrate a soil. The level of SWR can then be classified in five groups (Bisdorff et al., 1993): wettable (0-5 s), slightly repellent (5-60 s), strongly repellent (60-600 s), severely repellent (600-3600 s) and extremely repellent ( $>3600 \text{ s}$ ). To link the *WDPT* to infiltration, we performed infiltration experiments in the dry season (July, 2015) on a bare and vegetated soil. Using the *WDPT* we classified the soils (in the top 5 cm) as being wettable and strongly/severely repellent respectively. We then simulated a typical 5 mm rain event, which was applied instantaneously while runoff of water was prevented using a ring with a diameter of 22 cm.

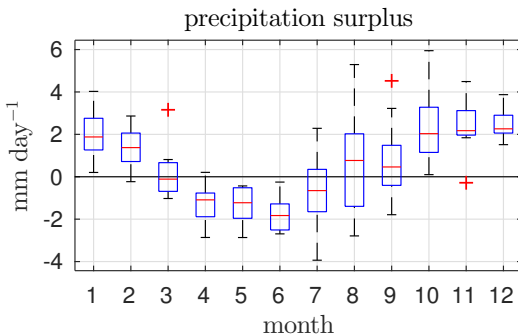


Figure 4.1: Monthly averages of daily precipitation surplus in  $\text{mm day}^{-1}$  for the nearby weather station at Wijk aan Zee, The Netherlands (period: 01-05-2001 - 30-04-2015; location:  $52^\circ 30' \text{N } 04^\circ 36'E$ ). The precipitation surplus was calculated by subtracting the (Makkink) potential evapotranspiration from the precipitation. The box and whisker plots show the median (central red lines) and the upper and lower quartiles (box limits) for each month. The whiskers indicate the variability outside the upper and lower quartiles and can extend to a maximum of 1.5 times the interquartile range. Values beyond the whiskers are regarded as outliers and indicated with the  $+$  markers.

Figure 4.2 shows that the resulting infiltration fronts differ strongly between the two soils. While the water infiltrates deep into the wettable soil (Figure 4.2a), it only wets the upper 1 cm of the repellent soil (Figure 4.2b). Water in this top layer can easily evaporate and therefore remains unavailable for plants whose root zones extend to much deeper layers. In addition, if not blocked by the ring, the water may be lost through runoff and infiltrate elsewhere. The common measure for SWR, can therefore be considered as a good proxy for infiltration of water into the root zone.

### 4.2.3 Soil variables controlling infiltration

We studied the effects two variables on infiltration: i) hydrophobic compound concentration in the soil and ii) initial soil moisture content. Links between these two variables and infiltration would give rise to feedbacks that potentially govern vegetation dynamics, as already briefly described in the introduction. To study the effects of these variables on infiltration we collected 15 soil samples from the Zuid-Kennermerland under a variety of plant species (grasses, mosses, shrubs, pines and oaks) at different soil depths ranging from 0 to 30 cm (see Mao et al., 2014, for more sampling details).

To determine the hydrophobic compound concentration, all soil samples were oven-dried at  $30^\circ\text{C}$  for two days and sieved (mesh size 1.4 mm) to remove leaf and root fragments. A sequential extraction procedure was applied to

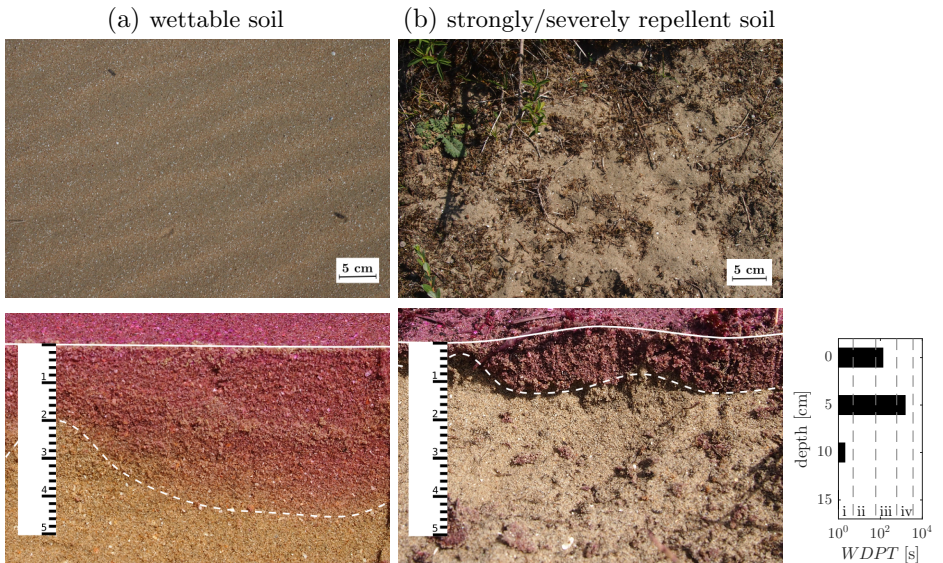


Figure 4.2: Infiltration fronts in a wettable soil (a) and a strongly/severely repellent soil (b) one hour after a 5 mm rain event. The upper images show the undisturbed soil from above. The  $WDPT$  in soil (a) was 0 seconds along the whole soil profile. The  $WDPT$  of soil (b) is depicted in the bar graph, with classes (i) wettable, (ii) slightly repellent, (iii) strongly repellent and (iv) severely water repellent. The  $WDPT$  for this soil equals zero for depths  $>10$  cm.

the soil samples using dichloromethane/methanol (DCM/MeOH) and isopropanol/ammonia solution (IPA/NH<sub>3</sub>) successively (Mao et al., 2014). All extracts were analyzed by gas chromatography - mass spectrometry (GC-MS) to identify and quantify the compounds. The total hydrophobic compound concentration (*THCC*) in Figure 4.3 represents the summed concentration of the dominant compound groups extracted from soils as described by Mao et al. (2015). For more details about the method and the identified compounds see Appendix 4.A. Figure 4.3a shows that the total hydrophobic compound concentration correlates with the *WDPT*, meaning that as hydrophobic compound concentration in the soil increases less water infiltrates. This finding suggests a negative feedback between plant biomass and available soil water: the accumulation of soil hydrophobic compounds through the decomposition of plant litter hampers infiltration and thereby negatively affects water availability and subsequent plant growth.

To determine soil moisture content we selected a subset of samples. From each soil sample, 40 gram of oven-dried soil was put in a plastic Petri dish ( $\varnothing$  90 mm, 1.5 mm height). Demineralized water was added until the soil became saturated. The dishes were put in a fume hood to let water evaporate. As the water evaporated over time, the dishes were weighed to calculate the gravimetric soil moisture content and the *WDPT* was measured by applying 10 water droplets to each soil (see Appendix 4.B for the equation used to calculate the gravimetric soil moisture content). Figure 4.3b shows that, in line with previous studies (Dekker and Ritsema, 1994; Doerr and Thomas, 2000; Dekker and Ritsema, 1996), a SWR threshold in soil moisture can be identified below which infiltration is hampered. Above this threshold, soils are wettable and infiltration is possible. The finding suggests the potential of a positive feedback between soil water availability and infiltration: a decrease in soil water reduces infiltration, leading to a further decrease in soil water.

## 4.3 Model description and analyses

### 4.3.1 Model description

A theoretical model was developed which captures our three empirical observations: (1) SWR hampers infiltration into the root zone (Figure 4.2b), (2) SWR increases with hydrophobic compound concentration (Figure 4.3a) and (3) SWR occurs only in dry soils (Figure 4.3b). The model is based on the water limitation model by Rietkerk et al. (1997), which was extended to include these observations. The model captures the dynamics in available soil

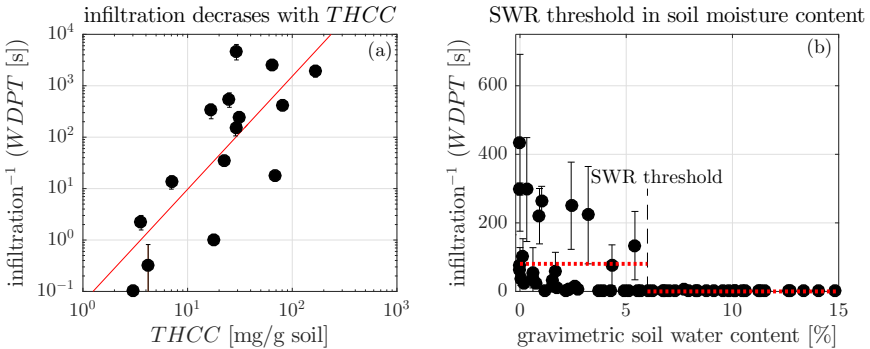


Figure 4.3: (a) Infiltration, measured as the inverse of the water droplet penetration time ( $WDPT^{-1}$ ), decreases with the total hydrophobic compound concentration ( $THCC$ ). A linear fit through this log-log plot gives the following equation:  $WDPT = 10^b THCC^a$  with  $a = 2.1979$ ,  $b = -1.2115$ ,  $R^2=0.61$  and  $p = 0.0006$ . The dots and the whiskers in this plot represent the average  $\pm$  the standard deviation of the penetration times of 20 individual water droplets on oven-dried soil samples. (b) SWR only occurs if the gravimetric soil moisture content drops below a threshold value of around 6%. Here the dots and the whiskers are based on the measured penetration times of 10 individual water droplets. The red dotted lines are the average  $WDPT$  below and above the threshold. More details about the methods can be found in Appendix 4.B.

water  $W$  [mm], plant biomass  $B$  [ $\text{g m}^{-2}$ ] and hydrophobic compound density  $C$  [ $\text{g m}^{-2}$ ]. All state variables are assumed to be uniformly distributed in space.

The dynamics in available water  $W$  are modeled with Equation 4.1:

$$\frac{dW}{dt} = pI(W, C) - U(W)B - rW \quad (4.1)$$

The first term represents the infiltration of water into the root zone. Here  $p$  is the precipitation rate [ $\text{mm day}^{-1}$ ] and  $I$  is the fraction of the precipitation that infiltrates into the root zone [-]. This fraction depends on the amount of water in the root zone  $W$  and the amount of hydrophobic compounds  $C$ :

$$I(W, C) = \frac{W^\alpha + W_0(C)k_1^\alpha}{W^\alpha + k_1^\alpha} \quad (4.2)$$

In Equation 4.2,  $k_1$  is the SWR threshold [mm] that we identified in Figure 4.3b. It is the value of  $W$  below which infiltration into the root zone is hampered. Above this value  $I$  asymptotically approaches 1 as  $W$  increases, meaning that all water infiltrates into the root zone. Below  $k_1$ , as  $W$  decreases,  $I$  approaches to a value of  $W_0$ , which is the fraction of precipitation that

infiltrates into dry soil. The steepness of the SWR threshold is controlled by the dimensionless exponent  $\alpha$  [-] ( $\alpha \gg 1$ ). To capture the increase in SWR with hydrophobic compound concentration (Figure 4.3a) we let the fraction of precipitation that infiltrates into dry soils  $W_0$  decline with hydrophobic compound density in the soil  $C$  as given by Equation 4.3:

$$W_0(C) = \frac{k_2}{C + k_2} \quad (4.3)$$

Here  $k_2$  is a half saturation constant [ $\text{g m}^{-2}$ ], it is the hydrophobic compound abundance at which the fraction of precipitation that infiltrates into dry soils equals  $\frac{1}{2}$ . The remaining terms of Equation 4.1 represent soil water uptake by plants (second term) and losses (third term) and are modeled as by Rietkerk et al. (1997). The uptake by plants is linearly related to plant biomass density  $B$  and asymptotically approaches a maximum uptake rate of  $u$  [ $\text{dm}^3 \text{ g}^{-1} \text{ day}^{-1}$ ] as the available water increases:

$$U(W) = u \frac{W}{W + k_3} \quad (4.4)$$

Here  $k_3$  is the value of  $W$  at which the uptake is half the maximum uptake rate [ $\text{mm}$ ]. Water losses, e.g. through percolation out of the root zone, are linearly related to the available water  $W$  and occur at a rate of  $r$  [ $\text{day}^{-1}$ ].

The dynamics in plant biomass  $B$  are modeled as by Rietkerk et al. (1997):

$$\frac{dB}{dt} = cU(W)B - mB \quad (4.5)$$

The first term represents plant growth, which increases linearly with water uptake (Equation 4.4). Parameter  $c$  is the conversion coefficient of water uptake by plants to plant growth [ $\text{g dm}^{-3}$ ]. The second term covers mortality losses, which increases linearly with plant biomass density  $B$ . Parameter  $m$  is the specific biomass loss rate [ $\text{day}^{-1}$ ].

The model by Rietkerk et al. (1997) was further extended with Equation 4.6, which captures the accumulation and decomposition of hydrophobic compounds in the soil:

$$\frac{dC}{dt} = f m B - d C \quad (4.6)$$

The accumulation of hydrophobic compounds occurs at the rate at which litter is produced  $mB$  [ $\text{g m}^{-2} \text{ day}^{-1}$ ] multiplied with the fraction of hydrophobic compounds in plant tissue  $f$  [ $\text{g g}^{-1}$ ]. The decomposition of hydrophobic

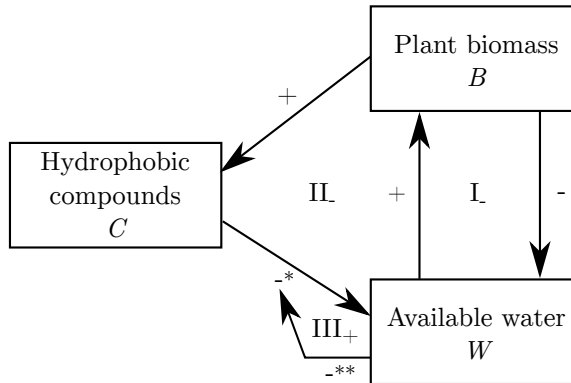


Figure 4.4: Interactions between the model components and the resulting feedbacks. Interactions are represented by the arrows and feedbacks are indicated with the latin numbers and are described in the main text. The + and - signs indicate positive and negative interactions/feedbacks respectively. The asterisks \* and \*\* refer to interactions derived from the empirical observations in Zuid-Kennermerland presented in Figures 4.3a and 4.3b respectively.

compounds takes place at a constant rate of  $d$  [day $^{-1}$ ]. All parameters in the model are listed and briefly described in Table 4.1.

Figure 4.4 shows the feedbacks in the described model. In the model, water promotes plant growth while plants deplete water, resulting in a negative feedback between plants and water (I $_$ ). Plants also produce hydrophobic compounds that potentially hamper infiltration, leading to less available water and decreased plant growth, which yields a second negative feedback loop (II $_$ ). However, because wet soils allow infiltration the negative effect of hydrophobic compounds is diminished by water in the soil, thereby yielding a positive feedback (III $_+$ ).

The three feedbacks depicted in Figure 4.4 do not occur at the same timescales. The effects of hydrophobic compounds and water on infiltration are instantaneous, meaning that the positive feedback (III $_+$ ) is fast. Plant dynamics, on the other hand, take place at longer time scales than infiltration, resulting in a slower plant-water feedback (I $_$ ). The negative plant-compound-water feedback (II $_$ ) can be considered to be even slower because hydrophobic compounds accumulate and decompose at a very low rate, due to the small fraction of hydrophobic compounds in plant tissue and the low decomposition rate of hydrophobic compounds (see Appendices 4.D and 4.E for observed fractions and rates respectively).

Table 4.1: Description and units of the model parameters and state variables.

Symbol	Description	Unit
$W$	Available soil moisture	mm
$B$	Plant biomass density	$\text{g m}^{-2}$
$C$	Hydrophobic compound density	$\text{g m}^{-2}$
$\alpha$	Exponent causing a threshold the infiltration function	-
$c$	The conversion of water uptake by plants to plant growth	$\text{g dm}^{-3}$
$d$	Decomposition rate of hydrophobic compounds	$\text{day}^{-1}$
$f$	Fraction of hydrophobic compounds in plant tissue	$\text{g g}^{-1}$
$k_1$	SWR threshold in the infiltration function	mm
$k_2$	Half saturation constant of infiltration into dry soil	$\text{g m}^{-2}$
$k_3$	Half saturation constant of soil water uptake	mm
$m$	Specific loss of biomass due to mortality and grazing	$\text{day}^{-1}$
$p$	Precipitation rate	$\text{mm day}^{-1}$
$r$	Specific soil water loss	$\text{day}^{-1}$
$u$	Maximum specific water uptake	$\text{dm}^3 \text{ g}^{-1} \text{ day}^{-1}$

### 4.3.2 Model analysis

In order to understand the potential role of SWR in dune vegetation dynamics the model was analyzed qualitatively, complemented with numerical simulations. The parameter values were adopted from Rietkerk et al. (1997) and parameters  $f$ ,  $d$ ,  $k_1$  and  $k_2$  have order-of-magnitude values that are based on our observations and related observations published elsewhere (Mao et al., 2015, see Appendices 4.D and 4.E). For more details on the parameter values and a list of the values per figure see Appendix 4.C.

During analysis it was assumed that the dynamics of the three state variables occur at different rates  $\frac{dW}{dt} > \frac{dB}{dt} > \frac{dC}{dt}$ . This assumption enables separating the timescales at which these dynamics occur, which helps in

obtaining a mechanistic understanding of the model dynamics. In Section 4.4.1 we first study the dynamics in the fast state variable  $W$ , while treating the slow dynamics in  $B$  and  $C$  as being static (i.e. as parameters). In Section 4.4.2 we add complexity by treating both  $W$  and  $B$  as a dynamic state variables. In Section 4.4.3 we consider the full model, and discuss the effect of dynamic  $C$ .

To study how the vegetation dynamics are affected by plant species traits the steady state behavior of the model was studied for different combinations water competitiveness, which is controlled by a number of different parameters, and the fraction of hydrophobic compounds in plant tissue  $f$ , which differs between species as shown in Appendix 4.D.

To study the role of SWR in droughts and the effect of increasing drought severity, droughts were simulated by reducing the precipitation rate  $p$  with 10%, 20% and 40% for soils with and without hydrophobic compounds.

## 4.4 Model results

### 4.4.1 SWR induced bistability in soil conditions

When treating the state variables plant biomass  $B$  and hydrophobic compound density  $C$  as parameters, the system can be analyzed by plotting the positive terms and the negative terms of Equation 4.1 against available soil water  $W$ , as shown in Figure 4.5. Water availability  $W$  increases where infiltration (positive) exceeds the sum of water uptake and losses from the soil (negative). The available water  $W$  decreases where infiltration exceeds the negative terms. For a soil without hydrophobic compounds this means that  $W$  asymptotically approaches the relatively wet equilibrium state depicted in Figure 4.5a, where infiltration equals uptake plus losses. For a soil with hydrophobic compounds the dynamics in available water are more complex. Hydrophobic compounds induce water repellency of dry soils (Figure 4.3b) preventing water from infiltrating into the rootzone (Figure 4.2b). This positive feedback mechanism results in three intersections of the infiltration curve with the uptake and loss curve, as shown in Figure 4.5b. Two of these equilibrium states are stable (they attract) and one is unstable (it repels). The system resides in one of the stable equilibrium states, meaning that soils are either wet and hydrophilic or dry and hydrophobic.

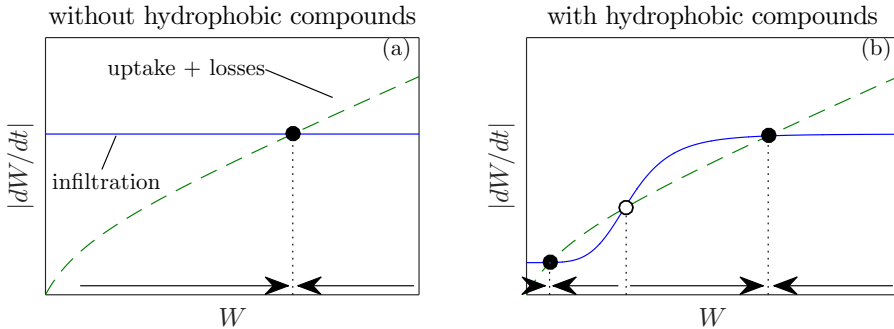


Figure 4.5: The positive (solid blue) and negative (dashed green) terms of Equation 4.1 plotted against available water  $W$ , for soils without hydrophobic compounds (a) and with hydrophobic compounds (b). Stable and unstable equilibria are depicted with the closed and open dots respectively. The arrows show the dynamics of the system when it is out of equilibrium. Available water increases where infiltration exceeds the uptake and losses, and decreases where the opposite occurs. For parameter values see Appendix 4.C.

#### 4.4.2 The water-plants cycle: repetitive regime shifts

Changes in infiltration and uptake may change the number of equilibrium states in soils that contain hydrophobic compounds. A decrease in rainfall  $p$  for example can lower the infiltration curve such that the hydrophilic wet state shown in Figure 4.5b vanishes. If the soil is in this state, a decrease in rainfall can trigger a sudden shift to a hydrophobic dry state, as we will discuss in Section 4.4.5. In our model however, such shifts need not be driven by external changes but may also be triggered by changes in plant biomass density. Plants may thrive and increase in biomass on the wet hydrophilic soils, but may not survive and decrease in biomass at dry hydrophobic soils. The gradual increase in water uptake from wet soils can initiate a shift to hydrophobic dry soils, as shown in Figure 4.6a (I-II-III). On hydrophobic dry soils plant biomass decreases and water uptake declines eventually resulting in a shift back to hydrophilic wet soils (III-IV-I). The coupled plant and water dynamics are therefore responsible for repetitive shifts between the two stable equilibrium states of  $W$  (Figure 4.6b). These repetitive regime shifts are fully internally driven, meaning that they occur without any external forcing.

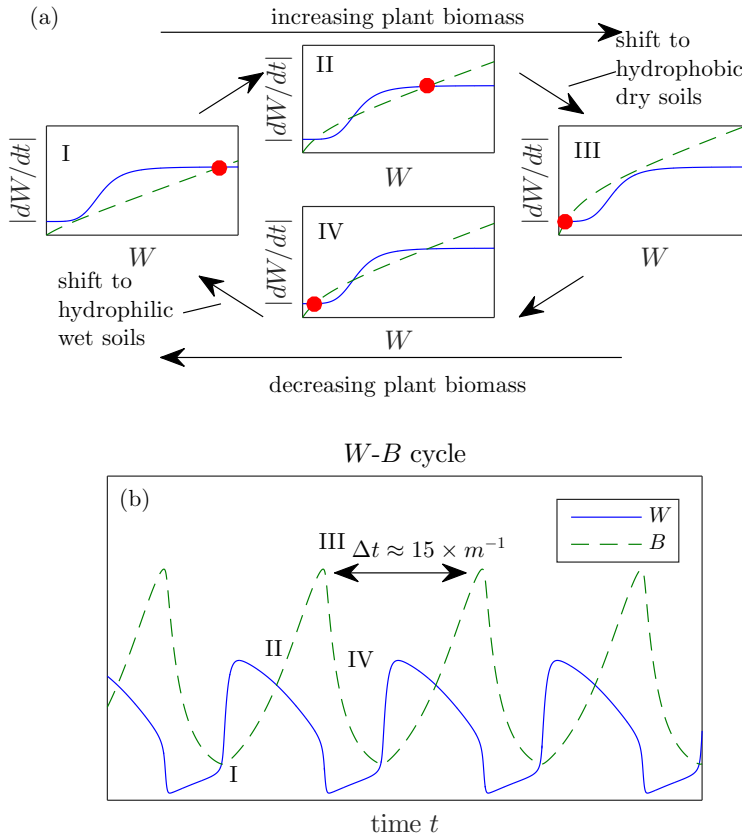


Figure 4.6: Repetitive regime shifts in available water. (a) The positive (solid blue line) and negative (dashed green line) terms of Equation 4.1 plotted against available water  $W$ , for a soil with hydrophobic compounds and dynamic plant growth. The red dot indicates the system state. (b) The dynamics in available water  $W$  and plant biomass  $B$  over time. The period of the cycles with the current parameter setting is just over 1 year, which corresponds to approximately 15 plant generations ( $m^{-1}$ ). For parameter values see Appendix 4.C.

### 4.4.3 Cyclic dynamics and the SWR lock

As plants grow and litter is produced, hydrophobic compounds accumulate in the soil. Over time, the system therefore moves from having one stable equilibrium state (Figure 4.5a) to a bistable system (Figure 4.5b), thereby giving rise to the repetitive regime shifts discussed in the previous section. Figures 4.7a and b show the phase planes of these two qualitatively different system modes. They show that, as hydrophobic compound density  $C$  increases, the stable equilibrium state becomes unstable after which the system alternates between two branches of the  $W$  isocline. Figure 4.7c shows that for high  $C$  there is a third system mode, in which the transition from a hydrophobic dry soil to a hydrophilic wet soil is blocked by a stable equilibrium state that emerges on the lower branch of the  $W$  isocline. At this stable equilibrium state, which we will call the SWR lock, plant density equals zero. This means that there is no accumulation of hydrophobic compounds and that over time, as hydrophobic compounds decompose, the SWR lock vanishes. The gradual accumulation and decomposition of hydrophobic compounds gives rise to a second cycle, the  $W$ - $B$ - $C$  cycle (see Figure 4.8), in which the system alternates between the two system modes depicted in Figures 4.7b and c. Since the dynamics in  $C$  are slower than the plant dynamics, this second cycle comprises a longer time interval than that of the repetitive shifts of the  $W$ - $B$  cycle.

### 4.4.4 The impact of SWR depends on plant species traits

The plant species traits that are included in this model can be captured with only two variables. The first variable is  $W^*$ , the  $B$ -isocline of Figure 4.7, which is given by:

$$W^* = \frac{mk_3}{cu - m} \quad (4.7)$$

The  $W^*$  gives the minimum resource abundance required for plant biomass to increase and is therefore inversely related to the water competitiveness of a species: species with low  $W^*$  will eventually outcompete species with high  $W^*$  (sensu Tilman, 1982). The second variable is the fraction of hydrophobic compounds in plant litter  $f$ , which appears to vary between plant species as shown in Appendix 4.D and controls the accumulation rate of hydrophobic compounds ( $= fmB$ ) and consequently the equilibrium value of  $C$ .

Figure 4.9 shows the equilibrium plant biomass  $B$  for different combinations of water competitiveness ( $W^*$ ) $^{-1}$  and hydrophobic compound fraction

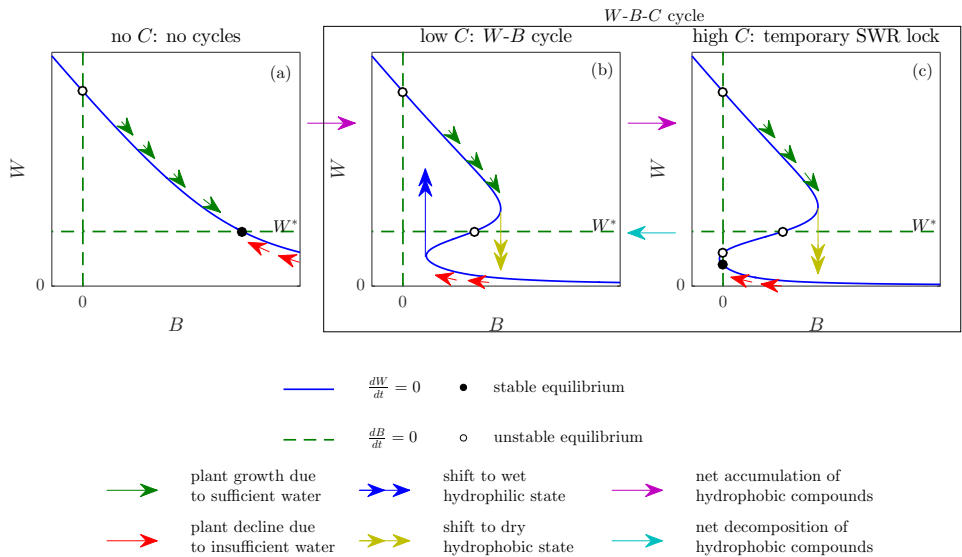


Figure 4.7: Phase planes for the model with different levels of hydrophobic compound density  $C$ . Above the horizontal plant isocline (green dashed line) plant density increases as a result of abundant available water. Below the plant isocline plant density decreases due to insufficient available water. Left from the water isocline (blue solid line), water increases due to a low uptake rates by plants. Right from the water isocline, water decreases as a result of elevated uptake rates. As the dynamics in available water are fast with respect to the plant dynamics, the system will usually be close to the water isocline. For parameter values see Appendix 4.C.

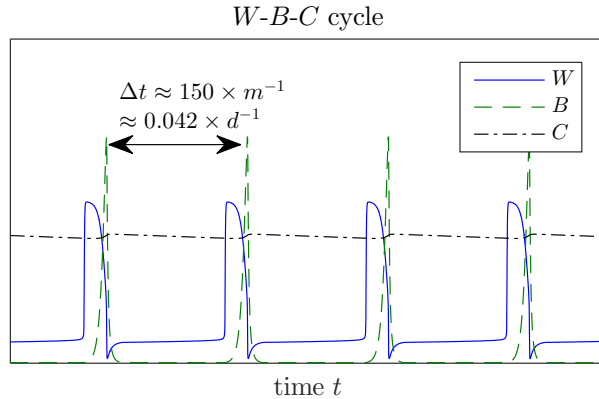


Figure 4.8: The dynamics in available water  $W$ , plant biomass  $B$  and hydrophobic compound density  $C$  over time. The period of the cycles for the current parameter setting is just over 10 years, which corresponds to approximately 150 plant generations ( $m^{-1}$ ) or 0.042 times the mean residence time of hydrophobic compounds ( $d^{-1}$ ). For parameter values see Appendix 4.C.  $C$  was scaled to match the order of magnitude of  $B$  and  $W$ .

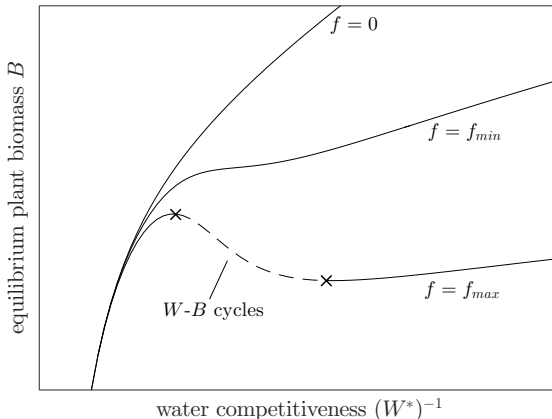


Figure 4.9: Water competitiveness  $(W^*)^{-1}$  and the fraction of hydrophobic compounds in plant litter  $f$  control the equilibrium plant biomass and the emergence of cyclic dynamics.  $f_{min}$  ( $= 0.0008 \text{ g g}^{-1}$ ) and  $f_{max}$  ( $= 0.0065 \text{ g g}^{-1}$ ) are the minimum and maximum measured value of  $f$  respectively, as listed in Appendix 4.D. For the other parameter values see Appendix 4.C.

$f$ . It shows that the previously described  $W$ - $B$  cycles occur only in a system with species that contain sufficient hydrophobic compounds and that have an intermediate water competitiveness. Species with a high water competitiveness do not display cyclic dynamics, as these species can cope with the dry conditions of hydrophobic soils such that plant biomass does not decrease to a level required for the shift from a hydrophobic dry state to a hydrophilic wet state. However, the equilibrium biomass of these competitive species is significantly reduced by SWR. This can be attributed to the fact that SWR only affects the dry soils on which these species live. Species with a low water competitiveness only live on wet soils that are unaffected by SWR, and therefore, their equilibrium biomass remains unaffected even if the fraction hydrophobic compounds in their litter is high. However, as we will show in the next section, the combination of SWR and droughts can significantly affect these species.

#### 4.4.5 SWR can amplify drought stress

The equilibrium states discussed in the previous section and shown in Figure 4.9 represent the long term dynamics of the undisturbed coastal dune ecosystem. However, the precipitation surplus strongly varies within one

year (Figure 4.1) and this variability is projected to increase over the coming decades (KNMI, 2014). Figure 4.10 shows how droughts of increasing severity affect a species that has a low water competitiveness on soils with and without hydrophobic compounds. For soils without hydrophobic compounds, plants respond in a rather linear way to a sudden drop in precipitation  $p$ , regardless of the drought severity. For plants on soils that do contain hydrophobic compounds the system response depends on drought severity. Minor droughts result in a similar linear response in vegetation as for soils without hydrophobic compounds. Slightly more severe droughts, however, have a disproportional effect on both available water and plant biomass. This is caused by a temporary shift from a hydrophilic wet state to a hydrophobic dry state (i.e. a single  $W-P$  cycle is triggered). An even greater reduction in precipitation can trigger a permanent shift to a hydrophobic dry state. Here the system gets trapped in the SWR lock, which leads to extinction of the species and can only be undone by an increase in precipitation or, on longer timescales, by decomposition of hydrophobic compounds. In Appendix 4.F we show that the presented shifts can only be triggered by a rapid decline in rainfall, e.g. by seasonality, and that a gradual decline in precipitation leads to a linear system response. We also show that increasing precipitation back to the original value allows soils to shift back to a hydrophilic wet state and enables vegetation to recover. Finally we show that, in contrast to the weak competitor modelled here, competitive species always respond in a linear way to declines in precipitation.

## 4.5 Discussion and conclusions

In this study we obtained relationships governing soil water repellency (SWR) from field and laboratory experiments to develop an ecological model which enabled us to systematically study the role of SWR in the vegetation dynamics of coastal dune ecosystems. The model suggests that SWR can result in bistable soil conditions (Figure 4.5b), meaning that soils are either in a hydrophilic wet state or in a hydrophobic dry state. If plants increase their biomass on hydrophilic wet soils and decrease their biomass on hydrophobic dry soils then cyclic vegetation dynamics can be triggered, in which soils alternate between the two stable states in soil water (Figure 4.6). The accumulation of soil hydrophobic compounds may trigger a SWR lock, which interrupts the water-plant cycle (Figure 4.7) and gives rise to a water-plants-hydrophobic compounds cycle which is characterized by long periods in which

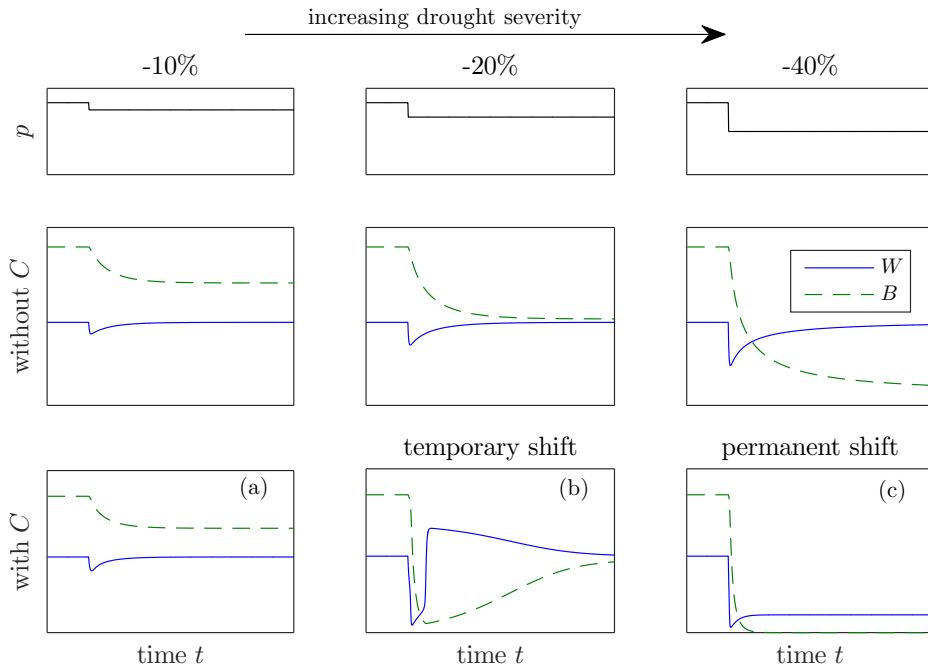


Figure 4.10: Amplification of drought stress for species with low water competitiveness caused by a (temporary) shift to the hydrophobic dry state. A period of 3000 days was modelled, which corresponds to 105 plant generations ( $m^{-1}$ ). For parameter values see Appendix 4.C. For runs with gradually declining precipitation, runs with precipitation increasing back to the original values and runs with a competitive species see Appendix 4.F.

vegetation is absent (Figure 4.8). The emergence of these cycles strongly depends on two plant species traits: i) hydrophobic compound concentration in plant tissues and ii) water competitiveness (Figure 4.9). Cyclic dynamics only occur if plant tissues contain a relatively high fraction of hydrophobic compounds. Depending on their water competitiveness, plants are affected by SWR in three different ways. Species with intermediate water competitiveness display SWR induced cyclic dynamics. Competitive species do not exhibit such cyclic dynamics but for these species SWR significantly reduces their productivity and equilibrium biomass. Cyclic dynamics are also not exhibited by species with low water competitiveness. However, such species are very sensitive to droughts. Depending on drought severity, soils covered by species with low water competitiveness may temporally or permanently shift to a hydrophobic dry state (Figure 4.10). This can result in a significant reduction in plant biomass or even a permanent shift to a bare state.

As noted above, our study highlights the importance of two species traits in coastal dune ecosystems: hydrophobic compound content of plant tissues and water competitiveness. The hydrophobic compound contents of woody species, e.g. pine and oak, are lower than of grasses (e.g. sheep fescue, red fescue, tufted grass; see Appendix 4.D). Water competitiveness is likely to be higher for woody plants than for grasses, herbs and mosses, since woody plants generally have deeper roots and lower wilting point (Scholes and Walker, 2004). Our model suggests that species with high water competitiveness and low hydrophobic compound content, i.e. woody species, are likely to exhibit stable vegetation dynamics, while less competitive species, i.e. grasses, would display cyclic dynamics or strong drought sensitivity.

Apart from the short term dynamics, our model suggests that SWR may also be important on longer timescales. As it can take centuries for hydrophobic compounds to decompose (see Appendix 4.E), their gradual accumulation may result in long periods in which vegetation is absent (the SWR-lock; see Figure 4.8). This, in combination with climatic variations and increased wind erosion during the absence of stabilizing vegetation, may contribute to the long term vegetation dynamics reported by Zagwijn (1970). Our model also suggests that SWR can increase the sensitivity of the dune ecosystem to disturbances such as shifts in precipitation (see Figure 4.10). Such disturbances are thought to be an important mechanism behind retrogression (Peltzer et al., 2010), which has been observed in dune systems of northwest Europe (Van der Maarel et al., 1985; Van Dorp et al., 1985). Our model suggests that, even in the absence of disturbances, SWR can result non-linear biomass development associated with retrogression (see Figure

4.8).

While our study shows that SWR is a potential driver of vegetation dynamics, externally driven shifts in vegetation composition could also change water repellency of soils. An example of such a community shift is the widely reported problem of grass encroachment, caused by elevated nitrogen deposition rates (Kooijman and Van der Meulen, 1996; Veer and Kooijman, 1997; Kooijman et al., 1998; Veer, 1997; Van den Berg et al., 2005; Remke et al., 2009). Grasses have a high hydrophobic compound content (see Appendix 4.D) and may therefore enhance SWR. In addition to shading (Veer and Kooijman, 1997), this may be an important mechanism to outcompete other plant species.

Focusing on dune ecosystems, our study raises the question whether our findings apply to other ecosystems with different climates and soil textures. Besides requiring water-limiting conditions for our model to be valid we expect that soil textures other than sandy will not allow cyclic dynamics to occur. We expect this because an important condition to be met for cyclic dynamics is that plants grow and increase their biomass on hydrophilic wet soils while they decrease biomass on hydrophobic dry soils. Whether this occurs is mainly controlled by the SWR threshold that separates the two soil states (see Figure 4.3b). Literature values suggest that this threshold moves towards higher soil moisture values for finer textured soils (measured ranges for sandy soils: 1.75-4.75 vol%, loamy sand/sandy loam soils: 28 grav% and peaty clay/clayey peat soils: 34.6-38.2 vol%; Dekker and Ritsema, 1994; Doerr and Thomas, 2000; Dekker and Ritsema, 1996). At these higher values, plants may not be stressed enough to sufficiently reduce their biomass, thereby not allowing a shift from a hydrophobic dry to a hydrophilic wet state to occur (Figure 4.6IV-I), meaning that cyclic dynamics are hampered. A second reason that other soil textures may not allow cyclic vegetation dynamics to occur could be a weaker relationship between soil hydrophobic compound concentration and SWR. While we found a significant correlation (see Figure 4.3a) between total hydrophobic compound concentration and SWR, we are not aware of studies on undisturbed finer textured soils that report significant correlations (Doerr et al., 2005; DeBano, 1991).

Climate change for the northwest European coastal dunes encompasses decreasing summer precipitation, increasing precipitation deficits in the growing season, a longer growing season, wetter winters and rising temperatures (KNMI, 2015; IPCC, 2013). Our model suggests that an increase in drought severity in combination with SWR could result in shifts from vegetated to bare ecosystem states (see Figure 4.10). This finding is in line with ex-

trapolations of a statistical model by Witte et al. (2008), that indicate an increasing fraction of bare soil as precipitation deficit increases. Witte et al. (2008) also hypothesize that, due to SWR, climate change may result in increased heterogeneity and enhanced patchiness, a hypothesis that we could not test with our model as it does not capture spatial processes. Besides changes in summer precipitation, vegetation dynamics may be affected by increasing winter precipitation and winter temperatures through enhanced decomposition rates of (hydrophobic) organic compounds (Davidson and Janssens, 2006; Kirschbaum, 1995; Laiho et al., 2004). The resulting decrease in soil hydrophobic compound concentrations would lower the likelihood of cyclic dynamics to occur. However, this effect may be diminished the increased turnover of biomass caused by the extended growing season.

Although the presented model captures our observations of SWR in Zuid-Kennermerland and the three key feedbacks (Figure 4.4) that potentially control the SWR driven vegetation dynamics on coastal sand dunes, it only partly captures the complexity of SWR on molecular scale and soil scale. The current model uses total hydrophobic compound concentration as a predictor for SWR of dry soils (Figure 4.3a and Equation 4.3). However, depending on their origin (plant species / plant tissues), hydrophobic compounds differ in their composition and consequently in their effect on SWR (Mao et al., 2014). Mao et al. (2015) identified a set of hydrophobic compounds, so-called SWR predictors, that can well predict SWR. These SWR predictors have a known origin and can therefore also be used to assess the relative contribution of different species and plant tissues to SWR. Mao et al. (2014) found that root-derived hydrophobic compounds (suberinins) are more hydrophobic than those originating from leaf waxes (free lipids). This may result in different impacts of hydrophobic compounds on SWR along the soil profile as leaves contribute relatively more to the organic matter in topsoils than roots, whereas in subsoils virtually all organic matter is derived from roots (Mao et al., 2014). Finally, the various hydrophobic compound groups also decompose at different rates (Weisberg, 2007; Feng et al., 2010; Spielvogel et al., 2010). A future model could incorporate this complexity by considering different hydrophobic compound groups or SWR predictors and by separating top- and subsoils and above and below-ground biomass. A drawback of such a comprehensive modelling approach would be that a qualitative analysis, as performed in our study, may not be possible, meaning that analysis would need to be done numerically. A second way our model can be extended is by including spatial processes such as surface runoff and preferential flow that commonly occur in water repellent soils. This may give insights in the role of SWR in

#### *4.A Composition of the hydrophobic compounds.*

the observed spatial heterogeneity and may be used to test the hypothesis of enhanced patchiness of vegetation resulting from climate change (Witte et al., 2008). Such models could also incorporate the temporal distribution of precipitation events, which is thought to play a key role in spatially extended ecosystems (Chapter 3) and is projected to change in the coming decades (Tebaldi et al., 2006). Finally, the model could be extended to include fires. Fires are known to be an important source of SWR in many ecosystems and may not only directly affect vegetation dynamics, but also indirectly through SWR and other soil surface changes (Ravi et al., 2009; Sankey et al., 2012).

Our findings, and those of future model studies, provide a more thorough understanding of the inherent complexity of the dune ecosystem and thereby they aid in assessing effect of climate change and human activities on the dune ecosystem.

### **Acknowledgments**

This study was funded by the Complexity programme of the Netherlands Organization for Scientific Research (NWO) and the Earth and Life Science and Research Council (ALW) with financial aid from NWO (Grant number 821.01.004). We would like to thank Aat Barendregt, Marcel C.G. van Maarseveen and Chris Roosendaal for providing ThetaProbe Soil Moisture Sensors.

### **Appendix 4.A Composition of the hydrophobic compounds.**

The total hydrophobic compound concentration was obtained by sequentially extracting hydrophobic compounds from the soils with dichloromethane/methanol (DCM/MeOH) and iso-propanol/ammonia solution (IPA/NH<sub>3</sub>) (Mao et al., 2014, 2015). Three fractions were obtained: DCM/MeOH extractable lipids (D), DCM/MeOH soluble part of IPA/NH<sub>3</sub> extract (AS) and DCM/MeOH insoluble part of IPA/NH<sub>3</sub> extract (AI). Ten main compound groups were identified in these three fractions: (D) fatty acid, (D) alcohol, (D) alkane, (AI) fatty acid, (AI) alcohol, (AI)  $\omega$ -hydroxy fatty acid, (AI)  $\alpha,\omega$ -dicarboxylic acid, (AS) fatty acid, (AS) alcohol and (AS)  $\omega$ -hydroxy fatty acid. The total hydrophobic compounds concentration is obtained by summing the concentrations of these ten compound groups. More details

on the extraction methods can be found in the papers by Mao et al. (2014, 2015).

## Appendix 4.B Gravimetric and volumetric soil moisture content

In Figure 4.3b soil moisture is presented as gravimetric soil moisture content, which is defined as:

$$\Theta_g = \frac{m_w}{m_b + m_w} \quad (4.8)$$

where  $m_w$  is the mass of water,  $m_b$  is the bulk mass of the oven-dried soil (40 gram) and  $m_b + m_w$  is the total weighted mass of the soil. If the density of the soil is known, the gravimetric soil moisture content can be converted to the volumetric soil moisture content using the following equation:

$$\Theta_v = \frac{\Theta_g}{1 - \Theta_g} \frac{\rho_b}{\rho_w} \quad (4.9)$$

where  $\rho_b$  is the density of the oven-dried soil (approximately  $1.6 \text{ g cm}^{-3}$  for sandy soils) and  $\rho_w$  is the density of water.

## Appendix 4.C Parameter values for the model

We adopted the parameters as used in the study by Rietkerk et al. (1997), but use a higher precipitation rate:  $p = 2.5 \text{ mm day}^{-1}$ ,  $u = 0.05 \text{ dm}^3 \text{ g}^{-1} \text{ day}^{-1}$ ,  $r = 0.1 \text{ day}^{-1}$ ,  $k_3 = 3 \text{ mm}$  and  $W^* = 7 \text{ mm}$ , where  $W^* = \frac{mk_3}{cu-m}$ . To account for the lower temperatures and incoming solar radiation, the dynamics in plant biomass  $B$  were assumed to be a factor 10 slower compared to the semi-arid regions for which the model by Rietkerk et al. (1997) was developed (i.e.  $c = 1 \text{ g dm}^{-3}$  and  $m = 0.035 \text{ day}^{-1}$ ). This assumption does not affect the presented dynamics, but merely sharpens the shifts between hydrophilic wet and hydrophobic dry soils (Figure 4.6b). For the infiltration function, the SWR threshold  $k_1$  was set to 7 mm and exponent  $\alpha$  was set to 5.

In this paper  $B$  and  $C$  are sometimes assumed to be constant, their values for the different figures are listed in Table 4.2. As indicated in the table,  $C$  is dynamic in Figures 4.8 and 4.9. In Figure 4.8 we triggered a SWR lock by selecting a low value of  $k_2$  ( $k_2 = 5 \text{ g m}^2$ ; which corresponds to a high impact of hydrophobic compounds on infiltration) and a high value of  $f$  ( $f = 0.0065$

$\text{g g}^{-1}$ ; which is the maximum measured value listed in Appendix 4.D). In Figure 4.9 we used a more realistic value for  $k_2$  ( $k_2=250 \text{ g m}^2$ ) and selected the lower and upper measured of  $f$  ( $f = 0.0008$  and  $f = 0.0065 \text{ g g}^{-1}$ ). For both figures  $d = 1 \times 10^{-5} \text{ day}^{-1}$ , which corresponds to a mean residence time of about 250 years (see Appendix 4.E). For the runs used to illustrate the drought stress amplification (Figure 4.10) we selected a species with low water competitiveness ( $W^* = 14 \text{ mm}$ ) by lowering the conversion coefficient  $c$  to a value of  $0.85 \text{ g dm}^{-3}$ .

Table 4.2: Values for  $B$  and  $C$  as used in the different figures. Hyphens indicate dynamic  $B$  or  $C$ .

Figure	$B [\text{g m}^{-2}]$	$C [\text{g m}^{-2}]$
4.5a	20	0
4.5b	20	$4k_2$
4.6a I	5	$4k_2$
4.6a I & IV	20	$4k_2$
4.6a III	35	$4k_2$
4.6b	-	$4k_2$
4.7a	-	0
4.7b	-	$4k_2$
4.7c	-	$9k_2$
4.8	-	-
4.9	-	-
4.10	-	0 / $4k_2$

## Appendix 4.D Hydrophobic compound content in plant tissues

The hydrophobic compound content of different plant tissues were obtained by summing the mass of the identified hydrophobic compounds in Mao et al. (2015) that comprise extractable lipids (alkanes, alcohols and fatty acids) and ester-bound lipids (alcohols, fatty acids,  $\omega$ -hydroxy fatty acids,  $\alpha,\omega$ -dicarboxylic acids) and dividing by the total mass of the plant tissue. The results are presented in Table 4.3. Part of the data (\*) refers to Mao et al. (2015) and part of the data (\*\*) refers to Mao et al. (under review).

Table 4.3: Hydrophobic compound content in plant tissues.

Species (Latin)	Species (common)	Tissue	Hydrophobic compound content [mg g <sup>-1</sup> dry weight]
<i>Festuca ovina</i> (*)	Sheep fescue	whole plant	4.10
<i>Hypnum lacunosum</i> (*)	Hypnum moss	whole plant	1.16
<i>Hippophae rhamnooides</i> (*)	Sea-buckthorn	leaves	1.20
<i>Crataegus</i> sp. (*)	Hawthorn	roots	3.76
<i>Pinus nigra</i> (*)	Black pine	leaves	4.30
<i>Quercus robur</i> (*)	Common oak	roots	2.83
<i>Festuca rubra</i> (**)	Red fescue	needles	2.77
<i>Poa nemoralis</i> (**)	Wood bluegrass	roots	0.84
<i>Phleum pratense</i> (**)	Timothy-grass	leaves	3.76
<i>Agrostis stolonifera</i> (**)	Creeping bentgrass	roots	5.13
<i>Holcus lanatus</i> (**)	Tufted grass	leaves	6.49
<i>Carex</i> sp.(**)	Sedge	roots	5.80
		leaves	3.58
		roots	4.14
		roots	2.59

## **Appendix 4.E    Decomposition rates of hydrophobic compounds in soils.**

Hydrophobic compounds in soils are decomposed by abiotic and biotic processes. The decomposition rate of organic matter is controlled by many internal and external factors, such as temperature (Davidson and Janssens, 2006), microorganisms, compound quality and water availability (Melillo et al., 1982; Riederer et al., 1993; Norby et al., 2001; Otto and Simpson, 2006) and land-use (Wiesenbergs, 2004). Table 4.4 lists the mean residence times (MRT) of different hydrophobic compounds in various soils.

Table 4.4: Mean Residence Times (MRT) of hydrophobic compounds in soils. MRT is the inverse of the decomposition rate ( $d^{-1}$ ).

hydrophobic compounds	MRT [years]	soil type	soil description	carbon labelling	reference
alkane	35	Haplic Phaeozem	grain-maize crop	$^{13}\text{C}$	Wiesenberg et al. (2004)
	60	Haplic Phaeozem	silage-maize crop	$^{13}\text{C}$	Wiesenberg et al. (2004)
fatty acid	21	Haplic Phaeozem	grain-maize crop	$^{13}\text{C}$	Wiesenberg et al. (2004)
	49	Haplic Phaeozem	silage-maize crop	$^{13}\text{C}$	Wiesenberg et al. (2004)
ester-bound long-chain fatty acid	31.8	Ultic alfisols	pine forest	$^{13}\text{C}$	Feng et al. (2010)
cutin-derived compounds	34.4	Ultic alfisols	pine forest	$^{13}\text{C}$	Feng et al. (2010)
suberin-derived compounds	33.2	Ultic alfisols	pine forest	$^{13}\text{C}$	Feng et al. (2010)
suberin/cutin	250	Leptic Cambisols	Europ. beech forest	$^{14}\text{C}$	Spielvogel et al. (2010)

## Appendix 4.F Additional drought simulations

In this appendix we show additional model runs akin the ones of Figure 4.10, but now with slowly decreasing precipitation (Figure 4.11) and precipitation shifting back to the original values (Figure 4.12). Figures 4.13 and 4.14 are the same as Figures 4.10 and 4.12, but show the response of a competitive species (low  $W^*$ ; right side of Figure 4.9) to changes in precipitation. All runs are on a soil with hydrophobic compounds ( $C = 4k_2$ ) as in the lower row of Figure 4.10.

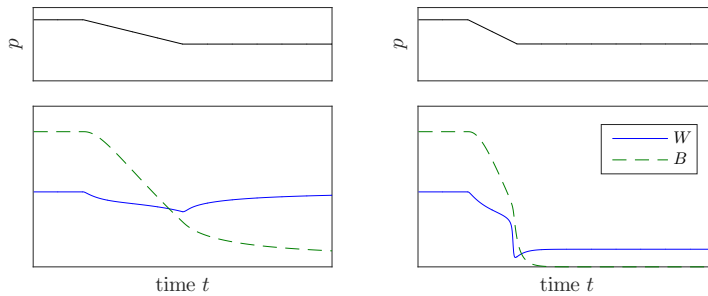


Figure 4.11: Only rapid decreases in precipitation can trigger a shift to a hydrophobic dry state without vegetation. Precipitation was reduced by 40 % over a period of 1000 days (left) and 500 days (right), corresponding to a rate of change of  $0.001 \text{ mm day}^{-2}$  ( $\approx 133 \text{ mm year}^{-2}$ ) and  $0.002 \text{ mm day}^{-2}$  ( $\approx 266 \text{ mm year}^{-2}$ ) respectively. Parameter values are the same as for Figure 4.10.

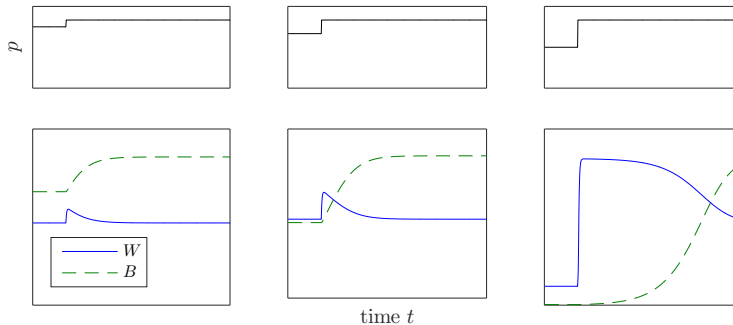


Figure 4.12: Restoring the original values of the precipitation of Figure 4.10 ( $2.5 \text{ mm day}^{-1}$ ) enables plants to recover. Parameter values are the same as for Figure 4.10.

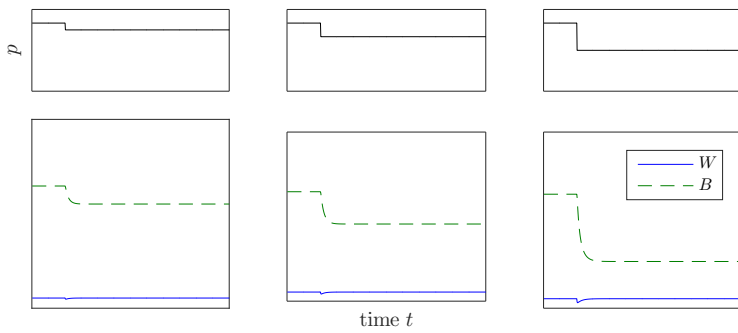


Figure 4.13: Competitive species respond in a linear way to decreases in precipitation. Parameter values are the same as for Figure 4.10, except  $W^* = 1.62$  mm, which was obtained by setting  $c$  to  $2 \text{ g dm}^{-3}$ .

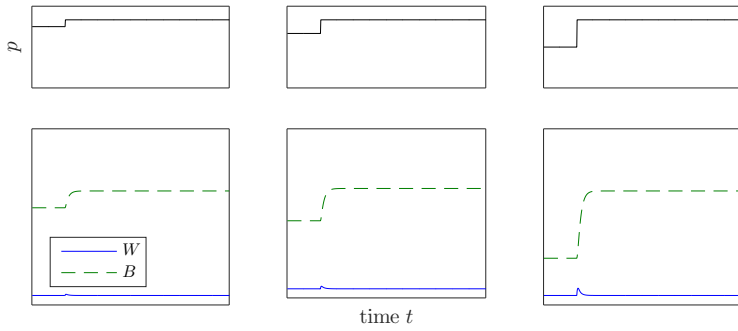


Figure 4.14: Same as for Figure 4.12, but now for the competitive species described in the caption of Figure 4.13.

# **5 Ecosystems off track: Rate-induced critical transitions in ecological models.**

Siteur, K., Eppinga, M. B., Doelman, A., Siero, E. and Rietkerk, M. (2016). Ecosystems off track: Rate-induced critical transitions in ecological models. Accepted for publication in *Oikos*.

## **Abstract**

Theory suggests that gradual environmental change may erode the resilience of ecosystems and increase their susceptibility to critical transitions. This notion has received a lot of attention in ecology in recent decades. An important question receiving far less attention is whether ecosystems can cope with the rapid environmental changes currently imposed. The importance of this question was recently highlighted by model studies showing that elevated rates of change may trigger critical transitions, whereas slow environmental change would not. This paper aims to provide a mechanistic understanding of these rate-induced critical transitions to facilitate identification of rate sensitive ecosystems. Analysis of rate sensitive ecological models is challenging, but we demonstrate how rate-induced transitions in an elementary model can still be understood. Our analyses reveal that rate-induced transitions (i) occur if the rate of environmental change is high compared to the response rate of ecosystems, (ii) are driven by rates, rather than magnitudes, of change and (iii) occur once a critical rate of change is exceeded. Disentangling rate-induced transitions from classical transitions in observations would be challenging. However, common features of rate-sensitive models suggest that ecosystems with coupled fast-slow dynamics, exhibiting repetitive catastrophic shifts or displaying periodic spatial patterns are more likely to be rate sensitive. Our findings are supported by experimental studies showing rate-dependent outcomes. Rate sensitivity of models suggests that the common definition of ecological resilience is not suitable for a subset of real ecosystems and that formulating limits to magnitudes of change may not always safeguard against ecosystem degradation.

## 5.1 Introduction

Theoretical studies have suggested that gradual changes in environmental conditions may trigger so-called critical transitions in ecosystems, which would explain unexpected ecosystem degradation and the sudden emergence of cyclic or chaotic dynamics (Holling, 1973; Scheffer et al., 2001; Scheffer, 2009). These studies found that gradual external change can undermine the resilience of ecosystems, thereby increasing their susceptibility to critical transitions. The resilience of ecosystems can be assessed with ecological models through steady state analysis. Steady state analysis allows determining critical magnitudes of change in external conditions and critical levels of disturbance beyond which ecosystems shift to alternative dynamics. The assumption behind steady state analysis is that an ecosystem is in a state in which all processes balance out and no change can be observed (i.e. in dynamic equilibrium). Although the assumption that ecosystems reside in such a steady state has been useful in assessing their resilience under static or slowly changing environmental conditions, it does not hold when changes in environmental conditions are rapid relative to the attractive capacity of a steady state. The fact rapid environmental changes may lead to unexpected ecosystem dynamics has received only little attention in the ecological community (Scheffer et al., 2008). This is remarkable as the environmental changes in the Anthropocene occur at unprecedented rates (Joos and Spahni, 2008; Kaplan et al., 2011; Klein Goldewijk et al., 2011) and may be too rapid for ecosystems to cope with (Walther et al., 2002). In this study, we show that models indeed suggest that some ecosystems may fail to respond to rapidly changing external conditions, which can lead to a novel type of critical transition. We identify mechanisms driving such rate-induced critical transitions, provide possible ways forward regarding identification of rate sensitive ecosystems and discuss the implications of rate-induced critical transitions for the general view on ecological resilience.

## 5.2 Critical transitions, Steady state analysis and Resilience

A critical transition is a shift of a system to a qualitatively different dynamical regime triggered by changing external conditions or by a disturbance. Critical transitions can be super- or subcritical. Supercritical transitions are continuous and reversible whereas subcritical transitions are discontinuous

and require disproportional efforts to reverse. Subcritical transitions that occur between steady ecosystem states are also referred to as catastrophic shifts (Scheffer et al., 2001). Well-known examples of catastrophic shifts are transitions of shallow lakes from clear to turbid states, triggered by increases in nutrient input (Scheffer et al., 1993), of grazing systems from vegetated to (bare) overgrazed states forced by an increase in herbivore density (Noy-Meir, 1975; May, 1977; Rietkerk et al., 1996, 1997) and of marine ecosystems driven by (combinations of) sea temperature rise, overfishing, habitat loss, invasive species and pollutants (Jackson et al., 2001; Petraitis, 2013). The alternative dynamics to which a system transitions do not necessarily have to be steady over time. Increases in primary production through nutrient enrichment, for example, are known to lead to cyclic dynamics between predators and preys (Huffaker et al., 1963; Rosenzweig, 1971). In addition to these predator-prey cycles more discrete repetitive catastrophic shifts can occur in ecosystems with coupled fast-slow dynamics (Rinaldi and Scheffer, 2000). Examples of such ecosystems are the spruce-budworm ecosystem, in which the recovery of trees from defoliation occurs at a much slower rate than the budworm outbreaks (Ludwig et al., 1978; Holling, 1988) and coastal dune ecosystems in which repetitive shifts between wet and dry soils are thought to occur due to soil water repellency, thereby controlling the much slower vegetation dynamics (Chapter 4). Besides cyclic and static dynamics, ecosystems may transition to apparently random dynamics when environmental conditions change. Such chaotic dynamics are solely caused by deterministic processes and can even occur if the mechanisms controlling the system are very simple and are ought to result in trivial behaviour (May, 1976; Tilman and Wedin, 1991). In addition to transitions towards alternative temporal dynamics, spatially extended ecosystems can change their spatial structure in response to environmental changes. In arid ecosystems for example, declining rainfall may trigger the formation of spatially periodic patterns in vegetation (Valentin et al., 1999; Klausmeier, 1999; Von Hardenberg et al., 2001; Rietkerk et al., 2002).

The notion that environmental change may trigger non-linear ecosystem response can largely be attributed to modelling efforts in the second part of the 20<sup>th</sup> century. In the field of mathematics, the description of natural phenomena using difference and differential equations is referred to as dynamical systems theory, which was introduced by Sir Isaac Newton back in the 17<sup>th</sup> century to lie the foundations of what is now known as classical mechanics (Newton, 1687) and which was later further developed by Henri Poincaré (Poincaré and Magini, 1899). Although the term *ecosystem* had already been

coined in the 1930s (Tansley, 1935; Willis, 1997) and population models had been used well before that (Pisano, 1202; Verhulst, 1838; Volterra, 1928), the dynamical systems approach only got widely applied in ecology in the 1970s (e.g. Rosenzweig, 1971; Noy-Meir, 1975; May, 1977).

The application of the dynamical systems approach to ecology was aided by graphical approaches that enabled analysis of ecological models (e.g. Rosenzweig and MacArthur, 1963). However, the rapid development of theoretical ecology was also closely related to advancements in the mathematical field of bifurcation theory, or more specifically catastrophe theory. Catastrophe theory, from which the term catastrophic shift is derived, was introduced by René Thom (Thom, 1975) and further developed by Christopher Zeeman (Zeeman, 1976; Zeeman and Barrett, 1979). It applies topology to families of fixed points (or steady states/equilibria) to obtain a set of elementary phenomenological models that show how “continuous causes can give rise to discontinuous effects” (Zeeman, 1982). One of the elementary models describes the so-called fold catastrophe. Equation 5.1 is one way this elementary model can be formulated (modified from Ashwin et al., 2012) and describes the dynamics of state variable  $x$  as function of itself and two parameters  $a$  and  $b$ :

$$\frac{dx}{dt} = b - (x - a)^2 \quad (5.1)$$

Figure 5.1a shows that a gradual decline in parameter  $b$  initially results in a minor response of state variable  $x$ . However, if parameter  $b$  decreases beyond a critical threshold value then a catastrophic shift occurs. This behaviour, as well as that of many ecological models, can very well be understood by applying a steady state approximation. As noted above, this approximation enables the derivation of steady states (i.e. dynamic equilibria). Over time, the actual state of a system will move to a steady state if it is stable, and will move away from it when unstable. If a stable steady state only attracts within a certain “basin of attraction” (Lewontin, 1969), it is said to be locally stable (as opposed to globally stable). The proximity of the system state to the boundaries of the basin of attraction and the change in parameters required to pass critical thresholds (i.e. the persistence of the basin of attraction) determines the resilience of an ecosystem. Thus, ecological resilience can be defined as a measure of the ability of ecosystems to absorb changes of state variables, driving variables, and parameters, and still persist (Holling, 1973).

Figure 5.1 shows that, as parameter  $b$  declines, the system closely follows a stable steady state (Figure 5.1a) until the basin of attraction vanishes (Figure 5.1b). Steady state analysis allows deriving the critical threshold value of

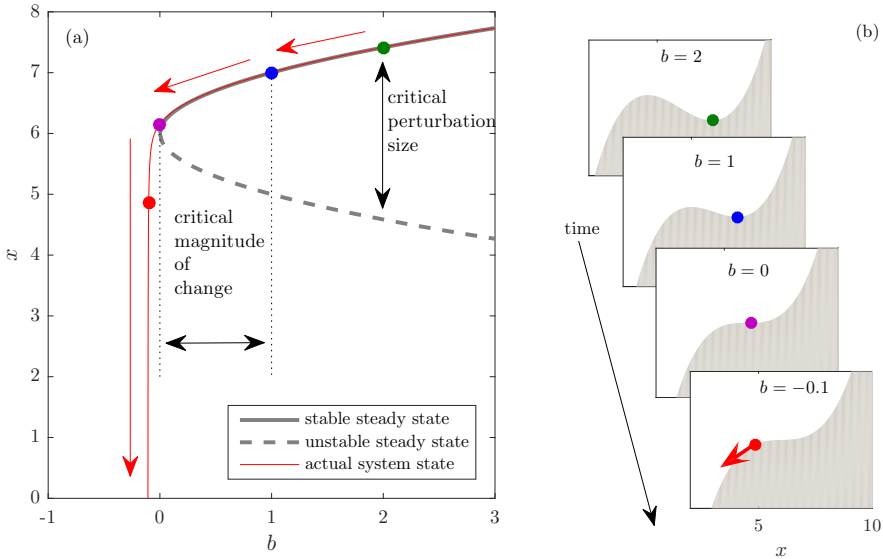


Figure 5.1: (a) Critical transition in a fold catastrophe model (Equation 5.1) triggered by a gradual decrease in parameter  $b$  ( $db/dt = -0.1$  and  $a = 6$ ). (b) Potential landscapes for different values of  $b$ , showing the vanishing of the basin of attraction as  $b$  declines. The coloured dots depict the system state at  $b = 2$  (green),  $b = 1$  (blue),  $b = 0$  (pink) and  $b = -0.1$  (red). In (a) the gray lines give the stable (solid) and unstable (dashed) steady states of the system (i.e. assuming  $db/dt = 0$ ). See Appendix 5.A for a derivation of the steady states and potential diagrams.

$b$  at which the basin of attraction vanishes, as well as the boundary of the basin of attraction, here given by the unstable steady state (see Appendix 5.A). Given the external conditions and the state of the system, this allows deriving the critical magnitude of change in  $b$  and the critical perturbation size in terms of  $x$ , beyond which the system shifts to alternative dynamics as depicted in Figure 5.1a. These properties directly relate to the definition of ecological resilience (Holling, 1973). The susceptibility of ecosystems to the types of critical transitions described so far can thus be assessed and understood through steady state analysis of ecological models.

### 5.3 Rate-induced critical transitions

As illustrated in Figure 5.1, steady state analysis can often properly explain the complex dynamics exhibited by ecological models. However, one can question the validity of the steady state assumption if external conditions

change more rapidly. From a mathematical perspective, models with explicit time dependency of one of the parameters (also referred to as non-autonomous, open or ramped systems; Wieczorek et al., 2010; Ashwin et al., 2012) do generally not have steady states. In analysis of ecological models it is therefore often implicitly assumed that external conditions change slowly compared to the attractive capacity of an ecosystem's stable steady state, such that it approximates the actual system state. While this may be true for ecosystems that are relatively isolated from human activities, the currently observed rates of anthropogenic environmental change could be much higher than the rate at which ecosystems can respond to these changes (Walther et al., 2002). This could result in dynamics that differ from the dynamics predicted by steady state analyses and may even trigger unexpected critical transitions. This would have consequences, not only for the validity of currently applied model analyses, but also for our view on ecological resilience (e.g. as defined by Holling, 1973).

Runs of the model described by Equation 5.1 suggest that if external conditions change rapidly, the actual system state can indeed strongly deviate from the stable steady state, as shown in Figure 5.2a. For relatively slow external changes, now simulated by increasing the value of parameter  $a$ , the actual system state simply lags behind the stable steady state. However, above some critical rate of change in  $a$ , the system is unable to cope with the rapid changes. The rapid increase in  $a$  then drives the system state out of the basin of attraction (Figure 5.2b) and away from the stable steady state. Notice that in this example the two classical measures for resilience identified in the previous section, i.e. the width and the persistence of a basin of attraction (Figure 5.1a), are not affected by changes in  $a$ . Yet, high rates of change in  $a$  can still trigger a critical transition.

The critical transition shown in Figure 5.1 occurs once a critical magnitude of change is exceeded, which can be derived by calculating the distance to the critical threshold value of  $b$ . In contrast, the transition depicted in Figure 5.2 occurs when external conditions (parameter  $a$ ) change with a rate that exceeds a certain critical rate of change. To distinguish between the two types of transitions we will refer to them with the terms “change-induced critical transition” and “rate-induced critical transition” respectively. Systems that are able and likely to display rate-induced critical transitions will be referred to as “rate sensitive systems”.

Although it is quite intuitive that some ecosystems may not be able to respond timely to rapidly changing conditions, this concept has only recently received attention in theoretical ecology (Scheffer et al., 2008). In the

field of neuroscience, however, rate sensitivity of neural cells is a well-known phenomenon. Neural cells are excitable, that is, if an electric current is passed through neural cell tissue excitation can occur, driving further transmission of the current. Excitation only occurs if the current exceeds a certain threshold value. However, accommodation occurs in response to the current, meaning that the critical threshold rises over time (Hill, 1936). As a result, excitation is rate dependent. A model that reproduces these dynamics is a modification of the Van der Pol oscillator (Van der Pol, 1920; FitzHugh, 1961) and shows that excitation can occur if sufficiently large “cathodal shock” is applied (FitzHugh, 1961).

More recently, rate-induced critical transitions have received considerable attention in the mathematical literature (Wieczorek et al., 2010; Ashwin et al., 2012; Perryman, 2015). A particularly well studied model is the model by Luke and Cox (2011). Their model shows that rising atmospheric temperatures may trigger enhanced soil microbial respiration which may further heat soils eventually resulting in a sudden loss of soil carbon and increased CO<sub>2</sub> emissions into the atmosphere. This non-linear response, which they refer to as the “compost-bomb instability”, only occurs if atmospheric temperatures rise quickly and is thus rate-induced.

In the ecological literature, a rate-induced critical transition was first described in a model study by Scheffer et al. (2008). In their model, which captures the dynamics of plants and herbivores, plants become less palatable as their biomass increases. An increase in plant productivity results in an increase of herbivore biomass, provided that the productivity rises slowly compared to the response rate of the herbivores. If, on the other hand, productivity rises rapidly, the model shifts from a herbivore controlled state to a plant dominated state without herbivores (Scheffer et al., 2008). In Box 5.1 we show that rate-induced critical transitions can occur more generally in systems with coupled resource and consumer dynamics.

## 5 Ecosystems off track

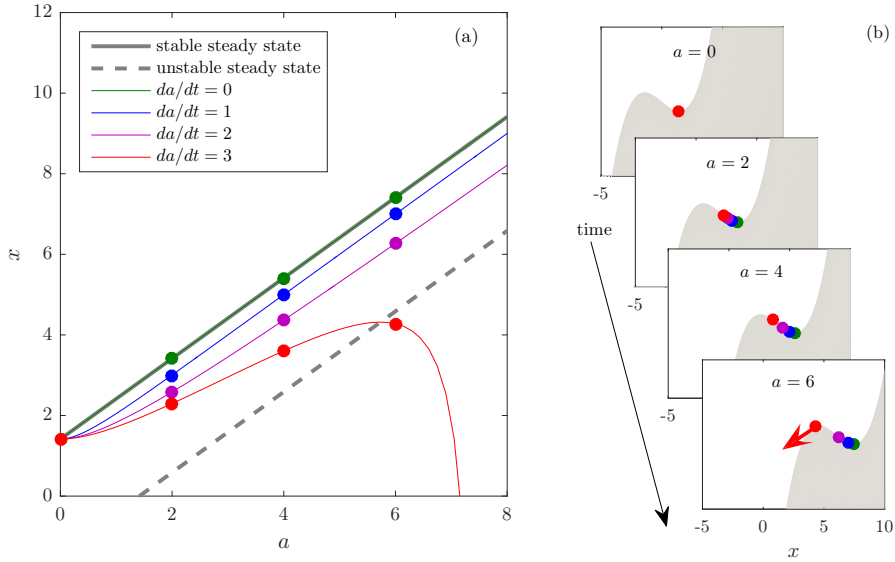


Figure 5.2: (a) Rate-induced critical transition in a fold catastrophe model (Equation 5.1) triggered by a rapid increase in  $a$ . Increases in  $a$  can trigger a critical transition, provided that the rate of change in  $a$  is sufficiently high. (b) The shape of the potential landscape is not affected by  $a$ , however rapid changes in  $a$  can pull the system out of the basin of attraction. In this figure  $b = 2$  and  $da/dt = 0-3$ . The coloured dots depict the actual system state at  $a = 0$ ,  $a = 2$ ,  $a = 4$  and  $a = 6$  for different rates of change. In (a) the gray lines give the stable (solid) and unstable (dashed) steady states of the system (i.e. assuming  $da/dt = 0$ ). See Appendix 5.A for a derivation of the steady states and potential diagrams.

**Box 5.1. An ecological example: rate-induced overconsumption in the Rosenzweig-MacArthur model**

An ecological model that can display rate-induced critical transitions is the model by Rosenzweig and MacArthur (1963) with slow consumer dynamics:

$$\frac{dR}{dt} = rR \left(1 - \frac{R}{K}\right) - \frac{aCR}{R + R_h} \quad (5.2)$$

$$\frac{dC}{dt} = \epsilon \left( \frac{eaCR}{R + R_h} - mC \right) \quad (5.3)$$

Here  $R$  and  $C$  are resource and consumer densities respectively (e.g. in  $\text{g m}^{-2}$ ),  $r$  is the resource growth rate (in  $\text{day}^{-1}$ ),  $K$  is the carrying capacity (in  $\text{g m}^{-2}$ ),  $a$  is the maximum consumption rate (in  $\text{day}^{-1}$ ),  $R_h$  is the resource density at which consumption is half this rate (in  $\text{g m}^{-2}$ ),  $e$  is an efficiency constant,  $m$  is the consumer mortality rate (in  $\text{day}^{-1}$ ) and  $\epsilon$  is a small dimensionless parameter that controls the difference in time scales between the fast resource dynamics and the slower consumer dynamics. Notice that what we consider here as consumers and resource is sometimes referred to as exploiter and victim (Rosenzweig, 1971), predator and prey (Rosenzweig and MacArthur, 1963) or herbivores and plants (Noy-Meir, 1975) respectively.

Figure 5.3 shows how the model responds to declining resource growth rate  $r$ . The steady states of the system predict that a change in  $r$  affects the consumer density, but not the resource density, as shown in Figure 5.3a. Model runs with declining  $r$  show something different (Figure 5.3b and c). Since the response of consumers is slow, due to the low value of  $\epsilon$ , the actual consumer density lags behind its steady state (Figure 5.3b). This means that consumption is higher than predicted with steady state analysis, thereby lowering the resource density (Figure 5.3c). The response to a slow decline in  $r$  is rather linear, since the decrease in consumer density is rapid enough to diminish consumption to a level that enables high resource densities to be maintained. If, however, the rate of change in  $r$  is slightly faster, the consumer density does not decline fast enough and overconsumption occurs resulting in sudden depletion of the resource. The rate of the consumer dynamics (controlled by  $\epsilon$ ), greatly

affects the occurrence of rate-induced critical transitions in this model, since the system can tolerate more rapid decreases in  $r$  if consumers are able to change their density faster (high  $\epsilon$ ).

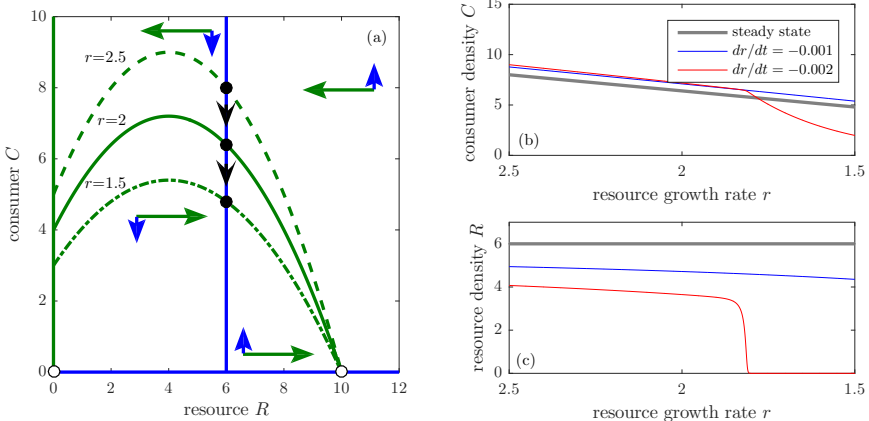


Figure 5.3: A rate-induced critical transition in the model by Rosenzweig and MacArthur (1963) (Equations 5.2 and 5.3) triggered by a decreasing resource growth rate  $r$ . (a) Phase plane of the Rosenzweig-MacArthur model. The green lines are resource isoclines ( $dR/dt = 0$ ) for  $r = 2.5$  (dashed),  $r = 2$  (solid) and  $r = 1.5$  (dash-dotted). The blue lines are consumer isoclines ( $dC/dt = 0$ ). Circles indicate stable (filled) and unstable (open) steady states ( $dR/dt = dC/dt = 0$ ). The black arrows show the movement of the stable steady state as  $r$  decreases. The blue and green arrows give the direction of change if the system is not in a steady state. (b,c) Model response to slowly and less slowly declining  $r$ . In this figure  $r = 1.5\text{--}2.5$ ,  $a = 1$ ,  $e = 1$ ,  $K = 10$ ,  $m = 0.75$ ,  $\epsilon = 0.01$  and  $R_h = 2$ . The model runs were initiated in the stable steady state of the system at  $r = 5$  ( $R = 6$ ,  $C = 16$ ).

## 5.4 Analysis of rate sensitive models

As can be deduced from the example shown in the previous section and in Box 5.1, steady state analysis is insufficient to describe the dynamics of rate sensitive models to rapid changes in parameters as it cannot predict rate-induced critical transitions and therefore may overestimate resilience. Brute force numerical techniques, such as model runs with varying rates of change (for example Figure 5.2a, Figure 5.3bc and Scheffer et al., 2008), can be used to study rate sensitivity and to estimate critical rates of change. However, to obtain more general insights into the mechanisms that drive rate-induced

transitions and to be able to derive explicit expressions for critical rates of change, analytical techniques are required. Unfortunately, an equivalent to steady state analysis that can be universally applied to study rate sensitive systems has not yet been developed. However, a comprehensive attempt to understand rate sensitivity in models with coupled fast-slow dynamics (such as the model by Rosenzweig and MacArthur (1963) described in Box 5.1) was introduced in a paper by Wieczorek et al. (2010). Their approach allows derivation of a critical rate of change through desingularization, time reversal and calculation of eigenvectors. Discussion of this approach goes beyond the scope of this paper, but in the following section we will present two less comprehensive alternative approaches that allow us to analyse the rate-induced critical transition in the model described by Equation 5.1. These alternative approaches are introduced here to provide a general mechanistic understanding of rate-induced critical transitions and to enable discussion on the outstanding challenges that come with the analysis of rate sensitive ecological models.

### 5.4.1 Graphical analysis of Equation 5.1

In Figure 5.2 we showed that a rate-induced critical transition occurs in the model of Equation 5.1 when the actual system state leaves the basin of attraction of the stable steady state, i.e. when it passes the unstable steady state of Equation 5.1. This event is triggered by the movement of unstable steady state, which in turn is driven by the change in parameter  $a$ . Whether the unstable steady state is able to overtake the actual system state, can be assessed graphically by comparing the maximum response rate of the system under static conditions (i.e. the maximum value of  $dx/dt$ ) with the movement rate of the unstable steady state, as shown in Figure 5.4. This graphical comparison shows that the movement rate of the unstable steady state exceeds the maximum response rate of the system if parameter  $a$  changes with a rate beyond a critical rate of change of  $da/dt = 2$ .

This result can also be obtained analytically by deriving both the maximum response rate and the movement rate of the unstable steady state. The maximum of Equation 5.1 is located at  $x = a$ , meaning that the maximum response rate equals:

$$\frac{dx}{dt} = b - (x - a)^2 = b \quad (5.4)$$

The unstable steady state is given by  $\bar{x}_- = a - \sqrt{b}$  (see Appendix 5.A) and its derivative to  $a$  equals 1. Thus, the moving rate of the unstable steady

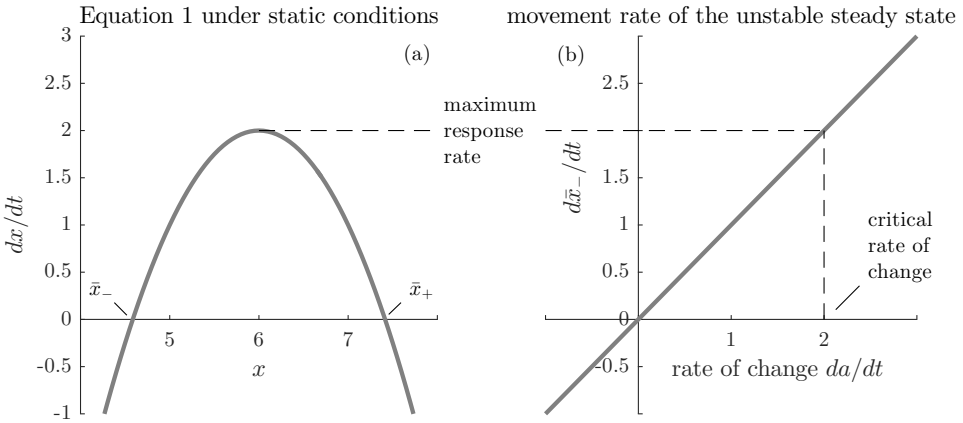


Figure 5.4: A rate-induced critical transition occurs in the model described by Equation 5.1 if the movement rate of the unstable steady state exceeds the maximum response rate of the system. (a) Dynamics in  $x$  under static conditions, for  $a = 6$  and  $b = 2$ . Here  $\bar{x}_+$  is the stable steady state and  $\bar{x}_-$  is unstable steady state, which moves with a rate depicted in (b) as  $a$  changes.

state is given by:

$$\frac{d\bar{x}_-}{dt} = \frac{d\bar{x}_-}{da} \frac{da}{dt} = \frac{da}{dt} \quad (5.5)$$

Equalizing Equations 5.4 and 5.5 yields a critical rate of change in  $a$  of:

$$\frac{da}{dt} = b \quad (5.6)$$

beyond which the unstable steady state is able to overtake the actual system state. Notice that both the graphical and the analytical result correspond with the model runs presented earlier in Figure 5.2.

### 5.4.2 Steady lag analysis of Equation 5.1

Figure 5.2a shows that under steady conditions ( $da/dt = 0$ ) the system can be assumed to reside in a stable steady state  $x = \bar{x}_+$ , but that as parameter  $a$  changes over time ( $da/dt \neq 0$ ) the actual state of the system starts to lag behind its stable steady state. The actual state of the system can then be written as the sum of the stable steady state  $\bar{x}_+$  and the lag of the system state  $\xi$ :

$$x = \bar{x}_+ + \xi \quad (5.7)$$

with  $\bar{x}_+ = a + \sqrt{b}$  (see Appendix 5.A). Rewriting gives  $\xi = x - \bar{x}_+$ , so that the change of the lag  $\xi$  over time can be written as:

$$\begin{aligned}
\frac{d\xi}{dt} &= \frac{d(x - \bar{x}_+)}{dt} \\
&= \frac{dx}{dt} - \frac{d\bar{x}_+}{dt} \\
&= b - (x - a)^2 - \frac{d\bar{x}_+}{da} \frac{da}{dt} \\
&= b - (\bar{x}_+ + \xi - a)^2 - \frac{d(a + \sqrt{b})}{da} \frac{da}{dt} \\
&= b - (a + \sqrt{b} + \xi - a)^2 - \frac{da}{dt} \\
&= b - (\sqrt{b} + \xi)^2 - \frac{da}{dt}
\end{aligned} \tag{5.8}$$

For linear changes in  $a$  (i.e. constant  $da/dt$ ) Equation 5.8 becomes autonomous. This means that, unlike Equation 5.1, it does not explicitly depend on the changing parameter  $a$ . Therefore, we can set  $d\xi/dt$  to zero to obtain the steady state of Equation 5.8, or the “steady lag” of  $x$  behind the steady state of Equation 5.1.

Two steady lags can be found of which  $\bar{\xi}_+$  is stable (see Appendix 5.B for stability analysis):

$$\bar{\xi}_{\pm} = \pm \sqrt{b - \frac{da}{dt}} - \sqrt{b} \tag{5.9}$$

This equation has no solution for  $da/dt > b$ . Indeed, Figure 5.5 shows that, in line with the analysis in the previous section and model runs of Figure 5.2a, this model has a critical rate of increase for parameter  $a$  of:

$$\frac{da}{dt} = b \tag{5.10}$$

above which the actual system state is unable to track the stable steady state. Notice that by rewriting in terms of  $\xi$ , the model reduces to the fold catastrophe model with  $da/dt$  being the driving parameter.

### 5.4.3 Understanding rate sensitivity of ecological models

The analyses of Equation 5.1 presented in Sections 5.4.1 and 5.4.2 provide a number of key insights regarding the general mechanisms that could be

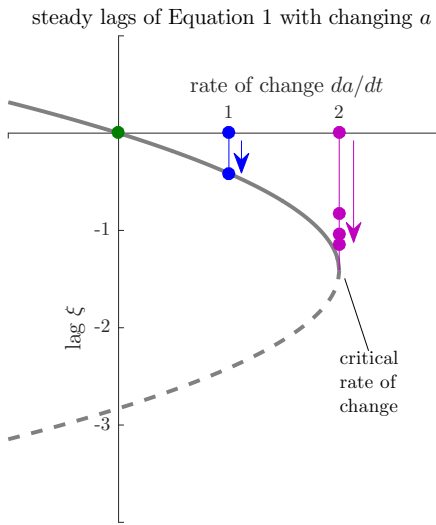


Figure 5.5: The model described by Equation 5.1 lags in a way equivalent to the fold catastrophe model with the rate of change  $da/dt$  as driving parameter. The gray solid lines are stable steady lags and the dashed lines are unstable steady lags. The colored lines and dots correspond to the model runs shown in Figure 5.2

responsible for rate-induced critical transitions in ecological models and real ecosystems. First, the graphical analysis of Section 5.4.1 suggests that rate-induced critical transitions are likely to occur when the rate of environmental change is high relative to the maximum response rate of ecosystems (Figure 5.4). Second, analysis of the lag of the system state behind its steady state revealed that rate-induced critical transitions are similar to change-induced critical transitions, e.g. they can be described by the fold catastrophe model (Figure 5.5), but are driven by rates, rather than magnitudes, of environmental change. Finally, both analyses suggest that rate-induced critical transitions occur once a critical rate of change is exceeded.

Although both analyses provide general mechanistic insights regarding rate sensitivity of models and possibly of real ecosystems, they are only of limited value when studying specific mechanisms that drive rate-induced critical transitions in a particular ecosystem or in more comprehensive ecological models. First, the graphical approach of Section 5.4.1 can only be applied to models with one state variable, such as Equation 5.1, or models with coupled fast-slow dynamics (e.g. Rosenzweig and MacArthur, 1963, Box 5.1) that

can be reduced to a system with one state variable through a quasi-steady state approximation. Second, both the maximum response rate and the movement rate of the unstable steady state of Equation 5.1 remain unaltered as parameter  $a$  changes, which is generally not the case for comprehensive ecological models. Applying this graphical approach on ecological models could therefore lead to erroneous critical rates of change. Finally, the steady lag approach has its limitations, as it can only be applied to models with an autonomous lag equation (Equation 5.8). For models other than Equation 5.1, the lag generally depends on the changing parameter, meaning that the lag is explicitly time dependent and a steady lag cannot be assumed.

In Appendices 5.C and 5.D we apply both analyses on the ecological model by Rosenzweig and MacArthur (1963, Box 5.1) to study whether the discussed limitations do indeed result in significant errors when applying the analyses to assess critical rates of change in parameters of ecological models. Both analyses yield a critical rate of change in parameter  $r$  of  $dr/dt = -1.5 \times 10^{-3}$  day $^{-2}$  or:

$$\frac{dr}{dt} = \epsilon r \left( \frac{ea(K - R_h)}{K + R_h} - m \right) \quad (5.11)$$

This value indeed differs from the critical rate of change of  $dr/dt = -2 \times 10^{-3}$  day $^{-2}$  found through model runs (Figure 5.3c). This suggests that, although helpful for identifying the general mechanisms behind rate sensitivity, the presented analyses can only be applied to a limited subset of models.

## 5.5 Identifying real rate sensitive ecosystems

While the critical thresholds that are responsible for change-induced transitions can be found relatively easily using steady state analysis, critical rates of change are more difficult to detect, as pointed out in the previous section. As a result, the identification of rate sensitive models and ultimately of rate sensitive ecosystems will be more challenging. There are, however, some common features of rate sensitive models that may be useful in doing so, as we will discuss in this section.

In contrast to change-induced critical transitions, ecosystems that respond slowly to environmental change are more sensitive to rate-induced critical transitions. This means that ecosystems with at least one slow state variable are more likely to exhibit rate-induced transitions. Such transitions may however not significantly affect the slow variable (Hughes et al., 2013), but may be prominent in a fast state variable with which it interacts. In

the model by Rosenzweig and MacArthur (1963, Box 5.1) for example, the slow consumers fail to cope with their declining resource, leading to overconsumption and a collapse in resource density. Other examples are the model by Luke and Cox (2011) with slow soil carbon dynamics and fast soil temperature dynamics and the model by Scheffer et al. (2008) with slow herbivore and fast plant dynamics, discussed in Section 5.3. In these models the fast variables have hump-shaped isolines. This means that the fast variables are controlled by non-linear processes. In the model by Rosenzweig and MacArthur (1963) for instance, both the logistic growth of the resource and its consumption are non-linear processes and in the model by Luke and Cox (2011) the soil carbon decomposition rate increases exponentially with soil temperature. These examples suggest that ecosystems that have coupled slow and fast non-linear processes may be more likely to undergo rate-induced critical transitions.

Models with coupled fast-slow dynamics are also known to exhibit repetitive catastrophic shifts, as previously mentioned in Section 5.2. These systems have the same properties as the rate sensitive systems described above, but are in an unstable regime. Ecosystems in which such cyclic dynamics have been observed may therefore be rate sensitive under slightly different environmental conditions. Observing such dynamics at one location may therefore be an indicator that elsewhere along an environmental gradient the ecosystem is rate sensitive. In coastal dune ecosystems for example, water repellency of soils results in nonlinear soil water dynamics (Dekker and Jungerius, 1990; Dekker and Ritsema, 1994). In these ecosystems the combination of slow plant dynamics and soil water repellency is thought to drive repetitive catastrophic shifts under some conditions and to trigger rate-induced critical transitions in response to declining precipitation under other conditions (Chapter 4).

Recent studies suggest that ecosystems with spatially periodic patterns may exhibit rate dependent behaviour (Chapter 2; Sherratt, 2013a; Chen et al., 2015). Such patterns are ubiquitously observed in arid ecosystems (Deblauwe et al., 2008), which are currently undergoing rapid climatic changes (Chapter 3; Tebaldi et al., 2006). In periodically patterned ecosystems patches of consumers (e.g. plants) compete for a limiting resource (e.g. water). As resource input declines, patches go extinct and the remaining patches rearrange to regain an optimal periodic pattern. If the rearrangement process occurs slowly with respect to the rate of decrease in resource input, a large fraction or even all of the patches may go extinct simultaneously. This is caused by a delayed transition, which forces the model to cross a so-called

period-doubling bifurcation (Siero et al., 2015, Chapter 2;). Rate sensitivity of spatially extended models suggests that spatially periodic patterns could serve as an indicator of real rate sensitive ecosystems.

The common properties of rate sensitive models could be used to determine the *ability* of ecosystems to undergo rate-induced critical transitions. To assess their *susceptibility* to rate-induced transitions, one could estimate the recovery rate of ecosystems to perturbations. As shown in Box 5.2 for the model described by Equation 5.1, ecosystems can be expected to become slower in recovering from perturbations when rates of change approach critical rates of change. When subject to natural variability, this could lead to increasing temporal autocorrelation and variance in an ecosystem's state variables. In addition, low diversity and high connectivity are architectural features known to make ecological networks susceptible to critical transitions (Scheffer et al., 2012). Finally, the susceptibility of ecosystems to rate-induced critical transitions could be assessed using the mechanistic insights provided by the analyses in Section 5.4. For example, maximum observed response rates in experiments or time series of real ecosystems could be used to assess the susceptibility of ecosystems to rate-induced critical transitions. Note that these types of analyses are now already being applied to real ecosystems (e.g. Carpenter et al., 2011, 2014), and could be extended to specifically study rate-induced critical transitions.

**Box 5.2. Generic early-warning signals for rate-induced critical transitions.**

As systems approach critical thresholds, they become increasingly slow in recovering from perturbations (Wissel, 1984; Scheffer et al., 2009). This phenomenon, known as “critical slowing down”, is expected to result in increasing variance and autocorrelation in systems that are subject to natural variability. Figure 5.6 shows that these early-warning signals also precede the rate-induced critical transition found for the model of Equation 5.1. The increases in recovery time, autocorrelation and variance are both predicted by the steady lag analysis (red curves) and model runs (blue crosses), but can not be regarded as trivial since flattening of the potential landscape associated with critical slowing down (Scheffer et al., 2009) does not occur as the rate of change approaches its critical value (see Figure 5.2b).

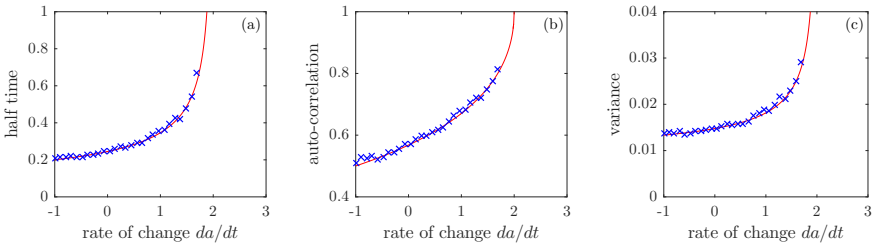


Figure 5.6: Increasing recovery time from perturbations (a), lag-1 auto-correlation (b) and variance (c) in state variable  $x$  of Equation 5.1 as the rate of change in parameter  $a$  approaches a critical rate of change of  $da/dt = 2 (= b)$ . The crosses represent the value of each statistic on detrended time series of  $x$  with a length of  $t = 2000$ . State variable  $x$  was perturbed with Gaussian noise with a standard deviation of  $\sigma = 0.1$ , which was applied with an interval of  $\Delta t = 0.2$ . The curves are derived by linearization around the steady lags. The half time is given by  $t_h = \frac{1}{\lambda} \ln(\frac{1}{2})$ , with  $\lambda = -2\sqrt{b - r}$  (see Appendix 5.B), the auto-correlation is given by  $\alpha = e^{\lambda \Delta t}$  and the variance by  $\text{VAR} = \frac{\sigma^2}{1 - \alpha^2}$ .

## 5.6 Discussion and conclusions

Current anthropogenic environmental changes occur at unprecedented rates (Joos and Spahni, 2008; Kaplan et al., 2011; Klein Goldewijk et al., 2011). In this paper we presented and discussed models that suggest that, for some ecosystems, rates of environmental change may be too high to cope with, thereby triggering a new type of critical transition. These rate-induced critical transitions are challenging to analyse in ecological models, but can be understood in elementary models by applying graphical analyses or by studying the lag behind a system's stable steady state. These analyses revealed that (i) rate-induced critical transitions occur if the rate of environmental change is high compared to the response rate of ecosystems, (ii) rate-induced critical transitions are similar to change-induced critical transitions but are driven by rates, rather than magnitudes, of environmental change and (iii) rate-induced critical transitions occur once a critical rate of change is exceeded. Identification of rate-sensitive ecosystems would also be challenging, but common features of rate-sensitive models suggest that ecosystems with coupled fast-slow dynamics, exhibiting repetitive catastrophic shifts or spatially periodic patterns are more likely to display rate-induced critical transitions.

Although we have suggested a number of common features of rate sensitive

models which may be useful in identification of rate sensitive ecosystems (Section 5.5), disentangling change- and rate-induced critical transitions in observations would still be challenging. Indeed, to our knowledge no observations of rate-induced critical transitions in real ecosystems have been reported. Rate dependent outcomes have however been reported in a number of experimental studies. Rate dependency is a well known problem for short-term experimental studies on the effect of the relatively gradual rise in atmospheric CO<sub>2</sub> on ecosystem structure and functioning (Luo and Reynolds, 1999; Klironomos et al., 2005; Luo and Hui, 2009). For example, Klironomos et al. (2005) have found that increasing the CO<sub>2</sub> concentrations instantly from 350 to 550 ppm resulted in a significantly different soil mycorrhizal community structure, whereas the same magnitude of change applied over a period of about 6 years had no significant effect. There is no reason to believe that such rate dependencies at the community level would have no effects at the ecosystem level, meaning that these experiments do not rule out the possibility of rate sensitivity of real ecosystems.

By using ordinary differential equations to model ecosystems, we implicitly assumed that ecosystems can only respond to environmental changes by adjusting the levels of their state variables. For example, consumers in the model by Rosenzweig and MacArthur (1963, Box 5.1), only respond to the declining resource density by lowering their own density. In real ecosystems however, populations are known to adapt to environmental changes in other ways too, namely by (i) evading to more suitable habitats or by adapting in situ through (ii) phenotypic plasticity and/or through (iii) micro-evolutionary adaptation (Holt, 1990). The rates of these three alternative response mechanisms are bounded, potentially leading to additional critical rates of environmental change. For example, Devictor et al. (2012) found that butterfly and bird populations in Europe do not meet the required displacement velocities to track shifting temperatures, and are building up what they call a “climatic debt”. Also micro-evolutionary adaptation has a limited rate, and theory suggests that critical rates of environmental change exist beyond which selective pressures become too high for positive population growth to be maintained (Lynch and Lande, 1993; Bürger and Lynch, 1995; Chevin et al., 2010). In order to predict the effect of rapid environmental changes on ecosystems, both the mechanisms behind rate-induced critical transitions on ecosystem level and behind the alternative responses on population level need to be understood.

The focus of steady-state analysis on long-term asymptotic behaviour of ecosystems is sometimes inappropriate and does not always match with

ecologically relevant time scales (Hastings, 2004; Hughes et al., 2013). Our study shows that steady state analysis is also insufficient to study rate-induced critical transitions. Steady state analysis has shaped the common view on concepts like ecological resilience, as we have pointed out in Section 5.2. Definitions of resilience (e.g Holling, 1973) are based on the view that ecosystems may shift to alternative dynamics when (external) change or perturbations drive ecosystems beyond a critical threshold. Hence a critical magnitudes of external change and disturbances can be regarded as measures for resilience (Figure 5.1a). However, these definitions and measures do not apply to rate sensitive ecosystems, which may or may not cope with a magnitude of change depending on the time scale over which the change occurs. This suggests that in some cases a broader definition of resilience that acknowledges critical rates of change would be more applicable.

The idea of alternative stable states and critical thresholds in ecosystems has motivated formulation of preconditions for human development on a global scale referred to as “planetary boundaries” (Rockström et al., 2009; Steffen et al., 2015; Scheffer, 2015). The proposed boundaries are however all critical levels (e.g. atmospheric carbon dioxide concentration) or rates controlling levels (e.g. the rate of phosphorous mining which controls phosphorous concentrations in the oceans). Rate sensitivity found in models suggests that, given the elevated rates of change in the environment that accompany human development, defining boundaries based on critical levels may not be enough to ensure a safe operating space. In order to define critical rates of change on ecosystem level or even on a global level and to identify rate sensitive systems, a better mechanistic understanding of rate-induced critical transitions is needed.

## Acknowledgements

We would like to thank Maria J. Santos, Jerry van Dijk and two anonymous reviewers for their insightful comments on the manuscript. This study is supported by a grant within the Complexity programme of the Netherlands Organization for Scientific Research.

## Appendix 5.A Steady states and potential diagrams for Equation 5.1

In this appendix we study the steady states of Equation 5.1 and derive its potential diagrams. The equation describes the change in state variable  $x$  over time as function of itself and at parameters  $a$  and  $b$ :

$$\frac{dx}{dt} = b - (x - a)^2 \quad (5.12)$$

The steady states ( $dx/dt = 0$ ) of this equation are given by  $\bar{x}_\pm = a \pm \sqrt{b}$ . In order for steady states to exist we require  $b \geq 0$ . General equations for perturbations are given by:

$$\frac{d(x + x')}{dt} - \frac{dx}{dt} = [b - (x + x' - a)^2] - [b - (x - a)^2] = 2(a - x)x' - x'^2 \approx \lambda x' \quad (5.13)$$

with  $\lambda = 2(a - x)$ . Filling in  $\bar{x}_\pm$  gives  $\lambda_\pm = \mp 2\sqrt{b}$ . This means that  $\bar{x}_+$  is stable and  $\bar{x}_-$  is unstable for  $b > 0$ . Notice that parameter  $a$  affects neither the existence nor the stability of the steady states. The potential landscapes of Figures 5.1b and 5.2b in the main text are given by:

$$p(x) = - \int (b - (x - a)^2) dx = a^2 x - ax^2 - bx + \frac{1}{3}x^3 + C \quad (5.14)$$

## Appendix 5.B Stability analysis for Equation 5.8

In this appendix we study the stability of the steady states of Equation 5.8 in the main text which describes the lag of Equation 5.1 behind the stable steady state as parameter  $a$  changes:

$$\frac{d\xi}{dt} = b - (\sqrt{b} + \xi)^2 - \frac{da}{dt} \quad (5.15)$$

Since this equation is autonomous for linearly changing  $a$ , say  $da/dt = r$ , we can set  $d\xi/dt$  to zero to obtain the steady states. This yields  $\bar{\xi}_\pm =$

$\pm\sqrt{b-r}-\sqrt{b}$ . The stability of  $\bar{\xi}_\pm$  can be determined by adding perturbations.

$$\begin{aligned}\frac{d(\xi + \xi')}{dt} - \frac{d\xi}{dt} &= \left[ b - (\sqrt{b} + \xi + \xi')^2 - r \right] - \left[ b - (\sqrt{b} + \xi)^2 - r \right] \\ &= -2(\sqrt{b} + \xi)\xi' - \xi'^2 \\ &\approx \lambda\xi'\end{aligned}\tag{5.16}$$

with  $\lambda = -2(\sqrt{b} + \xi)$ . Filling in  $\bar{\xi}_\pm$  gives  $\lambda_\pm = \mp 2\sqrt{b-r}$ . This means that  $\bar{\xi}_+$  is stable and  $\bar{\xi}_-$  is unstable. If  $r$  is greater than  $b$ , then the system is not able to track the stable steady state  $\bar{x}_+$  of Equation 5.1 (see Figure 5.5b in the main text), so a critical rate of change in  $a$  is given by  $r := r_c = b$ .

## Appendix 5.C Graphical analysis of the Rosenzweig-MacArthur model

In this appendix we apply the graphical analysis presented in Section 5.4.1 to the model by Rosenzweig and MacArthur (1963, Box 1):

$$\frac{dR}{dt} = rR \left(1 - \frac{R}{K}\right) - \frac{aCR}{R + R_h} \tag{5.17}$$

$$\frac{dC}{dt} = \epsilon \left( \frac{eaCR}{R + R_h} - mC \right) \tag{5.18}$$

In order to apply the graphical analysis, the model needs to be reduced to a model with one state variable, which can be accomplished by assuming fast state variable  $R$  to be in equilibrium (quasi-steady state approximation). This yields:

$$\frac{dC}{dt} = \epsilon \left( \frac{eaCR_\pm^*}{R_\pm^* + R_h} - mC \right) \tag{5.19}$$

with  $R_\pm^*(C) = \frac{1}{2}(K - R_h) \pm \sqrt{\frac{1}{4}(R_h + K)^2 - aCKr^{-1}}$  and  $R_-^*$  being unstable. The basin of attraction of the model described by Equation 5.1 was bordered by an unstable steady state. For this model, in contrast, the basin of attraction is bordered by the optimum in the resource isocline (Figure 5.3a; Wieczorek et al., 2010):

$$C_b = \frac{r(R_h + K)^2}{4aK} \tag{5.20}$$

### 5.C Graphical analysis of the Rosenzweig-MacArthur model

and moves with a rate of:

$$\frac{dC_b}{dr} = \frac{dC_b}{dr} \frac{dr}{dt} = \frac{C_b}{r} \frac{dr}{dt} \quad (5.21)$$

Figure 5.7 shows that by graphically comparing Equations 5.19 and 5.21 a critical rate of change in  $r$  can be found at  $dr/dt = -1.5 \times 10^{-3}$ .

This result can be found analytically by deriving the maximum response rate and comparing it with Equation 5.21. The maximum response rate of the system is given by the decline rate in consumer density  $dC/dt$  on the boundary of the basin of attraction  $C_b$ , which can be found by filling in Equation 5.20 in Equation 5.19:

$$\frac{dC}{dt} = \epsilon C_b \left( \frac{ea(K - R_h)}{K + R_h} - m \right) \quad (5.22)$$

Equalizing equations 5.22 and 5.21 and solving for  $dr/dt$  gives the critical rate of change in  $r$ :

$$\frac{dr}{dt} = \epsilon r \left( \frac{ea(K - R_h)}{K + R_h} - m \right) \quad (5.23)$$

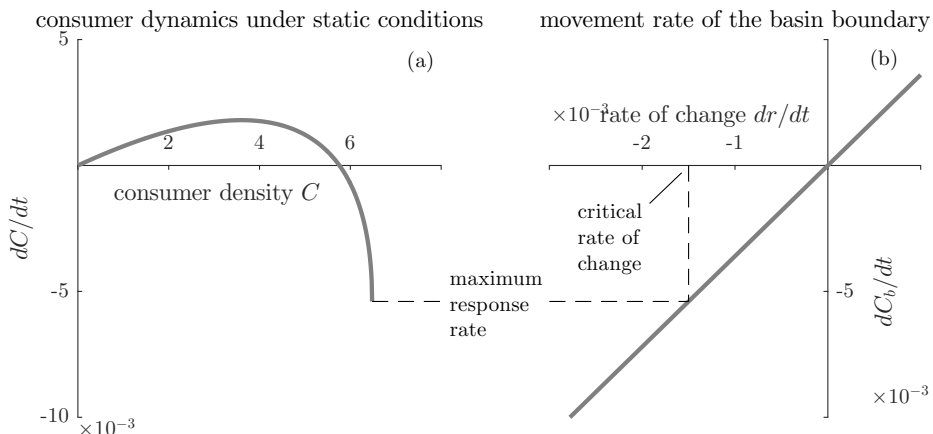


Figure 5.7: Rate-induced overconsumption occurs in the model by Rosenzweig and MacArthur (1963, Box 1) if the rate of basin boundary movement exceeds the maximum decline rate of consumers. (a) Consumer dynamics  $\frac{dC}{dt}$  under static external conditions when assuming the resource density to be in equilibrium (Equation 5.19). For parameter values see the caption of Figure 5.3 in Box 1 ( $r = 1.8 \text{ day}^{-1}$ ).

## Appendix 5.D Steady lag analysis of the Rosenzweig-MacArthur model

In this appendix we apply the steady lag analysis presented in Section 5.4.2 to the model by Rosenzweig and MacArthur (1963, Box 1):

$$\frac{dR}{dt} = rR \left(1 - \frac{R}{K}\right) - \frac{aCR}{R + R_h} \quad (5.24)$$

$$\frac{dC}{dt} = \epsilon \left( \frac{eaCR}{R + R_h} - mC \right) \quad (5.25)$$

For  $K < R_h \left(1 + \frac{2m}{ea-m}\right)$  this model has one stable steady state  $(\bar{R}, \bar{C})$  at  $\bar{R} = \frac{mR_h}{ea-m}$  and  $\bar{C} = r(1 - \bar{R})(\bar{R} + R_h)$ . If  $r$  changes with a rate of  $dr/dt$ , the actual system state  $(R, C)$  starts to lag behind the stable steady state. The lag of the actual system state  $(\rho, \gamma)$  behind the stable steady state can be described by:

$$\frac{d\rho}{dt} = r(\bar{R} + \rho) \left(1 - \frac{\bar{R} + \rho}{K}\right) - \frac{a(\bar{C} + \gamma)(\bar{R} + \rho)}{\bar{R} + \rho + R_h} - \frac{d\bar{R}}{dr} \frac{dr}{dt} \quad (5.26)$$

$$\frac{d\gamma}{dt} = \epsilon \left( \frac{ea(\bar{C} + \gamma)(\bar{R} + \rho)}{\bar{R} + \rho + R_h} - m(\bar{C} + \gamma) \right) - \frac{d\bar{C}}{dr} \frac{dr}{dt} \quad (5.27)$$

The steady state of this system (or steady lag  $(\bar{\rho}, \bar{\gamma})$ ) can be obtained by setting Equations 5.26 and 5.27 to zero. Figure 5.8, shows how the steady lag depends on the rate of change in  $r$ . The steady lag loses its stability at  $dr/dt = -1.5 \times 10^{-3}$ . As discussed in the main text, this result may be erroneous since Equations 5.26 and 5.27 are non-autonomous (i.e. depend on  $r$ ).

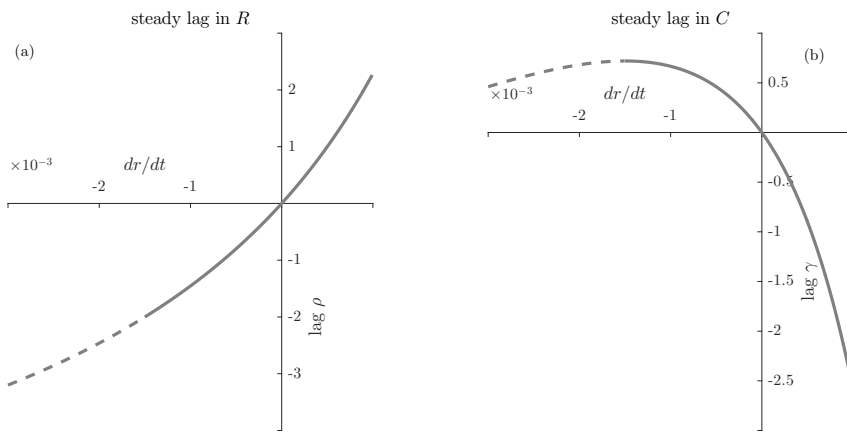


Figure 5.8: Steady lag for the model by Rosenzweig and MacArthur (1963, Box 1) with decreasing  $r$ . These figures were obtained by numerical continuation of Equations 5.26 and 5.27 using Grind for Matlab version 2.00, developed by Egbert van Nes (Wageningen University, NL).



# **6 Synthesis and perspectives**

## **6.1 Ecosystems "off the beaten track" and their response to environmental change**

The application of dynamical systems theory on ecological problems has provided a major contribution to the development of theoretical ecology and has led to key insights in the field of environmental sciences. Of particular interest is the fact that dynamical ecological models suggest that environmental change can trigger critical transitions in ecosystems. Through the application of equilibrium analysis, the mechanisms driving critical transitions from spatially uniform equilibrium states to alternative uniform equilibrium states, to cyclic dynamics and to spatially periodic patterns can be studied in detail (see Chapter 1). These transitions are well-understood because of analytical tractability of uniform equilibrium states. Although frequently assumed, many ecosystems do not reside in uniform equilibrium states. In this dissertation I tried to understand the response of ecological models that are “off the beaten track”, i.e. that are not in a uniform equilibrium state, because of spatial patterning (Chapter 2), because of pulsed resource input (Chapter 3), because of cyclic dynamics (Chapter 4) or because of rapid external change (Chapter 5).

In Chapter 2 I showed that through advanced analyses it is possible to assess the stability of spatially patterned states of ecological models, and demonstrated that insights in pattern stability are key to understanding the response of ecological models to environmental change. More specifically, I showed that a family of patterned states can be stable for a given set of environmental conditions (i.e. multistability) and that patterned ecosystems may respond gradually to environmental change, provided that the change occurs slowly. However, ecosystems are more likely to respond in a discontinuous way to rapid environmental change, meaning that patterned ecosystems may shift to a uniform (degraded) state even when alternative stable patterned states still exist. Continuous response of models to environmental change is bordered by a well-defined “period-doubling instability”, which may be

## *6 Synthesis and perspectives*

triggered by rapid change through a delayed transition. In real patterned ecosystems, period doubling can be explained by the (in)ability of patches to rearrange in response to environmental change, which may serve as an indicator for resilience.

In Chapter 3 I studied how changes in the frequency and magnitude of resource pulses could affect ecosystems with limited uptake capacity. More specifically I studied effect of changes in the frequency and intensity of rain events on arid ecosystems. By aggregating rain events I was able to apply equilibrium analysis to show that projected changes towards a rainfall regime with infrequent high intensity events may trigger a shift to a degraded state without any vegetation. In spatially patterned arid ecosystems, the same shift may be triggered by changes towards a rainfall regime with frequent low intensity rain events. These results suggest that patterned arid ecosystems are most resilient if rain events have an intermediate frequency and intensity. Whether changes in rainfall patterns are harmful or beneficial for arid ecosystems is therefore dependent on the current rainfall regime.

Cyclic dynamics of ecological models generally cannot be understood through equilibrium analysis. However, in combination with separation of timescales, it can explain the dynamics of ecosystems with processes at multiple timescales, as I demonstrated in Chapter 4. With this approach I was able to explain both the short-term and long-term dynamics of a coastal dune ecological model, consisting of rapid repetitive shifts in water availability and long periods in which the model is locked in a state without vegetation. The stagnation of the short-term cyclic dynamics of the model can be explained both by internal dynamics and by rapid external changes, such as a sudden decline in precipitation. This approach enabled identifying soil water repellency as a potential driver of vegetation dynamics in coastal dune ecosystems.

In Chapter 5 I discussed and introduced models that suggest that elevated rates of environmental change can trigger critical transitions in ecosystems, even if the same magnitude of slow environmental change would not (Figure 6.1). Understanding the mechanisms behind such rate-induced critical transitions is challenging, but analyses of an elementary model showed that rate-induced critical transitions are likely to occur when the rate of environmental change is high relative to the maximum response rate of ecosystems, that they are similar to change-induced critical transitions but are driven by rates, rather than magnitudes, of environmental change and that they occur once a critical rate of environmental change is exceeded. Common properties of rate sensitive ecological models suggest that ecosystems with

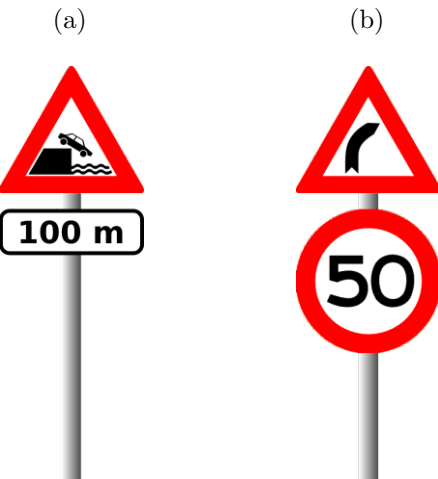


Figure 6.1: (a) When neglecting this traffic sign drivers may risk witnessing a critical transition of their vehicle to an alternative (degraded) state when the magnitude of change in the vehicle's position exceeds 100 meters. (b) Findings presented in Chapter 5 suggest that a critical transition may also occur when a critical rate, rather than magnitude, of change is exceeded (e.g. 50 km/h).

coupled fast-slow dynamics, that exhibit repetitive catastrophic shifts or that display spatially periodic patterns, may be prone to rate-induced critical transitions.

The findings presented in this dissertation did not only lead to new insights but also to open questions and new challenges that need to be addressed in future research, as I will discuss in the following sections.

## 6.2 Patterned ecosystems: multistability, gradual transitions and early-warning signals?

Stability analysis of spatially periodic patterned states in an arid ecosystem model presented in Chapter 2 suggests multistability of patterned ecosystems. Validating multistability with empirical data is challenging. An illustrative example is the bistability of the savanna and forest biomes due to a fire feedback, suggested by both simple (Beckage et al., 2009; Staver and Levin, 2012; Van Nes et al., 2014; Staal et al., 2015) and comprehensive models (Higgins and Scheiter, 2012; Baudena et al., 2015) based on insights from decades of experiments (Higgins et al., 2007) and supported by bimodality in tree cover data (Hirota et al., 2011; Staver et al., 2011; Yin et al., 2014) but

## 6 Synthesis and perspectives

currently still subject of an active debate in which both data and mechanisms are questioned (Hanan et al., 2014; Staver and Hansen, 2015; Veenendaal et al., 2015; Staal and Flores, 2015).

Validating multistability of patterned ecosystems would be even more challenging because the modelled stable patterned states make up a continuous family (a Busse balloon), whereas stable uniform states are generally separated by distinct unstable states. As a result, multimodality of data, frequently used as an indicator for multistability of well-mixed systems, is not expected to be found in the wavenumber data of patterned ecosystems. The unimodal data that is expected to arise from multistability is however also insufficient to validate multistability, because unimodality can as well result from monostability, as illustrated by Figure 6.2. Hence, the modality of wavenumber data would not provide the information needed to falsify or verify multistability of patterned ecosystems.

Another approach that may be more successful involves comparing areal images of a given region separated by a sufficiently long time interval. This would enable studying the temporal dynamics of patterned ecosystems. The model runs in Chapter 2 suggest that patterns do not adapt their wavenumber as long as they are stable. However, when losing their stability, patterns change their wavenumber to become stable again, i.e. to regain a position in the Busse balloon. When comparing two images one would expect stable patterns to show no significant changes in wavenumber, and unstable patterns to undergo significant wavenumber adaptations. If a continuous family of stable wavenumbers emerges, then this would indicate multistability. Prerequisites are that wavenumber estimates are accurate enough to detect wavenumber adaptations and that data is available of variables that can not be assumed spatially uniform in the considered region and that are known to affect the shape of the Busse balloon (i.e. slope in arid regions).

Finally, multistability of patterned ecosystems could be tested with planting experiments (Figure 6.3). These experiments would involve planting patterns with different wavenumbers and monitoring whether they persist over time. If multiple patterns persist, this would suggest multistability. Alternatively, one could manipulate existing patterns, as currently done in models (Bel et al., 2012; Zelnik et al., 2013), to see whether patterns with wavenumbers, other than the original wavenumber, are stable.

Besides multistability, the model analyses in Chapter 2 suggest that patterned ecosystems can respond in a gradual way to environmental change, instead of in an abrupt way as hypothesised by Rietkerk et al. (2004), provided that the environmental changes are slow. If environmental changes indeed

occur slow enough to enable gradual ecosystem response, one would expect no lower limit in pattern wavenumber that can be attained by patterned ecosystems. A study by Deblauwe et al. (2011) on vegetation patterns in Sudan however, shows rather sharp lower wavenumber limits of about 5 cycles per km for banded patterns and about 10 cycles per km for spotted patterns, which would suggest that changes in rainfall in arid regions may be too rapid to enable a gradual response. It is however possible that other mechanisms, such as grazing, could cause a “Busse balloon lift-off” (Siero, 2016, p. 133), meaning that the conditions under which low wavenumber patterns are stable simply do not exist. Further research is required to test whether processes like grazing are indeed able to cause a Busse balloon lift-off.

A recent extension of the analysis in Chapter 2 to two spatial dimensions, revealed that environmental change could trigger the break-up of banded patterns into dashed patterns (Siero et al., 2015). These dashed patterns have first been observed and classified as such in arid ecosystems by Ambouta (1997, “brousse en tirets”) and are hypothesized to be linked to declining rainfall by Valentin et al. (1999). In models dashed patterns are formed by a Turing-like instability in the direction parallel to the band. Since dashed patterns form as the environment becomes harsher, they may be used as an early-warning indicator for an upcoming transition to a uniform degraded state (Siero et al., 2015). To validate this finding further empirical research is required.

## 6.3 Towards (speed) limits for environmental change

Dynamical systems theory has shaped the common view on concepts like resilience and stability. Current research efforts focus on identifying the architectural features in (eco)systems that are responsible for critical transitions and on estimating their proximity to critical thresholds (Scheffer et al., 2012). The current theoretical framework has even been extended and build upon to establish preconditions for human development on a global scale (planetary boundaries; Rockström et al., 2009; Steffen et al., 2015; Scheffer, 2015).

However, the findings presented in this dissertation suggest that one has to acknowledge rapid environmental change and slow internal dynamics in order to understand how and when ecosystems undergo critical transitions and ultimately to formulate a safe operating space for humanity. As these aspects were previously not covered by theory, future research will have to return to the drawing board by developing novel approaches that enable

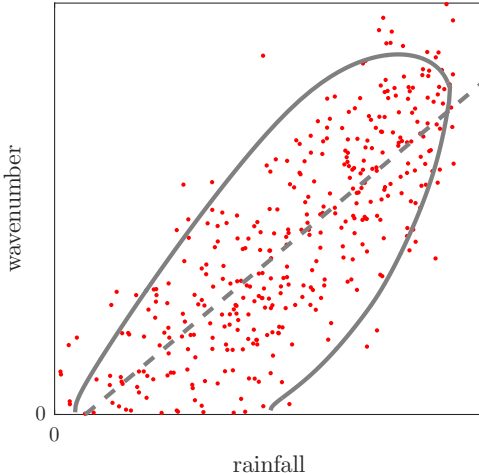


Figure 6.2: Multistability or a noisy signal of monostability? The solid line borders a Busse balloon and would explain the observations, but a linear fit through the data, indicated by the dashed line, would also explain the data. The data points in this figure are artificially generated. The Busse balloon is for the extended Klausmeier model with sloped terrain introduced in Chapter 2.

studying ecosystems subject to rapid external change and/or with slow internal dynamics. In addition, processes on population level that may affect the magnitudes and rates of change ecosystems can absorb before shifting to alternative dynamics will need to be considered in dynamical models. Such a new theoretical framework may eventually enable establishing (global) speed limits for environmental change, which may be used to safeguard ecosystems against degradation (Figure 6.1).

### 6.3.1 Advanced model analysis and long-term experiments

To obtain insights into the mechanisms behind observed ecosystem dynamics, ecologists generally rely on two approaches. They can either develop of statistical or dynamical models that explain the observed dynamics and/or they can perform manipulative experiments. These approaches are especially useful when studying how ecosystems respond to environmental change.

To get a detailed understanding of the behaviour of dynamical models, equilibrium analysis can be applied. However, as discussed in Chapter 5, the applicability of equilibrium analysis is limited to cases of slow external changes relative to the rate of internal ecosystem dynamics (upper left corner

### 6.3 Towards (speed) limits for environmental change



Figure 6.3: Vegetation patterns planted by the KKL-JNF in the northern Negev desert (Israel, 31°17' N, 34°49' E; ©2013 Google Earth. ©2013 DigitalGlobe). The dimensions of the depicted area are 1 × 1 km.

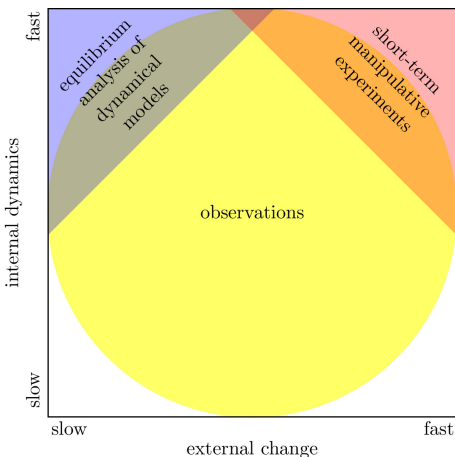


Figure 6.4: Equilibrium analysis of dynamical models and short-term manipulative experiments explain part of the observed ecosystem dynamics (overlapping regions), but may not explain all observations.

of Figure 6.4). As a result, equilibrium analysis of dynamical models can be expected to explain only part of the observed ecosystem dynamics (Hastings, 2004), possibly excluding phenomena like rate-induced critical transitions (Chapter 5), 'locked' ecosystem dynamics (Chapter 4) and slowly unfolding catastrophic shifts (Hughes et al., 2013).

Another way to assess ecosystem response to environmental change is by performing manipulative experiments, in which with different treatments, one or more environmental variable(s) is/are altered. In these treatments, the changes in environmental variables are often applied instantaneously, which is known to be problematic when studying the effect of observed gradual environmental changes (Luo and Reynolds, 1999; Luo, 2003; Klironomos et al., 2005; Luo and Hui, 2009). Furthermore, short-term experiments on the effects of environmental change are generally performed on species or ecosystems that respond relatively quickly to the applied treatment. Therefore, such short-term experiments can only provide explanations for part of the observed ecosystem dynamics (upper right corner of Figure 6.4).

To get a better understanding of the complex ecosystem dynamics that are observed, advanced (possibly partly numerical) analyses are required that acknowledge the transient dynamics of ecological models (e.g. Perryman, 2015). In addition, longer-term manipulative experiments are needed to study the effects of slow changes on ecosystems with slow internal dynamics.

### 6.3.2 Acknowledging adaptations on population level

An implicit assumption behind most ecological models, including the ones presented in this dissertation, is that ecosystems can only respond to environmental change by adjusting the values of their state variables, e.g. through changing population densities. However, on a population level also other types of adaptation are active, potentially affecting ecosystem response to environmental change. Populations may adapt *in situ* through phenotypic plasticity and/or through micro-evolutionary adaptation, or may evade to more suitable habitats (Holt, 1990).

The magnitudes and rates of environmental change that can be absorbed through these population level adaptations are bounded. Adaptations through phenotypic plasticity occur relatively fast (i.e. within one generation). However, plastic adaptations can only absorb limited magnitudes of change (e.g. Kleijn et al., 2010). Micro-evolutionary adaptations can absorb high magnitude changes, but generally occur at a very slow pace, meaning that critical rates of environmental change exist beyond which selective pressures become too high for positive population growth to be maintained (Lynch and Lande, 1993; Bürger and Lynch, 1995; Chevin et al., 2010; Gienapp et al., 2013). The ability of populations to evade to more suitable habitats in response to environmental change is limited by both the rate and magnitude of change and depends on environmental gradients, geographical barriers and the maximum displacement rate of the species (Burrows et al., 2011, 2014; Devictor et al., 2012; Sandel et al., 2011; Brooker et al., 2007; Schippers et al., 2011; Cobben et al., 2011; Bertrand et al., 2011).

Integrating these potentially important adaptations on population level in ecological models, e.g. using the adaptive dynamics framework, would give access to a detailed understanding of the effects of rapid continuous change on ecosystems.

## 6.4 Final remarks

In the first half of the 20th century, the science of ecology often operated on the presumption that the presence and spatial distribution of species (and ecosystems) is dictated by the abiotic environment (Von Humboldt, 1805; Watson, 1847; Wallace, 1976; Browne, 1983). However, over time examples accumulated of species actively modulating flows of resources, and thereby their local environment (i.e. ecosystem engineering; Jones et al., 1994). More recently, research has shown how ecosystem engineering can be

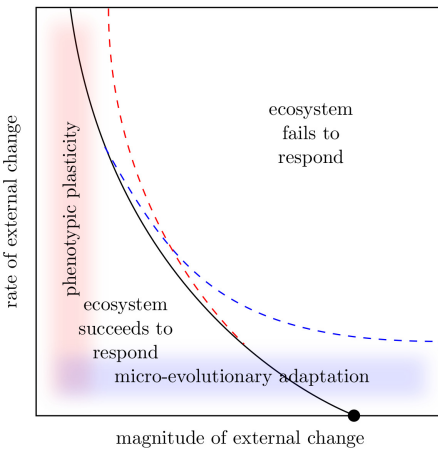


Figure 6.5: Slow change beyond a critical threshold value (black dot) can trigger critical transitions in ecosystems. The theory presented in Chapter 5 suggests that rapid external change can cause critical transitions even if the same magnitude of slow change would not (solid line). Besides responses in population density, phenotypic plasticity and micro-evolutionary adaptations may respectively absorb rapid low magnitude changes (red dashed line) and slow high magnitude changes (blue dashed line). Notice that, theoretically, the blue dashed line could also bend inwards ("evolutionary suicide"; Haldane, 1932; Rankin and López-Sepulcre, 2005).

responsible for feedbacks that trigger critical transitions such as catastrophic shifts and spatial pattern formation (Scheffer et al., 2001; Rietkerk et al., 2004). The combination of these theoretical insights and quantitative studies (e.g. planetary boundary studies; Rockström et al., 2009; Steffen et al., 2015; Scheffer, 2015) or experiments (e.g. planting experiments as in the Negev desert; Figure 6.3) may eventually prevent ecosystem degradation and enable ecosystem regeneration.

However, over the course of this scientific progress, it has also become increasingly clear that humans are currently modulating the global environment at unprecedented rates, involving changes in the major biogeochemical cycles, land surface transformations and climate change. This dissertation highlights that future research will also need to address the fact ecosystems are continuously exposed to rapid anthropogenic change. I hope that the findings I have presented will motivate future studies on this issue and that the yielded insights will one day guide measures to safeguard ecosystems against degradation.

# Bibliography

- Aagaard, T., Orford, J., and Murray, A. S. (2007). Environmental controls on coastal dune formation; Skallingen Spit, Denmark. *Geomorphology*, 83(1-2):29–47.
- Adema, E. B. and Grootjans, A. P. (2003). Possible positive-feedback mechanisms: Plants change abiotic soil parameters in wet calcareous dune slacks. *Plant Ecology*, 167(1):141–149.
- Ambouta, J. (1997). Définition et catactérisation des structures de végétation. In D'Herbès, J., Ambouta, J., and Peltier, R., editors, *Fonctionnement et Gestion des Ecosystèmes Forestiers Contractes Sahéliens*, chapter 4, pages 41–57. Paris, France.
- Arens, B., Geelen, L., Van der Hagen, H., and Slings, R. (2007). Duurzame verstuiving in de Hollandse duinen: kans, droom of nachtmerrie. Eindrapport Fase 1. Technical report, Arens Bureau voor Strand- en Duinonderzoek, Amsterdam.
- Ashwin, P., Wieczorek, S., Vitolo, R., and Cox, P. (2012). Tipping points in open systems: bifurcation, noise-induced and rate-dependent examples in the climate system. *Philosophical transactions. Series A, Mathematical, physical, and engineering sciences*, 370(1962):1166–84.
- Assouline, S. and Mualem, Y. (1997). Modeling the dynamics of seal formation and its effect on infiltration as related to soil and rainfall characteristics. *Water resources research*, 33(7):1527–1536.
- Assouline, S. and Mualem, Y. (2002). Infiltration during soil sealing: The effect of areal heterogeneity of soil hydraulic properties. *Water Resources Research*, 38(12):22–1–22–9.
- Assouline, S. and Mualem, Y. (2003). Effect of rainfall-induced soil seals on the soil water regime: Drying interval and subsequent wetting. *Transport in porous media*, (617):75–94.

## Bibliography

- Baldwin, M. and Hawker, H. W. (1915). Soil survey of the Fort Lauderdale area, Florida. Field Operations of the Bureau of Soils. Technical report, US Department of Agriculture.
- Baudena, M., Boni, G., Ferraris, L., von Hardenberg, J., and Provenzale, A. (2007). Vegetation response to rainfall intermittency in drylands: Results from a simple ecohydrological box model. *Advances in Water Resources*, 30(5):1320–1328.
- Baudena, M., Dekker, S. C., Van Bodegom, P. M., Cuesta, B., Higgins, S. I., Lehsten, V., Reick, C. H., Rietkerk, M., Scheiter, S., Yin, Z., Zavala, M. A., and Brovkin, V. (2015). Forests, savannas, and grasslands: Bridging the knowledge gap between ecology and Dynamic Global Vegetation Models. *Biogeosciences*, 12(6):1833–1848.
- Baudena, M. and Provenzale, A. (2008). Rainfall intermittency and vegetation feedbacks in drylands. *Hydrology and Earth System Science*, 12:679–689.
- Beckage, B., Platt, W., and Gross, L. (2009). Vegetation, Fire, and Feedbacks: A DisturbanceMediated Model of Savannas. *The American Naturalist*, 174(6):805–818.
- Bel, G., Hagberg, A., and Meron, E. (2012). Gradual regime shifts in spatially extended ecosystems. *Theoretical Ecology*, 5(4):591–604.
- Bertrand, R., Lenoir, J., Piedallu, C., Riofrio-Dillon, G., de Ruffray, P., Vidal, C., Pierrat, J.-C. J.-C., Gegout, J.-C., Riofrío-Dillon, G., and Gégout, J.-C. (2011). Changes in plant community composition lag behind climate warming in lowland forests. *Nature*, 479(7374):517–20.
- Bierkens, M. and Puente, C. (1990). Analytically Derived Runoff Models Based on Rainfall Point Processes. *Water Resources Research*, 26(11):2653–2659.
- Bisdom, E. B. A., Dekker, L. W., and Schoult, J. F. T. (1993). Water repellency of sieve fractions from sandy soils and relationships with organic material and soil structure. *Geoderma*, 56:105–118.
- Borgogno, F., D’Odorico, P., Laio, F., and Ridolfi, L. (2009). Mathematical models of vegetation pattern formation in ecohydrology. *Reviews of Geophysics*, 47:1–36.

- Brooker, R. W., Travis, J. M. J., Clark, E. J., and Dytham, C. (2007). Modelling species' range shifts in a changing climate: the impacts of biotic interactions, dispersal distance and the rate of climate change. *Journal of theoretical biology*, 245(1):59–65.
- Browne, J. (1983). *The Secular Ark: Studies in the History of Biogeography*. Yale University Press, New Haven and London.
- Burden, R. L. and Faires, J. D. (1985). The Bisection Method. In Julet, M., Taylor, M., and Seibert, D., editors, *Numerical Analysis*, chapter 2.1, pages 48–56. Brooks/Cole, Boston, USA, 9th edition.
- Bürger, R. and Lynch, M. (1995). Evolution and extinction in a changing environment: a qualitative-genetic analysis. *Evolution*, 49(1):151–163.
- Burrows, M. T., Schoeman, D. S., Buckley, L. B., Moore, P., Poloczanska, E. S., Brander, K. M., Brown, C., Bruno, J. F., Duarte, C. M., Halpern, B. S., Holding, J., Kappel, C. V., Kiessling, W., O'Connor, M. I., Pandolfi, J. M., Parmesan, C., Schwing, F. B., Sydeman, W. J., and Richardson, A. J. (2011). The pace of shifting climate in marine and terrestrial ecosystems. *Science*, 334(6056):652–5.
- Burrows, M. T., Schoeman, D. S., Richardson, A. J., Molinos, J. G., Hoffmann, A., Buckley, L. B., Moore, P. J., Brown, C. J., Bruno, J. F., Duarte, C. M., Halpern, B. S., Hoegh-Guldberg, O., Kappel, C. V., Kiessling, W., O'Connor, M. I., Pandolfi, J. M., Parmesan, C., Sydeman, W. J., Ferrier, S., Williams, K. J., and Poloczanska, E. S. (2014). Geographical limits to species-range shifts are suggested by climate velocity. *Nature*, 507(7493):492–5.
- Busse, F. (1978). Non-linear properties of thermal convection. *Reports on Progress in Physics*, 41:1929–1967.
- Carpenter, S. R. (2005). Eutrophication of aquatic ecosystems: bistability and soil phosphorus. *Proceedings of the National Academy of Sciences of the United States of America*, 102(29):10002–10005.
- Carpenter, S. R., Brock, W. A., Cole, J. J., and Pace, M. L. (2014). A new approach for rapid detection of nearby thresholds in ecosystem time series. *Oikos*, 123(3):290–297.

## Bibliography

- Carpenter, S. R., Cole, J. J., Pace, M. L., Batt, R., Brock, W. a., Cline, T., Coloso, J., Hodgson, J. R., Kitchell, J. F., Seekell, D. a., Smith, L., and Weidel, B. (2011). Early Warnings of Regime Shifts: A Whole-Ecosystem Experiment. *Science*, 332(6033):1079–1082.
- Chen, Y., Kolokolnikov, T., Tzou, J., and Gai, C. (2015). Patterned vegetation, tipping points, and the rate of climate change. *European Journal of Applied Mathematics*, pages 1–14.
- Chevin, L. M., Lande, R., and Mace, G. M. (2010). Adaptation, plasticity, and extinction in a changing environment: Towards a predictive theory. *PLoS Biology*, 8(4).
- Cobben, M. M. P., Verboom, J., Opdam, P. F. M., Hoekstra, R. F., Jochem, R., Arens, P., and Smulders, M. J. M. (2011). Projected climate change causes loss and redistribution of genetic diversity in a model metapopulation of a medium-good disperser. *Ecography*, 34(6):920–932.
- Couteron, P. and Lejeune, O. (2001). Periodic spotted patterns in semi-arid vegetation explained by a propagation-inhibition model. *Journal of Ecology*, 89(4):616–628.
- Davidson, E. A. and Janssens, I. A. (2006). Temperature sensitivity of soil carbon decomposition and feedbacks to climate change. *Nature*, 440(7081):165–173.
- De Blas, E., Almendros, G., and Sanz, J. (2013). Molecular characterization of lipid fractions from extremely water-repellent pine and eucalyptus forest soils. *Geoderma*, 206:75–84.
- DeAngelis, D. L., Post, W. M., and Travis, C. C. (1980). *Positive Feedback in Natural Systems*. Springer-Verlag, Berlin, Heidelberg, New York, Tokyo.
- DeBano, L. F. (1991). The effect of fire on soil properties. In Harvey, A. C. and Neuenschwander, L. F., editors, *Proceedings - Management and Productivity of Western-Montane Forest Soils*, pages 151–156. USDA.
- DeBano, L. F. (2000). The role of fire and soil heating on water repellency in wildland environments: a review. *Journal of Hydrology*, 232:195–206.
- Deblauwe, V., Barbier, N., Couteron, P., Lejeune, O., and Bogaert, J. (2008). The global biogeography of semi-arid periodic vegetation patterns. *Global Ecology and Biogeography*, 17(6):715–723.

- Deblauwe, V., Couteron, P., Bogaert, J., and Barbier, N. (2012). Determinants and dynamics of banded vegetation pattern migration in arid climates. *Ecological Monographs*, 82(1):3–21.
- Deblauwe, V., Couteron, P., Lejeune, O., Bogaert, J., and Barbier, N. (2011). Environmental modulation of self-organized periodic vegetation patterns in Sudan. *Ecography*, 34(6):990–1001.
- Dekker, L. W. and Jungerius, P. D. (1990). Water repellency in the dunes with special reference to The Netherlands. In *Dunes of the European coasts. Catena Supplement*, number 18, pages 173–183.
- Dekker, L. W. and Ritsema, C. J. (1994). How water moves in a water repellent sandy soil. 1. Potential and actual water repellency. 30(9):2507–2517.
- Dekker, L. W. and Ritsema, C. J. (1996). Variation in water content and wetting patterns in Dutch water repellent peaty clay and clayey peat soils. *Catena*, 28:89–105.
- Devictor, V., Van Swaay, C., Brereton, T., Brotons, L., Chamberlain, D., Heliölä, J., Herrando, S., Julliard, R., Kuussaari, M., Lindström, Å., Reif, J., Roy, D. B., Schweiger, O., Settele, J., Stefanescu, C., Van Strein, A., van Turnhout, C., Vermouzek, Z., Wallis De Vries, M., Wynhoff, I., and Jiguet, F. (2012). Differences in the climatic debts of birds and butterflies at a continental scale. *Nature climate change*, 2(February):121–124.
- D’Odorico, P., Bhattachan, A., Davis, K. F., Ravi, S., and Runyan, C. W. (2013). Global desertification: Drivers and feedbacks. *Advances in Water Resources*, 51:326–344.
- D’Odorico, P., Laio, F., and Ridolfi, L. (2005). Noise-induced stability in dryland plant ecosystems. *Proceedings of the National Academy of Sciences of the United States of America*, 102(31):10819–22.
- D’Odorico, P., Laio, F., and Ridolfi, L. (2006). Vegetation patterns induced by random climate fluctuations. *Geophysical Research Letters*, 33(19):1–5.
- Doedel, E. (1981). AUTO: A program for the automatic bifurcation analysis of autonomous systems. *Congressus Numerantium*, 30:265–284.

## Bibliography

- Doelman, A. and Kaper, T. J. (2003). Semistrong Pulse Interactions in a Class of Coupled Reaction-Diffusion Equations. *SIAM Journal on Applied Dynamical Systems*, 2(1):53–96.
- Doelman, A., Rademacher, J. D., and Van der Stelt, S. (2012). Hopf dances near the tips of Busse balloons. *Discrete and Continuous Dynamical Systems - Series S*, 5(1):61–92.
- Doerr, S. H., Llewellyn, C. T., Douglas, P., Morley, C. P., Mainwaring, K. A., Haskins, C., Johnsey, L., Ritsema, C. J., Stagnitti, F., Allinson, G., Ferreira, A. J. D., Keizer, J. J., Ziogas, A. K., and Diamantis, J. (2005). Extraction of compounds associated with water repellency in sandy soils of different origin. *Australian Journal of Soil Research*, 43(3):225–237.
- Doerr, S. H., Shakesby, R. A., and Walsh, R. P. D. (2000). Soil water repellency: Its causes, characteristics and hydro-geomorphological significance. *Earth Science Reviews*, 51:33–65.
- Doerr, S. H. and Thomas, A. D. (2000). The role of soil moisture in controlling water repellency: new evidence from forest soils in Portugal. *Journal of Hydrology*, 232:134–147.
- Dunkerley, D. (1997). Banded vegetation: development under uniform rainfall from a simple cellular automaton model. *Plant Ecology*, 129:103–111.
- Dunkerley, D. L. (2013). Vegetation Mosaics of Arid Western New South Wales, Australia: Considerations of their Origin and Persistence. In Mueller, E., Wainwright, J., Parsons, A., and Turnbull, L., editors, *Patterns of Land Degradation in Drylands: Understanding Self-Organised Ecogeomorphic Systems*, chapter 12, pages 315–345. Springer.
- Dunne, T., Zhang, W., and Aubry, B. (1991). Effects of rainfall, vegetation, and microtopography on infiltration and runoff. *Water Resources Research*, 27(9):2271–2285.
- Edelstein-Keshet, L. (1988). *Mathematical models in biology*. McGraw-Hill, New York.
- Elton, C. and Nicholson, M. (1942). The Ten-Year Cycle in Numbers of the Lynx in Canada. *Journal of Animal Ecology*, 11(2):215–244.
- Elton, C. S. (1924). Periodic fluctuations in the numbers of animals: their causes and effects. *British Journal of Experimental Biology*, 2:119–163.

- Eppinga, M. B., de Ruiter, P. C., Wassen, M. J., and Rietkerk, M. (2009). Nutrients and hydrology indicate the driving mechanisms of peatland surface patterning. *The American naturalist*, 173(6):803–18.
- Everard, M., Jones, L., and Watts, B. (2010). Have we neglected the societal importance of sand dunes? An ecosystem services perspective. *Aquatic Conservation: Marine and Freshwater Ecosystems*, 20(4):476–487.
- Feng, X., Xu, Y., Jaffé, R., Schlesinger, W. H., and Simpson, M. J. (2010). Turnover rates of hydrolysable aliphatic lipids in Duke Forest soils determined by compound specific  $^{13}\text{C}$  isotopic analysis. *Organic Geochemistry*, 41(6):573–579.
- FitzHugh, R. (1961). Impulses and Physiological States in Theoretical Models of Nerve Membrane. *Biophysical Journal*, 1(6):445–466.
- Fox, D., Le Bissonnais, Y., and Bruand, a. (1998). The effect of ponding depth on infiltration in a crusted surface depression. *Catena*, 32(2):87–100.
- Franco, C. M. M., Clarke, P. J., Tate, M. E., and Oades, J. M. (2000). Hydrophobic properties and chemical characterisation of natural water repellent materials in Australian sands. In *Journal of Hydrology*, volume 231-232, pages 47–58.
- Franco, C. M. M., Tate, M. E., and Oades, J. M. (1995). Studies on non-wetting sands .1. The role of intrinsic particulate organic-matter in the development of water-repellency in non-wetting sands. *Australian Journal of Soil Research*, 33(2):253.
- Gienapp, P., Lof, M., Reed, T. E., McNamara, J., Verhulst, S., and Visser, M. E. (2013). Predicting demographically sustainable rates of adaptation: can great tit breeding time keep pace with climate change? *Philosophical transactions of the Royal Society of London. Series B, Biological sciences*, 368(1610):20120289.
- Gierer, A. and Meinhardt, H. (1972). A theory of biological pattern formation. *Kybernetik*, 12(1):30–9.
- Gilad, E., von Hardenberg, J., Provenzale, a., Shachak, M., and Meron, E. (2004). Ecosystem Engineers: From Pattern Formation to Habitat Creation. *Physical Review Letters*, 93(9):1–4.

## Bibliography

- Gray, P. and Scott, S. (1984). Autocatalytic reactions in the isothermal, continuous stirred tank reactor. *Chemical Engineering Science*, 39(6):1087–1097.
- Grootjans, A. P., Everts, H., Bruin, K., and Fresco, L. (2001). Restoration of wet dune slacks on the Dutch Wadden sea islands: Recolonization after large-scale sod cutting. *Restoration Ecology*, 9(2):137–146.
- Guttal, V. and Jayaprakash, C. (2007). Impact of noise on bistable ecological systems. *Ecological Modelling*, 201(3-4):420–428.
- Haldane, J. B. S. (1932). *The Causes of Evolution*. Longmans, Green, London, England.
- Hanan, N. P., Tredennick, A. T., Prihodko, L., Bucini, G., and Dohn, J. (2014). Analysis of stable states in global savannas: Is the CART pulling the horse? *Global Ecology and Biogeography*, 23(3):259–263.
- Hastings, A. (1980). Disturbance, coexistence, history, and competition for space. *Theoretical Population Biology*, 18(3):363–373.
- Hastings, A. (2004). Transients: the key to long-term ecological understanding? *Trends in ecology & evolution*, 19(1):39–45.
- Higgins, S. I., Bond, W. J., February, E. C., Bronn, A., Euston-Brown, D. I. W., Enslin, B., Govender, N., Rademan, L., O'Regan, S., Potgieter, A. L. F., Scheiter, S., Sowry, R., Trollope, L., and Trollope, W. S. W. (2007). Effects of four decades of fire manipulation on woody vegetation structure in savanna. *Ecology*, 88(5):1119–1125.
- Higgins, S. I. and Scheiter, S. (2012). Atmospheric CO<sub>2</sub> forces abrupt vegetation shifts locally, but not globally. *Nature*, 488(7410):209–212.
- Hill, A. V. (1936). Excitation and accommodation in nerve. *Proceedings of the Royal Society of London. Series B, Biological Sciences*, 119(814):305–355.
- HilleRisLambers, R., Rietkerk, M., Bosch, F. V. D., Prins, H. H. T., and Kroon, H. D. (2001). Vegetation Pattern Formation in Semi-Arid Grazing Systems. *Ecology*, 82(1):50–61.
- Hirota, M., Holmgren, M., Van Nes, E. H., and Scheffer, M. (2011). Global resilience of tropical forest and savanna to critical transitions. *Science*, 334(6053):232–5.

- Holling, C. (1959). Some characteristics of simple types of predation and parasitism. *The Canadian Entomologist*, 91(7):385–398.
- Holling, C. S. (1973). Resilience and stability of ecological systems. *Annual review of ecology and systematics*, 4(1973):1–23.
- Holling, C. S. (1988). Temperate forest insect outbreaks, tropical deforestation and migratory birds. *Memoirs Of The Entomological Society Of Canada*, 0:21–32.
- Holt, R. D. (1990). The microevolutionary consequences of climate change. *Trends in Ecology and Evolution*, 5(9):311–5.
- Home, J. (2015). The influence of the microflora on the physical properties of soils . I . Effects associated with filamentous algae and fungi.
- Hoogmoed, W. B. (1981). Analysis of rainfall in some locations of West Africa and India. In Rawitz, E., Hoogmoed, W. B., and Morin, Y., editors, *Development of criteria and methods for improving the efficiency of soil management and tillage operations, with special reference to arid and semi-arid regions.*, page 260. Hebrew Univeristy of Jerusalem, Jerusalem, Israel.
- Horne, D. and McIntosh, J. (2000). Hydrophobic compounds in sands in New Zealand extraction, characterisation and proposed mechanisms for repellency expression. *Journal of Hydrology*, 232:35–46.
- Horsthemke, W. and Lefever, R. (2006). *Noise-Induced Transitions. Theory and Applications in Physics, Chemistry, and Biology*. Springer-Verlag, Berlin, Heidelberg, New York, 2 edition.
- Horton, R. E. (1939). Analysis of runoff-plot experiments with varying infiltration-capacity. *Transactions, American Geophysical Union*, 20(4):693–711.
- Hoyle, R. (2006). *Pattern Formation: An Introduction to Methods*. Cambridge University Press, Cambridge, UK.
- Huffaker, C., Shea, K., and Herman, S. (1963). Experimental studies on predation. Complex dispersion and levels of food in an acarine predator-prey interaction. *Hilgardia*, 34(9):305.

## Bibliography

- Hughes, T. P., Linares, C., Dakos, V., Van de Leemput, I. a., and Van Nes, E. H. (2013). Living dangerously on borrowed time during slow, unrecognized regime shifts. *Trends in ecology & evolution*, 28(3):149–55.
- IPCC (2013). Climate Change 2013: The Physical Science Basis. Contribution of Working Group I to the Fifth Assessment Report of the Intergovernmental Panel on Climate Change. Technical report, Cambridge, United Kingdom and New York, NY, USA.
- Jackson, J. B., Kirby, M. X., Berger, W. H., Bjorndal, K. A., Botsford, L. W., Bourque, B. J., Bradbury, R. H., Cooke, R., Erlandson, J., Estes, J. A., Hughes, T. P., Kidwell, S., Lange, C. B., Lenihan, H. S., Pandolfi, J. M., Peterson, C. H., Steneck, R. S., Tegner, M. J., and Warner, R. R. (2001). Historical overfishing and the recent collapse of coastal ecosystems. *Science (New York, N.Y.)*, 293(5530):629–37.
- Jensen, F. (1994). Dune management in Denmark: application of the Nature Protection Act of 1992. *Journal of Coastal Research*, 10(2):263–269.
- Jones, C., Lawton, J., and Shachak, M. (1994). Organisms as ecosystem engineers. *Oikos*, 69:373–386.
- Joos, F. and Spahni, R. (2008). Rates of change in natural and anthropogenic radiative forcing over the past 20,000 years. *Proceedings of the National Academy of Sciences*, 105(5):1425–1430.
- Kaplan, J. O., Krumhardt, K. M., Ellis, E. C., Ruddiman, W. F., Lemmen, C., and Goldewijk, K. K. (2011). Holocene carbon emissions as a result of anthropogenic land cover change. *The Holocene*, 21(5):775–791.
- Karssenberg, D. (2006). Upscaling of saturated conductivity for Hortonian runoff modelling. *Advances in Water Resources*, 29(5):735–759.
- Kealy, B. J. and Wollkind, D. J. (2012). A nonlinear stability analysis of vegetative turing pattern formation for an interaction-diffusion plant-surface water model system in an arid flat environment. *Bulletin of mathematical biology*, 74(4):803–33.
- Kéfi, S., Eppinga, M. B., Ruiter, P. C., and Rietkerk, M. (2010). Bistability and regular spatial patterns in arid ecosystems. *Theoretical Ecology*, 3(4):257–269.

- Kéfi, S., Rietkerk, M., Alados, C. L., Pueyo, Y., Papanastasis, V. P., Elaich, A., and de Ruiter, P. C. (2007). Spatial vegetation patterns and imminent desertification in Mediterranean arid ecosystems. *Nature*, 449(7159):213–7.
- Kefi, S., Rietkerk, M., and Katul, G. G. (2008). Vegetation pattern shift as a result of rising atmospheric CO<sub>2</sub> in arid ecosystems. *Theoretical population biology*, 74(4):332–44.
- Kelly, R. and Walker, B. (1976). The effects of different forms of land use on the ecology of a semi-arid region in south-eastern Rhodesia. *Journal of Ecology*, 64(2):553–576.
- Kinast, S., Zelnik, Y. R., Bel, G., and Meron, E. (2014). Interplay between Turing Mechanisms can Increase Pattern Diversity. *Physical Review Letters*, 112(7):078701.
- Kirschbaum, M. U. (1995). The temperature dependence of soil organic matter decomposition, and the effect of global warming on soil organic C storage. *Soil Biology and Biochemistry*, 27(6):753–760.
- Klausmeier, C. A. (1999). Regular and irregular patterns in semiarid vegetation. *Science*, 284(5421):1826–8.
- Kleijn, D., Schekkerman, H., Dimmers, W. J., and Van Kats, R. J. M. (2010). Adverse effects of agricultural intensification and climate change on breeding habitat quality of Black-tailed Godwits Limosa l. limosa in the Netherlands. *Ibis*, 152(3):475–486.
- Klein Goldewijk, K., Beusen, A., Van Drecht, G., and De Vos, M. (2011). The HYDE 3.1 spatially explicit database of human-induced global land-use change over the past 12,000 years. *Global Ecology and Biogeography*, 20(1):73–86.
- Kletter, A., von Hardenberg, J., Meron, E., and Provenzale, A. (2009). Patterned vegetation and rainfall intermittency. *Journal of theoretical biology*, 256(4):574–83.
- Klijn, J. A. (1990). Dune forming factors in a geological context. In Bakker, T. W., Jongerius, P. D., and Klijn, J. A., editors, *Dunes of the European coasts; Geomorphology, Hydrology, Soils*, pages 1–14. Catena Verlag, Cremlingen, Germany.

## Bibliography

- Klironomos, J. N., Allen, M. F., Rillig, M. C., Piotrowski, J., Makvandi-nejad, S., Wolfe, B. E., and Powell, J. R. (2005). Abrupt rise in atmospheric CO<sub>2</sub> overestimates community response in a model plantsoil system. *Nature*, 433:621–624.
- KNMI (2014). KNMI'14 : Climate Change scenarios for the 21st Century - A Netherlands perspective. Technical report.
- KNMI (2015). Daggegevens van het weer in Nederland. URL: [www.knmi.nl](http://www.knmi.nl). Accessed: July 1, 2015.
- Kolmogorov, A. (1936). Sulla Teoria di Volterra della Lotta per l'Esistenza. *Giornale Instituto Ital. Attuari*, 7:74–80.
- Konings, A. G., Dekker, S. C., Rietkerk, M., and Katul, G. G. (2011). Drought sensitivity of patterned vegetation determined by rainfall-land surface feedbacks. *Journal of Geophysical Research*, 116(G4):G04008.
- Kooijman, A. M., Dopheide, J. C. R., Sevink, J., Takken, I., and Verstraten, J. M. (1998). Nutrient limitations and their implications on the effects of atmospheric deposition in coastal dunes; lime-poor and lime-rich sites in the Netherlands. *Journal of Ecology*, 86:511–526.
- Kooijman, A. M. and Van der Meulen, F. (1996). Grazing as a control against 'grass-encroachment' in dry dune grasslands in the Netherlands. *Landscape and Urban planning*, 34(3-4):323–333.
- Laiho, R., Laine, J., Trettin, C. C., and Finér, L. (2004). Scots pine litter decomposition along drainage succession and soil nutrient gradients in peatland forests, and the effects of inter-annual weather variation. *Soil Biology and Biochemistry*, 36(7):1095–1109.
- Le Bagousse-Pinguet, Y., Forey, E., Touzard, B., and Michalet, R. (2013). Disentangling the effects of water and nutrients for studying the outcome of plant interactions in sand dune ecosystems. *Journal of Vegetation Science*, 24(2):375–383.
- Lefever, R. and Lejeune, O. (1997). On the origin of tiger bush. *Bulletin of Mathematical Biology*, 59(2):263–294.
- Lejeune, O., Couteron, P., and Lefever, R. (1999). Short range co-operativity competing with long range inhibition explains vegetation patterns. *Acta Oecologica*, 20(3):171–183.

- Lejeune, O. and Tlidi, M. (1999). A model for the explanation of vegetation stripes (tiger bush). *Journal of Vegetation Science*, 10(2):201–208.
- Lejeune, O., Tlidi, M., and Couteron, P. (2002). Localized vegetation patches: A self-organized response to resource scarcity. *Physical Review E*, 66(1):010901.
- Lejeune, O., Tlidi, M., and Lefever, R. (2004). Vegetation spots and stripes: Dissipative structures in arid landscapes. *International Journal of Quantum Chemistry*, 98(2):261–271.
- Lewontin (1969). The meaning of stability. *Brookhaven Symposia in Biology*, 22:13–24.
- Ludwig, D., Jones, D., and Holling, C. (1978). Qualitative analysis of insect outbreak systems: the spruce budworm and forest. *The Journal of Animal Ecology*, 47(1):315–332.
- Luke, C. M. and Cox, P. M. (2011). Soil carbon and climate change: from the Jenkinson effect to the compost-bomb instability. *European Journal of Soil Science*, 62(1):5–12.
- Luo, Y. (2003). Sustainability of terrestrial carbon sequestration: A case study in Duke Forest with inversion approach. *Global Biogeochemical Cycles*, 17(1):1–13.
- Luo, Y. and Hui, D. (2009). Gradual Global Environmental Change in the Real World and Step Manipulative Experiments in Laboratory and Field: The Necessity of Inverse Analysis. In Miao, S., Carstenn, S., and Nungesser, M., editors, *Real World Ecology. Large-Scale and Long-Term Case Studies and Methods*, chapter 10, pages 267–291. New York.
- Luo, Y. and Reynolds, J. F. (1999). Validity of extrapolating field CO<sub>2</sub> experiments to predict carbon sequestration in natural ecosystems. *Ecology*, 80(5):1568–1583.
- Lynch, M. and Lande, R. (1993). Evolution and extinction in response to environmental change. In Kareiva, P., Kingsolver, J., and Huey, R., editors, *Biotic interactions and global change*, chapter 14, pages 234–250. Sinauer Associates, Sunderland, MA.
- Macfadyen, W. (1950). Vegetation patterns in the semi-desert plains of British Somaliland. *Geographical Journal*, 116(4):199–211.

## Bibliography

- Malmström, C. (1923). *Degerö Stormyr. En botanisk, hydrologisk och utvecklingshistorisk undersökning över ett nordsvenskt myrkomplex*. PhD thesis, Uppsala University.
- Mao, J., Nierop, K. G. J., Rietkerk, M., and Dekker, S. C. (2015). Predicting soil water repellency using hydrophobic organic compounds and their vegetation origin. *Soil*, 1(1):411–425.
- Mao, J., Nierop, K. G. J., Sininghe Damsté, J. S., and Dekker, S. C. (2014). Roots induce stronger soil water repellency than leaf waxes. *Geoderma*, 232-234:328–340.
- Mathworks (2012). Matlab.
- May, R. M. (1976). Simple mathematical models with very complicated dynamics. *Nature*, 261(5560):459–67.
- May, R. M. (1977). Thresholds and breakpoints in ecosystems with a multiplicity of stable states. *Nature*, 269:471–477.
- McDonald, A., Kinucan, R., and Loomis, L. (2009). Ecohydrological interactions within banded vegetation in the northeastern Chihuahuan Desert, USA. *Ecohydrology*, 2:66–71.
- McGhie, D. A. and Posner, A. M. (1980). Water repellence of a heavy textured Western Australian surface soil. *Australian Journal of Soil Research*, 18(3):309.
- McGrath, G. S., Paik, K., and Hinz, C. (2012). Microtopography alters self-organized vegetation patterns in water-limited ecosystems. *Journal of Geophysical Research*, 117(G3):G03021.
- Meadows, D. H. (2008). *Thinking in Systems*. Earthscan, London, UK; Sterling, USA.
- Meinhardt, H. (1982). *Models of biological pattern formation*. Academic Press, London, New York.
- Meinhardt, H. (1995). *The algorithmic beauty of sea shells*. Springer-Verlag, Berlin, Heidelberg, New York.
- Melillo, J., Muratore, J., and Aber, J. (1982). Nitrogen and Lignin Control of Hardwood Leaf litter Decomposition Dynamics. *Ecology*, 63(3):621–626.

- Meron, E. (2012). Pattern-formation approach to modelling spatially extended ecosystems. *Ecological Modelling*, 234:70–82.
- Meron, E., Gilad, E., von Hardenberg, J., Shachak, M., and Zarmi, Y. (2004). Vegetation patterns along a rainfall gradient. *Chaos, Solitons & Fractals*, 19(2):367–376.
- Meron, E., Yizhaq, H., and Gilad, E. (2007). Localized structures in dryland vegetation: forms and functions. *Chaos*, 17(3):037109.
- Miller, T. (2005). *Living in the environment*. Brooks/Cole, Pacific Grove USA, 14 edition.
- Moran, P. A. P. (1949). The Statistical Analysis of Sunspots and Lynx Cycles. *The Journal of Animal Ecology*, 18(1):115–116.
- Nee, S. and May, R. M. (1992). Dynamics of Metapopulations: Habitat Destruction and Competitive Coexistence. *Journal of Animal Ecology*, 61(1):37–40.
- Newton, I. (1687). *Philosophiae Naturalis Principia Mathematica*. Royal Society, London, 1 edition.
- Norby, R. J., Cotrufo, M. F., Ineson, P., O'Neill, E. G., and Canadell, J. G. (2001). Elevated CO<sub>2</sub>, litter chemistry, and decomposition: a synthesis. *Oecologia*, 127(2):153–165.
- Novak, V., Šimánek, J., and Genuchten, M. (2000). Infiltration of water into soil with cracks. *Journal of Irrigation and ...*, (February):41–47.
- Noy-Meir, I. (1975). Stability of grazing systems: an application of predator-prey graphs. *Journal of Ecology*, 63(2):459–481.
- Odum, E. (1953). *Fundamentals of ecology*. Saunders, Philadelphia.
- Otto, A. and Simpson, M. J. (2006). Sources and composition of hydrolysable aliphatic lipids and phenols in soils from western Canada. *Organic Geochemistry*, 37(4):385–407.
- Pearson, J. E. (1993). Complex Patterns in a Simple System. *Science*, 261(5118):189–192.

## Bibliography

- Peltzer, D. A., Wardle, D. A., Allison, V. J., Baisden, W. T., Bardgett, R. D., Chadwick, O. A., Condon, L. M., Parfitt, R. L., Porder, S., Richardson, S. J., Turner, B. L., Vitousek, P. M., Walker, J., and Walker, L. R. (2010). Understanding ecosystem retrogression. *Ecological Monographs*, 80(4):509–529.
- Penny, G. G., Daniels, K. E., and Thompson, S. E. (2013). Local properties of patterned vegetation: quantifying endogenous and exogenous effects. *Philosophical transactions. Series A, Mathematical, physical, and engineering sciences*, 371(2004):20120359.
- Perryman, C. G. (2015). *How Fast is Too Fast? Rate-induced Bifurcations in Multiple Time-scale Systems*. PhD thesis, University of Exeter.
- Petraitis, P. (2013). *Multiple Stable States in Natural Ecosystems*. Oxford University Press, Oxford, UK.
- Philip, J. (1957). The theory of infiltration: 1. The infiltration equation and its solution. *Soil Science*, 83:345–357.
- Pisano, L. (1202). *Liber Abaci*. Rome, Italy.
- Poincaré, H. and Magini, R. (1899). Les méthodes nouvelles de la mécanique céleste. *Il Nuovo Cimento*, 10(1):128–130.
- Provoost, S., Jones, M. L. M., and Edmondson, S. E. (2009). Changes in landscape and vegetation of coastal dunes in northwest Europe: a review. *Journal of Coastal Conservation*, 15(1):207–226.
- Rademacher, J. D., Sandstede, B., and Scheel, A. (2007). Computing absolute and essential spectra using continuation. *Physica D: Nonlinear Phenomena*, 229(2):166–183.
- Rankin, D. J. and López-Sepulcre, A. (2005). Can adaptation lead to extinction? *Oikos*, 111(3):616–619.
- Ravi, S., Wang, L., White, C. S., Okin, G. S., Macko, S. A., and Collins, S. L. (2009). Post-Fire Resource Redistribution in Desert Grasslands: A Possible Negative Feedback on Land Degradation. *Ecosystems*, 12:434–444.
- Reid, W. V., Mooney, H. A., Cropper, A., Capistrano, D., Carpenter, S. R., Chopra, K., Dasgupta, P., Dietz, T., Duraiappah, A. K., Hassan, R., Kasperson, R., Leemans, R., May, R. M., McMichael, T. A., Pingali, P.,

- Samper, C., Scholes, R., Watson, R. T., Zakri, A., Shidong, Z., Ash, N. J., Bennett, E., Kumar, P., Lee, M. J., Raudsepp-Hearne, C., Simons, H., Thonell, J., and Zurek, M. B. (2005). Synthesis. In *Ecosystems and human well-being*, pages 1–137.
- Remke, E., Brouwer, E., Kooijman, A., Blindow, I., and Roelofs, J. G. M. (2009). Low Atmospheric Nitrogen Loads Lead to Grass Encroachment in Coastal Dunes, but Only on Acid Soils. *Ecosystems*, 12:1173–1188.
- Riederer, M., Matzke, K., Ziegler, F., and Kögel-Knabner, I. (1993). Occurrence, distribution and fate of the lipid plant biopolymers cutin and suberin in temperate forest soils. *Organic Geochemistry*, 20(7):1063–1076.
- Rietkerk, M. (1998). *Catastrophic vegetation dynamics and soil degradation in semi-arid grazing systems*. PhD thesis, Landbouwhogeschool Wageningen.
- Rietkerk, M., Boerlijst, M. C., Langevelde, F. V., Hillerislambers, R., Van, J., Koppelaar, D., Kumar, L., Prins, H. H. T., and Roos, M. D. (2002). Self-Organization of Vegetation in Arid Ecosystems. *The American naturalist*, 160(4):524–530.
- Rietkerk, M., Dekker, S. C., de Ruiter, P. C., and Van de Koppel, J. (2004). Self-organized patchiness and catastrophic shifts in ecosystems. *Science*, 305(5692):1926–9.
- Rietkerk, M., Ketner, P., Burger, J., Hoorens, B., and Olff, H. (2000). Multiscale soil and vegetation patchiness along a gradient of herbivore impact in a semi-arid grazing system in West Africa. *Plant Ecology*, 148:207–224.
- Rietkerk, M., Ketner, P., Stroosnijder, L., and Prins, H. H. T. (1996). Sahelian rangeland development; A catastrophe? *Journal of Range Management*, 49(6):512–519.
- Rietkerk, M. and Van de Koppel, J. (2008). Regular pattern formation in real ecosystems. *Trends in ecology & evolution*, 23(3):169–75.
- Rietkerk, M., Van den Bosch, F., and Van de Koppel, J. (1997). Site-specific properties and irreversible vegetation changes in semi-arid grazing systems. *Oikos*, 80:241–252.
- Rinaldi, S. and Scheffer, M. (2000). Geometric Analysis of Ecological Models with Slow and Fast Processes. *Ecosystems*, 3(6):507–521.

## Bibliography

- Ritsema, C. J., Dekker, L. W., Hendrickx, J. M. H., and Hamminga, W. (1993). Preferential Flow Mechanism in a Water Reppelent Sandy Soil. *Water Resources Research*, 29(7):2183–2193.
- Rockström, J., Steffen, W., Noone, K., Persson, Å., Chapin, F. S., Lambin, E., Lenton, T. M., Scheffer, M., Folke, C., Schellnhuber, H. J., Nykvist, B., De Wit, C. A., Hughes, T., Van der Leeuw, S., Rodhe, H., Sörlin, S., Snyder, P. K., Costanza, R., Svedin, U., Falkenmark, M., Karlberg, L., Corell, R. W., Fabry, V. J., Hansen, J., Walker, B., Liverman, D., Richardson, K., Crutzen, P., and Foley, J. (2009). A safe operating space for humanity. *Nature*, 461:472–475.
- Rodriguez-Iturbe, I., Porporato, A., Ridolfi, L., Isham, V., and Cox, D. R. (1999). Probabilistic modelling of water balance at a point: the role of climate, soil and vegetation. *Proceedings of the Royal Society A Mathematical Physical and Engineering Sciences*, 455(1990):3789–3805.
- Rosenzweig, M. (1971). Paradox of enrichment: destabilization of exploitation ecosystems in ecological time. *Science*, 171(3969):385–387.
- Rosenzweig, M. and MacArthur, R. (1963). Graphical representation and stability conditions of predator-prey interactions. *American Naturalist*, 97(895):209–223.
- Saco, P. M., Willgoose, G. R., and Hancock, G. R. (2007). Eco-geomorphology of banded vegetation patterns in arid and semi-arid regions. *Hydrology and Earth System Sciences*, 11(6):1717–1730.
- Safriel, U., Adeel, Z., Niemeijer, D., Puigdefabregas, J., White, R., Lal, R., Winslow, M., Ziedler, J., Prince, S., Archer, E., King, C., Shapiro, B., Wessels, K., Nielsen, T., Portnov, B., Reshef, I., Thonell, J., Lachman, E., and McNab, D. (2005). Dryland Systems. In *Ecosystems and Human Well-being: Current State and Trends*, pages 623–662.
- Sandel, B., Arge, L., Dalsgaard, B., Davies, R. G., Gaston, K. J., Sutherland, W. J., and Svenning, J.-C. (2011). The Influence of Late Quaternary Climate-Change Velocity on Species Endemism. *Science*, 334(November):660–664.
- Sankey, J. B., Ravi, S., Wallace, C. S. A., Webb, R. H., and Huxman, T. E. (2012). Quantifying soil surface change in degraded drylands: Shrub

- encroachment and effects of fire and vegetation removal in a desert grassland. *Journal of Geophysical Research*, 117:1–11.
- Scheffer, M. (2009). *Critical Transitions in Nature and Society*. Princeton Studies in Complexity. Princeton University Press, Princeton (NJ), USA.
- Scheffer, M. (2015). Creating a safe operating space for iconic ecosystems. *Science*, 347(November):1317–1319.
- Scheffer, M., Bascompte, J., Brock, W. a., Brovkin, V., Carpenter, S. R., Dakos, V., Held, H., Van Nes, E. H., Rietkerk, M., and Sugihara, G. (2009). Early-warning signals for critical transitions. *Nature*, 461(7260):53–9.
- Scheffer, M., Carpenter, S., Foley, J., Folke, C., and Walker, B. (2001). Catastrophic shifts in ecosystems. *Nature*, 413(6856):591–6.
- Scheffer, M., Carpenter, S. R., Lenton, T. M., Bascompte, J., Brock, W., Dakos, V., Van de Koppel, J., Van de Leemput, I. A., Levin, S. A., Van Nes, E. H., Pascual, M., and Vandermeer, J. (2012). Anticipating critical transitions. *Science*, 338(6105):344–8.
- Scheffer, M., Hosper, S., and Meijer, M.-l. (1993). Alternative equilibria in shallow lakes. *Trends in Ecology & Evolution*, 8(8):275–279.
- Scheffer, M., Nes, E. H., Holmgren, M., and Hughes, T. (2008). Pulse-Driven Loss of Top-Down Control: The Critical-Rate Hypothesis. *Ecosystems*, 11(2):226–237.
- Schippers, P., Verboom, J., Vos, C. C., and Jochem, R. (2011). Metapopulation shift and survival of woodland birds under climate change: will species be able to track? *Ecography*, 34(6):909–919.
- Schlesinger, W. H., Reynolds, J. F., Cunningham, G. L., Huenneke, L. F., Jarrell, W. M., Virginia, R. A., and Whitford, W. G. (1990). Biological feedbacks in global desertification. *Science*, 247(4946):1043–1048.
- Scholes, R. J. and Walker, B. H. (2004). *An African Savanna: Synthesis of the Nylsvley Study*.
- Schröder, a., Persson, L., and De Roos, a. M. (2005). Direct experimental evidence for alternative stable states: a review. *Oikos*, 110(1):3–19.
- Segel, L. A. and Jackson, J. L. (1972). Dissipative structure: An explanation and an ecological example. *Journal of Theoretical Biology*, 37(3):545–559.

## Bibliography

- Sherratt, J. A. (2013a). History-dependent patterns of whole ecosystems. *Ecological Complexity*, 14:8–20.
- Sherratt, J. A. (2013b). Numerical continuation of boundaries in parameter space between stable and unstable periodic travelling wave (wavetrain) solutions of partial differential equations. *Advances in Computational Mathematics*, 39(1):175–192.
- Sherratt, J. A. and Lord, G. J. (2007). Nonlinear dynamics and pattern bifurcations in a model for vegetation stripes in semi-arid environments. *Theoretical population biology*, 71(1):1–11.
- Siero, E. (2016). *A recipe for desert*. PhD thesis, Leiden University.
- Siero, E., Doelman, a., Eppinga, M. B., Rademacher, J. D. M., Rietkerk, M., and Siteur, K. (2015). Striped pattern selection by advective reaction-diffusion systems: Resilience of banded vegetation on slopes. *Chaos: An Interdisciplinary Journal of Nonlinear Science*, 25(3):036411.
- Solomon, S., Qin, D., Manning, M., Chen, Z., Marquis, M., Averyt, K. B., Tignor, M., and Miller, H. L. (2007). *IPCC, 2007: Climate Change 2007: The Physical Science Basis. Contribution of Working Group I to the Fourth Assessment Report of the Intergovernmental Panel on Climate Change*, volume Geneva. Cambridge University Press.
- Spielvogel, S., Prietzel, J., and Kögel-Knabner, I. (2010). Lignin phenols and cutin-and suberin-derived aliphatic monomers as biomarkers for stand history, SOM source, and turnover. In *19th World Congress of Soil Science, Soil Solutions for a Changing World*, number August, pages 74–77, Brisbane, Australia.
- Staal, A., Dekker, S. C., Hirota, M., and Van Nes, E. H. (2015). Synergistic effects of drought and deforestation on the resilience of the south-eastern Amazon rainforest. *Ecological Complexity*, 22:65–75.
- Staal, A. and Flores, B. M. (2015). Sharp ecotones spark sharp ideas: Comment on "Structural, physiognomic and above-ground biomass variation in savanna-forest transition zones on three continents - How different are co-occurring savanna and forest formations?" by Veenendaal et al. (2015). *Biogeosciences*, 12(18):5563–5566.

- Staver, A. and Hansen, M. (2015). Analysis of stable states in global savannas: Is the CART pulling the horse? - a comment. *Global Ecology and Biogeography*, 24:985–987.
- Staver, A. C., Archibald, S., and Levin, S. (2011). Tree cover in sub-Saharan Africa: Rainfall and fire constrain forest and savanna as alternative stable states. *Ecology*, 92(5):1063–1072.
- Staver, C. A. and Levin, S. (2012). Integrating Theoretical Climate and Fire Effects on Savanna and Forest Systems. *The American Naturalist*, 180(2):211–224.
- Steffen, W., Richardson, K., Rockström, J., Cornell, S., Fetzer, I., Bennett, E., Biggs, R., Carpenter, S. R., de Wit, C. a., Folke, C., Mace, G., Persson, L. M., Veerabhadran, R., Reyers, B., and Sörlin, S. (2015). Planetary Boundaries: Guiding human development on a changing planet. *Science*, 347(6223):1 –10.
- Sun, W., Ward, M. J., and Russell, R. (2005). The Slow Dynamics of Two-Spike Solutions for the Gray–Scott and Gierer–Meinhardt Systems: Competition and Oscillatory Instabilities. *SIAM Journal on Applied Dynamical Systems*, 4(4):904–953.
- Tansley, A. (1935). The use and abuse of vegetational concepts and terms. *Ecology*, 16(3):284–307.
- Tebaldi, C., Hayhoe, K., Arblaster, J. M., and Meehl, G. a. (2006). Going to the Extremes. *Climatic Change*, 79(3-4):185–211.
- Thom, R. (1975). *Structural stability and morphogenesis: An Outline of a General Theory of Models*, volume 8. Benjamin Cummings Inc., Reading, Massachusetts.
- Thompson, S. and Katul, G. (2009). Secondary seed dispersal and its role in landscape organization. *Geophysical Research Letters*, 36(2):L02402.
- Thompson, S., Katul, G., Konings, A., and Ridolfi, L. (2011). Unsteady overland flow on flat surfaces induced by spatial permeability contrasts. *Advances in Water Resources*, 34(8):1049–1058.
- Thompson, S., Katul, G., and McMahon, S. M. (2008). Role of biomass spread in vegetation pattern formation within arid ecosystems. *Water Resources Research*, 44(10):n/a–n/a.

## Bibliography

- Thompson, S. E., Harman, C. J., Heine, P., and Katul, G. G. (2010a). Vegetation-infiltration relationships across climatic and soil type gradients. *Journal of Geophysical Research*, 115(G2):G02023.
- Thompson, S. E., Katul, G. G., and Porporato, A. (2010b). Role of microtopography in rainfall-runoff partitioning: An analysis using idealized geometry. *Water Resources Research*, 46(7):n/a–n/a.
- Tilman, D. (1982). Resource competition and community structure. *Mono-graphs in Population Biology*, 17(Princeton, NJ):1–296.
- Tilman, D. (1994). Competition and biodiversity in spatially structured habitats. *Ecology*, 75(1):2–16.
- Tilman, D. and Wedin, D. (1991). Oscillations and chaos in the dynamics of a perennial grass. *Nature*, 353:653–655.
- Turing, A. (1953). The chemical basis of morphogenesis. *Bulletin of mathematical biology*, 237:37–72.
- UNEP (2007). *Global environmental outlook*.
- Ursino, N. and Contarini, S. (2006). Stability of banded vegetation patterns under seasonal rainfall and limited soil moisture storage capacity. *Advances in Water Resources*, 29(10):1556–1564.
- Valentin, C., D'Herbès, J., and Poesen, J. (1999). Soil and water components of banded vegetation patterns. *Catena*, 37(1-2):1–24.
- Van de Koppel, J. and Crain, C. M. (2006). Scale-dependent inhibition drives regular tussock spacing in a freshwater marsh. *The American naturalist*, 168(5):E136–47.
- Van de Koppel, J., Rietkerk, M., Dankers, N., and Herman, P. M. J. (2005). Scale-dependent feedback and regular spatial patterns in young mussel beds. *The American naturalist*, 165(3):E66–77.
- Van den Berg, L. J., Tomassen, H. B. M., Roelofs, J. G. M., and Bobbink, R. (2005). Effects of nitrogen enrichment on coastal dune grassland: A mesocosm study. *Environmental Pollution*, 138:77–85.
- Van der Maarel, E., Boot, R., Van Dorp, D., and Rijntjes, J. (1985). Vegetation succession on the dunes near Oostvoorne, The Netherlands; a comparison of the vegetation in 1959 and 1980. *Vegetatio*, 187:137–187.

- Van Der Meulen, F., Bakker, T., and Houston, J. (2004). The costs of our coasts: examples of dynamic dune management from Western Europe. In *Coastal Dunes: Ecology and Conservation*, volume 171, pages 259–277.
- Van der Pol, B. (1920). Een theory voor de amplitude van vrije en gedwongen triode trillingen. *Radio Review*, 1:701–710, 754–762.
- Van der Stelt, S. (2012). *Rise and Fall of Periodic Patterns in a Generalized Klausmeier-Gray-Scott Model*. PhD thesis, Universiteit Leiden.
- Van der Stelt, S., Doelman, A., Hek, G., and Rademacher, J. D. M. (2013). Rise and Fall of Periodic Patterns for a Generalized Klausmeier-Gray-Scott Model. *Journal of Nonlinear Science*, 23(1):39–95.
- Van Dorp, D., Boot, R., and Van Der Maarel, E. (1985). Vegetation succession on the dunes near Oostvoorne, The Netherlands, since 1934, interpreted from air photographs and vegetation maps. *Vegetatio*, 136:123–136.
- Van Nes, E. H., Hirota, M., Holmgren, M., and Scheffer, M. (2014). Tipping points in tropical tree cover: Linking theory to data. *Global Change Biology*, 20(3):1016–1021.
- Van 't Woudt, B. D. (1959). Particle coatings affecting the wettability of soils. *Journal of Geophysical Research*, 64(2):263.
- Van Wijngaarden, W. (1985). *Elephants Trees Grass Grazers; relationships between climate, soil, vegetation and large herbivores in a semi-arid savanna ecosystem (Tsavo, Kenya)*. PhD thesis, Landbouwhogeschool Wageningen.
- Veenendaal, E. M., Torello-Raventos, M., Feldpausch, T. R., Domingues, T. F., Gerard, F., Schrodt, F., Saiz, G., Quesada, C. A., Djagbletey, G., Ford, A., Kemp, J., Marimon, B. S., Marimon-Junior, B. H., Lenza, E., Ratter, J. A., Maracahipes, L., Sasaki, D., Sonké, B., Zapfack, L., Villarroel, D., Schwarz, M., Yoko Ishida, F., Gilpin, M., Nardoto, G. B., Affum-Baffoe, K., Arroyo, L., Bloomfield, K., Ceca, G., Compaore, H., Davies, K., Diallo, A., Fyllas, N. M., Gignoux, J., Hien, F., Johnson, M., Mougin, E., Hieraux, P., Killeen, T., Metcalfe, D., Miranda, H. S., Steininger, M., Sykora, K., Bird, M. I., Grace, J., Lewis, S., Phillips, O. L., and Lloyd, J. (2015). Structural, physiognomic and above-ground biomass variation in savanna-forest transition zones on three continents - How different are co-occurring savanna and forest formations? *Biogeosciences*, 12(10):2927–2951.

## Bibliography

- Veer, M. A. C. (1997). Nitrogen availability in relation to vegetation changes resulting from grass encroachment in Dutch dry dunes. *Journal of Coastal Conservation*, 3:41–48.
- Veer, M. A. C. and Kooijman, A. M. (1997). Effects of grass-encroachment on vegetation and soil in Dutch dry dune grassland. *Plant and Soil*, 192(1):119–128.
- Verhulst, P. F. (1838). Notice sur la loi que la population suit dans son accroissement. *Correspondance Mathématique et Physique*, 10:113–121.
- Volterra, V. (1928). Variations and fluctuations of the number of individuals in animal species living together. *Journal du Conseil / Conseil Permanent International pour l'Exploration de la Mer*.
- Von Hardenberg, J., Meron, E., Shachak, M., and Zarmi, Y. (2001). Diversity of Vegetation Patterns and Desertification. *Physical Review Letters*, 87(19):3–6.
- Von Humboldt, A. (1805). Essai sur la géographie des plantes; accompagné d'un tableau physique des régions équinoxiales. *Levrault, Paris*.
- Voortman, B. R., Bartholomeus, R. P., van der Zee, S. E. a. T. M., Bierkens, M. F. P., and Witte, J. P. M. (2015). Quantifying energy and water fluxes in dry dune ecosystems of the Netherlands. *Hydrology and Earth System Sciences*, 19(9):3787–3805.
- Wallace, A. (1976). *The geographical distribution of animals*. Macmillan, London, England.
- Walther, G. R., Post, E., Convey, P., Menzel, A., Parmesan, C., Beebee, T. J. C., Fromentin, J. M., Hoegh-guldberg, O., and Bairlein, F. (2002). Ecological responses to recent climate change. *Nature*, 416:389–395.
- Watson, H. (1847). *Cybele Britannica: or British plants and their geographical relations*. Longman, London, England.
- Weisberg, M. (2007). Richard Levins' Philosophy of Science. *Biology & Philosophy*, 21(5):603–605.
- Wessel, A. T. (1988). On using the effective contact angle and the water drop penetration time for classification of water repellency in dune soils. *Earth Surface Processes and Landforms*, 13(6):555–561.

- Wieczorek, S., Ashwin, P., Luke, C. M., and Cox, P. M. (2010). Excitability in ramped systems: the compost-bomb instability. *Proceedings of the Royal Society A: Mathematical, Physical and Engineering Sciences*, 467(2129):1243–1269.
- Wiesenberg, G. L. B. (2004). *Input and turnover of plant-derived lipids in arable soils*. PhD thesis, Universität zu Köln.
- Wiesenberg, G. L. B., Schwarzbauer, J., Schmidt, M. W. I., and Schwark, L. (2004). Source and turnover of organic matter in agricultural soils derived from n-alkane/n-carboxylic acid compositions and C-isotope signatures. *Organic Geochemistry*, 35(11-12):1371–1393.
- Willis, A. J. (1997). The ecosystem: an evolving concept viewed historically. *Functional Ecology*, 11:268–271.
- Wissel, C. (1984). A universal law of the characteristic return time near thresholds. *Oecologia*, 65:101–107.
- Witte, J. P. M., Bartholomeus, R. P., Cirkel, D. G., and Kamps, P. W. T. J. (2008). Ecohydrologische gevolgen van klimaatverandering voor de kustduinen van Nederland. Technical report.
- Worrall, G. (1959). The Butana grass patterns. *Journal of Soil Science*, 10(1):34–53.
- Xu, L., Myneni, R. B., Chapin III, F. S., Callaghan, T. V., Pinzon, J. E., Tucker, C. J., Zhu, Z., Bi, J., Ciais, P., Tømmervik, H., Euskirchen, E. S., Forbes, B. C., Piao, S. L., Anderson, B. T., Ganguly, S., Nemani, R. R., Goetz, S. J., Beck, P. S. a., Bunn, a. G., Cao, C., and Stroeve, J. C. (2013). Temperature and vegetation seasonality diminishment over northern lands. *Nature Climate Change*, 3(3):581–586.
- Yin, Z., Dekker, S. C., M. Van Den Hurk, B. J. J., and Dijkstra, H. A. (2014). Bimodality of woody cover and biomass across the precipitation gradient in West Africa. *Earth System Dynamics*, 5(2):257–270.
- Yizhaq, H., Gilad, E., and Meron, E. (2005). Banded vegetation: biological productivity and resilience. *Physica A: Statistical Mechanics and its Applications*, 356(1):139–144.

## Bibliography

- Zagwijn, W. (1970). Vegetational history. In Jelgersma, S., de Jong, J., Zagwijn, W., and Altena, J. v. R., editors, *The coastal dunes of the western Netherlands; geology, vegetational history and archeology.*, chapter IV, pages 122–132. Rijksdienst voor het oudheidkundig bodemonderzoek.
- Zeeman, E. C. (1976). Catastrophe Theory. *Scientific American*, 234(4):65–83.
- Zeeman, E. C. (1982). Bifurcation and catastrophe theory. Lectures by E.C. Zeeman. *Contemporary Mathematics*, 9:207.
- Zeeman, E. C. and Barrett, T. W. (1979). Catastrophe Theory, Selected Papers 1972-1977. *IEEE Transactions on Systems, Man, and Cybernetics*, 9.
- Zelnik, Y. R., Kinast, S., Yizhaq, H., Bel, G., and Meron, E. (2013). Regime shifts in models of dryland vegetation. *Philosophical Transactions of the Royal Society A*, 371(2004).

# Summary

Globally, ecosystems are exposed to human-induced changes in the environment. Understanding the effect of these changes on ecosystems is of crucial importance and is currently one of the main challenges in the field of environmental science. To gain insights into the effects of human-induced environmental changes there is a strong need to develop methods and tools that enable better understanding of ecosystem dynamics. Dynamical systems theory is a field in mathematics that uses differential and difference equations (i.e. dynamical models) to describe natural phenomena and it provides ways to study the effect of (human-induced) environmental changes on ecosystems.

The application of dynamical systems theory on ecological problems has led to a number of key insights in the field of environmental science. Of particular interest is the fact that dynamical ecological models suggest that environmental change can trigger critical transitions in ecosystems. A critical transition is a shift of a system to a qualitatively different dynamical regime. Critical transitions occur when conditions change beyond some critical threshold and include discontinuous, hard to reverse shifts to alternative stable regimes (catastrophic shifts), transitions from static to cyclic dynamics and the formation of spatially periodic patterns out of uniform states. Through equilibrium analysis the mechanisms behind these critical transitions can be studied in detail by assuming that ecosystems are spatially uniform and in equilibrium. However, although frequently assumed, ecosystems often do not reside in a uniform equilibrium state.

This dissertation investigates the response of ecological models that are “off the beaten track”, i.e. that are not in a uniform equilibrium state, because of spatial patterning (Chapter 2), because of pulsed resource input (Chapter 3), because of cyclic dynamics (Chapter 4) or because of rapid environmental change (Chapter 5).

In Chapter 2 I show that through advanced analysis it is possible to assess the stability of spatially patterned states of ecological models, and demonstrate that knowledge about pattern stability is key to understanding the response of ecological models to environmental change. More specifically, I show that a family of patterned states can be stable for a given set of

## *Summary*

environmental conditions (i.e. multistability) and that patterned ecosystems may respond gradually to environmental change, provided that the change occurs slowly. However, patterned ecosystems are more likely to respond in a discontinuous way to rapid environmental change, meaning that patterned ecosystems may shift to a uniform (degraded) state even when alternative stable patterned states still exist. Gradual response of models to environmental change is bordered by a well-defined “period-doubling instability”. The period-doubling instability can be triggered by rapid change through a delayed transition. In patterned ecosystems, period-doubling can be explained by the (in)ability of patches to rearrange themselves in response to environmental change, which may serve as an indicator for resilience.

In Chapter 3 I study how changes in the frequency and magnitude of resource pulses could affect ecosystems with limited uptake capacity. More specifically I study the effect of projected changes in the frequency and intensity of rain events on arid ecosystems. By aggregating rain events I was able to apply equilibrium analysis to show that projected changes towards a rainfall regime with infrequent high intensity events may trigger a shift to a degraded state without any vegetation. In spatially patterned arid ecosystems, the same shift may be triggered by changes towards a rainfall regime with frequent low intensity rain events. These results suggest that patterned arid ecosystems are most resilient if rain events have an intermediate frequency and intensity. Whether changes in rainfall patterns are harmful to or beneficial for arid ecosystems is therefore dependent on the current rainfall regime.

Cyclic dynamics of ecological models generally cannot be understood through equilibrium analysis. However, in combination with separation of timescales, it can explain the dynamics of ecosystems with processes at multiple timescales, as I demonstrate in Chapter 4. With this approach I was able to explain both the short-term and long-term dynamics of a coastal dune ecological model, consisting of rapid repetitive shifts in water availability and long periods in which the model is locked in a state without vegetation. The stagnation of the short-term cyclic dynamics of the model can be explained both by internal dynamics and by rapid external changes, such as a sudden decline in precipitation. This approach enabled identifying soil water repellency as a potential driver of vegetation dynamics in coastal dune ecosystems.

In Chapter 5 I discuss and introduce models that suggest that elevated rates of environmental change can trigger critical transitions in ecosystems, even if the same magnitude of slow environmental change would not. Studying

the mechanisms behind such rate-induced critical transitions is challenging, but analyses of an elementary model showed that rate-induced critical transitions are likely to occur when the rate of environmental change is high relative to the maximum response rate of ecosystems, that they are similar to change-induced critical transitions but are driven by rates, rather than magnitudes, of environmental change and that they occur once a critical rate of environmental change is exceeded. Common properties of rate sensitive ecological models suggest that ecosystems with coupled fast-slow dynamics, that exhibit repetitive catastrophic shifts or that display spatially periodic patterns, may be prone to rate-induced critical transitions.

This dissertation highlights that much of the ecosystem dynamics “off the beaten track” is yet to be explored. Future studies on patterned ecosystems should focus on validating multistability using areal imagery and manipulative experiments, on identifying possible mechanisms and processes, aside from rapid environmental change, that can cause non-gradual response of patterned ecosystems to environmental change and on extending stability analysis of patterned ecosystem models to two spatial dimensions. In addition, this dissertation calls for advanced analyses of ecological models in combination with long-term manipulative experiments in order to understand the response of ecosystems to environmental change regardless the rate of external change or the rate of internal dynamics. Furthermore, to formulate speed limits to environmental change for ecosystems, the theory on rate-induced critical transitions needs to be further developed and integrated with the established theory on population level adaptations.



# **Samenvatting**

Wereldwijd worden ecosystemen blootgesteld aan door de mens veroorzaakte veranderingen in het milieu. Het is belangrijk om het effect van deze milieuveranderingen op ecosystemen te begrijpen om toekomstige degradatie van ecosystemen te kunnen voorkomen. Dit is een van de belangrijkste uitdagingen binnen de milieuwetenschappen. Om inzichten te verkrijgen in de effecten van milieuveranderingen is het belangrijk om methoden en middelen te vinden die ons in staat stellen ecosysteemdynamiek bestuderen. Dynamische systeemtheorie is een onderzoeksgebied binnen de wiskunde en gebruikt differentiaal- en differentievergelijkingen (ofwel dynamische modellen) om natuurlijke fenomenen te beschrijven. Dynamische systeemtheorie kan gebruikt worden om effecten van veranderingen in de omgeving op ecosystemen te onderzoeken.

De toepassing van dynamische systeemtheorie op ecologische vraagstukken heeft tot een aantal belangrijke inzichten geleid binnen de milieuwetenschappen. Met name interessant is het feit dat dynamische ecologische modellen suggereren dat milieuveranderingen kunnen leiden tot kritische overgangen. Een kritische overgang is een verschuiving binnen een systeem naar een kwalitatief anders dynamisch regime. Kritische overgangen vinden plaats wanneer een kritische drempelwaarde wordt overschreden en omvatten discontinue en moeilijk te herstellen omslagen naar alternatieve stabiele regimes (catastrofale omslagen), overgangen van statische naar cyclische dynamiek en de vorming van ruimtelijk periodieke patronen uit uniforme toestanden. De mechanismen achter deze kritische overgangen kunnen in detail worden bestudeerd met behulp van evenwichtsanalyse. Hierbij moet worden aangenomen dat ecosystemen ruimtelijk uniform en in evenwicht zijn. Vaak zijn echte ecosystemen echter niet uniform of in evenwicht.

In dit proefschrift wordt het effect van milieuveranderingen bestudeerd met ecologische modellen die “buiten het gebaande pad” zijn getreden - ofwel modellen die niet in een uniform evenwicht zijn - door ruimtelijke patroonvorming (Hoofdstuk 2), door gepulseerde instroom van voedingsstoffen (Hoofdstuk 3), door cyclische dynamiek (Hoofdstuk 4) of door snelle milieuveranderingen (Hoofdstuk 5).

## *Samenvatting*

In Hoofdstuk 2 laat ik zien dat door middel van geavanceerde analyse het mogelijk is om de stabiliteit van ruimtelijke patronen in ecologische modellen te bepalen en demonstreer ik dat kennis over de stabiliteit van patronen essentieel is om het effect van milieuverandering in ecologische modellen te begrijpen. Ik laat zien dat een familie van patronen stabiel kan zijn voor een gegeven set van milieuomstandigheden (multistabiliteit) en dat ecosystemen met ruimtelijke patronen op een geleidelijke manier kunnen reageren op milieuveranderingen als de veranderingen langzaam plaatsvinden. Echter, ecosystemen met patronen reageren waarschijnlijk op een discontinue manier op snelle veranderingen, wat betekent dat er een omslag plaatsvindt van een toestand met patronen naar een uniforme (gedegradeerde) toestand. De geleidelijke aanpassing van modellen op milieuveranderingen wordt begrensd door een “periodeverdubbelingsinstabiliteit”, welke wordt overschreden als milieuveranderingen snel plaatsvinden. Of periodeverdubbelingen kunnen plaatsvinden lijkt af te hangen van de mobiliteit van (vegetatie-)clusters. De mobiliteit van deze clusters zou kunnen worden gebruikt als een indicator voor de veerkracht van ecosystemen.

In Hoofdstuk 3 onderzoek ik het effect van voorspelde veranderingen in de frequentie en intensiteit van regenbuien op aride ecosystemen. Door het cumulatieve effect van regenbuien te beschouwen kon ik een evenwichtsanalyse toepassen waarmee ik laat zien dat de voorspelde veranderingen richting een regenregime met infrequeute en intense buien kunnen leiden tot een omslag naar een gedegradeerde toestand zonder vegetatie. Veranderingen richting frequentere maar minder intense buien kunnen echter tot eenzelfde omslag leiden in aride ecosystemen met ruimtelijke vegetatiepatronen. Deze resultaten suggereren dat aride ecosystemen met ruimtelijke vegetatiepatronen het meest veerkrachtig zijn in een regenregime met tussenliggende frequentie en intensiteit. Dit betekent dat veranderingen in het regenregime zowel schadelijk als gunstig kunnen zijn voor aride ecosystemen, afhankelijk van de huidige frequentie en intensiteit van regenbuien.

Cyclische dynamiek in ecologische modellen kan over het algemeen niet worden bestudeerd met evenwichtsanalyse. In Hoofdstuk 4 laat ik echter zien dat evenwichtsanalyse kan worden toegepast wanneer processen binnen een ecosysteem sterk verschillen in het tijdbestek waarover ze plaatsvinden, omdat hierdoor de snelle en de langzame dynamiek apart geanalyseerd kunnen worden. Ik laat zien dat op deze manier zowel de korte- als langetermijndynamiek van een ecologisch kustduinmodel verklaard worden, bestaande uit zich herhalende snelle omslagen in beschikbaar bodemwater en lange perioden zonder vegetatie. De korttermijn cyclische dynamiek in het model stagniert

door interne mechanismen dan wel door snelle externe veranderingen, zoals een plotselinge afname van de neerslag. De gedetailleerde analyse van dit model maakte het mogelijk om waterafstotende bodems aan te wijzen als potentiële veroorzaker van de vegetatiedynamiek in kustduinen.

In Hoofdstuk 5 worden modellen gepresenteerd die suggereren dat kritische overgangen in ecosystemen kunnen worden veroorzaakt door snelle milieuvveranderingen. De mechanismen die verantwoordelijk zijn voor deze “snelheid geïnduceerde overgangen” zijn moeilijk te bestuderen, maar analyses van een simpel model laten zien dat snelheid genduceerde overgangen plaatsvinden als de snelheid van milieuvveranderingen hoog is in vergelijking met de maximale aanpassingssnelheid van ecosystemen en dat ze vergelijkbaar zijn met “verandering geïnduceerde overgangen” maar plaatsvinden als een kritische snelheid van verandering wordt overschreden. Snelheidsgevoelige ecologische modellen suggereren dat snelheid geïnduceerde overgangen kunnen plaatsvinden in ecosystemen met gekoppelde snelle en langzame dynamiek, in ecosystemen waarin herhaaldelijk omslagen plaatsvinden en in ecosystemen met ruimtelijk periodieke patronen.

Dit proefschrift benadrukt dat een groot deel van de ecosysteemdynamiek “buiten de gebaande paden” nog tot onontgonnen terrein behoort. Toekomstig onderzoek aan patronen in ecosystemen zou zich moeten richten op het valideren van multistabiliteit met luchtfoto’s en manipulatieve experimenten, het vinden van mechanismen en processen - naast snelle milieuvveranderingen - die verantwoordelijk kunnen zijn voor abrupte degradatie van deze ecosystemen en het uitbreiden van stabiliteitsanalyse van patronen naar twee ruimtelijke dimensies. Daarnaast zijn geavanceerde modelanalyses en langetermijnexperimenten nodig om het effect van milieuvveranderingen op ecosystemen te kunnen begrijpen, onafhankelijk van de snelheid van verandering en de snelheid van de interne ecosysteemdynamiek. Daarnaast kunnen snelheidslimits voor milieuvveranderingen worden bepaald als de theorie van snelheid geïnduceerde overgangen wordt doorontwikkeld en wordt geïntegreerd met de theorie over aanpassingen op populatieniveau.



# Dankwoord

Het schrijven van een proefschrift bleek niet zo makkelijk als ik aan het begin van mijn promotietraject dacht. Hoe zorg ik ervoor dat onzekerheid, stress en perfectionisme niet verlammend werken tijdens het schrijven van mijn artikelen? Hoe ga ik om met de vrijheid die ik krijg in mijn onderzoek? Hoe zorg ik voor voldoende afleiding? Dankzij mijn begeleiders, collega's, vrienden en familie kijk ik toch terug op een geweldige periode en ben ik zeer tevreden met het eindresultaat.

Max en Maarten, het was een voorrecht jullie als begeleiders te hebben. Bedankt voor de vrijheid die jullie mij gaven om m'n eigen pad te bewandelen en het vertrouwen dat jullie in mij stelden. Max, altijd enthousiast en kritisch waar nodig. Het blijft me verbazen dat de teksten die ik je stuurde je nooit leken te vervelen, zelfs als je ze al tig keer gelezen had. Bedankt ook voor de vele complimenten die ik soms nodig had en waar ik veel energie uit gehaald heb. Maarten, grondig en creatief. Je keek vaak in meer detail naar mijn werk dan ikzelf en dat motiveerde mij om het onderste uit de kan te halen. Onze discussies over die details en jouw kijk op de rode draad in mijn manuscripten hebben mij gevormd tot de zelfstandige onderzoeker die ik nu ben. Dank daarvoor.

Ik heb ook veel geleerd van de samenwerking met onze projectpartners van het Mathematisch Instituut van de Universiteit Leiden. Eric, onze bijeenkomsten hadden een gemiddelde duur van  $\pm$  7 uur. Die bijeenkomsten, waarin we verdwaalden in het doolhof dat wiskunde heet, hebben geleid tot ons gezamenlijke hoofdstuk waar we trots op kunnen zijn. Buiten onze succesvolle samenwerking zal ik nooit vergeten hoe in het eerste jaar het slechtste hostel van Londen hebben overleefd. Ik hoop ook de forehand die je me in de Kensington Gardens probeerde bij te brengen niet te vergeten. Arjen, de enorme hoeveelheden tekst in de kantlijnen van mijn manuscripten hebben me geholpen mijn hoofdstukken Wiskundig Correct te maken en ik ben blij te zien dat onze samenwerking weer tot nieuwe projecten heeft geleid. Ik wil jullie bedanken voor de fijne samenwerking.

Tijdens mijn promotietraject heb ik samengewerkt met milieuwetenschappers, wiskundigen, hydrologen en geochemici. Ik wil de co-auteurs van mijn

## Dankwoord

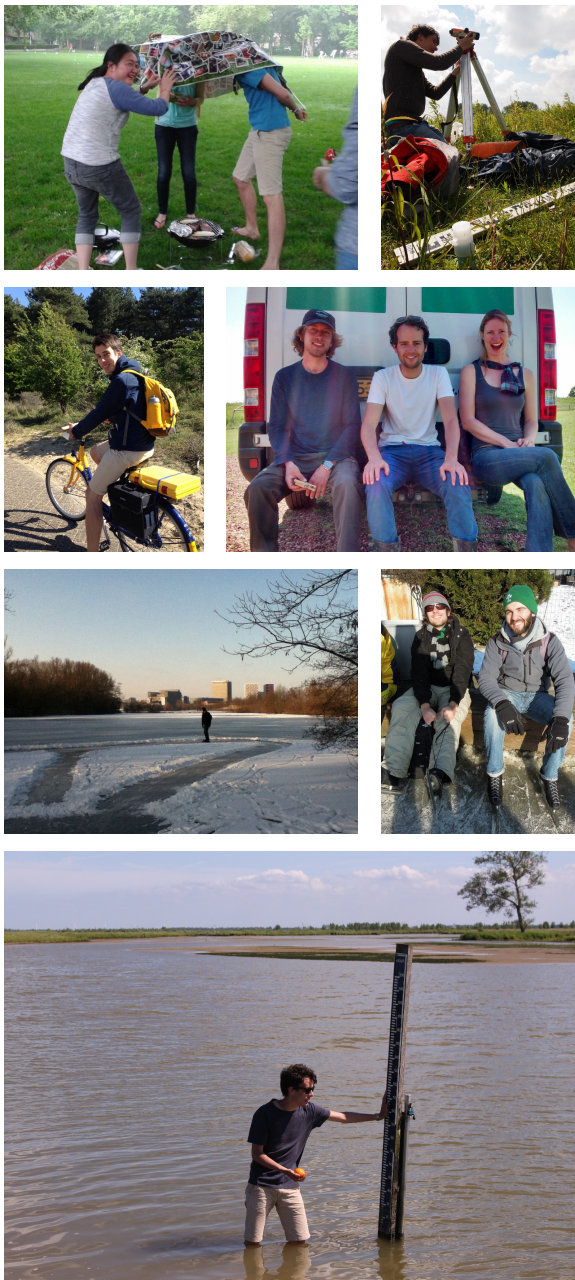
hoofdstukken bedanken voor alles wat ik van hen geleerd heb: Jens, Derek, Marc, Mara, Klaas, Jiefei en Stefan.

Ik heb het de afgelopen jaren erg naar mijn zin gehad op de 11e verdieping. Het departement Milieu-natuurwetenschappen is inmiddels zo groot dat ik onmogelijk iedereen kan bedanken. Zun, Jiefei, Roos, Luli, Didi, Shuquiong, Vincent en Natalie, jullie waren geweldige kamergenoten en ik heb altijd genoten van onze koffie/thee pauzes. Jiefei, you are a great roommate, friend and co-author and I wish we could have dinner together at restaurant Super House every day of the week. I'm looking forward to visiting you in China next year. Mara, thank you for introducing me to the espresso of Tricolore and for your contributions to Chapter 3. Brian, Mart en Maarten, ik zal ons schaatsavontuur in Broek in Waterland nooit vergeten. Aat, Iris, Floris, Rémon en Myrna, het jaarlijkse veldwerk op Tiengemeten voelde als vakantie voor mij en ik heb er altijd naar uit gekeken. Bedankt allemaal voor de geweldige werksfeer!

Buiten werktijd heb ik tijdens mijn periode als promovendus genoeg afleiding gehad dankzij mijn huisgenoten Francis, Miriël, Yosta, Lisanne en Jan en ook oudhuisgenoten Huib, Irene en Iris. Ik ben nog altijd met veel plezier thuis en geniet van de keukendisco's, eilandweekenden, kamerkroegentochten en zelfs de maandelijkse huisvergaderingen. Bedankt voor alle gezelligheid!

I would like to thank Manuel and Sija for not excommunicating me after leaving Hydrology. I appreciate our friendships and I enjoyed complaining about our miserable PhD lives. Sara, Vero, thank you for our friendship. Mats, aan jou heb ik mijn interesse in wiskunde en programmeren te danken. Terwijl we misschien beter hadden kunnen opletten bij natuurkunde programmeerden we samen onze grafische rekenmachines om  $\pi$  tot op tientallen decimalen nauwkeurig te berekenen. Bedankt allemaal!

Ik wil mijn familie bedanken voor hun steun in de afgelopen jaren en hun interesse in mijn onderzoek. Marjon en Rinus, hoe kun je geen milieuwetenschapper worden als je opgroeit in de klei en op het water en met al die rondjes over het erf? Floor en Jikke, bedankt voor alle positieve energie en gezelligheid. Tenslotte, Maaike, bedankt voor de onvoorwaardelijke steun, zorgzaamheid en liefde.





# **Curriculum Vitae**

Koen Siteur was born on September 27, 1987 in Utrecht. He grew up in Loenen aan de Vecht where he went to primary school. After finishing secondary school (VWO, RSG Broklede, Breukelen) he studied Environmental Sciences at Utrecht University. He obtained his BSc degree in Environmental Sciences in 2009 and continued his studies at Utrecht University in the master programme Hydrology. Within the Earth Surface Hydrology track he wrote his MSc thesis under supervision of dr. Derek Karssenberg and prof. dr. Marc Bierkens on the topic of early-warning signals for critical transitions in water-limited grazing systems. He obtained his MSc degree (*cum laude*) in 2011. In the same year he started his PhD research within the NWO Complexity programme under the supervision of dr. Maarten Eppinga and prof. dr. Max Rietkerk at Utrecht University and in collaboration with dr. Eric Siero and prof. dr. Arjen Doelman (Leiden University) and prof. dr. Jens Rademacher (University of Bremen). The results of this research are presented in this dissertation.



# **Publications by Koen Siteur**

## **Published chapters of this dissertation**

Siteur, K., Eppinga, M. B., Doelman, A., Siero, E. and Rietkerk, M. (2016). Ecosystems off track: Rate-induced critical transitions in ecological models. Accepted for publication in *Oikos*. (Chapter 5)

Siteur, K., Eppinga, M. B., Karssenberg, D., Baudena, M., Bierkens, M. F. P. and Rietkerk, M. (2014). How will increases in rainfall intensity affect semiarid ecosystems? *Water Resources Research* 50(7):5980-6001. (Chapter 3)

Siteur, K., Mao, J., Nierop, K. G. J., Rietkerk, M., Dekker, S. C. and Eppinga, M. B. (2016). Soil water repellency: a potential driver of vegetation dynamics in coastal dunes. Accepted for publication in *Ecosystems*. (Chapter 4)

Siteur, K., Siero, E., Eppinga, M. B., Rademacher, J. D. M., Doelman, A. and Rietkerk, M. (2014), Beyond Turing: The response of patterned ecosystems to environmental change. *Ecological Complexity* 20:81-96. (Chapter 2)

## **Other publications**

Doelman, A., Eppinga., M. B., Hek, G., Rademacher, J. D. M., Rietkerk., M., Siero., E. and Siteur, K. (2013). Klimaatverandering, verwoesting en biljart. *Nieuw Archief voor Wiskunde* 15(3):200-204.

Siero, E., Doelman, A., Eppinga, M. B., Rademacher, J. D. M., Rietkerk, M. and Siteur, K. (2015). Striped pattern selection by advective reaction-diffusion systems: Resilience of banded vegetation on slopes. *Chaos: An Interdisciplinary Journal of Nonlinear Science* 25(3):036411.